

Portable spectroscopy system for ultra-sensitive, real-time measurement of breath ethane

Claire Siobhan Patterson MSci (Hons.)

Thesis presented for the degree of Doctor of Philosophy

University of Glasgow
Department of Physics and Astronomy

December 2008

© Claire S. Patterson

Abstract

This thesis describes the development, characterisation and application of a portable spectroscopy system for ultra-sensitive, real-time detection of breath ethane. In healthcare, breath ethane is a widely accepted marker of free radical-induced cell damage and may be used to indicate changes in oxidative stress.

The aim was to deliver a compact instrument capable of long-term, on-site use in a clinical environment, while also retaining the high performance previously achieved by lab-based systems at the University of Glasgow. The newly developed instrument has a sensitivity of 70 parts per trillion with a 1 Hz sampling rate. The system incorporates a cryogenically-cooled lead-salt laser and uses a second derivative wavelength modulation detection scheme. A thermally-managed closed-loop refrigeration system has eliminated the need for liquid coolants.

The instrument has been field-tested to ensure target performance is sustained in a range of environments, both indoor and outdoor. It has since been used in a number of pilot clinical studies, both off-site and on-site, in which breath ethane was monitored as a marker of oxidative stress. The three main clinical areas investigated were dialysis, radiotherapy and intensive care. In the intensive care study, the instrument was modified to enable automatic breath sampling of inspired and expired gases of ventilated patients. This technique proved highly successful and the instrument then remained at the Southern General hospital, where it continued to be used as part of a wider study into breath ethane in intensive care patients.

The use of the new spectroscopy system has enabled ultra-sensitive, rapid analysis of a

large number of breath samples. The use of the new instrument, in particular for continual breath monitoring, has enabled the detection of short-lived fluctuations in breath ethane, yielding some interesting findings in a number of pilot clinical studies. Our results suggest that breath ethane may be used as an indicator of dynamic changes in oxidative stress. Further studies will be required to determine if such monitoring is of clinical benefit.

Chapter 1 gives a general introduction to spectroscopy and some background to our project. A number of spectroscopic techniques and laser sources are discussed, along with a review of previous work in ethane detection. In chapter 2 some background theory of molecular spectroscopy is given, with a more detailed discussion of the wavelength modulation technique. Chapter 3 describes in detail the development of the portable spectroscopy system. The achieved performance and factors contributing to this performance are discussed in chapter 4. The field test of the instrument is reported on in chapter 5. In chapter 6 the application of the technology to breath analysis and the current challenges in this field are discussed. Example breath ethane measurements for healthy controls are provided. The clinical pilot studies conducted using the new system in areas of dialysis, intensive care and radiotherapy are discussed in chapters 7, 8, and 9 respectively. Chapter 10 contains the thesis summary and conclusions, with suggestions for future work.

Contents

Preface	xiii
Acknowledgements	xviii
Declaration	xx
1 Introduction to spectroscopy	1
1.1 Spectroscopy	1
1.2 Gas detection	2
1.3 Spectroscopic trace gas detection	3
1.3.1 Source requirements	3
1.3.2 Direct mid-IR laser sources	5
1.3.3 Mid-IR sources based on nonlinear frequency conversion	7
1.4 Optical spectroscopic techniques	8
1.4.1 Wavelength or frequency modulation spectroscopy	9
1.4.2 Cavity-enhanced spectroscopy	10
1.4.3 Photoacoustic spectroscopy	12
1.5 Trace ethane detection	13
1.5.1 Background to our project	13
1.5.2 Related work in ethane detection	14
1.6 Discussion	16
2 Molecular absorption spectroscopy	17
2.1 Molecular transitions	17
2.1.1 Transition broadening	18
2.1.2 Ethane transitions	20

2.2	Absorption spectroscopy	21
2.3	The wavelength modulation technique	22
2.3.1	Mathematical description	23
2.3.2	Graphical description	26
2.3.3	Residual amplitude modulation	26
3	Development of the portable spectroscopy system	28
3.1	Instrument overview	28
3.1.1	Laser and optical configuration	29
3.1.2	Detection scheme	31
3.1.3	Electronics and interfacing	32
3.2	Laser cooling	37
3.2.1	Closed-loop cooling system	37
3.2.2	Temperature control	38
3.2.3	Thermal management	39
3.3	Power requirement	40
3.4	Zero referencing and calibration	41
3.5	Herriott cell	42
3.5.1	Alignment	42
3.5.2	Estimate of number of passes	46
3.6	Discussion	46
4	Characterisation of the spectroscopy system	48
4.1	Performance	48
4.1.1	Sensitivity	48
4.1.2	Accuracy	50
4.1.3	Selectivity	53
4.2	Theoretical contribution of noise sources	56
4.2.1	Detector noise	56
4.2.2	Shot noise	57
4.3	Experimentally determined contribution of noise sources	59
4.3.1	Measured noise spectra	59
4.3.2	Effect of reducing power	62
4.3.3	Comparison of vibrational noise	62

4.4	Laser parameters	64
4.4.1	Temperature and current	64
4.4.2	Modal purity	67
4.5	Further system parameters	67
4.5.1	Modulation	67
4.5.2	Optical pathlength	68
4.5.3	Pressure	70
4.6	Other factors affecting performance	74
4.6.1	Ambient temperature	74
4.6.2	DC light levels	75
4.6.3	Optical fringes	77
4.7	Discussion	78
5	Field-trial of the portable spectroscopy system	81
5.1	Background	81
5.2	Outdoor field trial	82
5.2.1	Overview	82
5.2.2	Gas release	84
5.3	Results	84
5.3.1	Measurement while stationary	85
5.3.2	Measurements while in a moving vehicle	85
5.4	Discussion	87
6	Breath analysis	89
6.1	Background	89
6.2	Challenges	91
6.2.1	Ambient levels and compensation methods	91
6.2.2	Previous studies and techniques	92
6.3	Oxidative stress	93
6.3.1	Definition	93
6.3.2	Associated conditions	94
6.3.3	Biomarkers	94
6.3.4	Ethane as a biomarker	94
6.4	Ethane levels	96

6.4.1	Ambient ethane	96
6.4.2	Breath ethane intra-variability	97
6.4.3	Breath ethane inter-variability	97
6.5	Discussion	98
7	Dialysis study	100
7.1	Background	100
7.2	Materials and Methods	101
7.2.1	Participants	101
7.2.2	Breath ethane analysis	102
7.2.3	Study Design	103
7.3	Results	105
7.4	Discussion	108
8	Radiotherapy study	113
8.1	Background	113
8.1.1	Ethane as a dose mediator	114
8.2	Study Design	115
8.2.1	Previous study	115
8.2.2	Automated collection system	116
8.2.3	Patients	121
8.3	Results	121
8.4	Discussion	124
9	Intensive care study	126
9.1	Background	126
9.2	Study design	127
9.2.1	Physiological data collection	128
9.2.2	Breath sample collection	128
9.2.3	System modifications	131
9.2.4	Ventilator modes	133
9.2.5	Medical gases	135
9.3	Results	135
9.3.1	Ethane in medical gases	135
9.3.2	Ventilator mode safety tests	136

9.3.3	Control experiment	137
9.3.4	Manual measurement of breath ethane	140
9.3.5	Automated measurement of breath ethane	143
9.4	Discussion	146
10	Summary and conclusions	148
10.1	Summary	148
10.2	Conclusions	149
10.3	Future work	151
A	Circuit diagrams	154
B	Rayleigh range approximation	157
C	Radiotherapy sampling equipment staff instructions	159
D	ITU patient physiological data	161

List of Tables

2.1	Fundamental bond stretching frequencies	19
4.1	Theoretical noise contributions and calculated effect on ethane sensitivity .	59
4.2	Measured noise contributions and calculated effect on ethane sensitivity . .	60
4.3	Effect of modulation depth on ethane sensitivity	68
4.4	Instrument specification	78
8.1	Mean breath ethane concentration for 6 radiotherapy patients	123
9.1	Mean measured net ethane concentration each day for ITU patient 3	142

List of Figures

1.1	Diagram of a double-heterojunction lead-salt laser	6
1.2	Experimental set-up for wavelength modulation spectroscopy	9
1.3	Experimental set-up for CRD spectroscopy	11
1.4	Experimental set-up photoacoustic spectroscopy	12
2.1	The independent vibrational modes of water	18
2.2	Selected ethane transitions	21
2.3	Graphical illustration of the wavelength modulation technique	25
3.1	Photograph of the portable spectroscopy system	29
3.2	Photographic view of the instrument sections	30
3.3	Schematic of the instrument optical configuration	31
3.4	$2f$ sample lineshapes as the laser wavelength is scanned over the ethane transition	32
3.5	The transfer function of the sample filter and electronics	34
3.6	An example of the results section from the LabVIEW software	35
3.7	Comparison of cooling times between closed-loop and liquid nitrogen systems	38
3.8	Instrument thermal management	40
3.9	Instrument power requirement	41
3.10	The Herriott multipass cell and visible spot pattern	45
4.1	Measurement of ambient ethane and nitrogen gas	49
4.2	Example breath ethane measurements	50
4.3	Instrument calibration	51
4.4	Instrument repeatability	54
4.5	Water, methane and ethane transitions from the HITRAN database	55

4.6	Calculated noise to signal ratios	58
4.7	Measured noise spectra	60
4.8	Effect of reducing the power on ethane sensitivity	63
4.9	Comparison of intensity noise between lab-based and portable instrument	64
4.10	Example laser modechart supplied by Laser Components	65
4.11	Laser current and temperature values corresponding to an ethane transition	66
4.12	Theoretical power transmission and sensitivity gain when increasing number of Herriott cell passes	69
4.13	Theoretical Voigt transition profiles found using HITRAN for direct absorption at 7 different pressures	71
4.14	Measured effect of sample cell pressure on the $2f$ sample lineshape and reported ethane concentration	73
4.15	Effect of photodetector light levels on reported ethane concentration	76
5.1	Photograph of field trial set-up showing van, generator and anemometer	83
5.2	Overhead view of test track indicating static measurement and plume traverse locations	84
5.3	Photograph of the four-arm natural gas release	85
5.4	Measured ethane concentration and wind velocity at two locations	86
5.5	Traverses of the gas release plume	86
5.6	Comparison of the measured ethane plume with a simple Gaussian model	87
6.1	Lipid peroxidation	95
6.2	Intra-variability of breath ethane of a healthy volunteer over one day	96
7.1	Breath sample collection apparatus	102
7.2	Elevation of ethane in first 30 min of dialysis for 6 patients	106
7.3	Comparison of ambient ethane, control subject breath ethane and dialysis patient breath ethane	106
7.4	Patient clinical data and measured peak ethane values	107
7.5	Peak ethane dependence on Period on Dialysis	109
8.1	The breath collection assembly	118
8.2	The custom-designed sampling rig and peristaltic pump	119
8.3	Circuit diagrams for sampling rig electronics	120

8.4	Breath ethane of 6 patients during radiotherapy treatment	122
9.1	Portable instrument and breath collection apparatus photographed in the ITU ward	130
9.2	Gas flow rate dependence on Herriott cell pressure	133
9.3	Ethane concentration of medical air and medical oxygen	136
9.4	Control ITU data using artificial lung in place of patient	137
9.5	Second ITU control experiment with varying inspired oxygen concentration	139
9.6	Breath ethane results for ITU patient 1	141
9.7	Breath ethane results for ITU patient 2	141
9.8	Breath ethane results for ITU patient 3	144
9.9	Breath ethane results for ITU patient 4	145
A.1	Sinewave generator circuit diagram	155
A.2	Bandpass filter circuit diagram	155
A.3	Summing operational amplifier circuit diagram	156
A.4	AC amplification circuit diagram	156
C.1	Equipment instruction sheet for radiotherapy staff	160
D.1	Key to physiological data	162
D.2	DocVu recorded data for ITU patient 1	162
D.3	DocVu recorded data for ITU patient 3	163
D.4	DocVu recorded data for ITU patient 4	164

Preface

During my PhD I was supervised by Dr Ken Skeldon and Prof Miles Padgett. I developed the portable instrument mainly under the supervision of Ken, who had previously developed the lab-based system in the Glasgow Optics group. I designed and set-up the more compact optical configuration. I modified the software previously controlling the lab-based instrument for use with the portable instrument and integrated all hardware and software components. Later I further modified the software for use with the automatic sampling system along with other instrument adjustments. Ken assisted me with the development of the electronics, the incorporation of the instrument components into the flight-case housing and the resolution of thermal management issues. Upon instrument completion I characterised the performance and determined the contributing noise factors. The Appleton outdoor field-trial was a team effort overall with Ken, Graham Gibson and I working on the instrument operation in the field.

I played a key role in the three main clinical studies. In the dialysis study I developed and subsequently modified the breath sampling protocol. I collected and measured a large number of patient breath samples, analysed the data and liaised with the clinicians. I worked closely with Lesley McMillan, who also collected and measured a large number of the breath samples and performed the statistical analysis of the data. In the radiotherapy trial I developed the electronic sampling rig. Lesley and I designed and constructed the other sampling apparatus such as the mask assembly. Together we collected the breath samples from radiotherapy patients at Ninewells hospital, Dundee and subsequently analysed them in the lab.

During the intensive care study I spent a large proportion of my time working in the Southern General hospital with the instrument based on-site. I manually collected and measured the majority of the breath ethane samples obtained from a number of ventilated patients. Recording of other clinical parameters was enabled by the clinical and medical physicists at the Southern General hospital. I modified the instrument to enable automated gas sampling from the ventilator. In addition to instrument use during the trial I also worked to maintain instrument performance and resolve any problems that arose before and during the trial. Ken assisted with problems encountered with laser cooling while the instrument was based on-site. These were eventually resolved by the replacement of the compressor used in the cooling system. During all periods of automated breath collection at the patient bedside I remained in the hospital to monitor the instrument operation and performance. Later, the intensity of breath sampling was increased and I worked closely with Lesley to monitor breath ethane in patients regularly over periods of up to four days. Ethical approval for all clinical studies was dealt with by Lesley or by our clinical collaborators.

There were also a number of parallel strands to our project including investigations of breath ethane analysis in areas such as exercise, zoology and other clinical conditions. I was involved in collection and measurement of breath samples and maintenance of both the previous lab-based instrument and the portable instrument throughout the course of these studies.

Publications

- K. Stevenson, K. Radhakrishnan, C. S. Patterson, L. C. McMillan, K. D. Skeldon, L. Buist, M. Padgett, and P. G. Shiels. Breath ethane peaks during a single haemodialysis session and is associated with time on dialysis. *J. Breath Res.*, 2(2):026004 (8pp), 2008.
- C. S. Patterson, L. C. McMillan, K. Stevenson, K. Radhakrishnan, P. G. Shiels, M. J. Padgett, and K. D. Skeldon. Dynamic study of oxidative stress in renal dialysis patients based on breath ethane measured by optical spectroscopy. *J. Breath Res.*, 1(2):026005, 2007.
- C. S. Patterson, L. C. McMillan, C. Longbottom, G. M. Gibson, M. J. Padgett, and K. D. Skeldon. Portable optical spectroscopy for accurate analysis of ethane in exhaled breath. *Meas. Sci. Technol.*, 18:1459–1464, 2007.
- K. D. Skeldon, L. C. McMillan, C. A. Wyse, S. D. Monk, G. Gibson, C. Patterson, T. France, C. Longbottom, and M. J. Padgett. Application of laser spectroscopy for measurement of exhaled ethane in patients with lung cancer. *Resp. Med.*, 100(2):300–306, 2006.
- K. D. Skeldon, C. S. Patterson, C. A. Wyse, G. M. Gibson, M. J. Padgett, C. Longbottom, and L. C. McMillan. The potential offered by real-time, high-sensitivity monitoring of ethane in breath and some pilot studies using optical spectroscopy. *J. Opt. A: Pure Appl. Opt.*, 7:376–384, 2005.

Accompanying material

Both of the publications for which I am first author have been included at the end of this thesis.

Presentations

July 07 Poster presentation at Tunable Diode Laser Spectroscopy conference in Reims, France

June 07 Invited oral presentation at Optical Radiation Measurement Club, NPL, Teddington

May 07 3rd year PhD talk in Department of Physics and Astronomy, University of Glasgow

Apr 07 Poster presentation at Interdisciplinary meeting, Oran Mor, Glasgow

Apr 07 Oral presentations to clinical staff at Southern General hospital, Glasgow and at Ninewells hospital, Dundee

Jan 07 Poster presentation at Medical Photonics Workshop, University of St Andrews

Oct 06 Oral presentation at PhotonEX06, Birmingham

Sep 06 Oral presentation at Photon06 conference, University of Manchester

Nov 05 Poster presentation at SET for BRITAIN event in House of Commons

Aug 05 Oral presentation at Unilever, Port Sunlight

May 05 Poster presentation at Breath analysis for Clinical Diagnosis and Therapeutic Monitoring conference, University of Innsbruck, Austria.

Apr 05 Poster presentation at IoP conference 2005, University of Warwick

In addition I have also been heavily involved in a number of science outreach activities and have developed and delivered a number of science shows and workshops for school and general public audiences. Towards the end of my PhD I also gave a short talk at the Lord Kelvin Reception in the House of Commons and attended the Rank-prize Symposium entitled Making Light Work.

Prizes

My end of 1st year report submitted to the Physical Sciences Graduate School in September 2005 was awarded the Hunter/Cumming Memorial prize.

I won a bottle of champagne for my 3rd year PhD talk in the Department of Physics and Astronomy.

Acknowledgements

It's difficult to know where to start with acknowledgements as I have so many people I would like to thank. Firstly, thank you to my supervisor Ken. I have come to realise that the feeling I had of being 'thrown in at the deep end' was the experience of real training. Throughout my PhD, even at inconvenient times, Ken gave me help when I really needed it and even when things were tough we usually managed to have a really good laugh. I learned a lot from him about science and science outreach. Thanks to my supervisor Miles for all his advice about my research, science and careers. It is much appreciated. Thanks also to Lesley, who was great fun to work closely with and always made time to help me, and to Graham, who must have lifted almost every heavy piece of equipment during my PhD.

I really appreciate the general support of the whole Optics group, or as we called it, the Optics 'family'. Laura was always there for chat and laugh over a cup of tea. Eric always had both a cheery smile and a ridiculously large supply of chocolate. I won't name everyone but I know that every group member helped me out in some way at some point and made the three years I spent in the Optics group enjoyable and often hilarious.

For the clinical studies, our project team is indebted to the staff and patients in the hospitals at which the trials took place: The dialysis clinics of Gartnavel Hospital and the Western Infirmary, both in Glasgow; the radiotherapy clinic at Ninewells hospital, Dundee; and the intensive therapy unit and medical physics department at the Southern General hospital, Glasgow. Assistance is appreciated from collaborators at the University Department of Surgery, Glasgow Royal Infirmary and the financial support of both the

EPSRC and Unilever is acknowledged.

Throughout the last few years I have had continual support and encouragement from my friends and family. In West Kilbride, Glasgow and St Andrews I've been lucky enough to be surrounded by lovely people who have kept me smiling. Thank you to Fraser, who has been there for me whether he was nearby or on the other side of the world. Those people who are closest to me have been with me through all the highs and the lows. Thanks for everything.

Author's declaration

I hereby declare that this thesis is my own composition, that it is a record of work done by myself and that it has not been presented in any previous application for a degree at this or any other institution.

.....

Claire Siobhan Patterson

Chapter 1

Introduction to spectroscopy

This chapter gives a general introduction to laser spectroscopy. A number of laser sources and spectroscopic techniques are described. An overview of previous work in ethane detection is given along with some background to our project.

1.1 Spectroscopy

Spectroscopy is defined as the measurement and interpretation of electromagnetic radiation absorbed or emitted by molecules, atoms, or ions undergoing transitions between allowed energy levels [1]. Spectroscopy has provided and continues to provide qualitative and quantitative analysis of materials, ranging from the biochemical constituents of cells [2] to the atmospheric composition of extra-solar planets [3]. The field of spectroscopy is rapidly expanding and many spectroscopic techniques are commonly applied across a wide range of applications including medical imaging, environmental monitoring, security and defence and energy research. Spectroscopy is both a subject of study, to further the knowledge of fundamental science, and a practical tool throughout scientific, and in many cases interdisciplinary, research [4].

Progress in the field of spectroscopy rapidly gained momentum through the invention of the laser. When Theodore Maiman built the first laser in 1960 he described it as a ‘solution seeking a problem’. Over the next few years, however, the potential use of lasers was envisaged and a massive effort was made to find materials that showed lasing action [5]. Since then, the technology has undergone huge development and lasers have found their place in the heart of applications such as sensing, communications, welding and medicine. In addition to the numerous practical applications, lasers have also enabled the discoveries of new phenomena and opened up new branches of physics.

In terms of spectroscopy, the application of lasers has been described as ‘an unprecedented revolution’. Compared with other light sources, lasers offer higher power, monochromaticity and coherence. The unique properties of lasers have increased sensitivity and selectivity of traditional spectroscopic techniques such as infrared (IR) absorption spectroscopy, overcoming problems of lower source intensity and poor detector sensitivity. In addition to the enhancement of previous spectroscopic techniques, lasers have enabled the development and introduction of new spectroscopic methods, such as those based on the stimulated Raman effect [6], and techniques involving nonlinear processes such as multi-photon excitation [7]. Spectroscopy has significantly benefited from the use of tunable diode lasers, first developed in the mid-1960s. Tunable diode lasers, particularly the lead-salt diode, quickly found broad use in high-resolution laser absorption spectroscopy [8]. Spectroscopy using tunable laser diodes, often referred to as Tunable Diode Laser Absorption Spectroscopy (TDLAS), is widely used as a technique for the detection of trace gases.

1.2 Gas detection

Gas detection is important in a wide variety of areas such as environmental and industrial monitoring, agriculture, and medicine. In industry, monitoring of gas emissions is important for safety and pollution control and, more recently, also as a control tool for manufacturing processes [8]. Environmental applications include monitoring of greenhouse gases or pollutants. Agricultural applications include the monitoring of food production processes or storage conditions. For example, a number of volatile organic compounds are emitted during fruit fermentation or meat degradation [9]. In medicine a growing area of

research in gas detection is breath analysis, which is motivated by the prospect of non-invasive clinical diagnosis, therapeutic management or monitoring of disease or conditions. The field of breath analysis has gained much momentum in recent years, due in part to the relatively recent developments of real-time trace gas sensor technologies [10, 11, 12, 13].

There are a variety of gas sensing techniques including gas chromatography (GC), mass spectrometry (MS) or combinations of the two (GC-MS), chemiluminescence, Fourier transform infrared spectroscopy (FTIR) and electrochemical sensors [14]. Laser-based gas detection systems can offer analysis at high sensitivity and selectivity, and often in real-time. Therefore they are commonly applied in applications where there is a need for rapid, specific and precise measurements of trace gases. For example, fast, precise and highly sensitive measurement of ammonia is required for process control both in the semiconductor industry and air quality monitoring [15].

1.3 Spectroscopic trace gas detection

Absorption spectroscopy is a method of determining the concentration of a gas, or gases, from the measured optical absorption spectrum (or fragment) of the gas mixture. Infrared absorption spectra result from the absorption of electromagnetic radiation as molecules undergo transitions between allowed electronic, vibrational and rotational states. Infrared laser absorption spectroscopy is an extremely effective tool for the detection and quantification of molecular trace gases, with a demonstrated sensitivity ranging from parts-per-million (ppm 10^{-6}) to parts-per-trillion (ppt 10^{-12}) levels depending on the specific gas species and the detection method employed [16].

1.3.1 Source requirements

For trace gas detection using infrared absorption spectroscopy it is vital that the infrared source can be tuned to the precise wavelength corresponding to an absorption transition of the target gas. The ideal source would offer high power to achieve high signal-to-

noise ratios, a narrow linewidth to enable selectivity and resolve absorption features and single-mode operation to avoid contamination from other species. Other desirable features are room temperature operation, high beam quality, ease of tunability to the required wavelength, low but fast tuning rates, low amplitude modulation, compact package size, and reliable long-term performance with minimal susceptibility to changing environmental conditions [17].

The majority of gases have their fundamental absorption bands in the mid-IR spectral region ($\sim 2 - 25 \mu\text{m}$) [18]. However the usefulness of laser spectroscopy in this region has been limited by the availability of convenient tunable laser sources [19]. The field of trace gas detection lacks the mid-IR equivalent of broadly tunable lasers such as dye lasers for the visible region or Ti:Saph for the near-IR region [20]. Advances in technologies include optical parametric oscillators, sources based on difference frequency generation, tunable solid-state lasers and quantum cascade lasers [10]. Despite recent developments, there still exists a distinct lack of choice with respect to commercially available, widely and continuously tunable sources around $3.5 \mu\text{m}$. The use of a variety of mid-infrared laser sources for sensitive, selective, and quantitative trace gas detection is discussed in a review by Tittel *et al* [17].

Overtone molecular transitions generally correspond to frequencies in the near-IR region, where widely tunable continuous-wave (cw) semiconductor lasers and detectors are more readily available with room temperature operation. Common commercial diode lasers, made from the III-V group of semiconductor materials, emit at red and near infrared wavelengths from about $0.63 \mu\text{m} - 1.55 \mu\text{m}$ [8]. For example, near-infrared InP-based lasers, which were primarily developed for optical telecommunication, are commonly used in trace gas sensing. These technologically matured devices of high reliability emit in the $1.1 - 2.0 \mu\text{m}$ range, where overtone absorption bands of many molecules are present [21]. However, overtone absorption coefficients are typically a factor of $\sim 30 - 300$ weaker than those of the fundamental [19] so there is a balance to be struck when deciding on the laser choice for a particular application.

Further development of gas sensors incorporating the new laser technologies combined with a variety of spectroscopic techniques could enable remote sensing using portable, automated devices without compromise to the high sensitivity, selectivity and speed already associated

with many types of laser spectroscopy.

A brief description of several mid-IR sources follows:

1.3.2 Direct mid-IR laser sources

Lead-salt lasers

When lead-salt tunable diode lasers were first developed at the MIT Lincoln Laboratory in the mid-1960s they found immediate application as tunable sources for high resolution laser absorption spectroscopy [8]. Available across the 3–30 μm spectral range, these lasers are based on IV-VI semiconductor materials, such as binary compounds like PbTe, PbSe, and PbS or tertiary compounds like PbSnTe, PbSnSe and [22]. A simple lead-salt diode laser consists of a single crystal of these semiconductor materials to form a p-n junction. When a sufficiently large forward bias current is applied, charge carriers (electrons or holes) are injected across the p-n junction. Stimulated emission across the band gap between the conduction and nearly full valence band provides the gain mechanism for lasing action. The cleaved ends of the crystal act as mirrors to form the optical cavity [23]. A considerable reduction in threshold current can be achieved through the use of a double heterostructure (DH) laser, in which a thin layer of a semiconductor is sandwiched between layers of a different semiconductor [24]. A diagram of a DH laser is shown in figure 1.1.

The output lasing wavelength is determined by the energy band gap, which is dependent upon semiconductor composition and crystal temperature. Any given device can be actively tuned in wavelength over $\sim 100\text{ cm}^{-1}$ by changing the device temperature, or over tens of cm^{-1} by changing the injection current [17]. As lead-salt lasers are generally compact, offer wide tuning and are commercially available in the mid-IR range, they are widely used in spectroscopy. At present, lead-salt tunable diode lasers manufactured by Laser Components (Olching, Germany) are suitable for cw operation around 3.5 μm . However, sensors based upon lead salt diode lasers are typically large in size as cryogenic cooling is required [19]. The lasers are therefore thermally cycled many times over their lifetime. This can result in permanent changes in lasing wavelength, tuning properties, modal structure

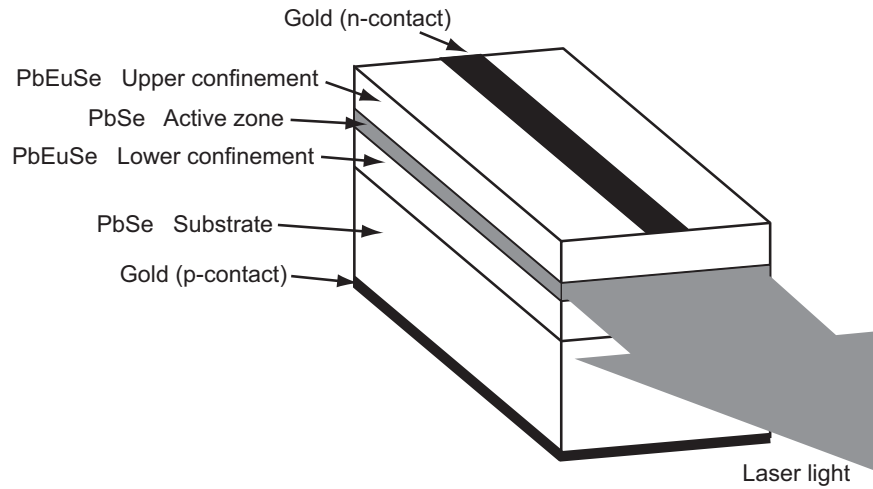


Figure 1.1: Diagram of a double heterostructure lead-salt diode laser

and output power. Other disadvantages include low power output (typically < 1 mW) and poor beam quality [25].

Quantum cascade lasers

Recent advancements in quantum cascade (QC) lasers have led to an attractive mid-IR source option for ultra-sensitive laser absorption spectroscopy [26].

QC lasers are semiconductor lasers based on intersubband transitions in a multiple-quantum-well heterostructure, designed by means of band-structure engineering and grown by molecular beam epitaxy [27]. The optical transitions in QC lasers occur between conduction band sublevels (subbands), rather than between the conduction band and valence bands [28]. A key advantage of this is that the wavelength of the emitted light is therefore dependent on the properties of the quantum heterostructure, rather than the bandgap of the material [25].

The design, fabrication and operation of the first QC laser was described by Faist *et al* in 1994 [29]. QC lasers can now be fabricated to operate over a wide range of wavelengths

from $\sim 3 - 24 \mu\text{m}$ [30]. However, material systems that can provide reliable operation at wavelengths shorter than $4 \mu\text{m}$ are still under development. Recently, Revin *et al* reported the realization of a InGaAs/AlAsSb/InP QC laser operating at wavelength range $3.05 \mu\text{m} \leq \lambda \leq 3.6 \mu\text{m}$ [31]. Interband cascade (IC) lasers based on interband transitions have also been reported in the $3 - 5 \mu\text{m}$ region [32].

QC and IC lasers could play an important role in future sensing applications as they offer high power and narrow linewidths [30]. Most QC laser spectrometers currently use distributed feedback (DFB) single-mode QC lasers, which can be operated at room temperature in pulsed mode, but usually require operation at liquid nitrogen temperatures for continuous output [25].

1.3.3 Mid-IR sources based on nonlinear frequency conversion

Difference frequency generation

Difference frequency generation provides a convenient means of generating mid-IR radiation using available near-IR and visible robust laser sources [16]. A number of mid-IR sources based on difference frequency generation (DFG) have been designed and used in spectroscopy.

If two laser beams at frequencies ω_2 and ω_3 are incident on a second order nonlinear optical crystal, a beam can be generated at the difference frequency $\omega_1 = \omega_3 - \omega_2$. By convention, the laser beam with the highest frequency ω_3 is called the ‘pump’, the one with the lowest frequency ω_1 is the ‘idler’ and the remaining one is the ‘signal’ at a frequency ω_2 [20]. The idler wavelength can be tuned by tuning the pump laser, or signal laser or both.

In order for this process to take place, both energy and momentum need to be conserved. ‘Phase-matching’ requires that the wavevectors of the pump, signal and idler beam obey $k_1 = k_3 - k_2$. This ‘phase-matching’ condition can be fulfilled in birefringent crystals by taking advantage of the fact that refractive index changes as a function of the incident angle, temperature or wavelength. Alternatively, it can be fulfilled in ‘quasi-phasematched’

crystals with a period modulation in the nonlinearity such as periodically poled lithium niobate (PPLN) [33].

Radiation at around $3.4\ \mu\text{m}$ can be generated by difference frequency mixing of a diode pumped Nd:YAG laser at 1064 nm and an external-cavity diode laser at 808 nm in PPLN [34].

Optical parametric oscillators

Frequency conversion using optical parametric oscillators is an effective way of generating broadly tunable mid-infrared light [20]. Recent advances in robustness and compactness make them an attractive source for a number of spectroscopic applications.

An optical parametric oscillator (OPO) consists of a nonlinear optical crystal placed inside an optical cavity. An incident input ‘pump’ beam with frequency ω_3 is converted to two output waves at lower frequencies ω_1 and ω_2 (named ‘signal’ and ‘idler’) via a non-linear interaction [7]. Energy conservation requires $\omega_3 = \omega_1 + \omega_2$. The optical cavity resonates either the signal or idler wave (singly resonant) or both (doubly resonant). How the frequency is divided between the new signal and idler waves is determined by the phase-matching condition that the sum of the signal and idler wavevectors (k -vectors) must equal that of the pump [16]. The parametric process can also be used in optical parametric amplifiers (OPAs) to boost infrared output powers.

Radiation at around $3.4\ \mu\text{m}$ can be produced using a PPLN-based OPO pumped by a Nd:YAG laser at 1064 nm [35].

1.4 Optical spectroscopic techniques

Laser sources such as those described above can be used in conjunction with number of optical techniques to enable trace gas detection by enhancing the signal or reducing noise.

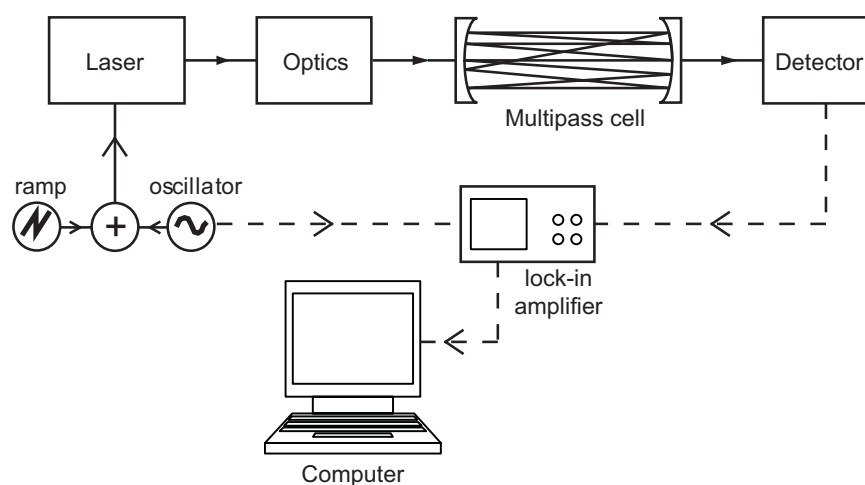


Figure 1.2: Typical experimental set-up for wavelength modulation spectroscopy

A brief description of a selection of these techniques is described below.

1.4.1 Wavelength or frequency modulation spectroscopy

Wavelength modulation spectroscopy

Wavelength modulation spectroscopy (WMS), also known as harmonic detection or derivative spectroscopy, involves modulation of the laser light at a particular frequency (\sim kHz) while tuning the wavelength through the absorption feature of an absorbing species. This leads to the generation of signals at different harmonics of the modulation frequency, the strength of which are proportional to the absorption [36]. The required harmonic can be detected using a lock-in amplifier. A diagram of a typical WMS experimental set-up is shown in figure 1.2. This is our adopted technique and is discussed in more detail in section 2.3.

Frequency modulation spectroscopy

Wavelength modulation (WM) and frequency modulation (FM) techniques are extremely similar. Each method attempts to maximize sensitivity by shifting the detection band to high frequencies to avoid excess ($1/f$) laser noise [37]. However WM techniques are characterised by a modulation frequency that is much smaller than the linewidth of the absorption feature and a modulation amplitude that is of the order of this linewidth [8]. On the other hand, FM spectroscopy is characterised by a modulation frequency that is larger than the width of the absorption linewidth and a small modulation amplitude [36]. This results in distinct frequency sidebands, spaced from the strong optical carrier frequency by multiples of the modulation frequency. The spectral feature of interest can therefore be probed by a single isolated sideband. Absorption can be measured by monitoring the heterodyne beat signal that occurs when the FM spectrum is distorted by the effects of the spectral feature on the probing sideband [38].

One-tone FMS detects the signal at the modulation frequency while two-tone FMS uses a pair of closely spaced frequencies to modulate the laser and quantifies absorbance by demodulating the detector output at the difference [37].

1.4.2 Cavity-enhanced spectroscopy

Cavity-enhanced spectroscopy takes advantage of long optical pathlength absorption in high finesse optical cavities and there are a number of developed techniques.

Cavity ring-down spectroscopy

Cavity ring-down (CRD) spectroscopy is a sensitive absorption technique based upon the measurement of the rate of absorption of a light pulse confined in an optical cavity [39]. In a simple CRD set-up a short laser pulse is coupled into the cavity and the subsequent decay, due to transmission and absorption losses, is monitored by detection of the light pulses exiting through an output mirror. The sample absorbance and therefore concentration

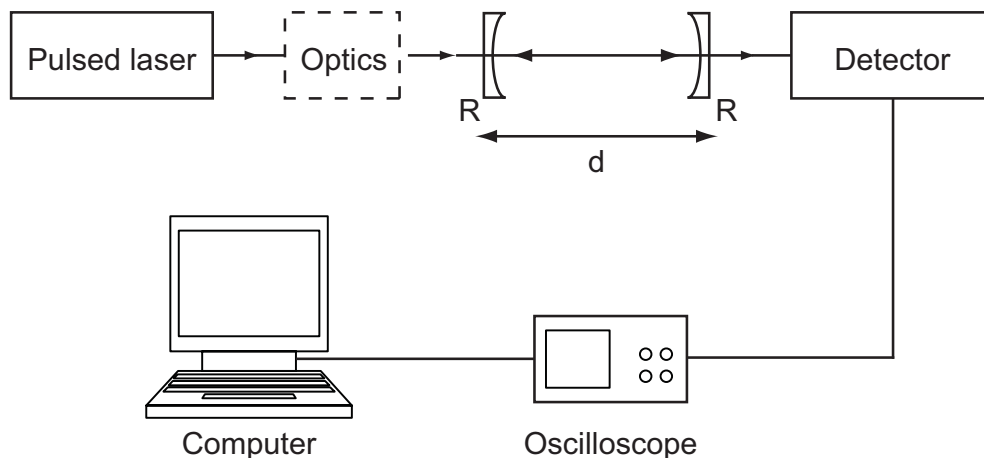


Figure 1.3: Typical experimental set-up for CRD spectroscopy, with optional mode matching optics [39].

can then be deduced by comparison of the decay time of the light due to absorption and transmission losses in an empty cavity with the decay time for a cavity also containing the absorbing gas sample. A schematic diagram of a typical experimental set-up is shown in figure 1.3. The technique achieves extremely high sensitivities, $\sim 10^{-9} \text{ cm}^{-1}$, by using high finesse cavities and pathlengths of several km and it has the advantage that the decay rate is independent of the laser amplitude. However the use of highly reflective mirrors with reflectivities of $> 99.995\%$ is required making the technique extremely sensitive to mirror degradation [40]. The continuous-wave version of the CRD technique is sometimes known as cavity leak-out spectroscopy (CALOS).

Cavity-enhanced absorption spectroscopy

Another CRD variant is cavity-enhanced absorption spectroscopy (CEAS) also known as integrated cavity output spectroscopy (ICOS). In this scheme the cavity length is dithered and the laser light is coupled into the high finesse cavity via accidental coincidences of the light with many cavity modes. The absorption of the gas sample within the cavity is determined by the time-integrated decay of radiation, which is effectively a time integration of the ring-down curve [17].

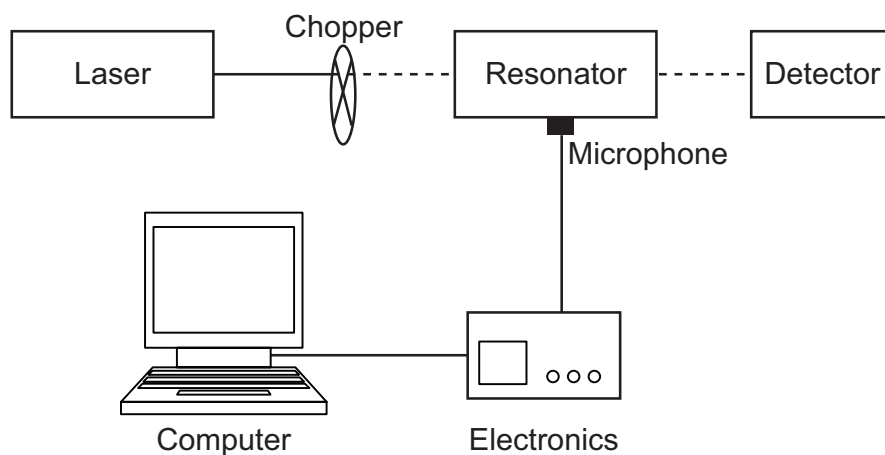


Figure 1.4: Typical experimental set-up for photoacoustic spectroscopy [41].

A review by Berden *et al* gives an overview of a number of CRD experimental schemes [39].

1.4.3 Photoacoustic spectroscopy

Photoacoustic spectroscopy (PAS) is based on the photoacoustic effect, in which acoustic waves result from the absorption of radiation [16]. When radiation is directed into a photoacoustic cell containing the target gas, molecular absorption of photons results in the excitation of molecular energy levels. The excited states lose energy by radiative processes (such as spontaneous or stimulated emission) or by collisional relaxation which results in localized heat release in the sample gas [41]. Modulating the radiation at an acoustic frequency periodically changes the temperature of the sample gas, giving rise to a pressure change at that frequency. The resulting acoustic signal can be detected using a sensitive microphone. A typical experimental set-up is shown in figure 1.4. As the generated signal is very weak, a photo-acoustic cell is used as an acoustic resonator, with the laser modulation frequency chosen to match a resonance frequency of the cavity. Further sensitivity improvements are possible by using multipass or intracavity arrangements and using microphone arrays instead of single microphones [40]. PAS can achieve high sensitivities with a large dynamic range and has the advantage that it can be easily used with a variety of

laser sources. However integration times tend to be longer than 1 s and sufficient sampling pressures (~ 100 torr – 1 atm) are required [17].

1.5 Trace ethane detection

Ethane gas, C_2H_6 , has sparked interest in applications as diverse as oil prospecting and healthcare. Such applications often require rapid concentration measurements at the part per billion (ppb) or even sub-ppb levels presenting a considerable technological challenge.

1.5.1 Background to our project

Researchers in the Optics group at the University of Glasgow working in collaboration with Shell Global solutions developed a trace ethane gas sensor, motivated by the potential application to oil prospecting [42]. Since oil and gas reservoirs are known to gradually leak hydrocarbon gases to the surface their detection may assist in the identification of new locations of such reservoirs. Measurement of ethane concentration along with wind speed and direction can be inverted to establish a source distribution, allowing rapid and remote surveying of a large area. This concept was demonstrated following the development of the real-time ethane gas sensor. The system was a modification of a commercial instrument from Aerodyne systems. A liquid N_2 cooled lead-salt laser combined with a second derivative wavelength modulation scheme was used to achieve a sensitivity to ethane of 100 ppt with a 1Hz sampling rate. A number of field trials were conducted in the Middle East [43] (See chapter 5).

Subsequently, the potential of ethane in healthcare was realised. Ethane gas is a widely accepted marker of free-radical-induced cell damage. It is exhaled in the breath, typically at a concentration of ~ 2 ppb. As it can be measured non-invasively ethane is of interest as a breath biomarker in a number of healthcare applications. However, as with many breath gases, there are a number of challenges in both in the detection and the interpretation of the results. Many previous studies in this field have made use of off-line techniques such

as GC-MS. Ultra-sensitive, rapid detection technology is required to further investigate ethane's clinical potential. The motivation behind breath ethane analysis is discussed in detail in chapter 6.

Given the increasing interest in the field of breath analysis and, in particular, the potential applications of breath ethane detection, a spectroscopy system was developed by the Glasgow Optics group and dedicated to the breath ethane research [44]. The achieved sensitivity corresponding to a 1 Hz sampling rate was better than 100 ppt. The system was used in a variety of applications in healthcare and life science [45, 46]. The short analysis time allowed a large number of breath samples to be rapidly measured with high sensitivity and selectivity. However, the system required discrete sampling methods for the breath collection followed by lab-based analysis due to its size and bulk along with the requirement for liquid nitrogen. Therefore it was not possible to fully exploit the real-time nature of the technology.

The development of a portable system was therefore required to enable breath ethane detection on-site in a clinical environment. It was uncertain if a system based on the previous technology could be made more compact, without compromise to the previously achieved performance. Therefore, a large proportion of the work undertaken was concerned with the development and characterisation of this new portable ethane spectroscopy system. Following the completion of the new system, a considerable amount of time and effort was spent applying the technology in a number of pilot clinical studies.

1.5.2 Related work in ethane detection

The traditional technique for analysis of the majority of breath gases, including ethane, is GC combined with MS or other variants. These techniques have a number of limitations, further described in section 6.2.2. Optical techniques are inherently better suited to breath monitoring applications due to the combination of sensitivity, selectivity and speed.

A number of groups have used optical techniques for the measurement of breath ethane. The first work demonstrating ppb-level ethane measurements in human breath was reported

in 2001 by Dahnke *et al* who used a liquid N₂-cooled tunable CO-overtone sideband laser to perform high cavity leak-out spectroscopy [47]. Under optimum conditions, an integration time of 5 s corresponded to a minimum detection limit of the order of 100 ppt ethane. Ethane was analysed in the breath of a smoker a few minutes after they had smoked a cigarette. The technique was later used to measure online ethane traces across individual exhaled human breaths, with a stated sensitivity of 500 ppt and a time resolution of \gtrsim 800 ms [48]. However breath ethane was only recorded after controlled inhalations following exposure to a high concentration of 1 ppm ethane.

The same group also developed a portable spectrometer by replacing the CO laser with a source based on both difference frequency generation (DFG) in a periodically poled lithium niobate (PPLN) [34] and later with an optical parametric oscillator (OPO) [49]. By using an OPO combined with cavity leak-out spectroscopy and further improving the technology, an extrapolated ethane detection limit of 6 ppt Hz^{-1/2} was reported in 2004 [50]. An example breath ethane measurement of 2.4 ± 0.5 ppb ethane was given. However this was not significantly different from the concentration of the ambient air, measured to be 2.7 ± 0.5 ppb. There may have been issues with the use of the transition at 2966.9 cm⁻¹, which overlaps with a methane transition. In 2006 the group reported on a mid-IR laser cavity leak-out spectrometer based on continuous-wave difference frequency generation with an ethane precision of 270 ppt and a time resolution of 1 s [51]. Although the sensitivity was lower than that previously reported, the room temperature operation enabled a size reduction of the system, allowing transportation by car.

Müller *et al* have developed an OPO based on PPLN for photoacoustic trace gas detection between 3.1 and 3.9 μ m. Applying this OPO in an photoacoustic spectrometer, an ethane detection limit of 110 ppt was achieved with an integration time of 10 s [35]. This was further improved to a detection limit of 25 ppt for ethane with a 30 s time constant [52]. However these detection limits were calculated from noise measurements. Since the concentration measurements were taken at atmospheric pressure the ethane concentrations couldn't be accurately determined due to interference from neighbouring species such as water. Therefore a liquid nitrogen cooling trap was required to freeze out disturbing gases. A example measurement of ambient air yielded an ethane concentration of $4. \pm 0.5$ ppb. Similarly, an OPO was used with photoacoustic spectroscopy by van Herpen *et al* to measure ethane [53]. The detection limit was determined to be 0.1 ppb, with a scan time 40 s.

A higher power OPO was subsequently developed, which had the potential to improve the ethane sensitivity [54].

Over the last few years there have been considerable developments in interband cascade (IC) laser and quantum cascade (QC) laser technologies. For example, a continuous-wave distributed feedback (DFB) ICL fabricated by the NASA–JPL was used in a trace ethane gas sensor [55]. The laser was liquid nitrogen cooled to ~ 80 K and had a maximum power of 12 mW. The instrument incorporated a 100 m optical path Herriott multipass cell and used wavelength modulation spectroscopy (WMS) to achieve an ethane sensitivity of 0.15 ppb with a 1 s acquisition time. Wysocki *et al* recently reported on a dual trace-gas sensor which incorporates two liquid nitrogen cooled IC lasers operating at 3.33 μm and 3.56 μm [56]. Second derivative wavelength modulation at two different frequencies was used to enable simultaneous detection of both ethane and formaldehyde. Minimum detection limits of 3.5 ppb for formaldehyde and 150 ppt for ethane were demonstrated with a 1 s integration time. Breath ethane results have not yet been reported using these systems.

Parameswaran *et al* used an IC laser together with off-axis integrated cavity output spectroscopy (OA–ICOS) to develop a portable system with a calculated minimum detectable ethane concentration of 0.12 ppb $\text{Hz}^{-1/2}$. The system was used for measurement of breath ethane in smokers, at 30 min intervals after they had smoked a cigarette [57].

1.6 Discussion

An introduction to the field of spectroscopy and to our work has been given along with a brief description of a number of mid-infrared sources and optical techniques. An overview of current and previous breath ethane detection using optical techniques has been presented. While the technology is greatly advancing, due to developments in both laser sources and detection systems, the majority of the breath ethane clinical studies are carried out using the traditional non-optical techniques. Therefore a principal aim of the work reported here was not only to develop an ethane spectroscopy system that could be used in a clinical setting but also to use it to record novel clinical data in the hope of furthering pilot studies and knowhow in the field of breath ethane analysis.

Chapter 2

Molecular absorption spectroscopy

This chapter gives background and theory behind molecular absorption spectroscopy. The chosen technique of wavelength modulation is examined in more detail.

2.1 Molecular transitions

The energy E_1 of a molecule can be changed to another allowed energy level E_2 by the exchange of energy. This energy change can result from the absorption or emission of a photon and must obey

$$\Delta E = h\nu \tag{2.1}$$

where $\Delta E = E_2 - E_1$, ν is the frequency and h is Planck's constant. If radiation of a particular frequency is incident on a material and satisfies the condition that the photon energy corresponds to that of an allowed energy transition, then some of the radiation will be absorbed by the material. This principle is used in molecular absorption spectroscopy.

Most molecules have their fundamental vibrational transitions in the mid-infrared region

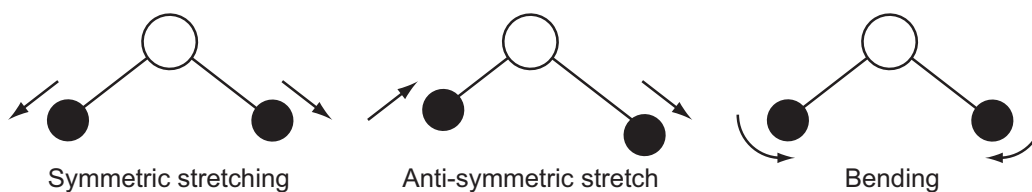


Figure 2.1: The independent vibrational modes of water, of which all three are infrared active

($\sim 2-25\ \mu\text{m}$) [18]. Transitions between vibrational energy levels are typically at a spacing of $20 \times 10^{-21}\ \text{J}$ [1]. A commonly used unit in molecular spectroscopy is the wavenumber, $\bar{\lambda}$, defined by

$$\bar{\lambda} = \frac{1}{\lambda} \quad (2.2)$$

Wavenumbers are traditionally expressed in cm^{-1} units and are a convenient way of expressing the frequencies corresponding to molecular transitions.

Molecular vibrations can be subdivided into two classes: stretching, where the distance between the atoms in a molecule is changed, or bending, where the angle between the atoms in a molecule is changed. For example, water undergoes three independent types of vibration, shown in figure 2.1. All three types of vibrations are infrared active. For a molecule to absorb infrared radiation it must undergo a net change in dipole moment as a result of vibrational or rotational motion. Diatomic molecules such as N_2 and H_2 do not absorb IR because stretching does not change the dipole moment.

The stretching vibration frequencies depend on the strength of the bond, which depends on the particular atoms in the bond and the bond type (i.e. single, double or triple). Typical fundamental frequencies for a number of different types of bond are given in table 2.1.

2.1.1 Transition broadening

Molecular energy transitions are always broadened due to three main causes:

Bond	$\bar{\lambda}$ (cm ⁻¹)
O-H	3600–3700
N-H	3000–3400
C-H	2850–3000
C≡N	2200–2300
C≡C	2050–2300
C=C	1500–2000

Table 2.1: Fundamental stretching frequencies for a selection of bonds [58].

Natural broadening

As a result of the Heisenberg uncertainty principle the energy transitions in a molecule are not truly discrete but have a finite width ΔE . This linewidth is determined by the mean lifetime τ as

$$\Delta E \sim \frac{\hbar}{\tau} \quad (2.3)$$

This leads to a natural broadening of the lineshape which can be described by a Lorentzian function. Natural linewidths in the infrared are relatively narrow, typically $\sim 10^{-4}$ cm⁻¹.

Collisional (Pressure) broadening

Absorption and emission processes are disturbed by the collision of other molecules with the absorbing molecule. Molecular collisions decrease the lifetime of the state, increasing the uncertainty in photon energy, and therefore broadening the transition linewidth. Collisional broadening depends on both the pressure and the temperature of the gas and the broadening effect is described by a Lorentzian profile. The half linewidth is given by

$$\gamma_L = \gamma_0 \frac{P}{P_0} \sqrt{\frac{T_0}{T}} \quad (2.4)$$

where T is the temperature, P is the pressure and γ_0 is the half linewidth at temperature

T_0 and pressure P_0 .

Doppler broadening

Doppler broadening arises due to the thermal motion of the molecules in the gas. The transition frequencies of each molecule will be red or blue shifted from the centre line frequency by the Doppler effect depending on the velocity of the molecule. The higher the temperature of the gas, the greater the distribution of velocities in the gas and therefore the broader the line. The lineshape is described by a Gaussian profile and the half linewidth is given by

$$\gamma_D = \frac{\nu_0}{c} \sqrt{\frac{8kT \ln(2)}{M}} \quad (2.5)$$

where ν_0 is the centre frequency, k is the Boltzman constant, T is the temperature and M is the molecular weight all in SI units.

In the regions where the Doppler and pressure broadened widths are comparable the total effective lineshape is given by the convolution of the Gaussian (Doppler) profile with the Lorentzian (pressure broadened) profile. This is known as a Voigt lineshape.

In tunable diode laser absorption spectroscopy (TDLAS) the laser wavelength is usually scanned over an absorption line of the target gas. High selectivity is achieved by reducing the pressure of the gas so that a sharp absorption feature is seen, isolated from nearby contaminants. Reducing the pressure does reduce the sensitivity but this is not significant until the linewidth starts to become Doppler limited. Typically, TDLAS systems are operated between 10 and 50 mbar [8]. This is further discussed in section 4.5.3, where example theoretical ethane absorption lineshapes are provided for a range of pressures.

2.1.2 Ethane transitions

The HITRAN molecular spectroscopic database provides information about molecular spectra in the 1 to 20500 cm^{-1} region [59]. MOLSPEC is a Microsoft Windows program

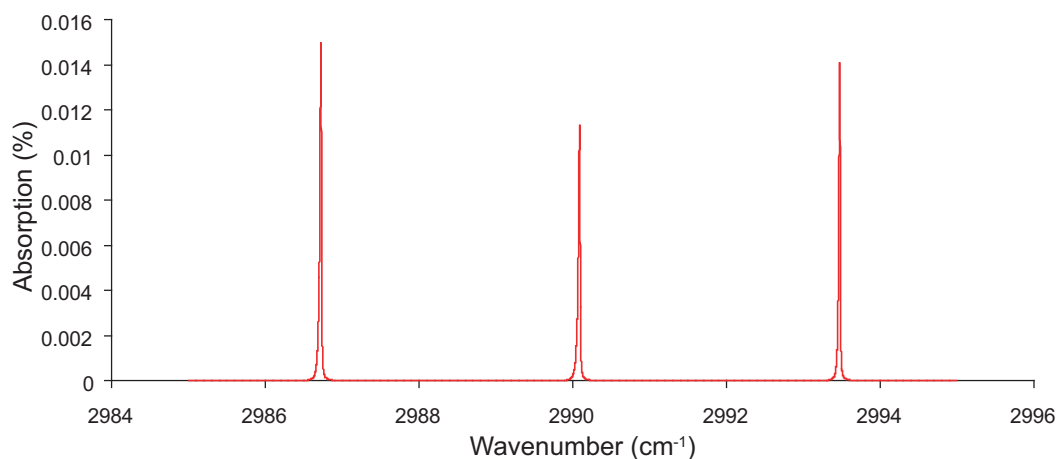


Figure 2.2: Three of the strongest transitions for ethane are at frequencies of 2986.72 cm^{-1} , 2990.09 cm^{-1} and 2993.47 cm^{-1} . The absorption is shown for 1 ppb ethane over a 100 m pathlength at a pressure of 40 mbar and temperature of 296 K.

that uses the HITRAN 2000 database to calculate and display molecular spectra based on parameters entered by the user. Data in the following section was obtained using the MOLSPEC program.

Ethane, C_2H_6 , has strong molecule transitions around $3.4\text{ }\mu\text{m}$. Three of these transitions are at frequencies of 2986.72 cm^{-1} , 2990.09 cm^{-1} and 2993.47 cm^{-1} . These correspond to C-H stretching vibrations. Figure 2.2 shows the absorption for 1 ppb ethane over 100 m pathlength, at a pressure of 40 mbar and temperature of 296 K, for each of the three transitions.

2.2 Absorption spectroscopy

The Beer-Lambert law, or Beer's law as it is commonly known, expresses the relationship between the absorbance of light and the properties of the material through which the light is travelling. It can be expressed as

$$I_T = I_0 \exp^{-\alpha(\nu)bc} \quad (2.6)$$

where $\alpha(\nu)$ is the absorption coefficient of the material at frequency ν , b is the path length through the material, c is the concentration of the absorbing species in the material, I_T is the transmitted intensity and I_0 is the incident intensity. The quantity $\alpha(\nu)bc$ is known as the absorbance. In the case of small absorbance the Beer law can be approximated as

$$I_T \approx I_0[1 - \alpha(\nu)bc] \quad (2.7)$$

Rearranging equation 2.7 gives the fractional absorption of light as

$$\frac{I_0 - I_T}{I_T} = \alpha(\nu)bc \quad (2.8)$$

At 2990 cm^{-1} , 1 ppb ethane at 296 K, 40 mbar over a 100 m pathlength has a fractional absorption of 1.1×10^{-4} (see figure 2.2). Hence the absorption coefficient at line centre $\alpha(\nu_0) \approx 11 \text{ cm}^{-1}$. Since ultra-low gas concentrations produce an extremely small change in light intensity the optical pathlength of the laser light is often extended. This increases the absorption in order to achieve the high sensitivity required for trace gas detection. This can be done by using cavity-enhanced methods [39] or by the use of a multi-pass cell, such as a Herriott cell [60]. However, even in conjunction with a long-path length, direct absorption measurements alone often cannot offer the required sensitivity, particularly when overtone transitions with significantly weaker absorption coefficients are used. Therefore a detection technique such as wavelength modulation spectroscopy is often used in conjunction with an increased pathlength.

2.3 The wavelength modulation technique

As described in section 1.4.1, wavelength modulation spectroscopy (WMS) involves modulation of the laser light at a particular frequency ($\sim \text{kHz}$) while tuning the wavelength through the absorption feature of an absorbing species. This leads to the generation of signals at different harmonics of the modulation frequency. As the laser is scanned through

the absorption line, the desired harmonic signal is acquired from a lock-in amplifier, or phase sensitive detector (PSD). A PSD takes an input signal, multiplies it by a reference signal and passes the result through a low pass filter, giving a maximum output voltage if the two input signals are coherent. In this case, the output voltage is proportional to the amplitude of the input signal. PSDs usually enable phase adjustment over 360 degrees to ensure that the signals are in phase and therefore maximise the signal. The modulation signal, or a multiple of this frequency, is used as the PSD reference signal. Applied to laser spectroscopy, wavelength modulation and subsequent phase sensitive detection allows the detection frequency to be increased to a level where noise sources such as $1/f$ laser noise are significantly reduced.

The technique requires that the linewidth of the laser is less than the width of the absorption peak. With a semiconductor laser, the modulation can be easily achieved by direct modulation of the laser current. Other techniques include mechanical dithering of the mirror and using external phase modulators.

2.3.1 Mathematical description

If the laser frequency ν is sinusoidally modulated at the frequency Ω and we assume pure frequency modulation (FM) then the resulting transmitted intensity I_{T} can be expressed as a function of ν and time t as follows

$$I_{\text{T}} = f(\nu + m \sin \Omega t) \quad (2.9)$$

where the function f will take into account absorption, and other transmission losses for each frequency ν . Assuming that the modulation frequency Ω and amplitude m are much smaller than the linewidth of the absorption peak we can expand equation 2.9 using a Taylor expansion [61] to give

$$f(\nu + m \sin \Omega t) = f(\nu) + m \sin \Omega t \frac{df}{d\nu} + \frac{m^2}{2!} \sin^2 \Omega t \frac{d^2 f}{d\nu^2} + \frac{m^3}{3!} \sin^3 \Omega t \frac{d^3 f}{d\nu^3} + \dots \quad (2.10)$$

Using the identities

$$\cos 2\Omega t = 1 - 2 \sin^2 \Omega t \quad (2.11)$$

$$\sin 3\Omega t = 3 \sin \Omega t - 4 \sin^3 \Omega t \quad (2.12)$$

and combining terms equation 2.10 becomes

$$I_{\text{T}} = [f(\nu) + \frac{m^2}{4} \frac{d^2 f}{d\nu^2} + \dots] + \sin \Omega t [m \frac{df}{d\nu} + \frac{m^3}{8} \frac{d^3 f}{d\nu^3} + \dots] + \cos 2\Omega t [-\frac{m^2}{4} \frac{d^2 f}{d\nu^2} + \dots] + \dots \quad (2.13)$$

Several terms are obtained in the transmitted intensity: A DC term, a term oscillating at 1Ω , a term at 2Ω and so on. Phase sensitive detection at the n^{th} multiple of the modulation frequency yields the n^{th} derivative of the transmission profile.

However, the Taylor expansion can be used by assuming m is small. i.e the modulation amplitude is much smaller than the width of the absorption peak. That is true for FM spectroscopy but not necessarily for WM spectroscopy. In WM, the low modulation regime results in low sensitivity. In practice, the modulation amplitude is chosen to be close to the linewidth to maximise the signal amplitude. However, it transpires that even in this case the resultant signal at the n^{th} harmonic of the modulation frequency is still similar to the n^{th} derivative of the absorption lineshape and is approximately proportional to the concentration of absorbing gas [8]. In our regime we use a large modulation amplitude, which results in a significant distortion of the absorption lineshape.

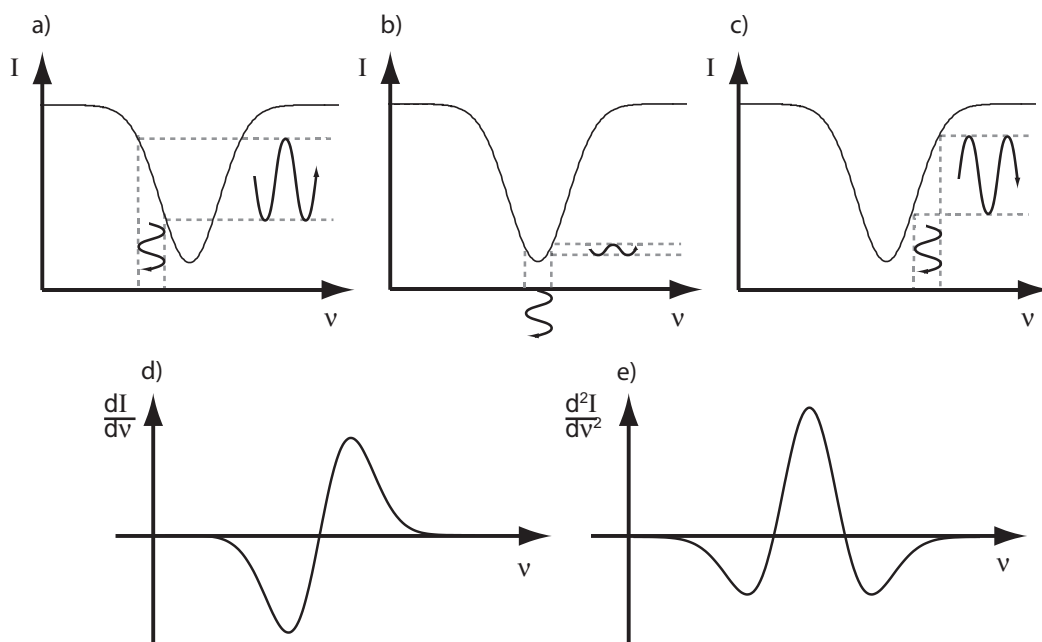


Figure 2.3: Graphical illustration of the wavelength modulation technique. (a)-(c) As the laser wavelength is scanned across the absorption transition the laser wavelength modulation is converted to amplitude modulation at the same frequency. The extent of this conversion varies across the absorption profile. (d) The first derivative of the absorption profile, obtained by phase sensitive detection at the modulation frequency. (e) The second derivative of the absorption profile, obtained by phase sensitive detection at twice the modulation frequency.

2.3.2 Graphical description

If the laser wavelength is in the vicinity of an absorption transition of the gas, the frequency modulation (FM) is converted to amplitude modulation (AM) at the same frequency, as shown in figure 2.3 a–c. The amplitude modulated signal is detected using a photodetector and then de-modulated using a PSD. As the wavelength is scanned across the absorption profile the magnitude of the resultant amplitude modulation varies and is dependent on the slope (or derivative) of the absorption profile. Therefore, plotting the ratio of the FM to AM conversion against frequency yields the first derivative of the absorption profile, as shown in figure 2.3 d. Similarly, plotting the rate of change of the FM to AM conversion yields the second derivative of the absorption profile, shown in figure 2.3 e. The 2nd order spectrum is useful as it has a peak at line centre, which is proportional to the absorption.

2.3.3 Residual amplitude modulation

According to equation 2.13, if the laser wavelength is scanned away from an absorption line the 1st and 2nd derivative signals should be reduced to zero. However in a semiconductor laser modulation of the injection current produces a combined wavelength modulation (WM) and intensity modulation (IM), with a phase shift between the two modulations [36]. In WM spectroscopy the IM is an unwanted effect which distorts the detected signal and is detected even in the absence of an absorbing gas. The IM, often referred to as residual amplitude modulation (RAM), depends on the wavelength characteristics of the laser diode.

A conventional way of obtaining quantitative information about the target absorbing gas despite the presence of RAM is to compare the measured signal to that generated by a calibration gas of known concentration. This is the method we adopt in our spectroscopy system. An alternative, calibration-free approach is to make use of the phase lag between the WM and the RAM, which depends on the laser structure and the modulation frequency. Duffin *et al* maximised this phase lag by optimising the modulation frequency and then nulled the WM derivative signal to isolate the RAM, yielding absolute gas-line transmission functions and enabling accurate measurements of linewidth and therefore pressure [62].

CHAPTER 2. MOLECULAR ABSORPTION SPECTROSCOPY

This chapter has provided some background theory in the area of molecular spectroscopy and has examined wavelength modulation spectroscopy, our chosen detection technique. The following two chapters describe the development and characterisation, respectively, of the portable ethane spectroscopy system.

Chapter 3

Development of the portable spectroscopy system

This chapter describes the development of the portable spectroscopy system for the ultra-sensitive, real-time measurement of ethane. An overview of the technology is first given with the construction described in more detail in the following sections.

3.1 Instrument overview

The system is based on high resolution absorption spectroscopy across a transition for ethane gas at 3.34 μm using a cryogenically-cooled lead-salt laser diode. A second derivative wavelength modulation detection scheme is used. All components are housed in a portable unit, dimensions 1 m x 0.5 m x 1 m (L x W x H), as shown in figure 3.1.

The portable unit consists of three sections: The base section houses a compressor used for laser cooling and a vacuum pump used to draw the gas sample through the system. The upper section, which can be completely separated from the base, supports the optical table on which the laser and optics are mounted, and a platform on which the laser controller

and the detection electronics are attached. These sections are shown in figure 3.2. Finally, there is a lid (see figure 3.1), which can also be removed.



Figure 3.1: Photograph of the ultra-sensitive, real-time portable ethane spectroscopy system. The self-contained instrument has dimensions 1 m x 0.5 m x 1 m (L x W x H)

The system is therefore a self-contained instrument and the only additional requirement is hydrocarbon-free nitrogen gas for zero referencing (see section 3.4). The instrument is controlled from a laptop computer using software written in LabVIEW.

3.1.1 Laser and optical configuration

A schematic of the optical configuration is shown in figure 3.3. A lead-salt laser diode (IR-2990-GMP-WM, Laser Components) emits ~ 0.2 mW of light which undergoes multiple

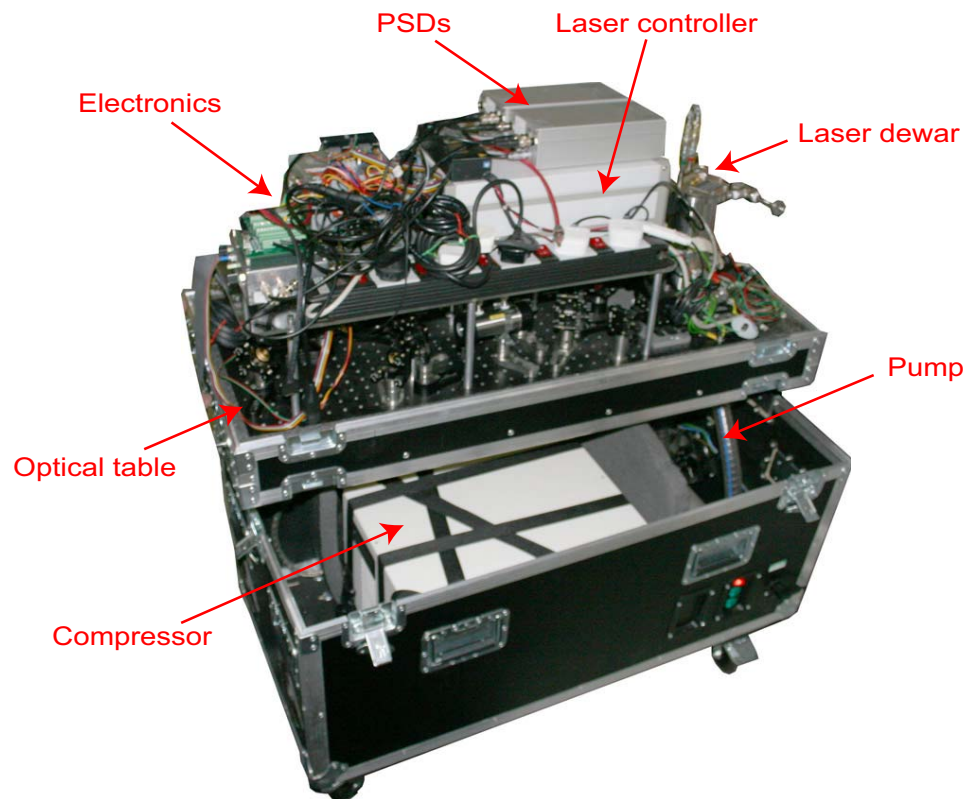


Figure 3.2: Photographic view of the instrument sections. The base houses the compressor and vacuum pump. In the upper section the laser and optics are mounted on an optical table. Above this a platform is supported on which the laser controller, PSDs and electronics are mounted.

passes in a Herriott sample cell 0.55 m in length. Exiting light is detected using a low noise thermo-electrically cooled HgZnCdTe photodetector, PD1 (PVI-2TE, Vigo). Sample gas is drawn through a sample inlet pipe to the Herriott cell by a 240 l min^{-1} pump (Varian Inc.). An air filter and regulator valve on the inlet to the cell maintains a pressure of 40 mbar, corresponding to a sample inlet flow rate of $\sim 3 \text{ l min}^{-1}$. Around 5% of the light is split off before the Herriott cell and directed through a 10 cm long reference cell containing ethane at a concentration of $500 \text{ ppm} \pm 2\%$ also at 40 mbar and onto a second photodetector, PD2. This reference cell allows for continual calibration and wavelength stability checks.

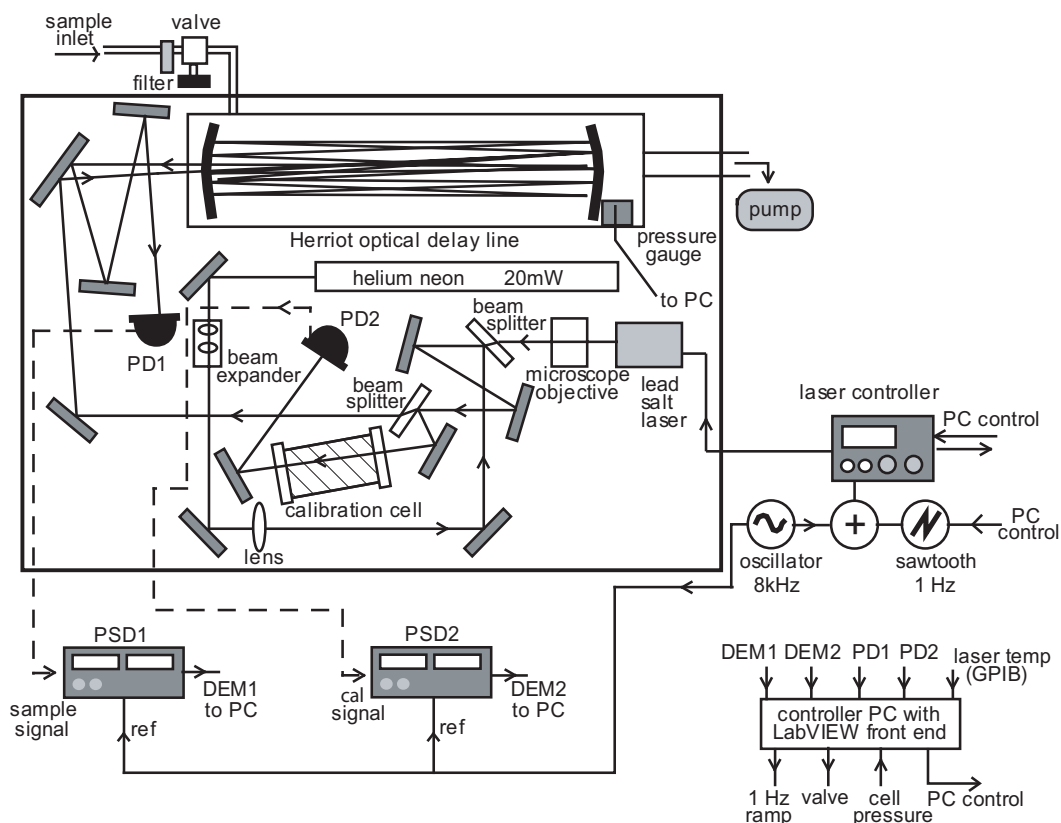


Figure 3.3: Schematic of the optical configuration. All optics are mounted on a 90 cm by 45 cm lightweight optical table.

3.1.2 Detection scheme

A second harmonic wavelength modulation scheme is used, where the laser light is sine-wave modulated at 8 kHz and ramped through the ethane transition at 1 Hz. Two phase sensitive detectors (PSDs) (LIA-MV-200-H, Femto) provide demodulated signals at twice the modulation frequency. The reported sample cell concentration is based on curve fitting between the demodulated signals from PD1 and PD2. See figure 3.4. This is achieved using a least squares fitting algorithm in the LabVIEW software, which compares the $2f$ lineshape from the sample channel to that of the reference channel and reports coefficients for the scaling factor and offset. The first of these coefficients is used to calculate the

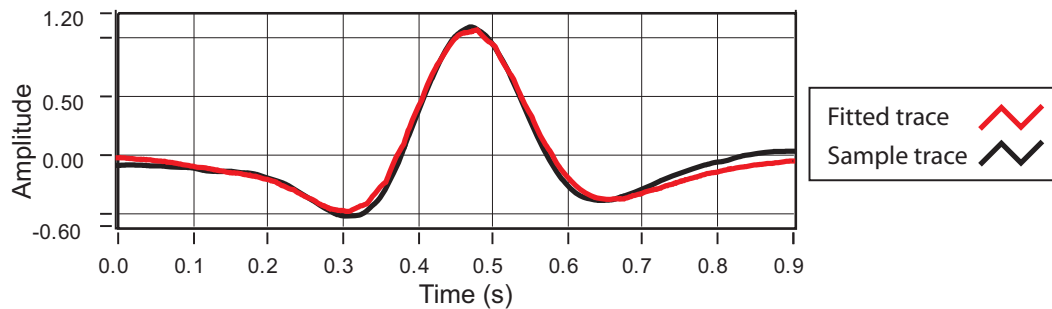


Figure 3.4: $2f$ sample lineshape and fitted lineshape as the laser wavelength is scanned over the ethane transition. A LabVIEW least squares fitting algorithm is used to calculate the ethane concentration.

ethane concentration. As the magnitude of the measured signal in the sample and reference channels is linearly proportional to the DC light levels at PD1 and PD2 respectively, the calculated concentration is also multiplied by the ratio of the light levels at PD1 and PD2. This normalises for changes in the overall light level and also for relative changes in the light levels between the photodetectors.

3.1.3 Electronics and interfacing

Modulation

The entire modulation scheme and data analysis process is controlled by the LabVIEW software controlling a commercial laser controller (PRO8000, Profile). All electronics for modulation and signal processing are custom-designed with the exception of the two PSDs. The laser temperature and current are set in the software and are regulated by the laser controller. The modulation signal at 8 kHz is produced by a high-frequency waveform generator (MAX038CPP, Maxim). The sinusoidal signal is then improved using a filter (UAF42AP Burr-Brown series, Texas Instruments). A ramped signal at a frequency of 1 Hz is produced directly in the LabVIEW software and is output via an analogue channel of the data acquisition (DAQ) card (6026E, National Instruments). An operational amplifier (OPA620 Burr-Brown series, Texas Instruments) is used to add the sinusoidal signal to

the ramp signal, and the resulting signal is applied to the laser current via the modulation input on the laser controller. The strength of the modulation signal is controlled using a variable resistor.

Signal amplification and filtering

The detected AC signals from the photodetector modules for both the sample and calibration cells are amplified by a factor of 10 using two op-amps (LT1028, Linear Technology). These are chosen due to their low noise voltage density (typically $1.0 \text{ nV Hz}^{-1/2}$). The amplified signals are then also filtered (UAF42AP). For second harmonic detection the filters were optimised at twice the modulation frequency. The centre frequency of each of the bandpass filters is easily adjusted using a variable resistor via a calibration dial. The necessary resistor values to achieve the desired bandpass filter parameters were calculated using a simple program supplied with the filter specifications. The transfer functions of the various stages of the detection electronics were measured with a spectrum analyser (SR780, Stanford Research Systems). A white noise source was used to measure the transfer function of the filter. The quality (Q) factor of the sample filter was determined to be 7.5 with a peak gain of 4.05. The overall transfer function for the sample channel electronics (AC gain and filter) were measured, this time using a swept sine wave source, and was found to have a Q factor of 7.8 and an overall peak gain of 44.3. Figure 3.5 shows both the measured transfer function for the sample channel filter and the measured overall transfer function for the sample channel electronics (AC amplification and filter).

As described, the two PSDs provide demodulated signals at twice the modulation frequency for both the sample and calibration channels. The filtered sinusoidal waveform from the MAX038 oscillator is used as the input reference signal for the PSDs, which are chosen to function in the $2f$ mode. See appendix A for all circuit diagrams.

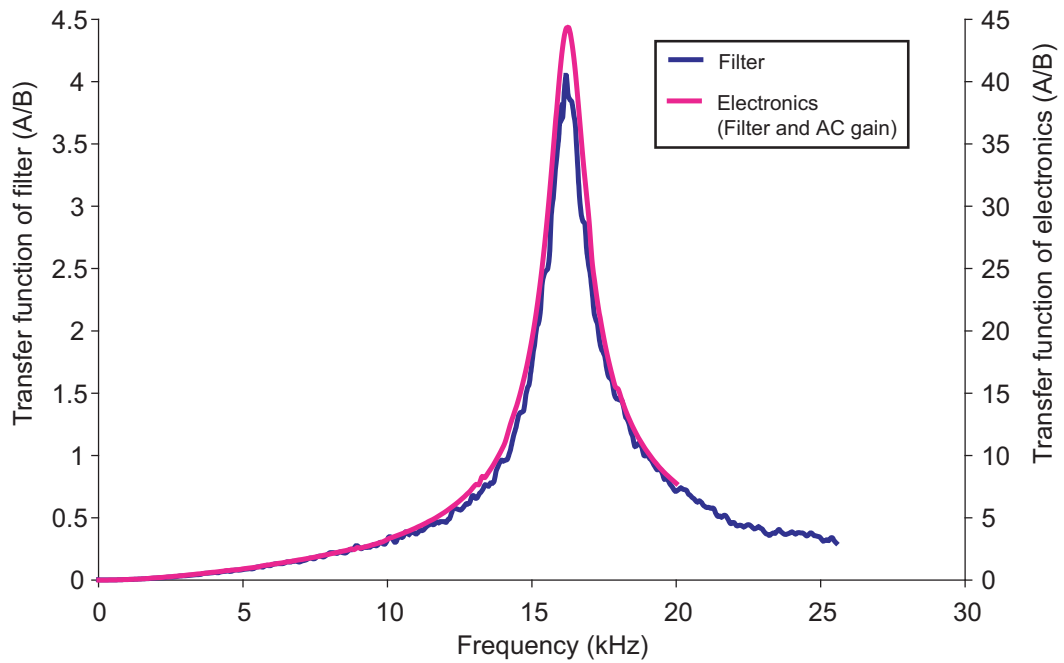


Figure 3.5: The measured transfer function of both the sample channel filter and the overall transfer function of the electronics, which includes the AC gain by a factor of ~ 10 provided by a low noise op-amp.

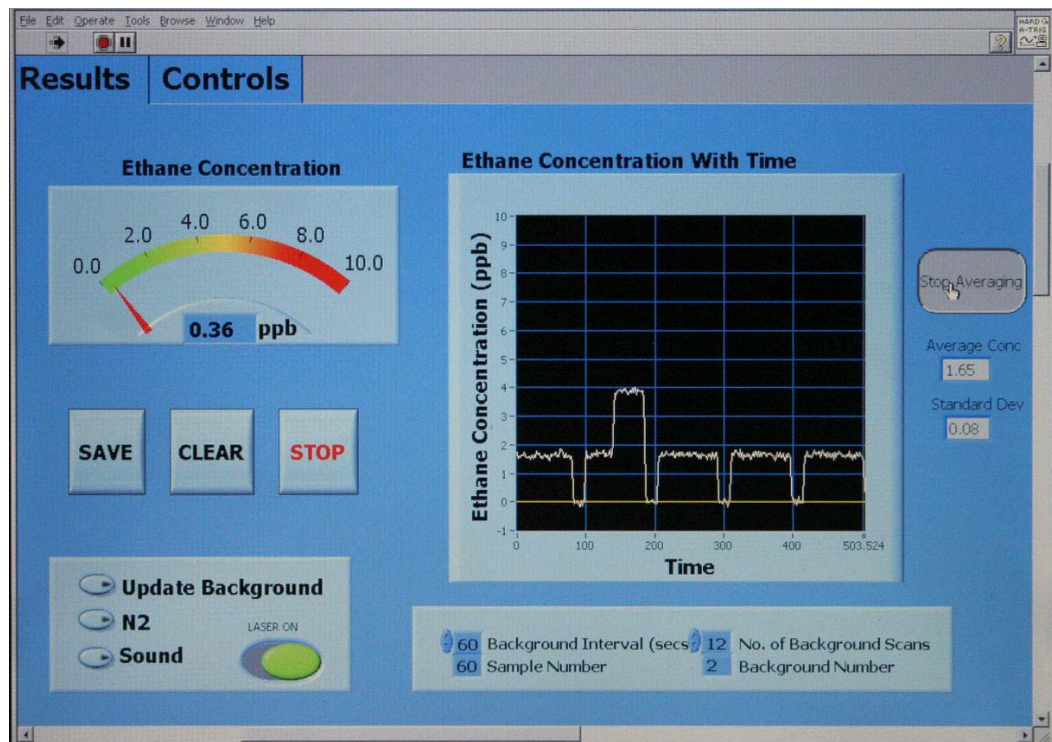


Figure 3.6: An example of the results section on the front panel of the LabVIEW control software.

Interfacing

The instrument is controlled from a laptop computer by software written in LabVIEW and is designed for simple operation. The ‘results’ section of the front panel of the LabVIEW program displays the measured ethane concentration against time. A user can easily view the measured concentration results, average the ethane concentration over time, save results in Excel format, clear the ethane-time chart, switch input lines to measure nitrogen gas, and modify time intervals between zero-referencing (see section 3.4). Figure 3.6 shows an example of the front panel results section. The control section of the front panel is used to set the laser temperature and current, frequency of sampling, and monitor light levels, calibration and sample $2f$ lineshapes and pressure.

The software previously developed to control the lab-based spectroscopy system was modified for use with the new portable system. The laser and temperature controllers are connected via a GPIB connection and PCMCIA card and are fully controlled by the software. All detected analogue and digital signals are input to the software via the DAQ card and corresponding connector block (6026E, National Instruments). These input signals include the following: Sample and reference photodetector DC light levels; sample and reference demodulated signals output from the PSDs and the Herriott cell pressure. The cell pressure is maintained at 40 mbar and is monitored using a pressure gauge (BOC Edwards, APG100) fitted between the cell and the scroll pump. Signals output via the DAQ card comprise the current ramp (analogue) and the digital signals used to switch a solid state relay, which opens/closes the valves used for zero-referencing (See section 3.4). Two computer power supplies are used to power all components including the electronics, photodetector modules, valves and pressure gauge.

3.2 Laser cooling

3.2.1 Closed-loop cooling system

To achieve the desired output wavelength of $\sim 3.34 \mu\text{m}$ the lead-salt laser requires operation at cryogenic temperatures. Lab-based ethane spectroscopy systems previously developed by the Glasgow Optics group used liquid nitrogen (N_2) for the laser cooling. However, there would be clear disadvantages of its use for portable technology: Firstly, the dewar required to contain the laser is large. Secondly, the liquid N_2 must be added before instrument use and the temperature can take up to one hour to stabilise. Further, it must be topped up when necessary, preventing long term uninterrupted use. Another factor to consider for on-site use in a hospital is the potential lack of readily available liquid N_2 .

The portable instrument uses a closed loop cooling system (Cryotiger, Megatech Ltd) to cool the laser to a temperature of around 88 K. The entire cooling system consists of a cold end, compressor and two gas transfer lines. This system has enabled a more compact laser cold finger to be incorporated and therefore the entire laser dewar has been downsized by around a factor of two in volume from the previous lab-based systems. Dispensing with the need for liquid N_2 has enabled use in a clinical environment. Issues such as intermittent filling with liquid nitrogen causing unpredictable laser behaviour have been eliminated.

Initial cooling from room temperature to $\sim 80 \text{ K}$ takes several hours (see figure 3.7) but once cooled, this temperature can be maintained over a period of weeks or even months. Before cooling, the dewar is evacuated to a pressure of $< 10^{-4}$ mbar using a turbo pump. Occasionally the laser was ‘thermally-cycled’ by allowing the system to reach room temperature, then re-evacuating the dewar, before re-cooling.

The two photodetector modules are thermo-electrically cooled to a temperature of $\sim 230 \text{ K}$. This is assisted by the addition of a computer fan with a heat sink to each module. It is necessary to cool mid-IR detectors as the bandgap is smaller than it is for near-IR detectors (approximately half since the wavelength is doubled). Thermal excitation of carriers would lead to higher dark current noise unless the detector is cooled. Since the important factor

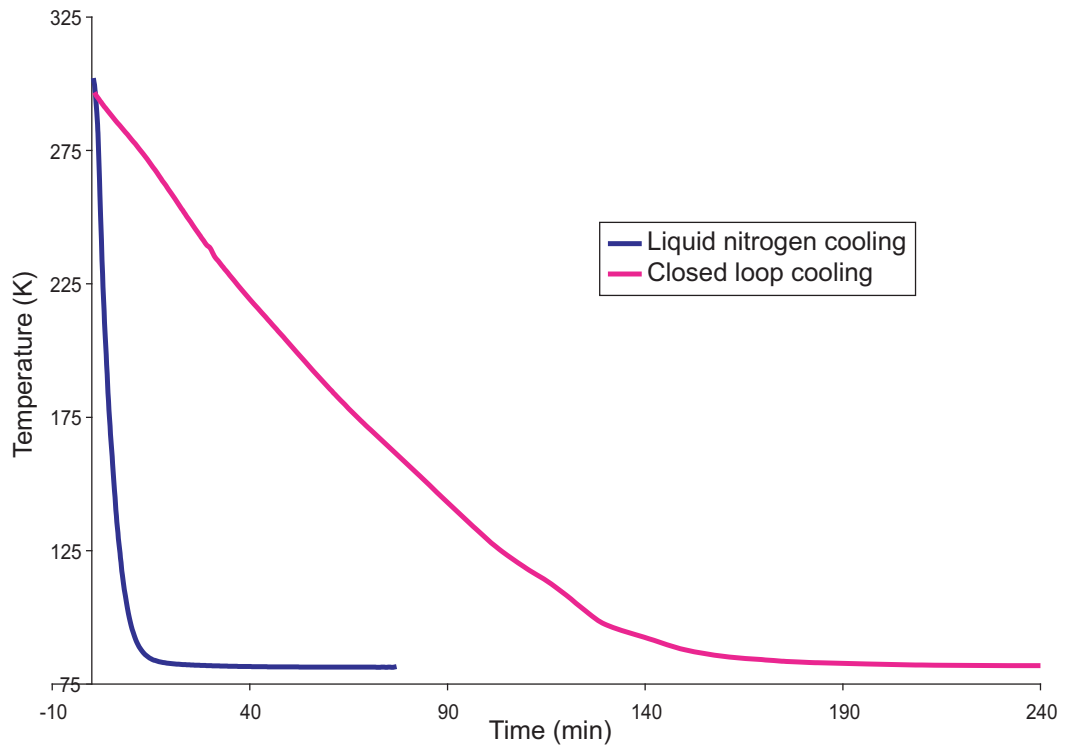


Figure 3.7: Comparison of cooling times between closed-loop and liquid nitrogen systems. Although laser cooling using the closed-loop system initially takes several hours, a key advantage is the low temperature can be maintained for periods of months.

is $\exp^{-E/kT}$, the smaller bandgap energy E at mid-IR wavelengths requires a reduction in temperature T to match performance at near-IR wavelengths.

3.2.2 Temperature control

The laser temperature is set and monitored via a temperature controller (Pro8000, Profile) using a silicon diode sensor (PT-1000) in the laser dewar. The sensor reports a resistance, R_A , which is converted to a temperature T in the software using the following formula:

$$T = \frac{233841 - R_A}{525.9} \quad (3.1)$$

The laser could be cooled to a minimum temperature of 77 K but it was typically operated at a temperature of 88 K. This is further discussed in section 4.4.1. The required temperature is achieved by setting the target resistance, R_S , on the temperature controller. When the temperature has stabilised, the actual resistance, R_A , is reported as lower than the target resistance, R_S , by 2.32 k Ω , corresponding to a temperature difference of +4.4 K. The resistance offset was easily compensated for in the software by automatic adjustment of the target resistance. During instrument operation the temperature controller is operated using the LabVIEW software via a GPIB connection and PCMCIA card (National Instruments).

A constant laser temperature was required during instrument operation for wavelength stability. The laser controller holds the temperature constant to within a few mK. After optimising the PID settings of the temperature controller, the temperature stability was found to be better than that of the previous lab-based systems which use liquid nitrogen for cooling.

3.2.3 Thermal management

The compressor is housed in the base section of the instrument along with the scroll pump. Thermal management for this section is achieved via four AC fans mounted on the case sides and with the use foam partitioning to direct the airflow. (See figure 3.8). The compressor and pump are tightly secured using straps and vibrations are reduced using rubber mounts. Two fans are also mounted on the case sides of the upper section. In addition, a computer fan with a heat sink is attached to each of the two thermo-electrically cooled photodetectors.

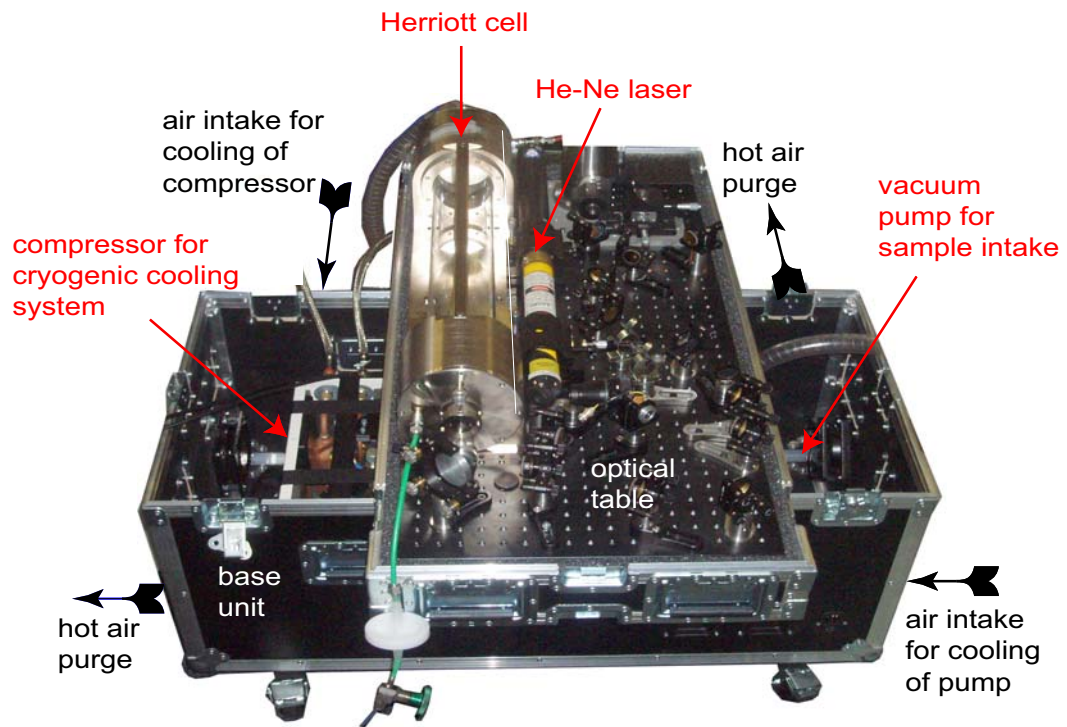


Figure 3.8: Photograph of instrument where the optical table section has been rotated to show the compressor and vacuum pump positions in the base. Thermal management is achieved via cooling fans with air flow controlled by foam partitioning.

3.3 Power requirement

The power requirement of the complete spectroscopy system, measured using an energy meter, is shown in figure 3.9. The power requirement of the instrument is dominated by the compressor of the laser cooling system and scroll pump used to draw gas through the sample cell. The total power requirement is $\sim 1.8 \text{ kW}$ (8 A at 230 V). On start-up, the power requirement is momentarily higher.

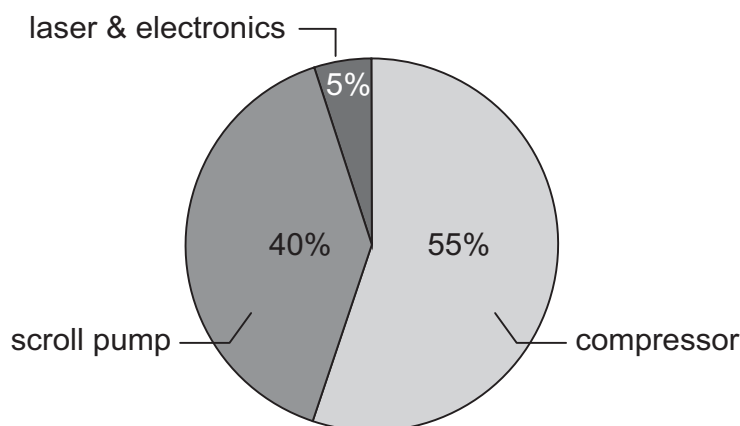


Figure 3.9: The total power requirement of the instrument is ~ 1.8 kW. This is dominated by the compressor and scroll pump.

3.4 Zero referencing and calibration

To provide a zero reference for the calculation of the ethane concentration, hydrocarbon-free nitrogen gas is measured at regular intervals, determined by the settings in the software. Typically zero-referencing occurs for 12 s after each 60 s measurement period. This is achieved by switching between the sample inlet and a second inlet from which there is a supply of nitrogen gas. In situations where the difference in ethane between two sources is to be examined the zero reference can be taken as one of these sources, eliminating the need for an external reference such as nitrogen. The zero referencing technique primarily eliminates the effects of slowly shifting optical fringing patterns in the Herriott cell, which can affect the sample $2f$ lineshape.

In addition, calibration is independently confirmed using a hydrocarbon reference standard certified in accordance with a ISO9001 (National Physical Laboratory). This contains ethane at 4.01 ppb with a certification accuracy of 2%. Upon measurement of the reference standard, a calibration factor in the software can be adjusted until the reported and known ethane concentrations are in complete agreement.

3.5 Herriott cell

The necessary optical pathlength to enable sub-ppb sensitivity to ethane is achieved using a Herriott cell. The Herriott cell is a multi-pass cell with astigmatic mirrors at each end. The laser light enters and exits the cell through a small aperture in the input mirror and during successive round trips the laser spot pattern undergoes a precessing ellipse, where the number of passes is dictated by the cell geometry [60]. Aerodyne Research produce multipass cells based on the Herriott configuration. A variety of pathlengths can be achieved using a fixed set of astigmatic mirrors through a combination of mirror rotation and separation changes. These cell configurations are nearly confocal [63]. The previous lab-based ethane spectroscopy systems at the University of Glasgow incorporated a Herriott cell 1 m in length (AMAC-200, Aerodyne). The beam was arranged to exit the cell after 174 passes and, with the mirror separation of 0.88 m, resulted in a total optical path length of 153.5 m. For compactness, the portable instrument incorporates a shorter Herriott cell (AMAC-100, Aerodyne), with a mirror separation of 0.54 m. Therefore to achieve approximately the same pathlength as previous systems 284 passes would be required. A Herriott cell with cell geometry configured for 366 passes was purchased. However, the gain in sensitivity due to increased pathlength must be offset against transmission losses (discussed in section 4.5.2). Therefore the cell was aligned for a lower number of passes than the maximum.

3.5.1 Alignment

A Helium Neon tracer beam, combined with the infrared beam using a calcium fluoride beam splitter, was used to align the Herriott cell. See figure 3.3. The collimated infrared and tracer beams were directed into the cell using two steering mirrors. These mirrors were adjusted until an exiting tracer beam was detected. However, significant difficulties in detecting the infrared beam were encountered when attempting to align the shorter 0.5 m Herriott cell in this way, in contrast to the alignment of the 1 m cells used in the previous lab-based systems.

When aligning the 1 m cells in the lab-based systems the input beams had been collimated

and directed into the cell without the need to focus the beam. The required exiting tracer beam and infrared beam had been detected by careful adjustment of the steering mirrors. However, to align the shorter cell, for which the mirrors have a smaller radii of curvature, it was necessary to calculate the beam size and focusing required at the entrance to the cell.

Input beam parameter calculations

For a stable cavity, the radius of curvature of the beam wavefront must match that of the mirrors. Each mirror in the Herriott cell is astigmatic, with radii of curvature $R_x = 67.6$ cm, $R_y = 74.0$ cm. Using $R = 70.8$ cm as the average of the two radii and the mirror separation $d = 54.5$ cm, the Rayleigh range, z_r , can be calculated (see appendix B) using

$$z_r \simeq \sqrt{\frac{d(2R - d)}{4}} = \sqrt{\frac{54.4(2 \cdot 70.8 - 54.4)}{4}} = 34.4 \text{ cm} \quad (3.2)$$

The beam waist, ω_0 , of the infrared beam is then

$$\omega_0 = \sqrt{\frac{z_r \lambda}{\pi}} = \sqrt{\frac{0.34 \cdot 3.4 \cdot 10^{-6}}{1. \pi}} = 6 \cdot 10^{-4} \text{ m} = 0.6 \text{ mm} \quad (3.3)$$

Therefore the input beam should be gently focused to achieve a beam radius at the centre of the Herriott cell of ~ 0.6 mm.

For a beam waist of 0.6 mm in the centre of the cell, the spot size on the mirrors (at $z = d/2 = 0.273$ m) is calculated using

$$\omega(z) = \omega_0 \sqrt{1 + \left(\frac{z}{z_r}\right)^2} = 0.06 \sqrt{1 + \left(\frac{0.27}{0.34}\right)^2} = 0.77 \text{ mm} \quad (3.4)$$

Similar calculations show that the He-Ne tracer beam will have a beam waist of $\omega_0 = 0.26$ mm and a spot size on the mirrors of 0.34 mm. However, the reflectivities of the mirror coatings are not optimised for this wavelength. In practice, larger spot sizes are observed for the tracer beam.

Calculation of the optimum position for the focusing mirror

A mirror with radius of curvature $R = 1.5$ m was then used to focus the collimated beams into the cell. To determine the optimum position for the curved mirror, ray transfer matrix (RTM) analysis was used:

RTM analysis uses the paraxial approximation of ray optics, where all rays have some small transverse distance (x) and angle (θ) relative to the optical axis of the system. The input and output beams are described by vectors $\begin{pmatrix} x_1 \\ \theta_1 \end{pmatrix}$ and $\begin{pmatrix} x_2 \\ \theta_2 \end{pmatrix}$ respectively. The transfer matrix \mathbf{M} describes the effect of an optical element on the input beam.

$$\begin{pmatrix} x_2 \\ \theta_2 \end{pmatrix} = \mathbf{M} \begin{pmatrix} x_1 \\ \theta_1 \end{pmatrix} \quad (3.5)$$

and

$$\mathbf{M} = \begin{pmatrix} A & B \\ C & D \end{pmatrix} \quad (3.6)$$

For a ray reflection off a mirror of radius of curvature R followed by free space propagation for a distance d the transfer matrix becomes

$$\mathbf{M} = \begin{pmatrix} 1 & d \\ 0 & 1 \end{pmatrix} \begin{pmatrix} 1 & 0 \\ -\frac{2}{R} & 1 \end{pmatrix} = \begin{pmatrix} 1 - \frac{2d}{R} & d \\ -\frac{2}{R} & 1 \end{pmatrix} \quad (3.7)$$

Before being focused into the Herriott cell the infrared and tracer beams were approximately collimated. The radius of the infrared beam was measured using a photodiode to be ~ 1 mm. This was done by placing the photodiode on an X-Y-Z translation stage and determining the distance over which the beam intensity fell from the maximum to $\sim 1/e^2$ of the maximum.

For $x_1 = 1$ mm, $\theta_1 = 0$ and $R = 1.5$ m

$$\begin{pmatrix} x_2 \\ \theta_2 \end{pmatrix} = \begin{pmatrix} 1 - \frac{2d}{R} & d \\ -\frac{2}{R} & 1 \end{pmatrix} \begin{pmatrix} x_1 \\ \theta_1 \end{pmatrix} = \begin{pmatrix} 1 - \frac{4d}{3} & d \\ -\frac{4}{3} & 1 \end{pmatrix} \begin{pmatrix} \frac{1}{1000} \\ 0 \end{pmatrix} \quad (3.8)$$



Figure 3.10: The Herriott multipass cell is aligned using a Helium Neon tracer beam. A spot pattern is visible on each of the cell mirrors.

yielding

$$x_2 = (1 - \frac{4}{3}d)/1000 \quad (3.9)$$

$$\theta_2 = -4/3000 \quad (3.10)$$

The required mirror distance d from the centre of the Herriott cell was calculated by setting $x_2 = 0$ mm in equation (3.9) to yield $d = 0.75$ m.

Therefore, to achieve the beam focus in the centre of the Herriott cell, a curved mirror, $R = 1.5$ m, should have been placed at a distance of 75 cm before the centre of the cell, i.e. 47.5 cm before the aperture on the input mirror of the cell. The curved mirror was fixed at a distance of ~ 48 cm before the input aperture mirror. A flat mirror was used immediately before the cell input aperture to direct the beam into the cell. With this arrangement cell alignment was more easily achieved than with a collimated beam and both an exiting tracer and infrared beam could be detected after multiple passes.

The detected tracer beam was then optimised for the infrared beam by adjustment of the steering mirrors. Although the number of passes at this point was unknown, a rough

estimate was made by immediately assessing the sensitivity to ethane using samples of known concentration. The alignment was adjusted until the exiting beam could be used to achieve a similar sensitivity to ethane as the lab-based system. To reach the higher passes the trace beam spot patterns on the cell mirrors were observed (see figure 3.10). The mirrors were then adjusted until the spot pattern appeared to resemble the required pattern, as depicted in diagrams provided by Aerodyne.

3.5.2 Estimate of number of passes

The Herriott cell mirrors are nickel-plated aluminum with broad-band dielectric coating mirrors, specified with a reflectivity, R , of 99.2%. Therefore, the theoretical power loss can be calculated using $T = R^n$, where T is the fraction of light exiting the cell after a certain number of passes n . Using the specified responsivity of the sample photodetector ($> 366600 \text{ VW}^{-1}$) and the measured voltage to estimate the power in the beam entering the Herriott cell gave a power of $\sim 38 \mu\text{W}$. The power at the sample photodetector after multiple passes in the Herriott cell was estimated to be $\sim 5 \mu\text{W}$. This measured transmission of 13%, equates to a maximum of 255 passes, assuming the specified mirror reflectivities of 99.2% were sustained. In practice, despite the use of air filters, the reflectivities will be lower and it is likely that the actual number of passes is also lower. It is important to note that, while the number of passes will affect performance, it is not necessary to know the precise number of passes in order to calibrate the instrument. Absolute calibration is achieved using a known reference standard as described in section 3.4.

3.6 Discussion

In this chapter the development of the portable instrument has been described in detail. The instrument design is based on that of the previously developed lab-based systems. However, the requirement for a on-site use in a clinical setting has required a size reduction and a key change to the laser cooling.

The closed-loop cooling system, which has dispensed with the need for liquid nitrogen, was purchased as a commercial piece of equipment (Cryotiger, Megatech Ltd) and overall has been extremely successful in the instrument. However, initially this aspect of the instrument development presented the greatest challenge. The need for careful thermal management and adequate ventilation for the compressor was difficult to achieve in accordance with the specification that the instrument be compact. However, successful thermal management was eventually achieved via the addition of more fans to the instrument case and careful foam partitioning, enabling long-term uninterrupted use. Given that the base section of the instrument, containing the compressor, accounts for almost one half of the instrument bulk, future generations of the technology could be made significantly more compact by incorporating a laser that is operational at room temperature.

The length reduction of the Herriott cell also presented new challenges not experienced in the development of the lab-based systems. Difficulties were encountered when aligning the cell for the higher number of passes due to the shorter cell being significantly more sensitive to input beam size and focusing. These difficulties were overcome by calculating the theoretically required beam parameters. Applying this in practice made the alignment process easier and a sufficiently long pathlength was obtained to enable sub-ppb ethane detection.

A number of additional factors contributed to the overall size reduction of the instrument: the optical breadboard supporting the injection optics has been made more compact through careful planning and design; smaller PSDs have been incorporated, all electronics has been custom-designed and are housed in a compact metal box. Despite the changes described above, the performance of portable system has not been compromised when compared to the lab-based system and higher performance has been observed with the portable system. The following chapter presents results and discussion of the characterisation of the portable instrument.

A paper reporting on the development and performance of the new instrument has been published in *Measurement Science and Technology* [64].

Chapter 4

Characterisation of the spectroscopy system

This chapter reports on the instrument performance in terms of sensitivity, accuracy and selectivity. Noise sources and other factors contributing to the performance are analysed and discussed.

4.1 Performance

4.1.1 Sensitivity

The instrument has a sensitivity to ethane of 70 ppt with a 1 Hz sample rate. Using the absorption coefficient $\alpha(\nu_0) \approx 11 \text{ cm}^{-1}$ (from section 2.2) this means that the instrument can detect a minimum absorbance of

$$\alpha(\nu)bc = 1.1 \cdot 10^{-3} \cdot 100 \cdot 70 \cdot 10^{-12} = 7.7 \cdot 10^{-6} \quad (4.1)$$

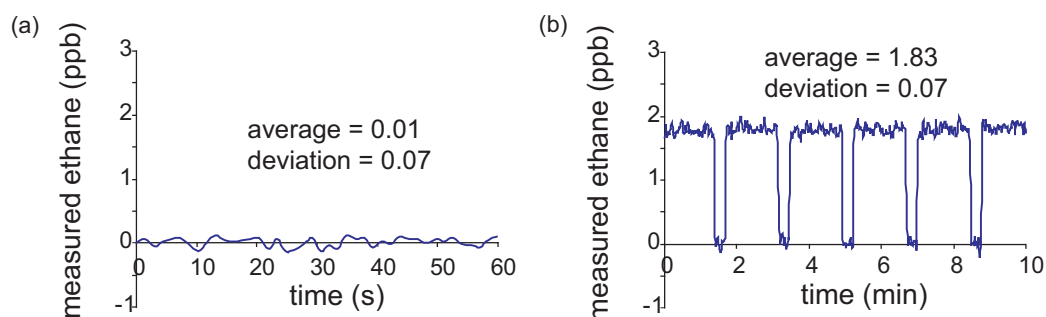


Figure 4.1: The performance of the ethane spectroscopy system. (a) Nitrogen gas measured over 60s. (b) Room air measured over 10 min, with regular nitrogen zero-referencing.

The sensitivity is defined as the standard deviation in the reported ethane concentration when measuring hydrocarbon-free nitrogen gas. Figure 4.1 a shows a measurement of nitrogen gas (BOC Gases) over one minute. The mean concentration was found to be 0.01 ppb with a standard deviation of 0.07 ppb. This typical measurement standard deviation is also seen over a time interval of a few seconds and is not significantly improved by further increasing the measurement (averaging) time interval. An example of ambient ethane measurement with regular nitrogen zero-referencing is shown in figure 4.1 b. For the reported ethane concentration of 1.83 ppb (a typical ambient ethane level) the standard deviation was again 0.07 ppb. Exhaled human breath also contains low concentrations (ppb) of ethane. Figure 4.2 shows example measurements of exhaled breath ethane for both online and off-line samples. In particular, online sampling with the achieved sensitivity allows the increase in ethane associated with the gas exchange regions within the lung to be observed over the course of a single exhalation (the so-called alveolar gradient). Analysis of breath ethane is discussed in detail in chapter 6.

The sensitivity of the instrument is limited by a combination of intensity noise, detector noise, electronic noise and optical fringing, further discussed in section 4.3. Although concentration measurements are taken in a 1 Hz bandwidth the instrument response time is 2.5s, limited by the flow rate of gas into the sample cell.

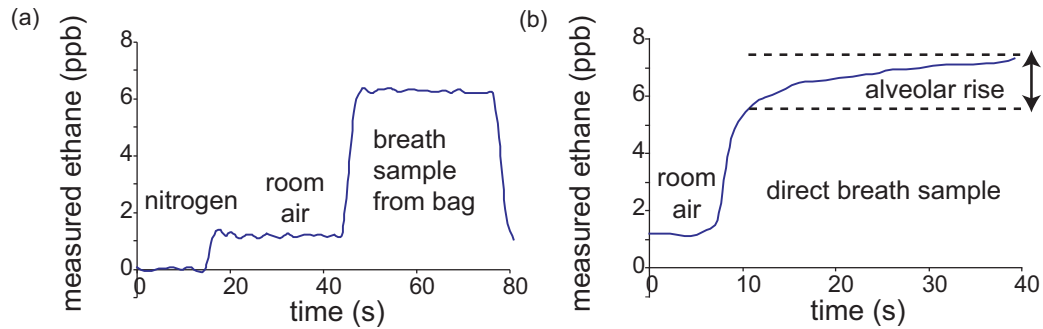


Figure 4.2: Example breath ethane measurements. (a) Room air followed by a breath sample contained in a Tedlar sample bag. (b) Room air followed by a breath sample exhaled directly into the instrument. In the latter case the rise in ethane can be detected over a single breath

4.1.2 Accuracy

The accuracy of the instrument is considered in terms of its absolute calibration and reproducibility as determined in the following experiments.

Calibration test 1

A test was performed to determine the agreement between the measured ethane concentrations and empirically calculated ethane concentrations of a series of gas samples. The instrument was initially calibrated by measuring an ethane sample certified at $4.01 \text{ ppb} \pm 2\%$ (National Physical Laboratory). The instrument calibration factor was adjusted accordingly via the control on the front panel in the LabVIEW software. The ethane concentration was then recorded to be 3.9 ppb with a standard deviation of 0.07 ppb over a 30 s period.

The empirical gas mixes were obtained by first filling a 100 l Tedlar gas sample bag (SKC Ltd) to its full capacity of 110 l with hydrocarbon-free nitrogen gas. Then 10 ml of ethane at a concentration of $50 \text{ ppm} \pm 2\%$ (BOC gases) was added to the sample bag through the septum at the inlet tap using a syringe with a fine needle. The septums reseal automatically

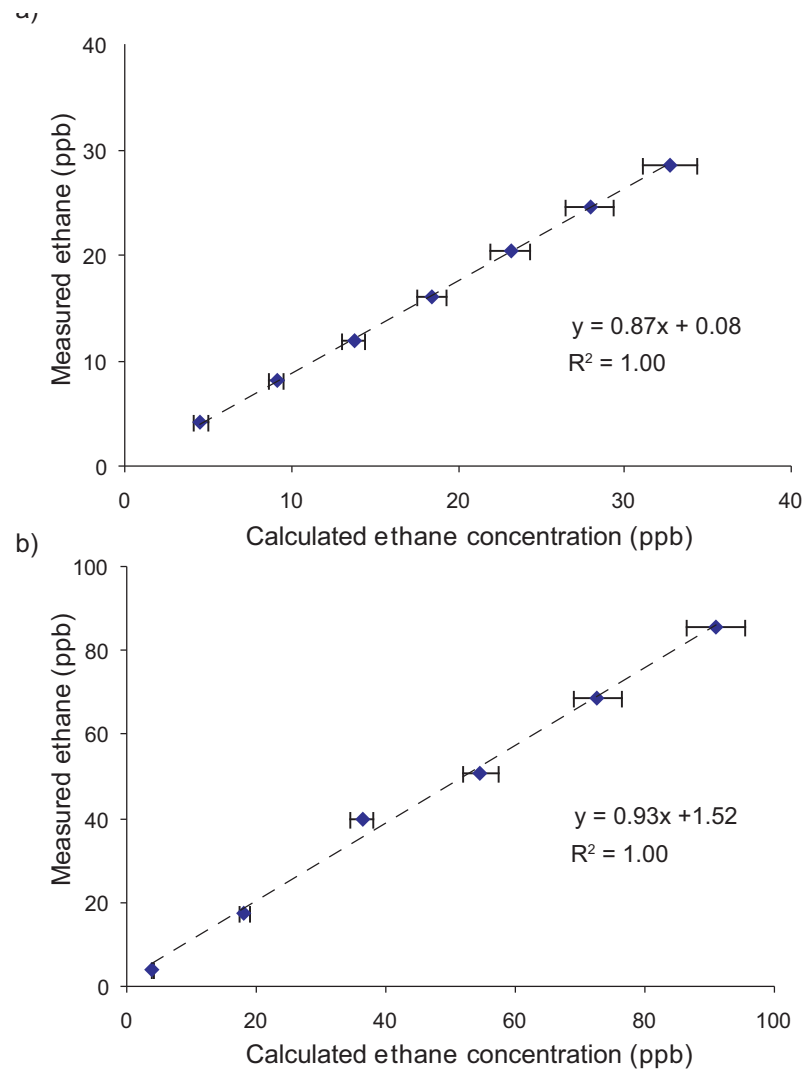


Figure 4.3: Instrument calibration. (a) A sequence of measured ethane concentrations showing agreement of 87 % with empirically calculated ethane concentrations. (b) A second sequence of measured ethane concentrations also showing agreement of 93 % with empirically calculated ethane concentrations. The agreement is seen to be highly linear for both sequences.

after being pierced. The gas mixture in the bag was allowed to mix for several minutes before measurement. Gas was drawn from the 100 l bag into the instrument for 20 s, corresponding to a removed volume of 1 l. The ethane concentration and standard deviation was recorded. 10 ml of 50 ppm ethane was then added to the remaining gas volume and the process was repeated five times. In addition a small bag was filled with nitrogen gas and measured as a zero reference. Errors on the empirically calculated mixes were approximately 10 % of the concentration while the measured errors (standard deviation during measurement) were less than 0.1 ppb. Figure 4.3 a shows a plot of the experimentally determined ethane concentrations against the calculated empirical concentrations with an added trendline. The R^2 value of 1.00 shows the relationship is linear and the gradient of the of 0.87 shows that the measured and empirical readings agree to an overall accuracy of 87%.

Calibration test 2

A second calibration test was performed using a modified technique to produce a series of gas samples at empirically calculated ethane concentrations. Six Tedlar bags were filled with nitrogen until they were at full capacity (5.5 l). Differing volumes of 50 ppm \pm 2 % ethane was then added to five of the bags using a syringe as described above. The added volumes were 2, 4, 6, 8 and 10 ml while the remaining bag contained only nitrogen. The empirical ethane concentration of each bag was calculated and the ethane concentration and standard deviation was then measured for each. The results were plotted and are shown in figure 4.3 b. Again the relationship is highly linear ($R^2 = 1$) with an agreement of 93 % between the empirically calculated and measured ethane concentrations.

These calibration techniques were repeated and it was found that the agreement between the empirical and measured ethane concentrations was generally better than 80 %. Since the agreement is always seen to be highly linear, the important factor appears to be the initial calibration of the instrument with a known concentration. Therefore, for breath ethane measurements obtained during our clinical trials, the instrument was regularly calibrated using a certified ethane sample 4.01 ppb \pm 2 %. For other applications where higher ethane levels were recorded, the calibration was checked using a source at \sim 90 ppb,

obtained from careful dilution of our 50 ppm ethane gas cylinder.

Repeatability test

Figure 4.4a shows the concentration reproducibility when measuring a constant ethane sample every 2 min over a period of 12 min. The mean ethane concentration was 4.58 ppb with a standard deviation of 0.04 ppb. The range in the measurements was 0.13 ppb. The ethane concentration was then measured approximately every 30 min for 4 hrs as shown in figure 4.4b. The mean ethane concentration over the 4 hr period was 4.53 ppb with a standard deviation of 0.05 ppb. The range in the measurements was 0.13 ppb. Therefore the error in repeatability for an ethane concentration of 4.5 ppb is found to be within the value of 0.07 ppb for the sensitivity. When measuring higher concentrations the range in the measurements is higher. For example a gas sample measured twenty times over a period of 4 hours and 30min was found to have a mean ethane concentration of 20.67 ppb, a standard deviation of 0.02 ppb and a range of 0.76 ppb. In general, repeated concentration measurements over a period of several hours were found to agree to within 3%.

The repeatability is limited by the effects of thermally induced changes in alignment, drift of electronic offsets and shifting optical fringing patterns. As described in section 3.4, zero-referencing with nitrogen gas is used to reduce the effects of optical fringing. Repeatability within each zero-referencing interval is maintained at ~ 0.07 ppb provided that the referencing intervals occur with sufficient regularity (\sim every 60 s). Longer term repeatability (within $\sim 3\%$) is affected by changes in light levels at the photodetectors (see section 4.6.2) and drifting electronic offsets. The instrument was always calibrated on start-up to take account of day to day variations in these parameters.

4.1.3 Selectivity

Operation at low pressure is vital for selectivity as it reduces the overlap between neighbouring transitions. Figure 4.5 shows the transmission of water, methane and ethane at a pressure of 40 mbar, temperature of 296 K over a 100 m pathlength from the HITRAN

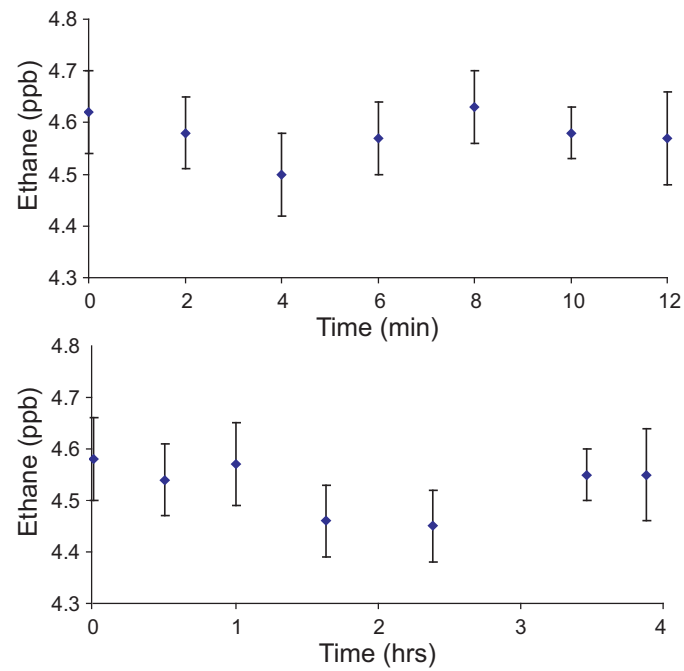


Figure 4.4: Reproducibility of measurements of a constant ethane sample over a period of (a) 12 min (b) 4 hrs. The readings agree to within 0.07 ppb. In general, the concentration reproducibility is better than 3%.

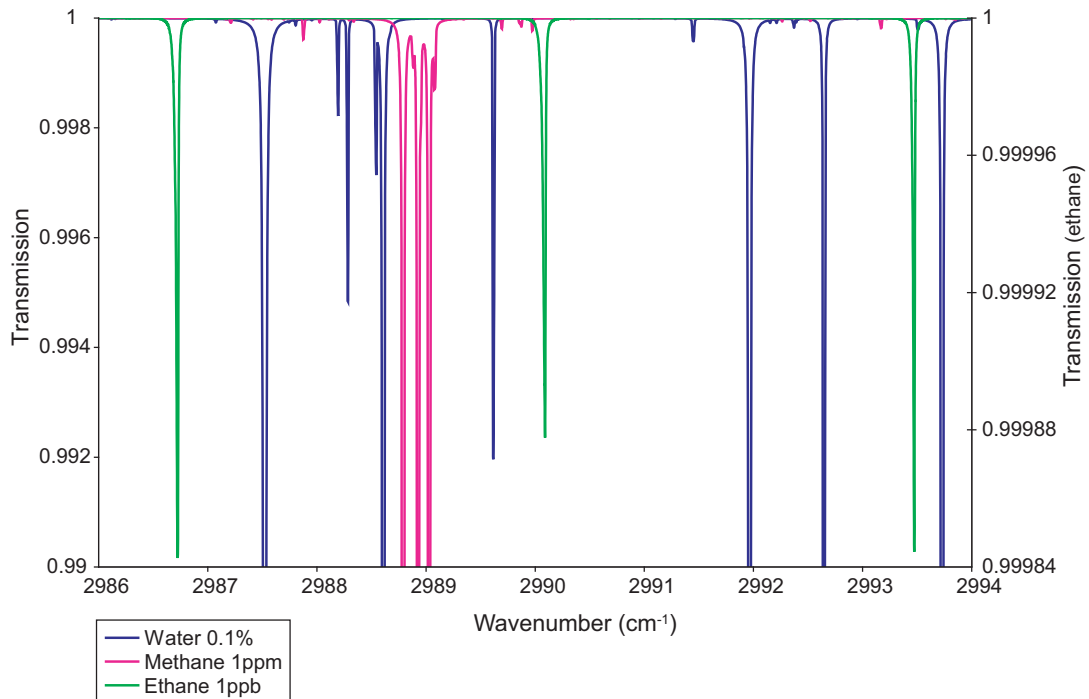


Figure 4.5: Water, methane and ethane transitions given by the HITRAN database for a pressure of 40 mbar, temperature of 296 K over a 100 m pathlength.

database. The ethane absorption lines of 2990.09 cm^{-1} and 2986.72 cm^{-1} are chosen due to their isolation from large absorption features of atmospheric species such as water and methane.

Ideally, rather than zero-referencing using nitrogen, a gas would be used containing all species in the sample to be measured in the same concentration with only ethane absent. This of course is impossible to achieve in practice and therefore low concentrations of background species remain a small source of error.

The cross sensitivity to other species depends on absorbance due to slight overlap with neighbouring transitions and also due to the fact that the laser emission may not be completely single-mode. Absorption of light from other laser modes can overlap with an absorption line of a contaminating species. The cross-sensitivity to methane, for example,

was found to vary between 10000:1 and 1000:1 as the modal properties of the laser were observed to decline over time.

The presence of significant interference from contaminants was easily established using our detection technique: Via the LabVIEW software, the profile of the ethane absorption transition could be continually monitored. In the rare case of contamination, the shape of the ethane transition was visibly distorted on the laptop screen. In such cases, the gas samples could be discarded. Generally, problems with contamination were not encountered but care was needed during our clinical trials, for which a range of cleaning fluids were used. This is further discussed in section 7.2.3.

4.2 Theoretical contribution of noise sources

Theoretical noise contributions were calculated using the datasheet specifications for photodetectors and electronic equipment and estimating the power at the sample photodetector. Experimental noise contributions from the detectors and electronics were then measured using a Stanford Research Systems SR780 analyser and the results compared.

4.2.1 Detector noise

The sample and reference detector modules (VIGO PVI-2TE) each consist of an infrared detector optimised for 3.4 μm operated in photovoltaic mode, combined with a DC coupled voltage preamplifier (VIGO MVPDC). These modules were chosen as they are extremely compact (dimensions 70 x 45 x 19 mm) and offer a high detectivity (D^*), specified to be $\sim 2 \cdot 10^{11} \text{ cm Hz}^{1/2} \text{ W}^{-1}$.

The noise equivalent power (NEP) gives an indication of the size of the minimum signal that can be detected with the photodetector modules. Using the stated detectivity of $D^* = 2 \cdot 10^{11} \text{ cm Hz}^{1/2} \text{ W}^{-1}$, the photodetector active area of $A = 1 \text{ mm}^2$ and the measurement bandwidth of $\Delta f = 33.3 \text{ Hz}$ (corresponding the PSD time constant setting of 30 ms), the

NEP was calculated as

$$NEP = \frac{\sqrt{A\Delta f}}{D^*} = \frac{\sqrt{0.01 \cdot 33.3}}{2 \cdot 10^{11}} = 2.89 \cdot 10^{-12} \text{ W} = 2.89 \text{ pW} \quad (4.2)$$

For a laser temperature $T = 89.7 \text{ K}$ and laser current $I = 0.565 \text{ A}$, the measured voltage at the sample photodetector is $\sim 1.8 \text{ V}$. From the specified responsivity of the photodetector module ($3.67 \cdot 10^5 \text{ V W}^{-1}$) this equates to an approximate power at the sample detector of $5 \mu\text{W}$.

Therefore

$$\text{Detector noise-to-signal} = \frac{NEP}{P} = \frac{2.89 \cdot 10^{-12}}{5 \cdot 10^{-6}} = 5.77 \cdot 10^{-7} \quad (4.3)$$

4.2.2 Shot noise

The ethane transition at 2990.01 cm^{-1} corresponds to a frequency of $\nu = 89.7 \text{ THz}$

Therefore the energy E of each photon

$$E = h\nu = 5.95 \cdot 10^{-20} \text{ J} \quad (4.4)$$

No of photons at a given power P

$$\text{Photon No. } (P) = \frac{P}{E} \quad (4.5)$$

For a power of $5 \mu\text{W}$ at the sample photodetector,

$$\text{Photon No. } (5 \mu\text{W}) = \frac{5 \cdot 10^{-6}}{5.95 \cdot 10^{-20}} = 8.4 \cdot 10^{13} \text{ s}^{-1} \quad (4.6)$$

$$\text{Shot noise-to-signal} = \frac{\sqrt{\text{Photon No. } (P)\Delta f}}{\text{Photon No. } (P)} = \frac{\sqrt{8.4 \cdot 10^{13} \cdot 33.3}}{8.4 \cdot 10^{13}} = 6.30 \cdot 10^{-7} \quad (4.7)$$

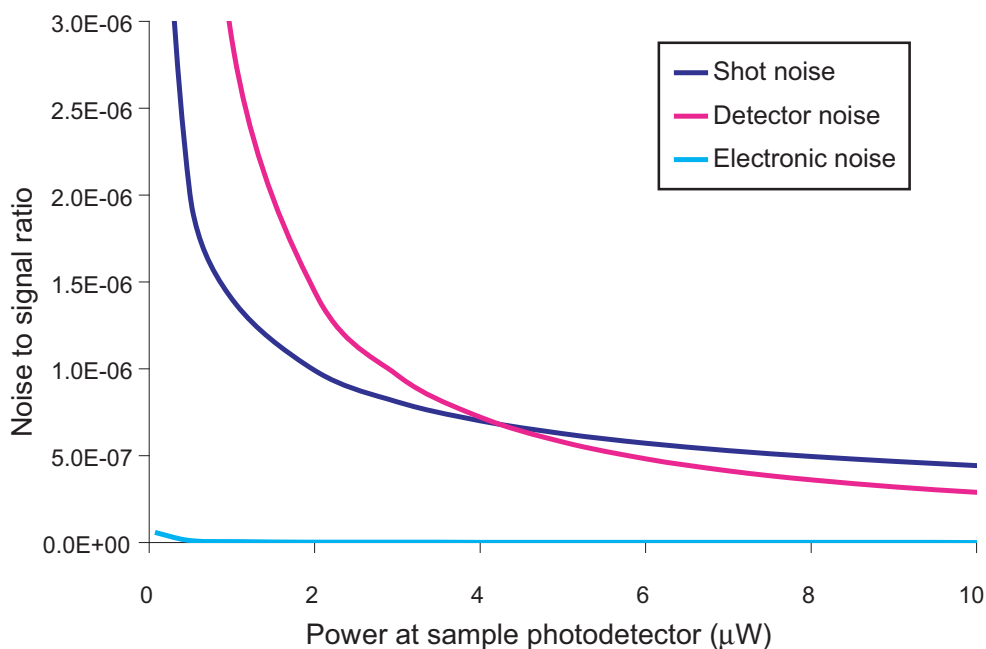


Figure 4.6: Calculated noise to signal ratios for shot, detector and electronic noise. At a power of $5 \mu\text{W}$ at the sample photodetector the shot noise is marginally dominant.

Therefore it appears that for a power at the sample photodetector of $5 \mu\text{W}$ the shot noise and detector noise are approximately equal, with the shot noise being marginally dominant.

Electronic noise was minimised by using low noise op-amps to amplify the detected AC signals pre-PSDs as described in section 3.1.3. In theory, the specified voltage noise of $1 \text{ nV Hz}^{-1/2}$ for the op-amps would dominate the electronic noise contributions.

Figure 4.6 shows how the theoretical contribution from the detector noise, shot noise and electronic noise vary with power at the sample photodetector. At a power of $5 \mu\text{W}$ at the sample photodetector the shot noise dominates. For power $\lesssim 4 \mu\text{W}$ the detector noise dominates the shot noise.

From the HITRAN database, the fractional absorption coefficient for 1 ppb ethane is $1.1 \cdot 10^{-6} \text{ m}^{-1}$ at $\bar{\lambda} = 2990.01 \text{ cm}^{-1}$, $P = 40 \text{ mbar}$, $T = 296 \text{ K}$. The theoretical contribution

Noise source	Theoretical signal to noise ratio	Ethane detection limit (ppt)
Electronic	$1.56 \cdot 10^8$	0.06
Detector	$1.70 \cdot 10^6$	5.34
Shot	$1.57 \cdot 10^6$	5.78
Combined	$1.15 \cdot 10^6$	7.87

Table 4.1: Theoretical noise contributions. The resulting ethane detection limit was calculated using the fractional absorption coefficient for 1ppb ethane at $\bar{\lambda} = 2990.01 \text{ cm}^{-1}$, $P = 40 \text{ mbar}$, $T = 296 \text{ K}$ and over a 100 m pathlength.

of each noise source to the ethane sensitivity was calculated using the signal to noise ratio and this fractional absorption coefficient over a 100 m pathlength. The results are shown in table 4.1.

4.3 Experimentally determined contribution of noise sources

4.3.1 Measured noise spectra

Figure 4.7 shows noise spectra measured at the detection frequency of 16 kHz at the output of the detection electronics but before the PSDs. The basic electronic noise was measured by grounding the circuit at the photodetector input with a 50Ω terminator. The combined contributions due to detector noise, electronic noise and intensity noise are also shown. The intensity noise includes shot noise, laser amplitude noise and vibration-induced noise. Since each noise measurement included the previous noise source the effective individual contributions due to detector noise and shot noise were calculated by quadrature subtraction. The corresponding signal to noise ratios and contributions to the ethane sensitivity were calculated and the results are shown in table 4.2.

The achieved working sensitivity of 70 ppt agrees extremely well with the sensitivity calculated from noise measurements. However, this value is a factor of 10 higher than that calculated directly from the theory using photodetector datasheet specifications.

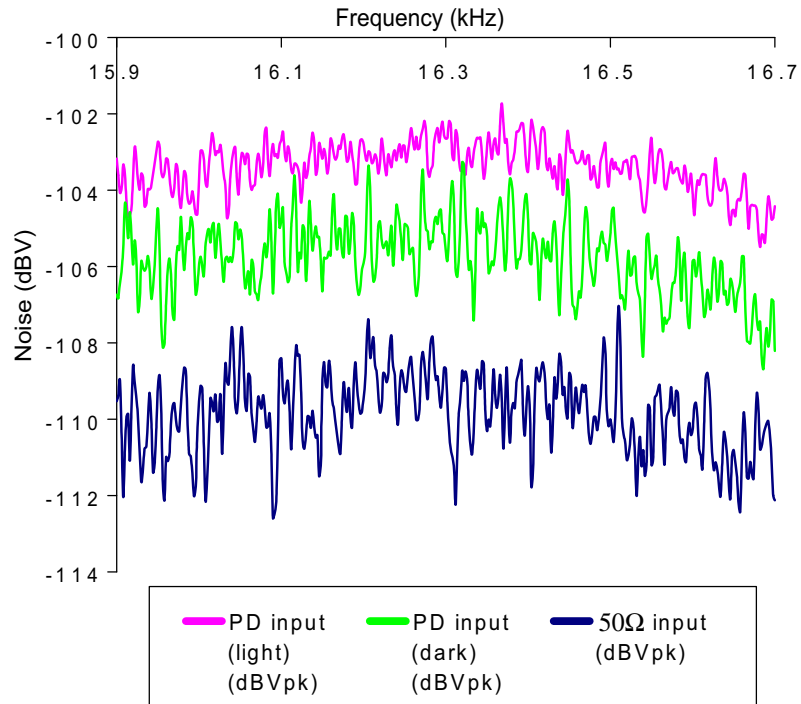


Figure 4.7: Noise spectra measured post-photodetector electronics but pre-PSDs. The contributions due to shot and laser amplitude noise, photodetector noise and electronic circuit noise (circuit grounded at photodetector input with a $50\ \Omega$ terminator) are shown.

Noise source	Measured noise ($\text{nV Hz}^{-1/2}$)	Signal to noise ratio	Ethane detection limit (ppt)
Electronic	1089	$2.86 \cdot 10^5$	32
Detector	1499	$2.08 \cdot 10^5$	44
Intensity	1416	$2.20 \cdot 10^5$	41
Combined	2332	$1.34 \cdot 10^5$	68

Table 4.2: Measured noise contributions. The resulting ethane detection limit was calculated using the fractional absorption coefficient for 1 ppb ethane at $\bar{\lambda} = 2990.01\ \text{cm}^{-1}$, $P = 40\ \text{mbar}$, $T = 296\ \text{K}$ and over a 100 m pathlength.

There are a number of possible reasons that the experimentally determined signal to noise ratio is lower than that calculated theoretically.

Thermal noise

An additional source of noise will be thermal (Johnson) noise due to the resistance, R , of the photodetector module. This resistance is the total equivalent resistance, including the internal resistance of the detector and the load resistance from the circuit, at the output of the detector [65]. The thermal noise current, i_{th} , (per root Hz) is given by

$$i_{th} = \sqrt{\frac{4kT}{R}} \quad (4.8)$$

Current noise

The optical signal to noise ratio has been computed for shot noise. This translates to photodiode current through

$$\text{signal-to-noise} = \frac{\Re P_{optical}}{\sqrt{2e\Re P_{optical}}} = \sqrt{\frac{\Re}{2e}} \cdot \sqrt{P_{optical}} = \sqrt{\frac{\eta P_{optical}}{2h\nu}} \quad (4.9)$$

where \Re is the responsivity and η is the quantum efficiency of the detector. Therefore the signal to noise ratio for shot noise is reduced through the quantum efficiency.

Second harmonic component

The signal to noise calculations have been made on the basis of the peak height of the direct absorption line. However it is the second harmonic component that is actually measured. At the optimum modulation index of 2.2 the central peak height is ~ 0.33 times that of the absorption line peak. Therefore the signal to noise ratios will be lower than those previously calculated.

Finally, it is worth noting that the calculated ethane sensitivity values in tables 4.1 and 4.2 are based on a signal to noise ratio of unity. In practice a higher ratio (≥ 2) is required.

4.3.2 Effect of reducing power

Since detector noise-to-signal is inversely proportional to the power and shot noise-to-signal is inversely proportional to the square root of the power the dominant noise source was determined experimentally by reducing the laser power at the sample detector by adjusting the beam alignment and measuring the resulting decrease in sensitivity. Figure 4.8 a shows the dependence of the standard deviation in measured ethane concentration (over 30 s) on the power at the sample photodetector module. The measured sample was at a constant concentration of 1.53 ppb. Changes in reported concentration due to the changes in light levels were compensated for. As shown in figure 4.8 b, the sensitivity appears to be proportional to the square root of the light level, suggesting that the shot noise does dominate the detector noise. These experimental results agree with the theoretical calculations that the shot noise dominates slightly over detector noise.

4.3.3 Comparison of vibrational noise

Vibrational noise is introduced from the compressor and vacuum pump within the base compartment of the instrument. However, the overall sensitivity is not compromised as compared to the previous lab-based system in which the pump is isolated and liquid nitrogen is used. A comparison of the DC light levels from the sample cell photodetector in the lab-based system and the portable system is shown in figure 4.9. Despite the considerable increase in vibration-induced intensity noise at the photodetectors there is no up-conversion of this noise compromising the signal at the detected frequency of 16 kHz. This is reassuring since it would otherwise be difficult to suppress such noise, given the need for a compact design.

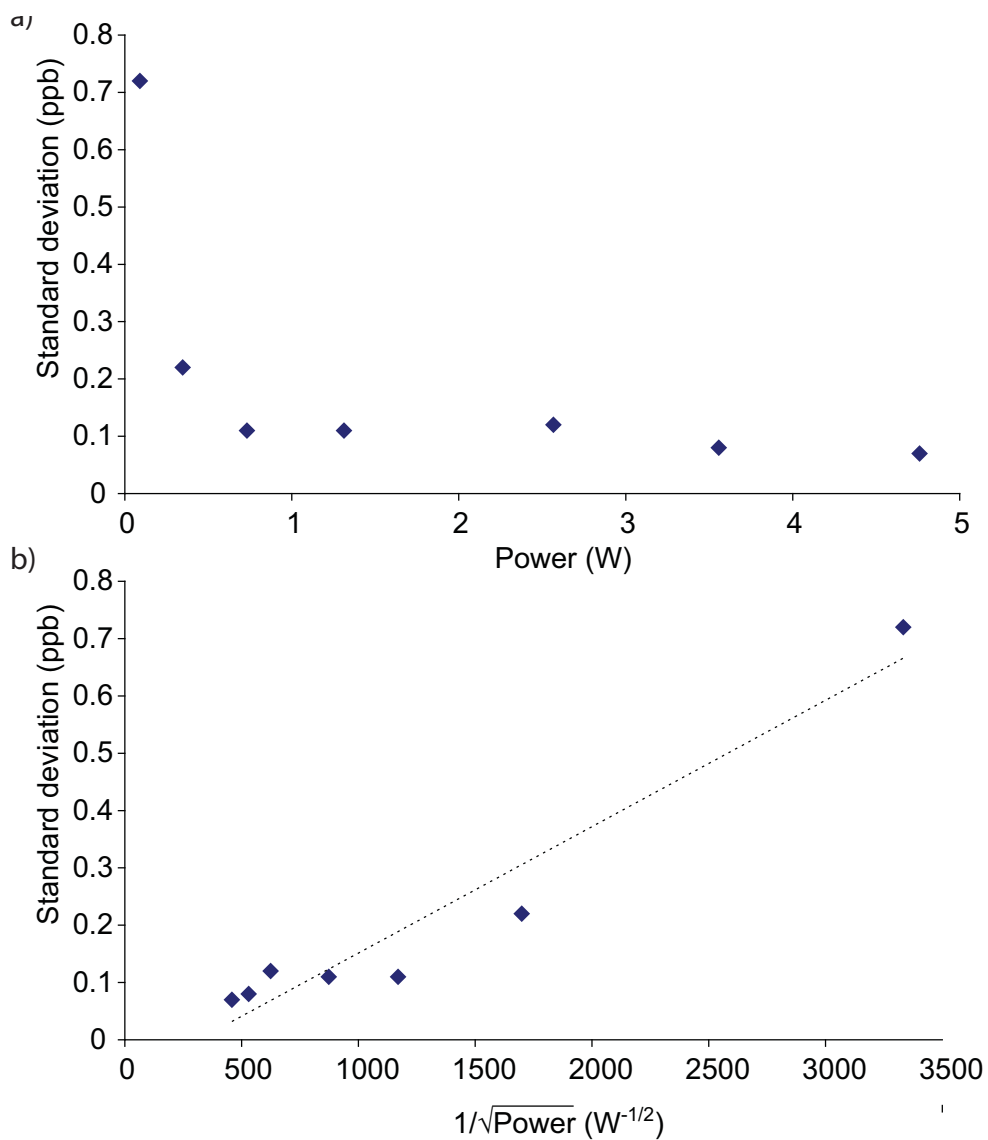


Figure 4.8: a) The effect of reducing the power at the sample photodetector on the standard deviation in reported ethane, for a constant concentration of ethane measured over a 30 s time period. b) It can be seen that the standard deviation is approximately inversely proportional to the square root of the sample light level, suggesting that the shot noise dominates the detector noise.

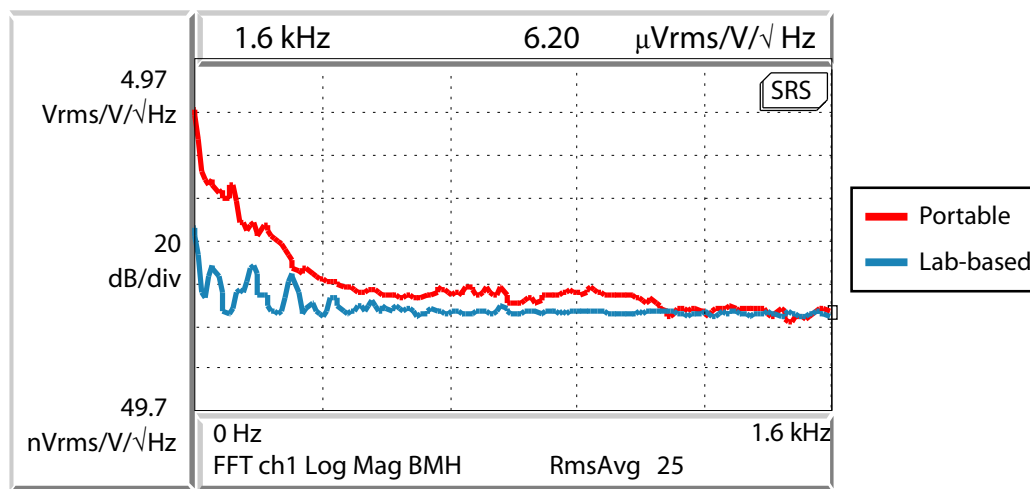


Figure 4.9: Comparison of DC-coupled intensity noise measured at the sample cell photodetectors in the new portable instrument and existing lab-based system. Despite clear coupling of vibration from the compressor and pump housed within the new unit, potential up-conversion of this noise has no noticeable effect on measured sensitivity.

4.4 Laser parameters

4.4.1 Temperature and current

The laser output wavelength is tuned to an ethane transition by adjusting the laser temperature and current. Increasing the laser temperature decreases the wavelength and vice versa. Increasing the current also has the effect of decreasing the wavelength. A change in wavelength of 1 cm^{-1} could be achieved by a temperature change of $\sim 2 \text{ K}$ or a current change of $\sim 20 \text{ mA}$. Datasheets are supplied for each laser (Laser Components) in which output wavelength, power and mode purity are specified for a range of current values at four different temperatures. Figure 4.10 shows one page of the datasheet for the laser used in the portable instrument.

The charts suggest that the optimum performance of the laser for our application would be at a temperature of 88 K and current of 630 mA . This choice of parameters should give

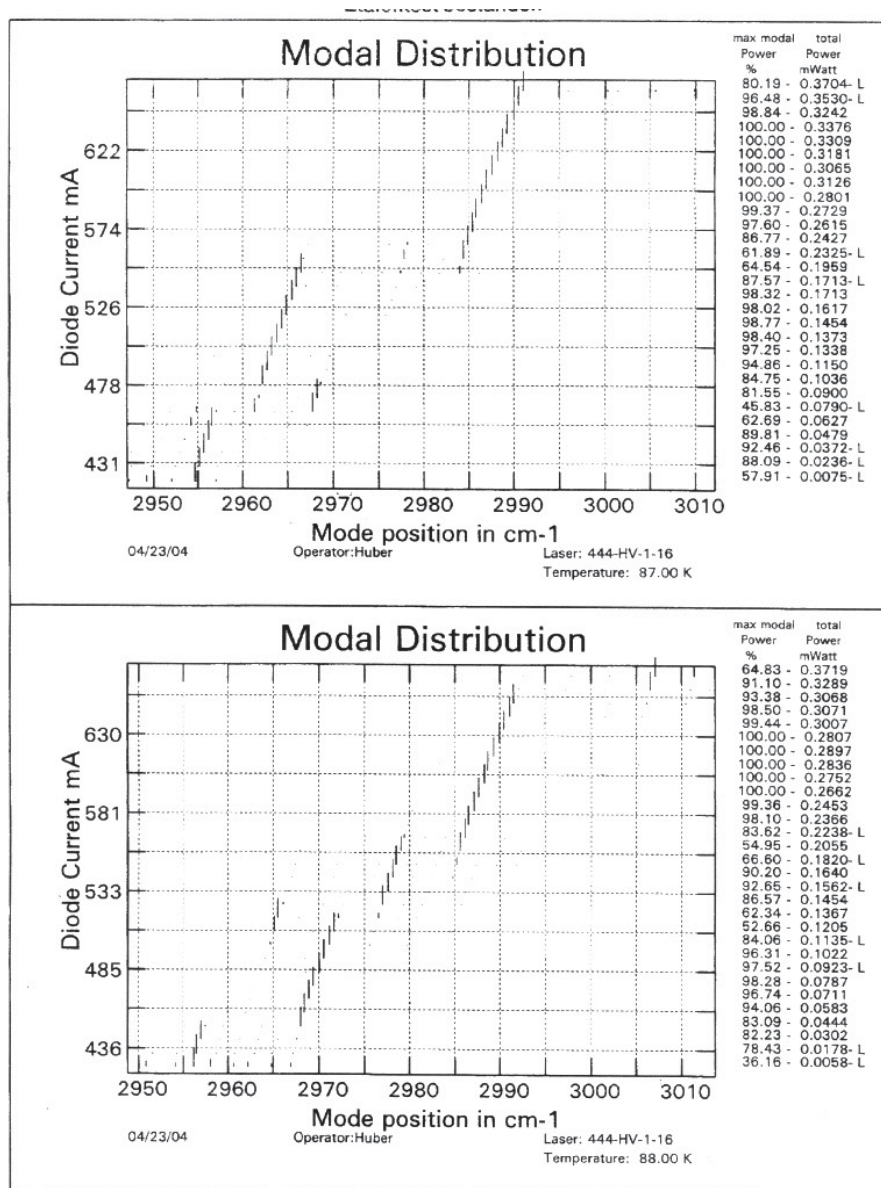


Figure 4.10: Datasheets are supplied for each laser (Laser Components). The charts provide a useful reference point for the initial selection of the laser and for use in locating temperature and current values for single-mode, highest power operation at the required wavelength.

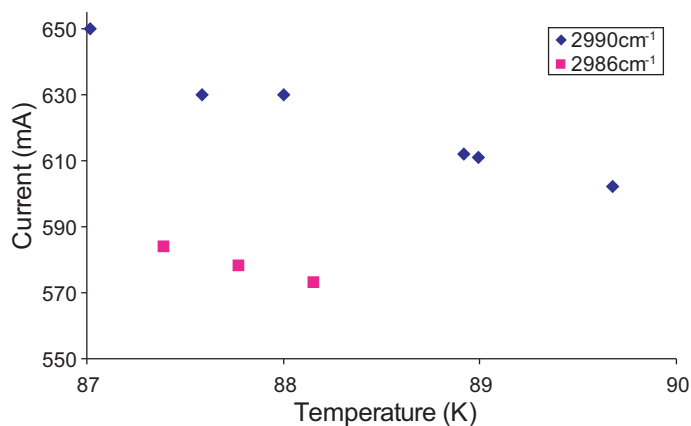


Figure 4.11: Laser current and temperature values which resulted in an output wavelength that corresponded to an ethane absorption transition.

single mode output at 2990 cm^{-1} , corresponding to one of our two target ethane transition wavelengths. These charts are useful guidelines as a starting point to locate the wavelength which corresponds to a particular gas transition. In practice, the precise temperature and current values corresponding to the wavelength of an ethane transition were obtained by systematic variation of these parameters while scanning the laser in the usual second derivative detection set-up and manually ‘searching’ for the gas transition using a high concentration of the gas in a reference cell. Once a transition was located in the reference channel, it was easy to verify if it was actually an ethane transition by filling the cell with a gas sample of high ethane concentration and observing the effect on the sample channel. Following the location and identification of an ethane transition, the corresponding temperature and current settings were saved in the LabVIEW software to enable the transition to be easily re-located upon instrument start-up.

Figure 4.11 shows the laser temperature and current values which produced an output wavelength that corresponded to an ethane transition. Using the supplied mode charts it was possible to estimate the wavenumbers of these transitions. The presence of a triplet of strong methane transitions centred around 2988.93 cm^{-1} made the identification of the 2990.09 cm^{-1} ethane transition easier (see figure 4.5). The ethane transitions were tracked by slowly adjusting the laser temperature and compensating for the induced wavelength change by adjusting the laser current accordingly. In order to also optimise the temperature

and current settings for modal quality the height of the reference second derivative signal was normalised to the detected light level and was monitored.

The laser was generally operated a temperature of 87.6 K with a current of 630 mA, corresponding to the ethane transition at 2990.1 cm^{-1} . These parameter settings were found to give the optimum performance, with a high detected power and best mode quality than at other allowable current/temperature combinations.

4.4.2 Modal purity

According to the datasheets the above temperature and current settings should have yielded single mode operation of the laser. The lack of interference from other species suggested that either the output was single mode or that any small fraction of power in other modes was not significant enough to cause noticeable interference. However the temperature and current parameters often required slight adjustment after thermal-cycling of the laser system. After the laser had been in use for over approximately two years this required adjustment became more significant. Despite the possibility of multimode operation, optimum instrument performance more recently was found to be at lower current and higher temperature values, of around $T=89.7\text{ K}$ and $I=565\text{ mA}$. It appeared that the modal properties of the laser had changed, as has been observed in the previous systems. This is further discussed in section 4.7.

4.5 Further system parameters

4.5.1 Modulation

The modulation parameters (frequency and depth) used were chosen in accordance with those calculated and optimised for maximum sensitivity in the previous systems. For the lab-based systems developed in the Glasgow Optics group, the modulation frequency was made variable and an optimum modulation frequency of $\sim 8\text{ kHz}$ was determined.

Current modulation (mA)	Wavelength change (nm)	Ethane sensitivity (ppb)
0.33	0.01	0.19
0.67	0.03	0.08
1	0.05	0.17

Table 4.3: Varying the modulation depth affected the ethane sensitivity, with an optimum performance when the peak wavelength change corresponded to the transition linewidth.

The major increase in noise introduced by the design of the portable instrument is due to vibration noise, which has been shown to be insignificant at 8 kHz (section 4.3.3). Therefore the modulation frequency of the oscillator chip was set at 8 kHz in keeping with previous systems and a fixed resistor was used to keep the control electronics compact.

The FWHM linewidth of the ethane transition at 2990 cm^{-1} at a pressure of 40 mbar and a temperature of 296 K is found from HITRAN to be $\Gamma = 0.03\text{ nm} = 780\text{ MHz}$. The laser linewidth is $\sim 30\text{ MHz}$. The wavelength modulation depth for the portable instrument was initially chosen to be approximately equal to the transition linewidth, as was used for the previous lab-based systems. The wavelength change of 0.03 nm corresponded to an adjustment of the laser current by 0.7 mA, achieved via the modulation signal input on the laser controller. By varying the strength of the modulation, it was found that this initial choice of modulation depth was approximately the optimum (See table 4.3). Details concerning the theoretical optimisation of both parameters for our detection scheme were discussed in [66].

4.5.2 Optical pathlength

The instrument sensitivity to ethane is dependent on the optical pathlength in the Herriott sample cell. Although increasing the pathlength increases the absorption, the exiting light level is also reduced. Therefore there will be an optimum number of passes to give the highest signal to noise ratio. Figure 4.12 a shows the theoretical transmitted fraction of incident power after light losses due to two window transmissions and n passes in the Herriott cell, using the specified mirror reflectivity of 99.2%. The theoretical gain in sensitivity for n passes as compared with 1 pass is shown in figure 4.12 b. However, the gain in sensitivity will scale either linearly or by the square root of the power, depending on the dominating

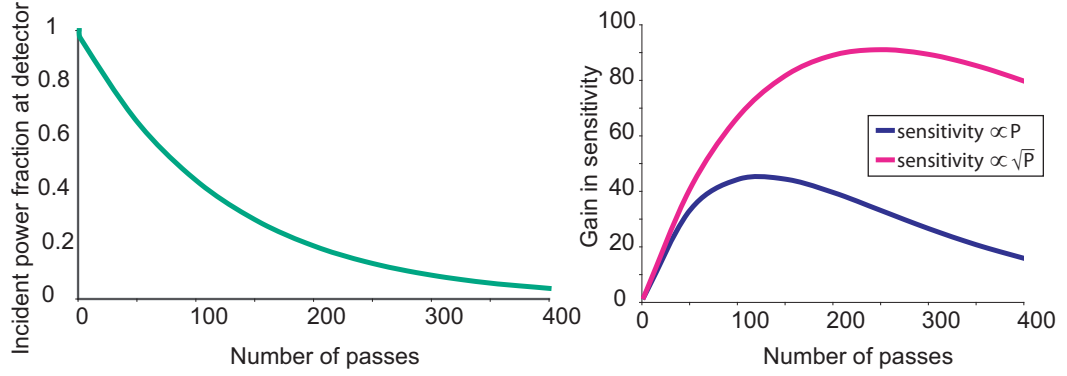


Figure 4.12: (a) The theoretical fraction of incident power exiting the Herriott cell after two transmissions and n reflections. (b) The theoretical gain in sensitivity by increasing n as compared with 1 pass. This is shown for both a linear and square root dependence on power at the sample detector

noise source. This is itself dependent on power. As calculated in section 4.2, for a power at the sample detector of $5 \mu\text{W}$, the shot noise and detector noise are approximately equal and therefore it is extremely difficult to theoretically determine the precise optimum number of passes. It appears from 4.12b that the optimum will be around 200 passes and estimates of pass number based on relative detected light levels (as described in section 3.5) suggest that this has been achieved.

These results can be made more general by using the sensitivity S as

$$S \propto nR^n \quad (4.10)$$

or in the case of shot noise limited sensitivity

$$S \propto \sqrt{nR^n} \quad (4.11)$$

Differentiating with respect to n and setting

$$\frac{dn}{dS} = 0 \quad (4.12)$$

gives the maximum S as

$$n = -\frac{1}{\ln R} \quad (4.13)$$

or in the case of shot noise limited sensitivity

$$n = -\frac{2}{\ln R} \quad (4.14)$$

With the mirror reflectivity of $R = 0.992$, this gives $n \sim 120$ or, for shot noise limited sensitivity, $n \sim 250$.

4.5.3 Pressure

Optimum pressure

The operating pressure of 40 mbar was chosen as it was previously determined to be a good compromise between sensitivity and selectivity [66]. As described in section 2.1.1, the transition linewidths depend on pressure and temperature. At a constant temperature the linewidth scales linearly with the pressure and the Lorentzian half linewidth is given by $\gamma_L = bP$, where b is the pressure broadening coefficient. For ethane the air broadening coefficient is $b = 0.67 \text{ cm}^{-1} \text{ MPa}^{-1}$ [67]. Decreasing the pressure reduces the linewidth, increasing selectivity, until Doppler broadening becomes significant. Since the reference cell in the instrument contains ethane in nitrogen gas while the sample cell contains ethane in ambient air, differences in pressure broadening may be a source of error.

For $\lambda_0 = 2990.09 \text{ cm}^{-1}$, $T = 296 \text{ K}$ and $M = 30 \text{ amu}$, the Doppler half linewidth is calculated to be $\gamma_D = 3.36 \cdot 10^{-3} \text{ cm}^{-1}$. At 40 mbar the Lorentzian half linewidth $\gamma_L = 3.95 \cdot 10^{-3} \text{ cm}^{-1}$, which is comparable with the Doppler half linewidth. In this region where the Doppler and pressure broadened widths are comparable the total effective line profile shape is given by the Voigt line shape. This lineshape is a convolution of the Gaussian (Doppler) lineshape with the Lorentzian (pressure broadened) profiles. Figure 4.13 shows the direct absorption Voigt lineshapes at 7 different pressures obtained from HITRAN corresponding to an ethane concentration of 1 ppm, temperature 293 K over a 100 m pathlength. A high ethane concentration was used to avoid a severely quantised output.

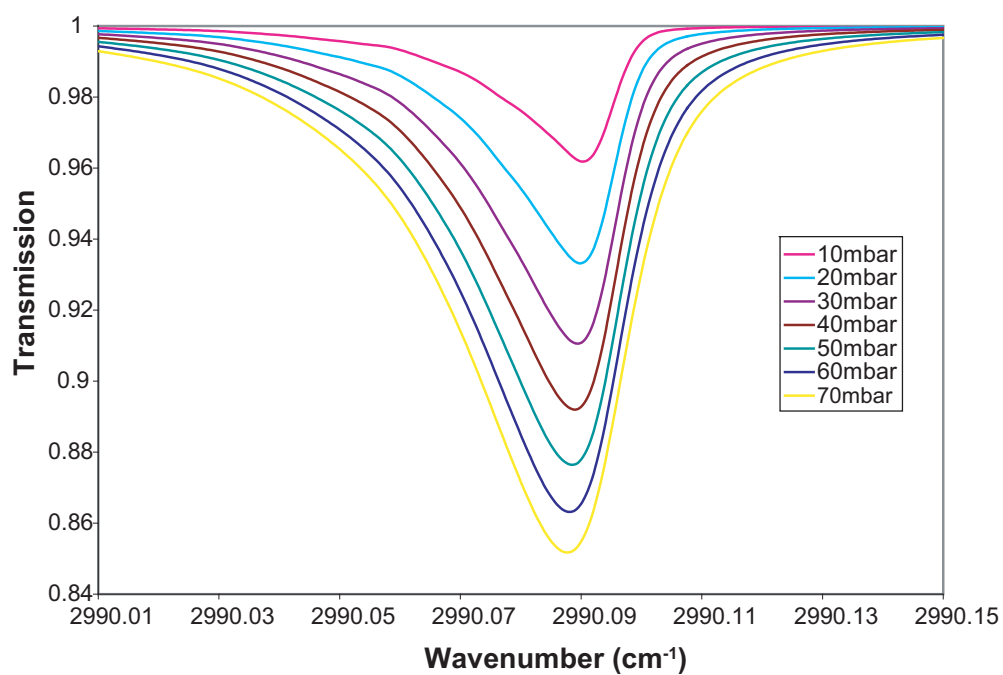


Figure 4.13: Theoretical Voigt transition profiles found using HITRAN for direct absorption at 7 different pressures. Ethane concentration 1ppm, temperature 293 K and 100 m pathlength.

Pressure monitoring

The Herriott (sample) cell is maintained at a pressure of 40 mbar to within 2% using a regulator valve on the inlet to the cell and monitored in the LabVIEW control software using a pressure gauge (BOC Edwards, APG100).

The reference cell is filled with ethane at a concentration of $500 \text{ ppm} \pm 2\%$ at a pressure of $40 \pm 0.1 \text{ mbar}$. For a fixed amplitude of scan (i.e. amplitude of laser current ramp) the observed width in the LabVIEW control software of the measured reference ethane transition is dependent on the cell pressure. Therefore any significant increase in pressure (i.e. a leak) is easily identified by an increase in the observed width of the ethane transition.

Effect of pressure variation

Changes in pressure affect the reported ethane concentration and the accuracy is therefore dependent on the average pressure being maintained at the constant value of 40 mbar. Fluctuations in pressure about the average value affect the sensitivity rather than the accuracy. As described in section 3.1 the reported sample cell concentration is based on curve fitting between the demodulated signals from the reference and sample photodetectors. The least squares fitting algorithm in the LabVIEW software compares the $2f$ lineshape from the sample channel to that of the reference channel and reports coefficients for the scaling factor and offset. It is the scaling factor that is used to calculate the ethane concentration. A increase in sample cell pressure will increase the absorption as there is more gas in the cell, as shown in figure 4.13. This will affect the $2f$ lineshape and leading to a change in reported ethane concentration. This was tested by adjusting the sample cell pressure via the valve on the inlet to the cell and recording the height of the sample $2f$ lineshape.

The results, shown in figure 4.14, show that the height of the $2f$ lineshape is directly proportional to the pressure. As expected, this has a direct effect on the reported ethane concentration, also shown in figure 4.14. The reported ethane concentration was found to be linearly proportional to the pressure over the 10–60 mbar range.

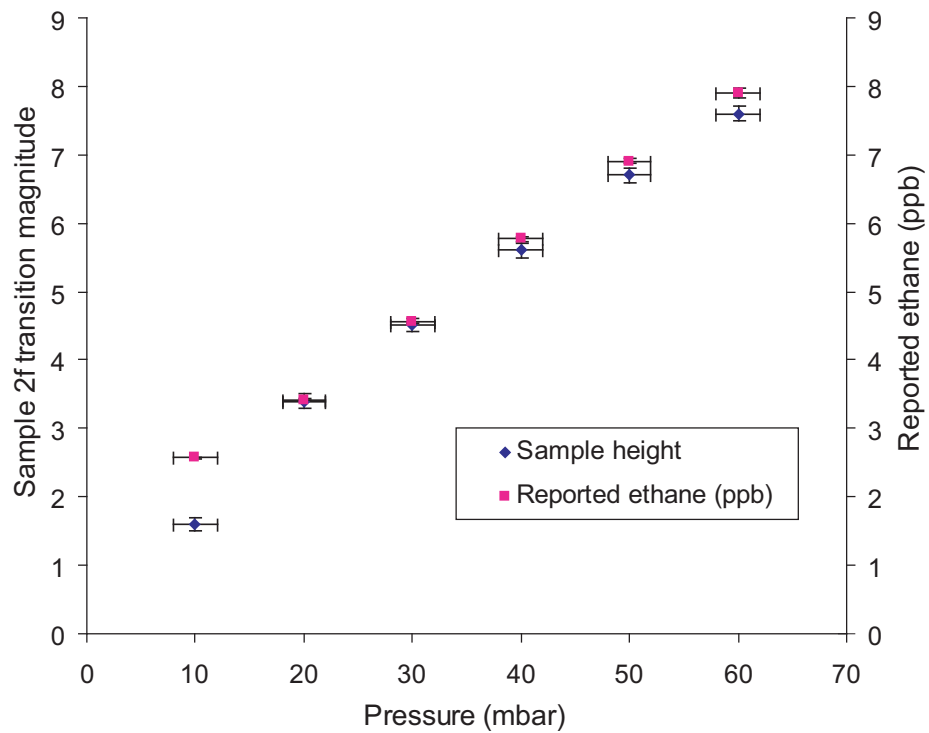


Figure 4.14: Measured effect of sample cell pressure on the magnitude of the $2f$ sample lineshape and on the reported ethane concentration. Both were found to be linearly proportional to the sample pressure (reference cell pressure kept constant).

The experimental results suggest that maintaining the Herriott cell pressure to within ± 2 mbar would reduce changes in reported ethane concentration to $<1.5\%$. The reference cell pressure is manually checked every few months and refilled if necessary.

4.6 Other factors affecting performance

4.6.1 Ambient temperature

The instrument was generally operated with good performance across a range of temperatures both indoor and outdoor and no problems were encountered with temperature variations during an outdoor field trial of the instrument (See chapter 5).

However, large increases in ambient temperature ($\gtrsim 22^\circ\text{C}$) were sometimes found to affect the overall instrument performance. Initially, overheating affected operation of the instrument only while the lid was on, decreasing the performance of the photodetectors and resulting in significant loss of sensitivity. This was solved by the addition of larger heatsinks and two computer cooling fans mounted on the photodetector modules. A more serious issue was that the compressor was occasionally unable to maintain the required laser temperature of around 90 K. This was usually solved with thermal-cycling. More recently, difficulties were encountered in even achieving the required low temperature for laser operation. The effect of ambient temperature and other factors on this was investigated. The problem was eventually solved by replacing the compressor, after it transpired that it had unexpectedly reached the end of its lifetime earlier than predicted.

An experiment was attempted to assess the effect of temperature on the instrument sensitivity. The instrument was operated in the lab and was measuring room air with all doors and windows closed while the ambient temperature was increased using the air conditioning/heating system and a number of electrical heaters. However in practice it was extremely difficult to control and measure the temperature the instrument was exposed to, as there were large spatial fluctuations in temperature across the room. No significant results were deduced from this experiment.

4.6.2 DC light levels

To centre the scan of the laser wavelength over the ethane transition the supplied laser current can require fine adjustment on instrument start-up and often requires greater adjustment after thermal-cycling. The DC light levels at the reference and sample photodetectors depend strongly on the laser current. In addition, these light levels can slowly vary during instrument operation due to thermally-induced changes in alignment. Therefore, the calculated ethane concentration was multiplied by the ratio of the light reference DC light level to the sample DC light level. This technique was used to normalize for changes in the overall light level and also for relative changes in the DC levels between the photodetectors. However the technique relies on the linearity of the photodetectors for both DC and AC signals.

The effect of varying the detected light levels on the reported ethane concentration was investigated by adjusting the beam alignment. The results are shown in figure 4.15. The slightly non-linear response of the detectors is significant when the light levels are aligned to below 50% of the maximum. However, thermally-induced alignment changes are normally within 25% of the maximum light levels and the impact on the reported ethane concentration is small.

In addition to genuine changes in light level at the photodetectors, the reported values vary due to drifting offsets of the various stages of detection electronics, particularly the photodetector modules. Offsets can be compensated for in the LabVIEW software by blocking the laser beam for a few seconds and manually adjusting the compensation value in the program. This technique was found to be preferable to switching off the laser: The heating caused by switching the laser back on results in a temporary change in wavelength of the laser light. This can require up to a few minutes to settle down, often requiring fine adjustment of the laser current to return to the necessary working wavelength.

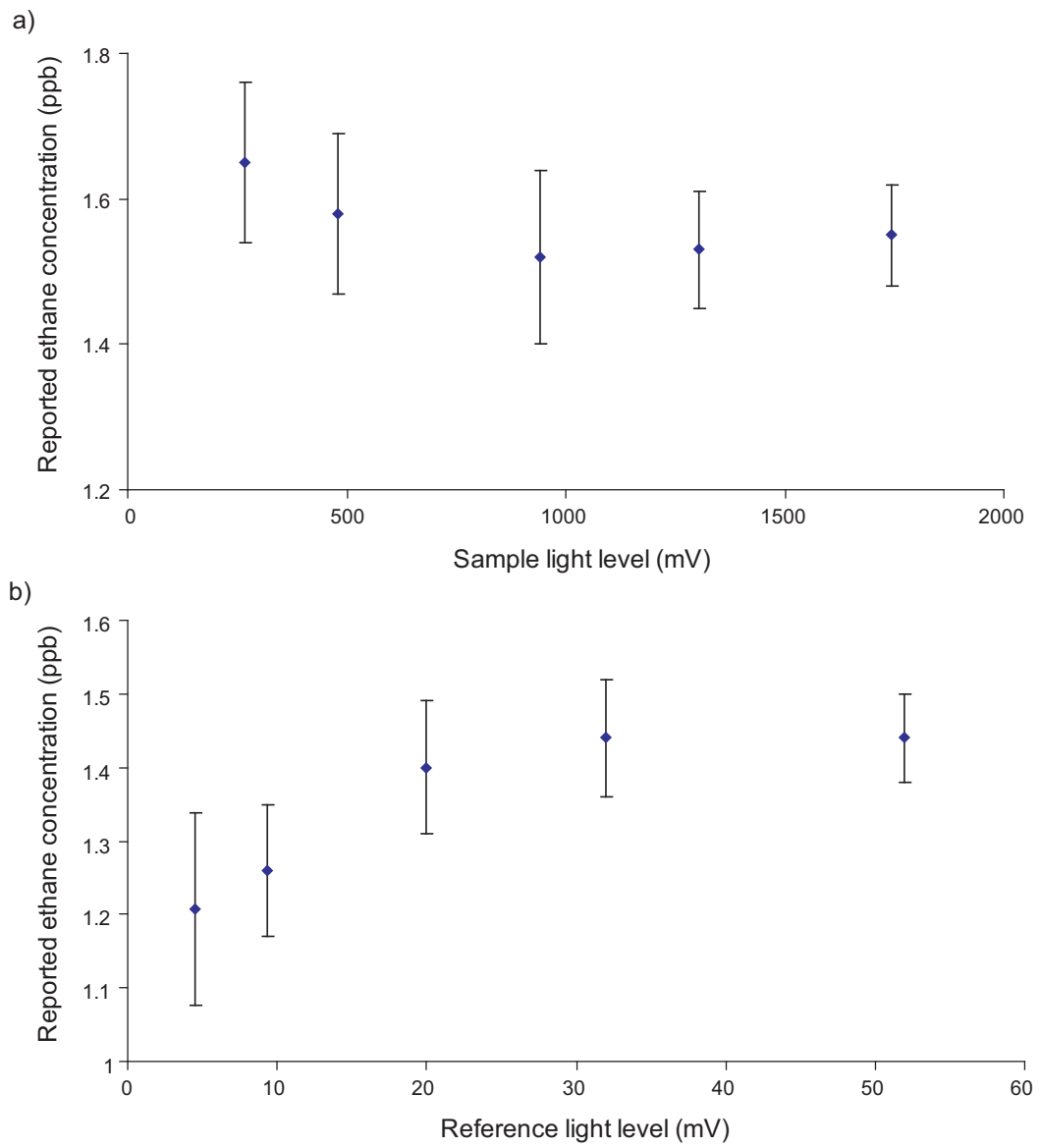


Figure 4.15: Changes in reported ethane concentration due to reduced light levels at sample and reference photodetectors

4.6.3 Optical fringes

Optical fringing affects the instrument accuracy and sensitivity, setting a limit on the time intervals between zero-referencing. The fringes arise from reflections between objects at a distance L apart. Optical fringes are observed in the reference channel with approximate spacing of 0.6 nm. The spacing between the two surfaces causing back reflections and therefore optical fringing can be calculated as follows:

Constructive interference occurs when $2L = m\lambda$, where m is an integer.

Constructive interference next occurs for the new wavelength $2L = (m + 1)\lambda_{\text{new}}$

$$m\lambda = (m + 1)\lambda_{\text{new}} \implies m = \frac{\lambda_{\text{new}}}{\lambda - \lambda_{\text{new}}} = \frac{\lambda_{\text{new}}}{\Delta\lambda} \simeq \frac{\lambda}{\Delta\lambda} \quad (4.15)$$

$$\therefore L = \frac{m\lambda}{2} = \frac{\lambda^2}{2\Delta\lambda} \quad (4.16)$$

For $\lambda = 3.34 \mu\text{m}$ and a fringe separation of $\Delta\lambda = 1 \text{ nm}$

$$L = \frac{(3.34 \cdot 10^{-6})^2}{2 \cdot 10^{-9}} = 0.0056 \text{ m} = 5.6 \text{ mm} \quad (4.17)$$

This separation corresponds to the distance between the reflecting surfaces in the calcium fluoride beam splitter (5 mm). These fringes were minimised by placing the beam splitter at an angle of 45° to the incident beam. Additional fringes were also observed in the reference channel of $\sim 0.05 \text{ nm}$ spacing corresponding to a separation distance $L = 11.2 \text{ cm}$. This distance corresponds to the length of the reference cell and the fringes were suppressed by maximizing the angle that the beam entered the reference cell. Weak optical fringes with spacing 0.3 nm were observed in both the sample and ref channel and may be due to back reflections between the microscope objective and the laser dewar window. These could have been reduced with the use of a parabolic mirror to collimate the light exiting the dewar, rather than the microscope objective.

Sampling time	1 s
Response time	2.5 s
Ethane sensitivity	0.07 ppb
Minimum detectable absorption coefficient	$1.05 \cdot 10^{-9} \text{ cm}^{-1} \text{ Hz}^{-1/2}$
Repeatability	3%
Cross-sensitivity to methane	0.1 – 1 ppb ethane per 1 ppm methane
Operating laser temperature	87.6 K
Operating laser current	630 mA
Modulation frequency	8 kHz
Modulation depth	780 MHz
Optical pathlength	$\sim 108 \text{ m}$
Sensitivity to pressure change	1.9% per mbar at 40 mbar
Maximum ambient operating temperature	$\sim 25^\circ \text{C}$
Required alignment	50%
Physical dimensions	1 m x 0.5 m x 1 m
Weight	$\sim 200 \text{ kg}$
Power requirement	1.8 kW

Table 4.4: Instrument specification

4.7 Discussion

In this chapter the instrument has been characterised in terms of its sensitivity, accuracy and selectivity. An instrument specification is given in table 4.4. The sensitivity to ethane of 70 ppt over a 1 Hz sampling rate corresponds to a minimum detectable absorption coefficient of $1.05 \cdot 10^{-9} \text{ cm}^{-1} \text{ Hz}^{-1/2}$. The noise sources contributing to this sensitivity were investigated. The measured intensity noise was found to be around a factor of 10 higher than the calculated shot noise. However the actual intensity noise will include additional factors such as such as laser amplitude noise and vibrational induced noise. Since the detector noise was also found to be almost a factor of 10 higher than expected a possible explanation is that the detector responsivity, specified to be $> 36000 \text{ V W}^{-1}$, was actually much higher than this and therefore the estimated power at the photodetectors was therefore too low. However, even taking this into account, the electronic noise was found to be significantly higher than expected. It is possible that electrical noise from the oscillator, the filters and/or the power supplies affected the detected signals. This would have been investigated much further had there not been a the need for immediate use of the instru-

ment in a number of clinical trials. On the whole, however, the achieved sensitivity of 70 ppt for the portable system is actually better than the previous lab-based system which had a sensitivity of 100 ppt.

The modulation depth, optical pathlength and operating pressure were also considered. These parameters are similar in the sense that the optimisation of each is a compromise. A large modulation depth gives a strong second derivative signal, but it must not be so large that the signal is averaged out. Increasing the optical pathlength will increase the absorption, but the reduced detected power results in a lower signal to noise ratio. While increasing the pressure also increases absorption, it must be kept low enough to achieve the required selectivity.

Thermal management issues were solved to a certain extent to deal with the effect of variations in ambient temperature. However the instrument performance is still affected by variation in detected DC light levels and electronic drift. Together with optical fringing, there is a limit to the length of time the instrument can be operated with good performance before zero-referencing. The photodetectors were carefully chosen from a limited number of suppliers and have a high specified detectivity. However it would perhaps have been useful to have considered more carefully the thermal stability to reduce drifting offsets. Optical fringing was reduced as far as possible. The use of a parabolic mirror rather than a microscope objective may have helped further reduced this.

Finally, single mode operation of the laser is required to prevent absorption signals from other modes interfering with the signal from the ethane transition. It has been found by the Glasgow Optics group that single mode operation at one of two transitions, 2986.7 cm^{-1} and 2990.09 cm^{-1} , is essential for our current and previously reported ethane sensitivity. While not an easily quantifiable source of noise in terms of sensitivity reporting, it does significantly contribute to practical sensitivity. The modal structure of the lasers tends to decline after prolonged periods, and particularly after thermal-cycling. Thermal-cycling for the portable instrument was required every few months as power levels and mode purity were found to decline. Over the three years of laser use, the time intervals required between thermal cycling decreased from several months to approximately one month. In our previous systems, after several years the decline of mode purity significantly affected the performance. By replacing the laser diode in our lab-based system a dramatic im-

provement was instantly seen in the overall performance. The replacement (or at least detailed re-characterisation) of the laser diode used in the portable instrument could be useful. However the next generation of the system will instead incorporate a quantum cascade laser or optical parametric oscillator.

Chapter 5

Field-trial of the portable spectroscopy system

This chapter describes an outdoor field trial in which the performance of the new portable spectroscopy system was evaluated and data was collected for the further development of gas dispersion models.

5.1 Background

There are many applications for spectroscopic trace gas detectors in industry [8, 15, 68]. The original motivation behind the development of a field-portable ethane sensor at the University of Glasgow was the potential application to oil prospecting as described in section 1.5.1. Measurement of ethane concentration along with wind speed and direction can be inverted to establish a source distribution, allowing rapid and remote surveying of a large area. Current research in this area also involves the optimisation of gas dispersion and inverse models for future trials [69]. A field trial of the portable instrument allowed us to gather information which was then used for further development of gas plume dispersion and inverse models by other members of the Glasgow Optics group. We were also able

to evaluate the instrument performance during outdoor use for measurements both while stationary and while in a moving vehicle.

5.2 Outdoor field trial

5.2.1 Overview

The trial was conducted at a disused airfield in northern England and comprised a controlled release of natural gas (5 % ethane 95 % methane) at a rate of 10 l min^{-1} . The resulting ethane concentration was measured using the portable instrument at over fifty locations around a track occupying the perimeter of the airfield. The instrument was housed in a van and, for the main part of the trial, was driven from one measurement location to another. At each location the ethane concentration was monitored on a second by second basis for a six min period via a sample inlet tube mounted above the vehicle. See figure 5.1. GPS position was also recorded for each location and measurement distances from the release ranged from $\sim 20\text{ m}$ to $\sim 500\text{ m}$. The instrument was also used to perform a number of real-time gas plume traverses. A map of the measurement locations and plume traverses is shown in figure 5.2. The wind speed and direction was simultaneously recorded by an anemometer permanently located at the base station of the site also shown in figure 5.2.

The total power requirement, of around 2 kW (see section 3.3) was met by a 4 kVA (2.7 kW continuous) portable petrol generator, capable of up to 13 hrs of operation between refueling. The generator was transported on a trolley behind the van to reduce the effect of the vibrational noise on the instrument performance (see figure 5.1). An additional air filter was added to protect against mirror losses in the Herriott cell due to the presence of airborne dust.



Figure 5.1: The portable instrument was housed in a van and the generator was transported on a trolley. Ethane concentration measurements were made via a sample inlet tube mounted at the top of the vehicle. Measurements of wind speed and direction were made using an anemometer (shown in the distance).

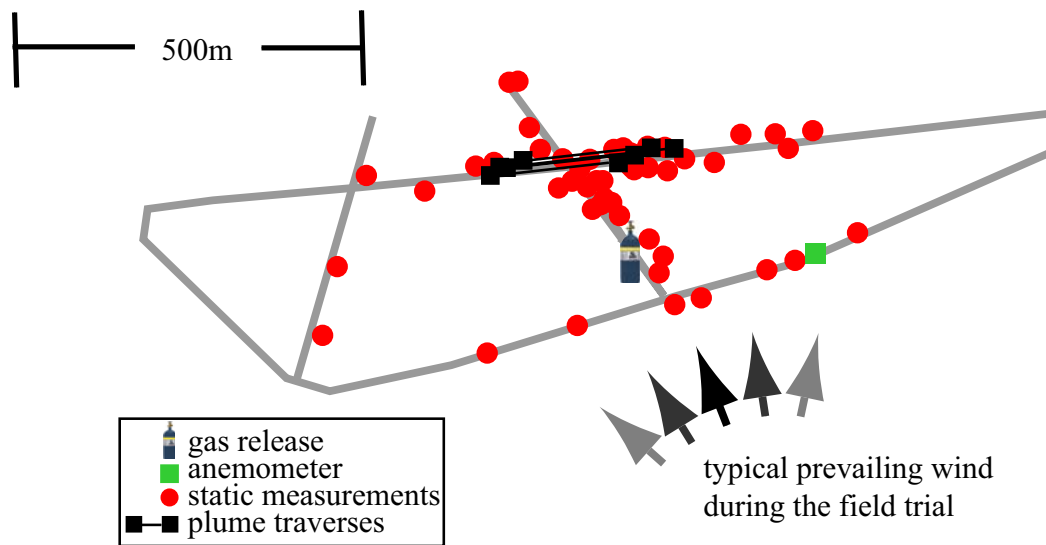


Figure 5.2: Overhead view of the test track showing the tarmac track sections in grey. The locations of static measurements (red circles) and plume traverses (black squares) are shown relative to the gas release point (cylinder) and anemometer (green square).

5.2.2 Gas release

A controlled gas release was set up on a road crossing the airfield, as shown in figure 5.2. A natural gas cylinder (Intertek) with validated ethane concentration of 5.03% was connected through a regulator to a four-arm tubing pattern, each arm of length 8 m as shown in figure 5.3. At typical measurement distances of >100 m from the cylinder this more closely resembled an extended area source. The gas release rate of 10 l min^{-1} was checked regularly by determining the time to fill gas sample bags of a known volume and by also measuring ongoing weight loss from the cylinder using a weigh scale platform.

5.3 Results

Throughout the four days of the field trial, an instrument sensitivity to ethane of around 150 ppt was observed. Very little degradation was observed over the trial, during which

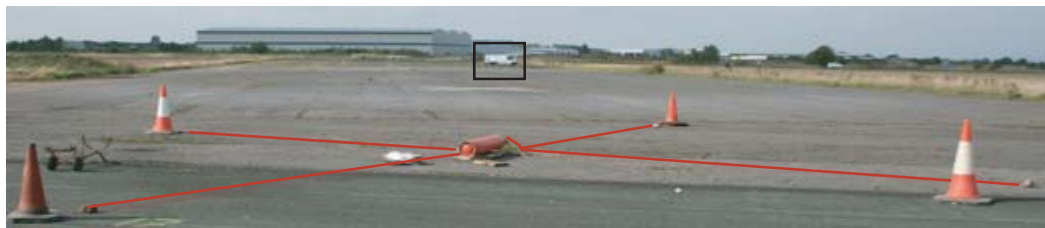


Figure 5.3: The four-arm natural gas release (foreground) and the instrument vehicle in the distance.

sampling was on an average ~ 8 hrs per day. This was frequently in the presence of airborne dust, for example due to crop harvesting in an adjoining field.

5.3.1 Measurement while stationary

Figure 5.4a shows background ethane recorded over one such 6 min period with zero-referencing using nitrogen gas every ~ 90 s. This location is outside the plume with an average ambient ethane concentration of 0.94 ppb and a standard deviation of 0.13 ppb. In figure 5.4b the location is downwind of the release point and ethane concentrations fluctuate as the plume direction alters with wind. The wind data was also recorded at a 1 Hz sampling rate as shown in 5.4c–d and later synchronised with the ethane data. This information is being used to optimise methods for gas dispersion and inverse modelling.

5.3.2 Measurements while in a moving vehicle

Sub-ppb sensitivity was achieved while moving at speeds of up to 5 km h^{-1} over relatively rough terrain, as the system is highly robust to vibration and is liquid nitrogen-free. A sequence of gas plume traverses were measured, in which the instrument was driven at $\sim 1 - 2 \text{ m s}^{-1}$ in a straight line perpendicular to the average wind direction. Since the ethane concentration is displayed in real-time, this allowed the driver to continue the traverse until after the plume had been fully measured.

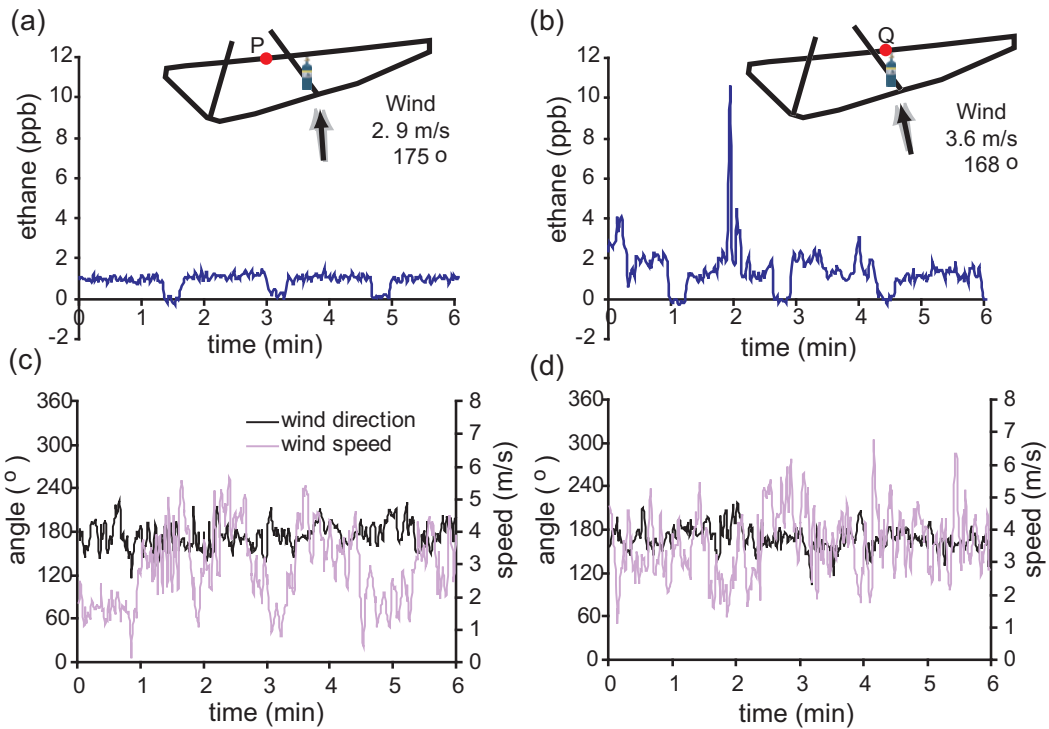


Figure 5.4: (a) & (b) Measured ethane concentration over 6 minutes for two locations P and Q. Zero-referencing with nitrogen occurs every ~ 90 s. In (a) the location is outside the plume and the instrument measures a stable background of 0.94 ± 0.13 ppb. In (b) the ethane concentrations fluctuate as the plume direction alters with the wind. Corresponding wind velocity data is shown in (c)-(d).

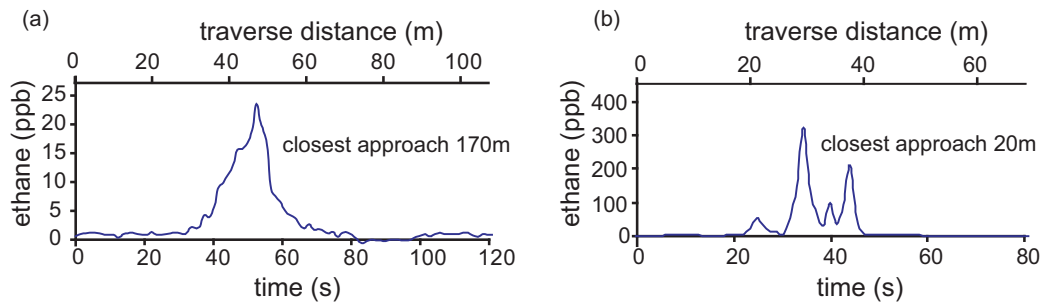


Figure 5.5: Traverses of the gas release plume obtained by driving through the plume at a speed of $\sim 0.9 \text{ ms}^{-1}$. In (a) a far field measurement resembles the plume shape associated with an area source, while in (b) a closer traverse reveals the individual plumes from the four points of the extended release.

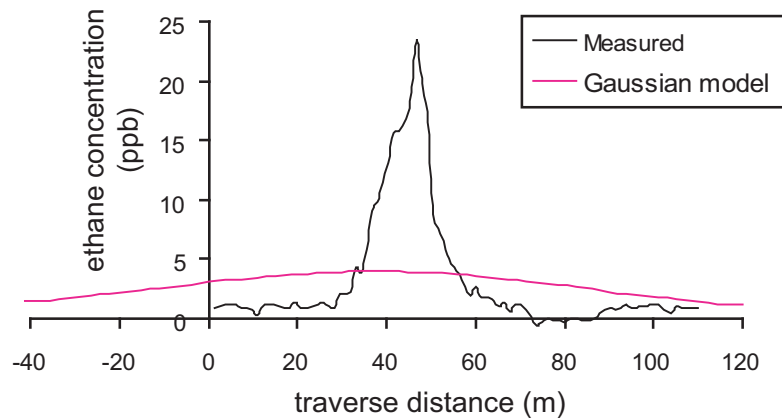


Figure 5.6: Comparison of the measured ethane plume with a simple Gaussian model, at a distance of 170m from the gas source. The Gaussian model shows the statistical ethane concentration over the plume based on 2 min averaging, while our measurements represent the instantaneous plume shape over the much shorter traverse time.

A typical result for the plume traverse at 0.9 ms^{-1} at two different proximities to the release is shown in figure 5.5. The second of these corresponds to being very close to the centre of the release location ($\sim 20 \text{ m}$) where the individual gas plumes originating from each arm of the release could be resolved. In figure 5.5 a at a measurement distance of $\sim 170 \text{ m}$ the source more closely resembled an area release. For this plume a peak value of 23 ppb with a plume width (FWHM) of 12 m was measured.

5.4 Discussion

A number of models are available to predict gas concentration from a known source [70, 71]. Many of these models, such as Gaussian plume dispersion models, rely on the averaging of wind and concentration data over measurement times comparable with the gas transit time. However, these models say little about the plume structure over much shorter timescales associated with a simple traverse of the plume. Employing a simple Gaussian model [69] with 2 min wind data averaging yielded a peak value of 5 ppb and width 75 m of the plume at our measurement distance of 170 m (figure 5.6). At the low wind speed of $\sim 1 \text{ ms}^{-1}$

convection may have influenced the plume, reducing the validity of the model.

As would be expected, since the Gaussian shape is a statistical model of the gas plume based on time-averaging, significant differences are seen compared to the measured instantaneous plume shape over the course of the traverse. However, it is reassuring to note that the integral of each curve in figure 5.6 is similar, confirming that the measured gas flux is in agreement with the set release rate of 10 l min^{-1} .

It has been shown that the location of an ethane gas source can be determined inversely using simultaneous measurements of gas concentration and wind data and a gas plume dispersion model such as a simple Gaussian model [69]. However, the use of a more complex plume dispersion model may enable a more accurate source reconstruction. For example, a model may be able to make use of instantaneous changes in ethane concentration rather than a time-averaged model. The ethane concentration data generated using the portable instrument during this field-trial is currently being used for the development of a new gas dispersion model, which may make use of the second by second concentration fluctuations.

In addition to the generation of new ethane data, the instrument performance was evaluated in a changing outdoor environment. A sensitivity to ethane of around 150 ppt was observed, with little degradation in performance throughout the trial. This is only a factor of two lower than the typical performance in a thermally controlled lab environment of ~ 70 ppt. The reduction in sensitivity during the trial is likely to be due to a combination of factors such as thermal fluctuations during outdoor use and the increase in vibration noise associated with the generator use. The instrument also enabled sub-ppb detection even whilst in a moving vehicle. Although a previous ethane spectroscopy system had been used in hostile environments such as the desert [42] it had, until now, been limited to stationary measurements. The portable system would not be of practical for use in a desert environment due to the high power requirement and thermal management issues associated with the compressor used to cool the laser. However, the trial gave us great confidence in the sustainability of the instrument performance in a changing environment, particularly since its main use would be in a far less hostile environment such as a hospital ward.

Chapter 6

Breath analysis

This chapter describes the motivation behind breath ethane analysis, along with the current detection techniques and technical challenges. The potential clinical application of breath ethane monitoring is discussed and examples of inter and intra-variability in breath ethane of healthy controls are given.

6.1 Background

The idea that human breath might provide information on health conditions dates back to the era of Hippocrates, who is said to have told his students to sniff the breath of their patients. Even today it is recognised that some breath odours are associated with particular diseases: uncontrolled diabetes leads to a smell similar to rotting apples due to acetone in the breath, chronic renal failure can cause a smell similar to stale urine and advanced liver failure can result in a musty fish-like smell in the breath [72]. Scientific analysis of the breath began as early as the 18th century, when Antoine Lavoisier detected CO_2 in exhaled air. In the 1970s Nobel prize winner Linus Pauling determined more than 200 volatile organic compounds (VOCs) in human breath using cold trapping and gas chromatography [73]. Since then more than 3000 VOCs have been identified in the breath

[74]. Breath mainly consists of a mixture of nitrogen, oxygen, carbon dioxide, water, and inert gases. The remaining small fraction of human breath consists of trace components including VOCs at concentrations in the ppb or ppt range [75]. Not only does the detection of such low concentrations presents technical challenges but interpreting the meaning of the results is also difficult. Phillips *et al* conducted a number of studies to build up a database of the composition of VOCs in the breath across the population [74, 76]. Phillips suggested that breath analysis could open up a non-invasive window on normal metabolic pathways, and possibly illustrate how these pathways are altered in disease.

Today, conventional tests for clinical diagnosis and monitoring focus on blood and urine analysis. Common blood tests include a full blood count, to detect conditions like infections, anaemia, and leukaemia, and tests for urea and electrolytes, to detect disease or kidney malfunction [77]. However, blood and urine tests are invasive, often causing discomfort and/or embarrassment. Results can be also subject to a significant delay. On the other hand, breath analysis is a non-invasive technique that could offer invaluable clinical information in real-time.

The field of breath analysis has gained much momentum in recent years, due in part to the relatively recent advent of accurate real-time measurement technologies. For example, nitric oxide (NO) and carbon monoxide (CO) are two breath gases that have attracted considerable interest in recent years as potential respiratory markers [72]. NO and CO have been studied for a over a decade in a variety of lung pathologies and conditions such as asthma [78, 79], chronic obstructive pulmonary disease (COPD) [80, 81] and cystic fibrosis (CF) [82, 83]. The use of fractional exhaled nitric oxide (FeNO) as a respiratory marker is close to being incorporated into clinical practice. In 2003 the US Food and Drug Administration cleared an FeNO analyzer for use in asthma management to be used in conjunction with standard asthma outcomes [84]. Progress in this field, reviewed in [85], is attributable to the large number of studies conducted in this area showing strong correlation between NO and airway inflammation and to the fact that portable FeNO analysers have recently become available [86, 87]. This has made routine testing a practical possibility, enabling home-monitoring of asthma symptoms.

Another area in which real-time breath monitoring may offer clinically useful information is in the assessment of oxidative stress (section 6.3).

6.2 Challenges

Despite promising research and progress in a small number of fields, such as those described above, breath analysis is not yet widely used in clinical practice. Progress has been restricted due to a number of complicating factors [88]: Firstly, breath gases reflect a huge variety of biochemical processes and it is often difficult to interpret the physiological meaning of the presence of such markers. Secondly, there are an enormous number of parameters that can influence results, including exhalation kinetics, ambient levels etc. Thirdly, substances are often present in the breath in extremely low concentration. Measurement techniques must be ultra-sensitive and rapid in order to detect dynamic processes. Ideally measurement would be in real-time with results immediately available to the clinicians. Therefore the technology must be portable so that it can be brought to the bedside.

6.2.1 Ambient levels and compensation methods

At rest a healthy adult has a respiratory rate of 12-15 breaths per minute with an average expiration volume of 500 ml per breath [89]. The first 150 ml of the breath is tidal, essentially ambient, air and the following 350 ml is alveolar air from the lungs [72]. It is the alveolar air that is of interest since it is at the alveolar membranes that blood gases diffuse into the lung. Tidal air tells us nothing of a patient's condition but breath samples contain a tidal component which dilutes the alveolar air and effects the total breath gas concentration. Therefore ambient levels must be taken into account.

Hydrocarbon-free air

One technique is to have the volunteer breathe only hydrocarbon-free (HCF) air [90]. Theoretically, this technique would give the most accurate results since the concentration of ethane in the exhaled breath would then be solely attributable to the production within the body. However, the breathing of HCF air has a number of practical constraints: Firstly a 'washout' period of time is required to rid the lungs of any remaining ambient ethane.

Secondly, for a volunteer to breathe only HCF air, a special mask is required. The delivery of HCF air has been investigated previously within the group. However, experience when recruiting patients for pilot clinical studies has shown that a significant proportion of recruited patients would not be comfortable wearing such a mask for prolonged periods of time. In general its use is impractical due to the expense, discomfort and prolonged time periods required [72]. Therefore, it must be accepted that patients will normally be breathing ambient air and that this must be corrected for.

Background subtraction

Exhaled breath gas concentration measurements are generally, and more practically, corrected by subtracting ambient levels. This standard technique [75, 72, 91] takes account of modest variations in ambient ethane levels. While this technique is not strictly correct in a mathematical sense, since the alveolar and tidal volumes are not equal, the technique is successful in highlighting changes in breath gas concentration arising from changes in the production within the body and distinguishing those changes from those resulting from fluctuations in ambient levels. This technique is widely used and was our chosen technique, ideal for use with large numbers of breath samples.

6.2.2 Previous studies and techniques

The majority of breath gases are analysed using Gas Chromatography (GC) combined with Mass Spectroscopy (MS) and other variants. GC-based techniques reach detection limits down to 0.2 ppb for ethane [92], enabling breath ethane analysis. Such methods are generally time-consuming for large numbers of samples, although improved techniques have been developed for sequential breath sampling [93]. Still, most GC based techniques require pre-concentration of the breath sample and the use of adsorbents and drying agents to deal with the large amounts of water vapour present in human breath [75]. Many compounds can be detected without significant delay using selected ion flow tube mass spectrometry (SIFT) [12]. However, this technique uses precursor ions and ethane cannot be detected due to the lack of a dipole moment. The standard technique of chemiluminescence for measuring

exhaled Nitric Oxide (NO) usually requires bulky and expensive analysers, although hand-held electrochemical sensors have also been developed [87]. In general, studies of exhaled carbon monoxide (CO) have used electrochemistry [94] or GC for measurement. While portable electrochemical units offer the advantage of on-site measurement they are usually less sensitive than GC analysis, which is generally lab-based [72]. Due to these requirements a fast, single-breath resolved breath analysis is not possible with GC [92].

Optical techniques are inherently better suited to breath monitoring applications due to the combination of sensitivity, selectivity and speed. Breath NO has been detected using tunable diode laser absorption spectroscopy [95, 96] and laser magnetic resonance spectroscopy (LMRS) [13]. An exhaled NO sensor (Breathmeter) based on laser absorption spectroscopy is commercially available from Ekips Technologies, Inc. Breath CO has been detected using absorption spectroscopy using tunable diode and quantum cascade lasers [97, 98] and cavity ring-down spectroscopy [99]. Narasimhan *et al* used photo-acoustic spectroscopy to measure breath ammonia in patients undergoing haemodialysis treatment [100]. Cavity-ring down spectroscopy has been used to enable rapid breath ammonia detection [101]. Such techniques are of interest for possible monitoring of kidney function and efficacy of dialysis.

Similarly, real-time techniques for the measurement of ethane could open up a new window on the monitoring of oxidative stress. Real-time ethane detection is currently only possible using optical techniques, such as those described in chapter 1.

6.3 Oxidative stress

6.3.1 Definition

Molecular oxygen readily accepts unpaired electrons to form a number of reduced (or ‘reactive’) oxygen species (ROS), including superoxide (O_2^-), hydrogen peroxide (H_2O_2), hydroxyl radical ($HO\cdot$) and peroxy ($ROO\cdot$) and alkoxy ($RO\cdot$) radicals [102]. In biological materials the generation of ROS is widespread and can lead to initiation and propagation

of free radical chain reactions, resulting in extensive damage to biomolecules [103]. In healthy organisms, normal production of free radicals and other ROS (eg. by metabolic processes) is offset to a certain extent by the antioxidant defence systems. However, the balance is not perfect, resulting in some continual cell damage [72]. The term ‘oxidative stress’ (OS) is defined as an imbalance between oxidants and antioxidants in favour of the oxidants [104].

6.3.2 Associated conditions

Although OS is a normal feature of our oxygen-fueled metabolism, it has also been recognised as playing a role in the development of a wide range of conditions and diseases such as lung cancer [91, 105], cystic fibrosis [106], chronic obstructive pulmonary disease (COPD) [107], acute respiratory distress syndrome (ARDS) [108] and asthma [109]. In addition, OS may be elevated by external factors such as cigarette smoke [110], environmental pollutants [111] and exposure to ionising radiation [102].

6.3.3 Biomarkers

A number of biomarkers can be used for the measurement of OS. Blood markers include malondialdehyde (MDA), thiobarbituric acid reactive substances (TBARS), F₂-isoprostanes, glutathione (GSH) and oxidised low density lipoproteins (LDL) [112, 113, 114, 115]. Breath markers such as exhaled hydrocarbons offer the advantage of non-invasive monitoring [75, 116, 90, 117].

6.3.4 Ethane as a biomarker

The free-radical-induced oxidative breakdown of cell membrane lipids, known as lipid peroxidation, is a main target of investigation into OS [118]. Ethane gas, (C₂H₆), is formed during the lipid peroxidation of omega-3 fatty acids in the cell membrane [119] as shown in figure 6.1. Ethane is a well established marker of OS [116, 90, 117] and is considered to be

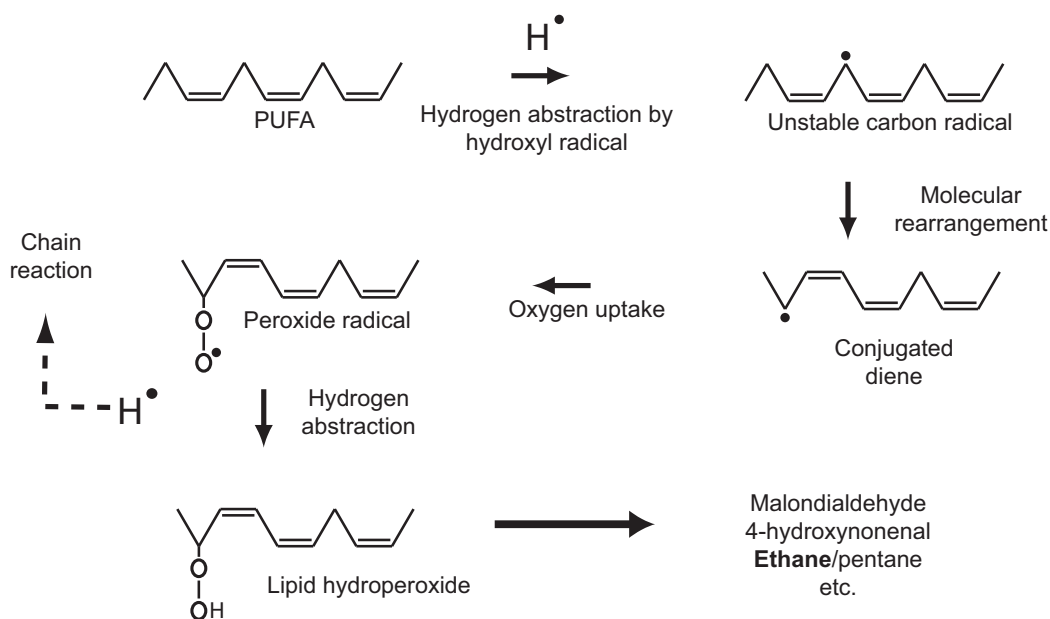


Figure 6.1: Free radical attack on a double bond of a polyunsaturated fatty acid (PUFA) initiates a chain reaction. Several possible products are generated, some of which can be measured as markers of lipid peroxidation [123]

a particularly good marker for several reasons: Its means of generation is well understood [75] and other potential sources (for example from the metabolism of bacteria in the colon) are not considered to contribute significantly [120]. More importantly, ethane appears in the breath within seconds of the release of free radicals in the tissue [72]. Being both poorly metabolised and poorly soluble in the body, volatile ethane diffuses rapidly into the bloodstream and is transported to the lungs where it is exhaled [120].

Breath ethane has been shown to quickly arise following reperfusion injury during organ transplantation [90] or during cardio pulmonary bypass [121, 122]. The speed of the ethane response could facilitate non-invasive patient monitoring applications provided an appropriately periodic and rigorous sampling regime is used. Such monitoring has been recognised as important for gaining insight into oxidative damage in various clinical conditions [75, 103].

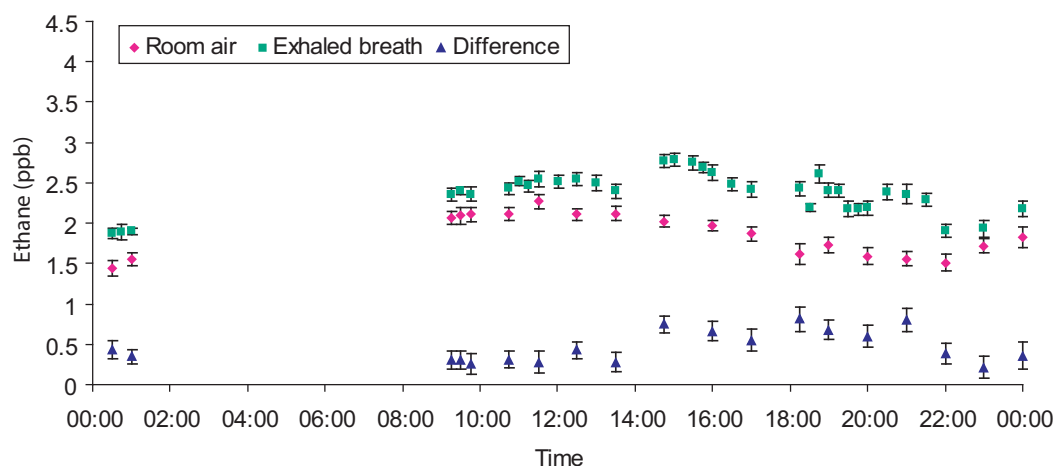


Figure 6.2: Intra-variability of breath ethane of a healthy volunteer over one day

6.4 Ethane levels

6.4.1 Ambient ethane

The average ambient concentration for ethane in the Northern hemisphere has been reported to be ~ 2 ppb [124]. Ambient levels observed by the Glasgow Optics group are typically in agreement with this. Oil reserves are believed to be the main contributor to ambient ethane levels (See chapter 5). Although ambient levels are low, exhaled breath ethane concentrations are often only higher than these levels by up to a few ppb. A key advantage of our technology is that it enables the resolution of even relatively small changes in breath ethane above higher ambient levels. It is even possible to resolve changes in ethane concentration across the breath, due to the increased proportional of alveolar air, as shown in figure 4.2. This level of resolution may provide additional clinical information over and above time-averaged ethane elevations. However, ambient ethane levels must be taken into account in order to resolve subtle changes in breath ethane production.

6.4.2 Breath ethane intra-variability

Since ethane is a ubiquitous marker of OS, breath ethane levels are known to vary considerably even between healthy controls [46] and can even vary significantly in a healthy individual from day to day. Figure 6.2 shows the variability in breath ethane of a healthy volunteer over a 24 hr period (except when the volunteer was asleep). Each breath sample was a single exhalation of vital capacity into a 5 l gas sample bag (Tedlar, SKC). For each breath sample, a corresponding ambient air sample was collected into a sample bag using an oil free pump. The gas samples were then measured using the newly developed spectroscopy system. The error bars represent the standard deviation over the measurement averaging time of ~ 30 s. Background subtraction was performed as described in section 6.2.1. The subtracted ethane levels are seen to vary between 0.21 ppb and 0.81 ppb.

The overall level in the absolute accuracy of the reported ethane concentration is higher than that of the standard deviation in the measurement of the single sample due to factors such as electronic drift, pressure, temperature as described in chapter 4. Subtraction of inspired ethane from the expired ethane concentration reduces some of the systematic errors associated with the above factors. Additional errors are introduced by the expiration and breath collection technique (e.g. dilution of alveolar air is dependant on expired volume). For the majority of our clinical studies, further described in chapters 7–9, it is the relative changes in a patient’s breath ethane from their own ‘baseline’ level that may be of interest. Therefore, the breath ethane results reported for our clinical studies are presented with error bars representing only the standard deviation over the measurement averaging time, to demonstrate the performance of the instrument over a single measurement. If absolute accuracy is required then other factors have to be carefully taken into account.

6.4.3 Breath ethane inter-variability

A previous study conducted by the Glasgow Optics group showed that background-corrected breath ethane in a group of 58 healthy control volunteers (26% smokers) ranged from 0 to 10.54 ppb [46]. The observed median of 1.9 ppb is a typical breath ethane level, with significantly higher levels typically observed in the breath of smokers. Smoking increases

breath ethane levels both directly, in the cigarette smoke, and also indirectly, due to the induced oxidative damage [110, 125].

6.5 Discussion

As described, increased oxidative stress has been associated with a large number of diseases and conditions. It has been proposed that breath ethane analysis could give insight into the biochemical processes occurring in a healthy or diseased human body [75]. However, although breath analysis is often motivated by the prospect of early diagnosis of disease [91], it appears more likely that the potential for breath ethane analysis is in monitoring applications. This is due to the large number of factors affecting breath ethane levels leading to significant inter and intra-variability of breath ethane levels even in healthy controls. Single breath measurements of ethane for a healthy individual have been observed to fluctuate by several ppb over a few days making it difficult to extract useful clinical information from one measurement alone. However, in monitoring applications, such as the assessment of response to therapy or disease progression, or in fields such as critical care and transplantation medicine, rapid analysis of ethane in the breath may provide valuable on-going clinical information.

A number of collaborative studies have been conducted by the Glasgow Optics group over the past few years in a variety of areas such as lung cancer, organ transplantation, exercise, respiratory inflammation in horses, and diet [45]. These trials required discrete sampling methods for breath collection, with later analysis using the lab-based spectroscopy system that was specifically dedicated to ethane breath analysis studies.

Following the development of the portable spectroscopy system, both discrete sampling and on-site breath ethane measurement was made possible. Due to practical reasons, such as the spread of geographical locations at which the trials were conducted, discrete sampling was often used with subsequent measurement performed centrally using the portable instrument. The instrument was then located on-site in the Southern General hospital, Glasgow where the real-time nature of the technique could be exploited.

CHAPTER 6. BREATH ANALYSIS

The following three chapters report on pilot studies in three areas of healthcare in which it was proposed that real-time breath ethane monitoring may offer clinical benefit. These areas are dialysis, radiotherapy and intensive care.

Chapter 7

Dialysis study

This chapter reports on a pilot clinical study in which breath ethane was monitored as a dynamic indicator of oxidative stress in patients as they received dialysis treatment.

7.1 Background

Over the last two decades, evidence linking oxidative stress (OS) and dialysis has grown. A number of groups have reported elevation in markers of OS in haemodialysis patients compared with healthy control groups [126, 127, 128, 129]. While increased OS is considered to be a major factor in morbidity and mortality in dialysis patients [112], the factors contributing to this increase are not clear [130, 131]. Suggested causes include the uremic state [130], vitamin C deficiency [132], inflammatory status and duration of treatment [126]. In particular, it has been reported that the dialysis treatment *per se* may cause oxidative damage due to dialysate quality or dialysing membranes, possibly by the stimulation of primed neutrophils [130, 133]. Techniques directed toward preventing the damage from OS are under investigation, such as the effect of antioxidants [134, 135] and bio-compatible or vitamin E-coated membranes [136].

Past studies of oxidative stress using breath ethane have often involved only a small number of ‘one-off’ measurements, for example before and after a treatment session. However, this approach lacks the resolution to track rapid or short-lived effects and this may have contributed to inconsistent results seen in the literature [129, 137, 138]. The aim of this study was to monitor dialysis patients’ changing breath ethane levels at regular intervals *during* single dialysis sessions.

7.2 Materials and Methods

7.2.1 Participants

Thirty subjects were recruited from patients presenting at the renal dialysis clinics at Glasgow Western Infirmary and Glasgow Gartnavel General Hospital. Patients were recruited subject to the requirement that they were non-smokers and had not consumed alcohol for at least 12 hrs prior to their arrival at the clinic. This was to minimise the risk of known contamination issues. Six patient samples sets were later excluded: four due to anaesthetic contamination, one due to unexplained excessive background fluctuation that swamped the breath samples and the other due to an inconsistent patient breathing technique. The remaining 24 patients (age 65 ± 16 yrs, mean \pm SD, range 39-85 yrs) comprised 19 males and 5 females. Patients had been on dialysis for periods ranging from 4 days to 12 years and received three four-hourly sessions (typically) per week using Polyflux[®] dialysis membranes. The distribution in this period was highly positively skewed (median 10 months, range 0.1 - 141 months).

Patients receiving dialysis treatment had a wide variety of underlying conditions including renovascular disease, polycystic kidney disease, glomerulonephritis, obstructive uropathy, IgA nephropathy, membranous nephropathy and diabetic nephropathy. Five of the twenty four patients were diabetic.

Informed consent was obtained from all participants and the study was approved by the Ethics committee of Universities West of Scotland NHS Trust.

7.2.2 Breath ethane analysis

Ethane concentrations were analysed using the newly developed spectroscopy system. Due to practical constraints, this pilot study involved breath collection using sample bags which were subsequently measured in the Optics lab at the University of Glasgow, only a short distance from the dialysis clinics used in the study. While the real-time nature of the portable technology was therefore not fully exploited in this study, it did facilitate the rapid turnaround of a large number of samples.

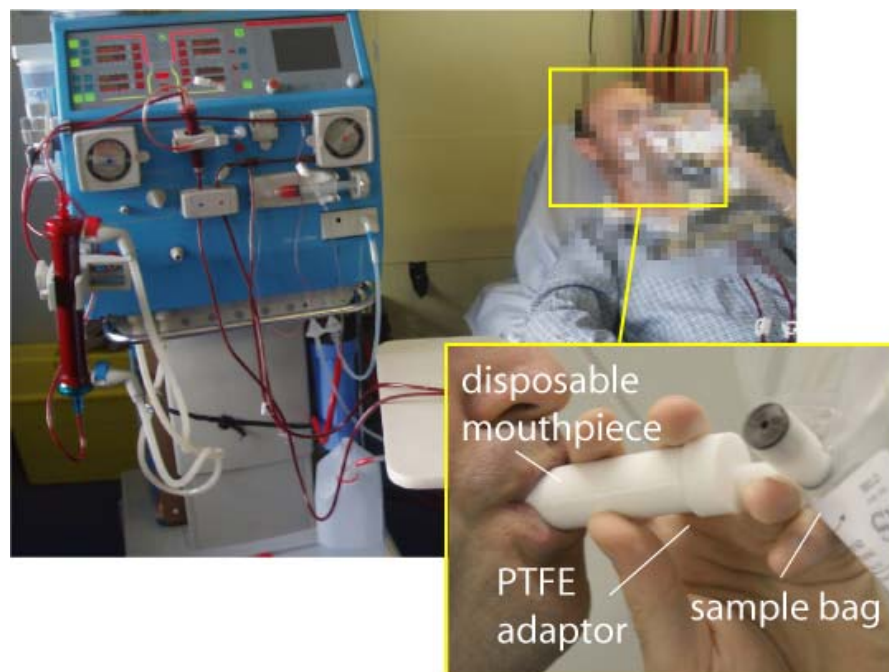


Figure 7.1: Breath samples were collected during dialysis treatment into Tedlar sample bags using a simple single breath filling technique.

A key advantage of the technology is that the direct analysis of gas samples requires no cooling or pre-concentration. Therefore each breath sample was analysed in less than one minute. For example, the 38 samples collected for each patient (as described below) required a total measurement time of less than 40 minutes. Typically, we collected and analysed the breath ethane of four patients in a day. The total number of samples analysed in the study was >1000 . This technique represents a considerable improvement in

measurement efficiency and sample turnaround compared to traditional methods of breath ethane detection.

7.2.3 Study Design

As previously outlined, the aim of the study was to monitor the OS level of patients during a single visit to the dialysis clinic by regular measurement of their breath ethane. Each patient acted as their own control. Baseline breath ethane levels vary between individuals and therefore, in order to validate the comparison of patient data, we measured the extent of the change in a patients breath ethane level from their respective baseline level. In other words, a common datum was defined with respect to patient baseline breath ethane levels by setting these to zero.

Healthy volunteers in close proximity to the patients also provided a concurrent series of breath samples using the same exhalation technique. This secondary control set was in order to verify that the observed effect was solely attributable to patient response and independent of environmental factors.

Frequent sampling throughout the whole of the treatment session was incompatible with the overriding requirement for good patient care. Fortunately, our early work had indicated raised exhaled ethane levels at the beginning of the treatment session and so the most rapid sampling was confined to this period. The collection protocol was set at one sample every 2 minutes during an 8 minute period prior to dialysis, then every 2 minutes for the first 10 min of dialysis followed by every 5 minutes during the next 20 minutes. Three samples were then collected at 10 min intervals and subsequent samples were collected at hourly intervals with a final sample being collected at the end of the dialysis session. The definition of the start of dialysis here is the point at which the dialysis machine commenced the blood flow returning to the patient, typically a few minutes after the initial attachment and flushing of the lines with saline. Precise times of breath collection were subject to small variations (typically ± 10 s) to avoid interference with clinical procedures or interventions. Patient care was considered paramount throughout.

Samples were collected in 5 l ethane-impermeable bags (Tedlar, SKC Ltd). Patients exhaled through a disposable cardboard mouthpiece (Bedfont Scientific Ltd), connected to the sample bags by a Teflon mouthpiece adaptor. The setup is shown in figure 7.1.

Breath sampling

To standardise the protocol, a consistent breath sampling technique was adopted. Each breath sample was a single expiration of vital capacity. Patients found this approach easy to reproduce as is evident from the consistent longitudinal baseline measurements. The initial deep inhalation ensured each exhalation was more than minimum volume (1 l) required for accurate ethane analysis. For each breath sample collected, a corresponding room air sample was obtained using an oil-free hand pump and corrected breath ethane measurements were obtained by subtraction of these ambient ethane levels (as described in section 6.2.1).

Contamination issues

As described in section 4.1.3 the presence of contaminants is easily established using our detection technique. Any contamination causes distortion of the continually monitored ethane transition lineshape displayed in the software. All sampling equipment used was checked for the production of ethane and/or contaminants and no source of either was found. Commonly used hospital cleaning solutions were investigated as sources of contamination. Chlorohexadine gluconoate solution is typically used for patients for whom access is by way of a central line. In the case of fistula access, chlorohexadine gluconoate solution containing ethanol is used. The detection technique is insensitive to both of these compounds. However, ethyl chloride, often used as a local anaesthetic, was found to be a contaminant and was therefore avoided. In this study samples from four patients were affected by contamination due to ethyl chloride and were discarded.

Data analysis

Data are presented as mean \pm standard deviation or median and range. The data were plotted to show the relationships between the magnitude of the ethane peak and other clinical scores, including period on dialysis, age, gender and co-morbidity factors. The Student t-test was used and where data were found not to conform to the parameters of a normal distribution, significance testing was performed using a Mann-Whitney test for non-parametric data. Statistical significance was accepted at $P < 0.05$.

7.3 Results

Patient breath ethane measurements were corrected for the ambient air ethane by subtracting corresponding values (as described in section 6.2.1) and plotted against time. Significant short-lived increases in breath ethane were observed in 14 out of the 24 patients within the first few minutes of the dialysis session. For clarity, since these peaks are largely coincident, a subset of 6 representative examples of the 24 are illustrated in figure 7.2. The effect was not observed in the healthy volunteers who acted as the secondary control group (See figure 7.3) and no further significant increases in breath ethane were observed after the initial 30 min of the treatment session.

Breath ethane levels prior to dialysis treatment (patient baseline levels) are seen to vary between individuals (median 0.6 ppb, range 0 - 12 ppb). This is seen in the positioning of the (background-corrected) traces along the y-axis in figure 7.2.

Ethane is a ubiquitous marker of OS and therefore a large number of factors will contribute to baseline ethane levels. In order to assess the contribution from the dialysis treatment *per se* the datasets were normalised by setting a common zero baseline ethane level. The peak level of ethane (PE) was defined as follows:

$$PE = E_{max} - E_0 \tag{7.1}$$

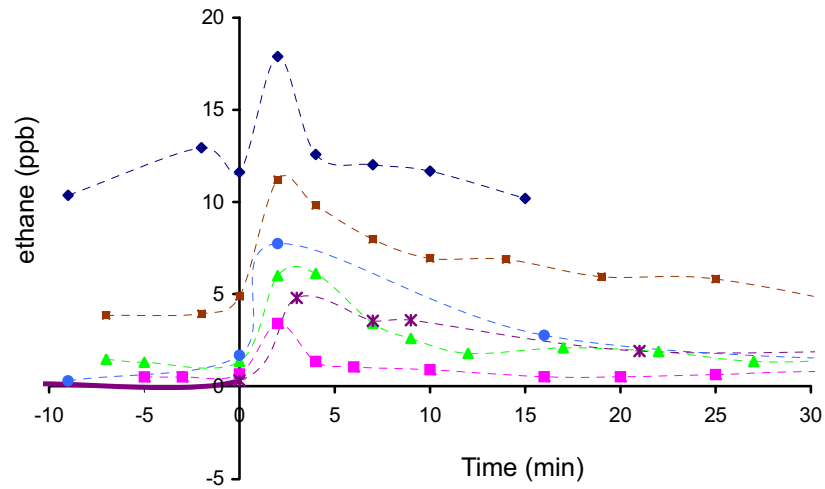


Figure 7.2: Elevation of ethane in first 30 min of dialysis, plotted for six patients. These values have been corrected for ambient ethane levels. The dotted lines have been added as a guide for the eye to make it easier to distinguish between the six different patient results.

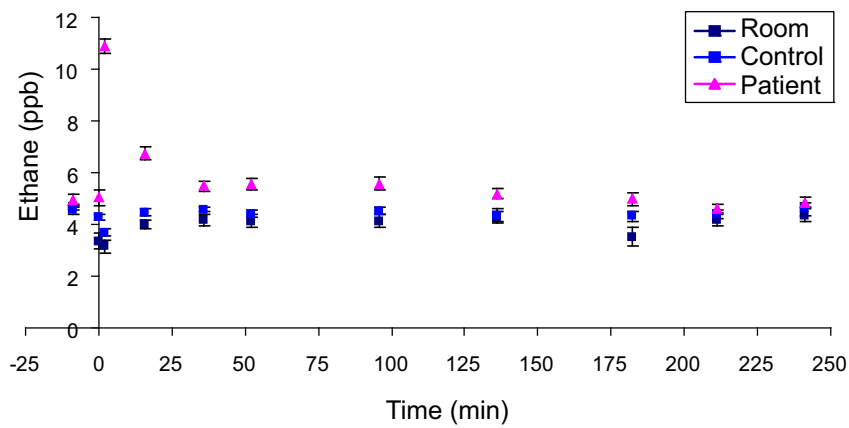


Figure 7.3: Comparison of room ethane, breath samples from a control subject and breath samples from a dialysis patient. This demonstrates that the ethane elevation effect is confined to the patient.

CHAPTER 7. DIALYSIS STUDY

where, E_{max} is the maximum background-corrected breath ethane concentration measured within approximately 5 mins of start of dialysis and E_0 is the mean background-corrected breath ethane concentration measured prior to the start of dialysis. The peak ethane measurements presented therefore correspond to the net change in breath ethane concentration. Peak ethane values for each of the 24 patients along with corresponding patient clinical data is shown in figure 7.4.

Patient	Underlying condition	Diabetes present (1=yes)	Period on dialysis (months)	Age (yrs)	Type of access (1=fistula)	Peak level of ethane (ppb)
1	Diabetic Nephropathy	1	4	43	0	4.77
2		1	4	74	1	7.45
3		1	15	48	0	3.02
4		1	1	82	1	4.66
5	Drug Induced-Lithium	0	11	80	1	0.85
6	Glomerulonephritis	0	60	57	1	0.34
7		0	141	39	1	0.15
8	IgA nephropathy	0	4	39	1	0.31
9		0	20	72	1	0.28
10		0	120	72	1	0.47
11	Membranous Nephropathy	0	0.1	47	0	6.28
12		0	6	85	0	7.28
13	Obstructive Uropathy	0	15	66	1	0.52
14	Polycystic kidney disease	0	0.3	44	1	14.93
15		0	60	50	1	0.62
16		0	115	77	1	0.13
17	Renovascular disease	0	6	67	1	0.15
18		0	6	79	1	0.4
19		0	28	81	1	1.88
20		1	4.5	75	0	2.9
21		0	5	78	1	0.22
22	Unknown	0	10	76	1	1.68
23		0	10	83	1	1.35
24		0	17	49	1	0.2

Figure 7.4: Clinical data and corresponding measured peak ethane values for the 24 recruited patients in the study

The distribution in peak levels of ethane generated by equation (7.1) was also highly positively skewed; median = 0.7 ppb, and range 0.1 - 14.9 ppb. The distribution in the Peak levels was not found to correlate with age. However, the distribution was found to be significantly different in the two patient groups that used either a fistula or a central line

for access. (Mann-Whitney test significant at 0.0069). For patients with a fistula access ($n = 19$) the median Peak level of Ethane = 0.5 ppb; range 0.1 - 14.9 ppb. For patients with a central line ($n = 5$) the median Peak level of Ethane = 6.3 ppb; range 2.9 - 7.5 ppb. However, this is likely to be misleading since patients new to dialysis treatment tend not to have had a fistula provided yet. Period on Dialysis and fistula use are therefore not independent and the ethane peak levels were found to be strongly dependent on the former.

A significant correlation was found between Peak level of Ethane and Period on Dialysis (PoD). See figure 7.5 a. Both variables demonstrated lognormal distributions and a natural log-log plot (figure 7.5 b) yielded a linear relationship ($R^2 = 0.43$). The fitted trendline follows

$$\ln(PE)_{alldata} = -0.5(\ln PoD) + 1.2 \quad (7.2)$$

Modified Charleson co-morbidity scores (CCS) were calculated for all patients (median 5, range 2-11). No significant correlation was found between Peak level of ethane and age, gender or co-morbidity. Although peak ethane appeared to be higher in diabetic patients (median 4.7 ppb, range 2.9 - 7.5 ppb) than non-diabetic patients (median 0.5 ppb, range 0.1 - 14.9 ppb), it was shown that diabetic status was not independent of fistula use and period on dialysis. This is discussed further in [139].

7.4 Discussion

Changes in oxidative stress (OS) have been monitored during dialysis treatment using exhaled ethane as a biomarker. As shown in figures 7.2 and 7.3 we observed a single, short-lived ethane peak on commencement of dialysis, suggesting that there is a significant increase in OS at this time. The absence of this effect in both of the concurrent sample sets of ambient air and exhaled breath from the healthy volunteers (see figure 7.3) suggests that the effect is solely attributable to patient response. The control trace essentially mirrors the relatively flat background air trace. It should be pointed out of course that the healthy volunteers did not receive dialysis treatment. This set of controls should not

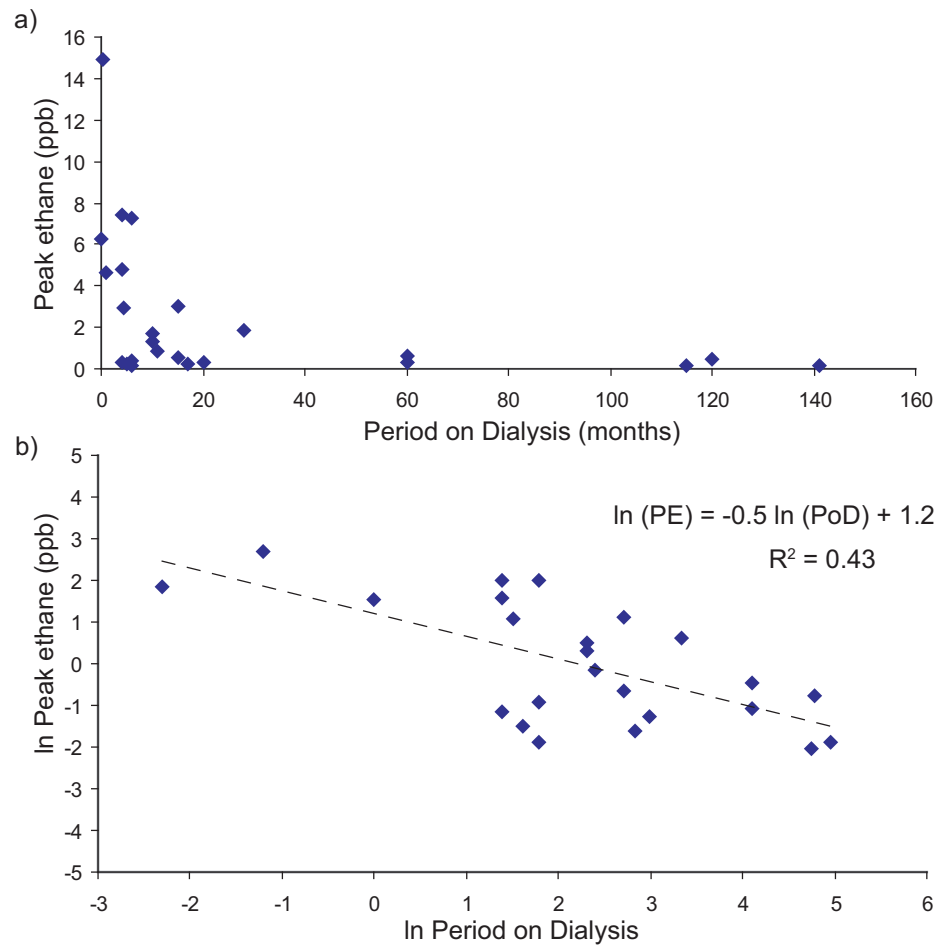


Figure 7.5: (a) Peak ethane dependence on Period on Dialysis. (b) The same data transformed to a natural log-log scatterplot.

be confused with the primary control group. In this study the patients effectively acted as their own control. Each patient provided a series of samples that were referenced to their own baseline breath ethane level, that is, the level measured immediately before the start of their treatment session.

Possible errors due to inconsistent breath sampling were reduced using the breath sampling protocol described in section 7.2.3. The consistency of the observed ethane elevation effect (observed in 14 out of the 24 patients) with ethane concentrations significantly higher than the breath to breath fluctuations found even in healthy controls suggests that the effect could not be solely attributable to patient breathing dynamics. The peaks in breath ethane are unlikely to be due to a reservoir of ethane stored in tissue since ethane is highly volatile and poorly metabolised, rapidly diffusing into the blood stream upon production [72].

It is recognised that a large number of factors affect the overall OS status of dialysis patients, such as age, lifestyle and underlying condition. For example, a higher level of OS has been reported in diabetic haemodialysis patients [128]. While we recognise these factors, this pilot study focused specifically on the detection of rapid *changes* in OS associated with the dialysis treatment *per se*. Normalising peak ethane levels to the patients' baseline ethane levels enabled us to look at this short-term effect across a limited number of patients with a broad range of underlying conditions. Ethane is a ubiquitous marker of OS and baseline ethane levels are known to vary considerably even between healthy control patients [46] and can even vary significantly in a healthy individual from day to day. For this reason it is difficult to extract relevant information from a single measurement of baseline ethane from individual patients in a study with small patient numbers. No significant relationship was found between baseline ethane level and pathology in this pilot study. However, trends may become apparent in a larger scale study. A paper has been published by our clinical collaborators in which the potential biological and clinical relevant factors affecting the breath ethane production during dialysis are further explored [139].

The relatively low level of noise in the expired ethane traces indicate that the consistent breath sampling protocol worked well and that possible variation in patient respiratory rate, expired volume and background ethane had a minimal effect. However, it is important to note that the peak ethane measured for each patient is a conservative estimate of the true maximum. This is due to the finite sampling intervals and the consequential limited

resolution with respect to the changing breath ethane concentration. This may explain the spread in the data shown in figure 7.5 and the relatively low value of R^2 in figure 7.5 b. More frequent sampling could help reduce this spread. However, in practice, acquiring breath samples from a patient more regularly than at 2 min intervals is difficult without disrupting clinical care.

Clearly the speed of the ethane response highlights the need for regular, continual sampling for the detection of such transient events. For example, had patient breath sampling been limited to pre- and post- dialysis, the effect would have been missed completely and the false conclusion drawn that ethane levels (and OS) are unchanged during dialysis treatment. This could explain the conflicting results from a number of previous studies of lipid peroxidation in dialysis patients [129, 137]. Our results are consistent with the findings of Ward *et al* [133, 140] that neutrophil priming, as a consequence of interaction with dialysis membranes, results in a respiratory burst that can lead to lipid peroxidation. Kuwahara *et al* also noted this neutrophil activation [141]. This requirement for frequent breath sampling has also been observed by Stenseth *et al*, who monitored exhaled breath ethane during cardiac surgery. They found that rapid surges of exhaled ethane had a very early onset, starting immediately during the surgical procedures [122]. A future possibility would be to employ the portable instrument directly into the ward with single expirations into the instrument, enabling the breath sampling frequency to be increased.

Figure 7.5 a suggests that haemodialysis patients do become conditioned to their treatment regime relatively quickly, since Peak Ethane levels decrease exponentially with Period on dialysis. This is in keeping with findings of Sezer *et al* that OS was negatively correlated with dialysis duration [142].

Since the observed ethane fluctuations are transient, suggesting only short-term periods of OS, it is unknown if there are any significant long-term consequences of this oxidative damage. It will be important to establish if the repetition of such events have an effect on morbidity or mortality outcomes. If so, it may be that the use of an appropriate intervention could reduce the OS response in patients new to dialysis treatment. Recent approaches include hemolipodialysis, infusion of antioxidants by dialysate and the use of vitamin E bonded membranes [131, 136, 143]. Breath ethane is a specific marker of lipid peroxidation, which antioxidants such as vitamin E can reduce. Therefore, breath ethane monitoring

could offer useful assessment of OS during hemodialysis and the effect of vitamin E-bonded membranes. For example, previous studies in other areas have shown that the production of breath ethane arising from reperfusion injury during organ transplantation [90] or during cardio pulmonary bypass [121] could be reduced using radical scavenging species. A review by Abuja & Albertini [103] suggests that the increasing use of antioxidants in medicine will lead to the requirement for monitoring of OS in a laboratory or hospital in the future.

Future studies with a much greater patient number and a more uniform sample will be necessary in order to determine the potential clinical benefit of such monitoring during dialysis. In this pilot study, practical constraints prevented the recruitment of the ideal patient group, resulting in highly skewed patient statistics (See section 7.2.1), which may have contributed to the R^2 value in figure 7.5 b. Increased patient numbers will also enable better understanding of the variability in baseline levels of ethane among the patients and the possible relationship with pathology and other factors.

A paper reporting on this study has been published in the Journal of Breath Research [144]. This was followed by the publication of a companion paper by our clinical collaborators [139].

Chapter 8

Radiotherapy study

This chapter describes the collection and analysis of breath ethane in radiotherapy patients with the motivation that such analysis may offer potential as a clinical dose mediator. For the first time breath ethane was monitored in patients *during* the radiotherapy treatment process.

8.1 Background

Cancer affects one in three of the population [145]. In the UK, radiotherapy is a key component of both radical and palliative treatment for cancer. Of those cured of their cancer (ie. go on to survive at least 5 years), the use of radiotherapy either alone or in combination with other treatments such as surgery contributes to that cure in $\sim 40\%$ of cases [145].

The main type of radiotherapy treatment is external beam radiotherapy in which high energy X-rays are produced using a linear accelerator and directed in a focused beam, from varying angles, onto the target area of the body. The X-rays used for treatment are at energies typically between 4 and 20 MeV, in contrast to the X-rays used for diagnosis,

typically at keV energies [146]. Radiotherapy is delivered in ‘fractions’ (treatment sessions over a number of days) to reduce the unwanted effects of large doses of radiation on normal tissue. Within our patient group, a typical treatment dose was 2 gray/fraction.

Radiotherapy doses are calculated to minimise the incidence of severe reactions in normal tissue. Due to the significant inter-patient variability of sensitivity to radiation, doses are limited by the minority of patients whose normal tissues are particularly sensitive [147]. Therefore patients given a standard treatment are typically consistently ‘under-dosed’. If the most sensitive patients could be identified prior to treatment then their doses could be lowered to reduce their risk of severe complications [148]. Similarly, therapeutic outcomes may be improved by increasing the dose in more resistant patients. One potential method to identify sensitive patients is the use of predictive assays to determine the radiosensitivity of fibroblasts [148]. However data in this research area is not consistent and predictive tests of cellular radiosensitivity do not allow clinical treatment decisions to be based upon them [149]. Another disadvantage is the lengthy analysis time [150].

8.1.1 Ethane as a dose mediator

The main mechanism behind radiotherapy is believed to be radiation-induced damage to the DNA of tumour cells, with subsequent cell death occurring after a number of cell cycles. The DNA damage occurs directly by ionisation or indirectly via the generation of free radicals [151]. The most reactive, and therefore potentially hazardous, oxygen-derived radical is the hydroxyl radical ($\text{HO}\cdot$). Ionizing radiation generates hydroxyl radicals either directly by oxidation of water, or indirectly by the formation of secondary partially reactive oxygen species (ROS), which may be subsequently converted to hydroxyl radicals in the cell [102].

Lipid peroxidation may be initiated by free radicals produced during radiotherapy treatment [102]. As described in section 6.3.4, ethane is a marker of free-radical induced breakdown of cellular lipids. Therefore we would expect an increase in breath ethane in response to radiotherapy treatment. Further, the amount of ethane produced would be expected to depend on the administered dose of radiation. Since each patient responds differently

to radiation, there may be a relationship between the amount of ethane produced and the patients' individual response to radiation. Therefore, there is a possibility that breath ethane may be useful in the determination of the optimum patient dose.

To determine if this is true it is necessary to first show that increases in breath ethane resulting from the radiotherapy treatment can be detected. This was the aim of our study. If the resultant breath ethane changes are large enough to be detectable above normal breath to breath fluctuations then future steps would involve establishing a link between the increase in breath ethane and the administered dose and investigating patient inter and intra-variability.

8.2 Study Design

8.2.1 Previous study

An earlier trial conducted by our group had attempted to detect increases in ethane resulting from the radiotherapy treatment via manual collection of pre-treatment and post-treatment patient breath samples. Breath ethane was observed to be marginally higher post-treatment [45]. However the results were not significant. Having seen short-lived ethane concentration spikes (over only around 5 - 15 minutes) in our dialysis study (chapter 7), it was thought that the ethane elevation effect was may have been too rapid and short-lived, i.e. that by the time the radiotherapy treatment had finished and patients were able to provide the first of the post-treatment samples, the effect had been missed.

The previous approach involved the collection of single exhalations of vital capacity in a Tedlar gas sample bag along with a corresponding room air sample. However, samples could not be obtained *during* treatment this way as the patients are required to remain in a fixed position on the treatment bed, to within a tolerance of 2 mm [150]. At Ninewells hospital, Dundee, where the trial took place, treatment sessions are typically scheduled every 15 min. The previous trial had required a double treatment session for each participating patient in order that breath samples could be collected pre and post-treatment. This limited the

number of patients who could participate in the study each day and, more importantly, restricted the number of patients that could receive treatment in one day. Since patient care is the overriding priority a new system had to be developed to enable the collection of the breath samples during treatment with the minimum disruption to the normal routine in the clinic.

Design specification for new system

1. Breath and room air samples to be collected *during* a single treatment session
2. Automated system required as personnel not able to access treatment room during treatment
3. Patient must be able to remain in completely fixed position on treatment bed
4. Total treatment session time of 15 min not to be compromised
5. Ability required to easily stop collection if necessary
6. Simple operation by non-specialists
7. Equipment must meet infection control standards

8.2.2 Automated collection system

According to the above specification the following system was developed:

Mask assembly

The set-up is illustrated and photographed in figure 8.1. Patients were fitted with a mask which was connected to a pair of non-returnable valves. This allowed room air to be inhaled by the patient, while the exhaled breath was directed into a 1.2 m length of open-ended tubing of diameter 22 mm (Flextube 1574, Intersurgical). This tubing acted as a reservoir

for the exhaled breath. Breath was continually sampled from the top of this open tubing (figure 8.1 b) using a peristaltic pump (313, Watson-Marlow). The breath was drawn at $\sim 600 \text{ ml min}^{-1}$ through a biofilter and pumped through a length of neoprene 4.8 mm-diameter tubing into Tedlar sample bags using an automated sampling rig, as described below. In addition, room air was also drawn through an identical length of the same neoprene tubing for corresponding background sample collection. The mask assembly was tested in the radiotherapy simulation room prior to patient use (figure 8.1 c).

Sampling rig

The peristaltic pump was fitted with two pump heads, enabling simultaneous collection of breath and room air. The gas samples were collected in 12 Tedlar bags: 6 for breath samples and 6 for the corresponding room air samples. The automated system was designed to direct the air drawn through the pump into the sample bags, filling them sequentially.

The sampling rig, shown in figure 8.2, contains the electronics to control the automated collection. Circuit diagrams are shown in figure 8.3. A timer (LM555, National Semiconductor) was used to produce a clock pulse and a counter (C4017, National Semiconductor) was used to sequentially count through 8 outputs each triggered by the next clock pulse. The first output from the counter corresponded to a delay before sample filling commenced, while the final output terminated the sequencing. The other outputs sequentially switched a pair of solid state relays, which in turn switched off a pair of 3-way valves (3/2 NC, Microsol). This sequentially directed the air flow through a series of manifolds into each pair of breath and room air sample bags. Immediately prior to the sample bag filling, and also when the sampling was complete, the air flow was automatically directed into the room. A switch on the outside of the sampling rig was used to reset the timer and counter, initiating a new collection sequence cycle.

The system was user friendly, housed within a black box with an attached 24V power supply. The clearly labeled switch could be set to *START* to initiate sample filling and to *STOP* to terminate the sample collection at any point. The time to fill each pair of sample bags was adjusted using a variable resistor via a calibration dial on the outside of

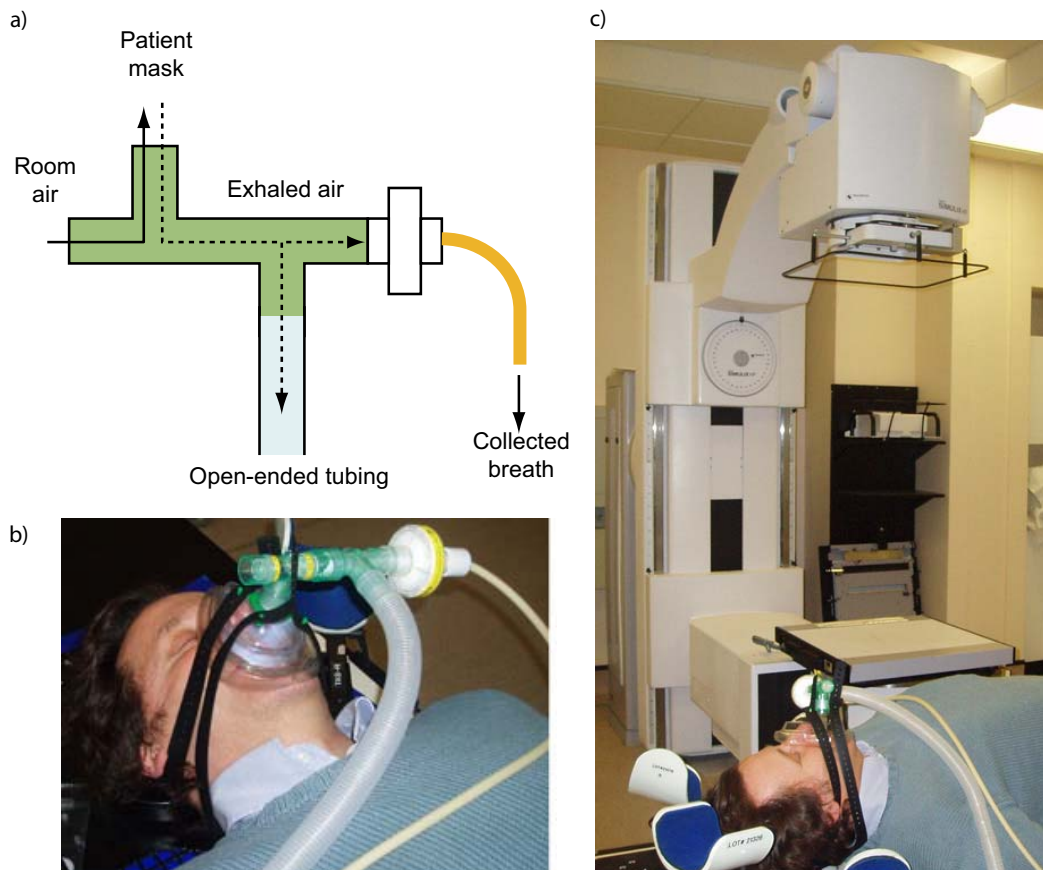


Figure 8.1: (a) Schematic of the breath collection assembly. The non-returnable valves allow only room air to be inhaled while exhaled breath is directed into a length of open-ended tubing from which gas is drawn through a filter for sample collection. (b) and (c) The mask assembly undergoing initial tests in the radiotherapy treatment simulation room.

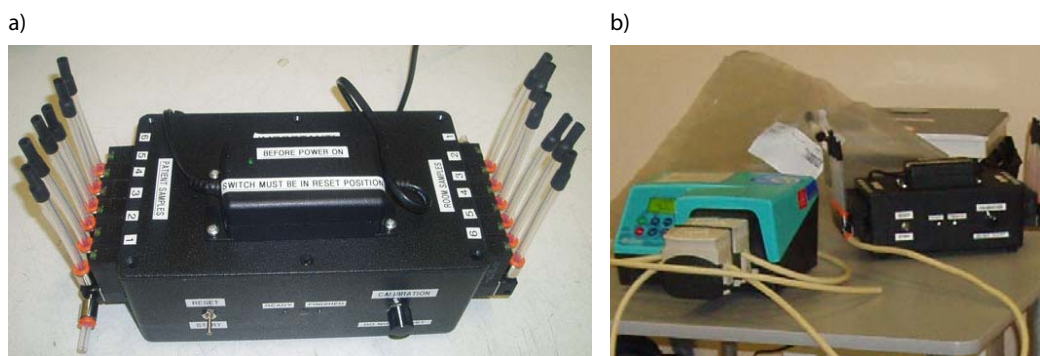


Figure 8.2: (a) The custom-designed sampling rig contains the electronics used to control the automated collection. (b) The sampling rig is used in conjunction with a peristaltic pump to sequentially fill the pairs of gas sample bags (only 1 bag is shown).

the box. Since a minimum volume of 1 l of gas is required for ethane analysis using our detection technique the filling time interval was made adjustable between 2 min and 3 min. During the trial, it was realised that these time intervals were required to be reduced if all sample bags were to be used during a single treatment session. The sampling tubing was then replaced with one of a wider diameter (6.4 mm) to increase the sample flow rate from $\sim 600 \text{ ml min}^{-1}$ to $\sim 1100 \text{ ml min}^{-1}$ and enable the collection of the minimum sample volume of 1 l in each bag. If the patient set-up in the treatment room was rapid, it would be possible to collect all 6 samples. The system was designed so that sample collection could easily be stopped early, as was often required. This ensured that we did not overrun the 15 min allocated to standard radiotherapy treatment sessions. Pre and post-treatment breath sampling was therefore not possible as the treatment session time was not to be compromised in any way for the reasons described above. The equipment was tested for electrical safety by the medical physics department at Ninewells hospital.

The sampling equipment was appropriately labeled and step-by-step instructions were provided for all staff (See appendix C). In addition, two lunch-time presentations were delivered to the radiographers and medical physicists in Ninewells hospital. This was in order to introduce ourselves and the project and to demonstrate the new equipment. The equipment was tested prior to use in the radiotherapy simulation room. This enabled Professor Alistair Munro (Surgery and Molecular Oncology, Ninewells) to experience using the mask assembly and identify potential problems before requesting patient participation. In addi-

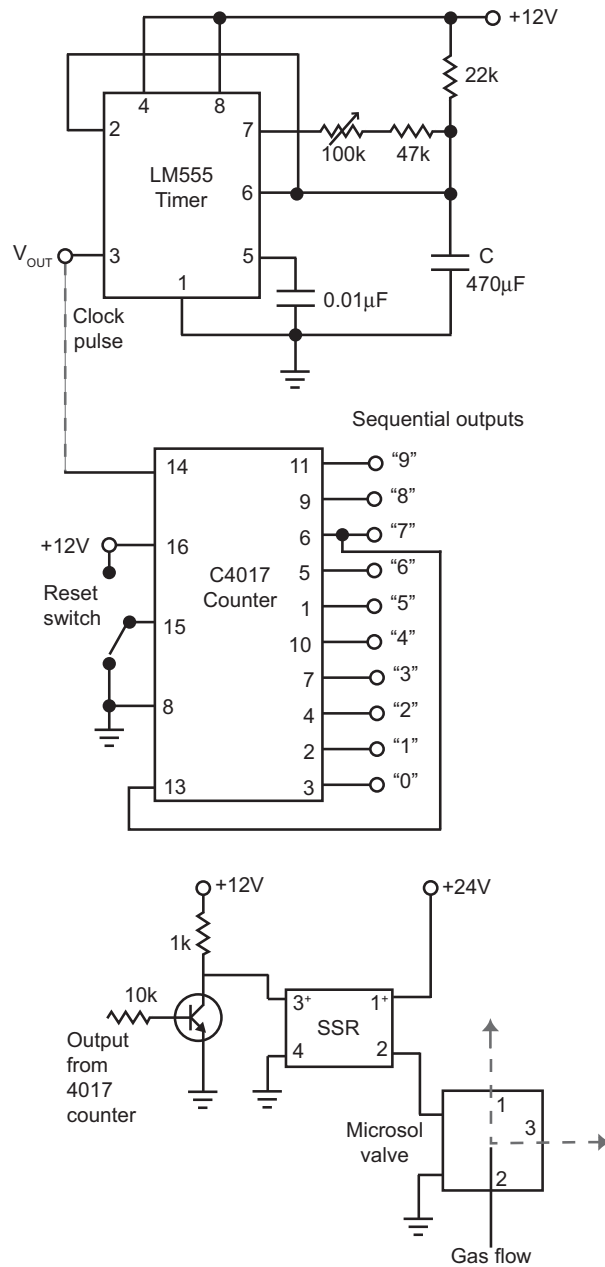


Figure 8.3: Circuit diagrams of the electronics that control the automated sample collection. A C4017 counter sequentially counts through 8 outputs, at a time interval determined by the clock pulse produced with a LM555 timer. The outputs sequentially switch a set of 3-way valves, each via a solid state relay (SSR) and direct the gas flow into the appropriate sample collection bags.

tion, the equipment demonstration was used to emphasise to the clinical staff that patient treatment session times would not be compromised.

Ethane analysis

Collected breath and rooms samples were transported to the Optics lab at the University of Glasgow and the ethane concentrations were measured using the newly-developed spectroscopy system. The samples volumes of ~ 1 l corresponded to a measurement averaging time of ~ 20 s for each sample.

8.2.3 Patients

16 patients were approached to consider participation in the study. Informed consent was obtained at least 24hrs before participation and breath samples were obtained on the 3rd day of each patient's treatment. Of the 6 patients who participated in the trial with successful sample collection, 4 were male and 2 female, aged between 54 and 71.

8.3 Results

Of those 16 patients approached

- 7: Successfully recruited
- 2: Glasgow researchers unavailable to collect samples (same day)
- 1: Patient unavailable
- 2: Patient had dementia/psychologically unsuitable
- 4: Patient anxious/unable to tolerate mask

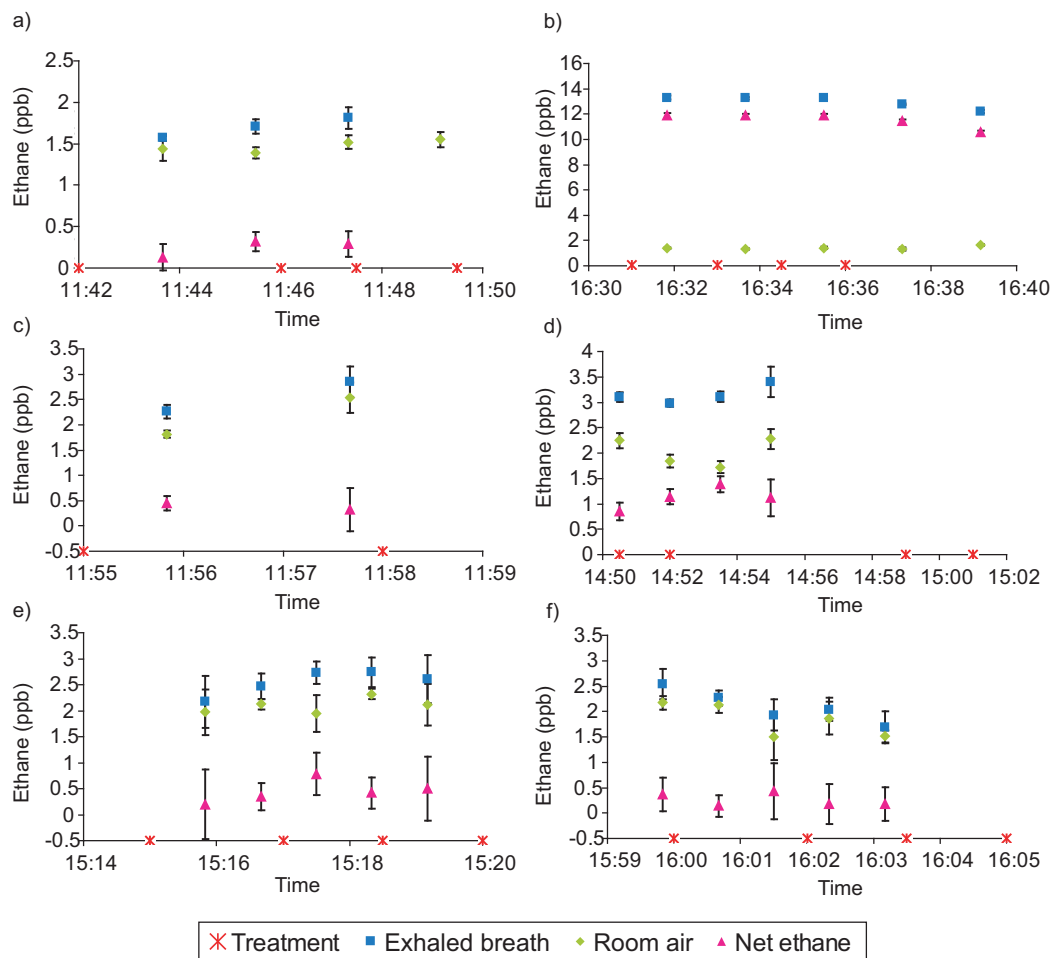


Figure 8.4: Exhaled breath, room air and background-corrected ethane for 6 patients, each during a single radiotherapy treatment session. An asterisk denotes a time when radiotherapy was administered

Patient	No. of breath samples	Mean ethane (ppb)	Std dev (ppb)
a	4	0.24	0.08
b	5	11.54	0.58
c	2	0.39	0.09
d	4	1.13	0.22
e	5	0.45	0.22
f	5	0.27	0.12

Table 8.1: Mean ethane concentration of each set of breath samples collected and analysed for six patients over the course of a single radiotherapy treatment. session.

The samples collected from the first successfully recruited patient were too small to analyse as the sampling rig calibration dial had been accidentally adjusted immediately before sample collection.

For the other 6 successfully recruited patients, the exhaled ethane concentrations were corrected for ambient air ethane by background subtraction, as described in section 6.2.1. The corrected ethane concentrations for all 6 patients were plotted against time for the duration of sample collection and are shown in figure 8.4. An asterix denotes a time when radiotherapy was being administered. The error bars show the standard deviation of the measurement over the sample measurement time (~ 20 s).

The mean ethane concentration and standard deviation of the background-corrected breath ethane samples, along with the number of samples obtained for each patient is shown in table 8.1. For 5 out of the 6 patients, the mean breath ethane concentration was <2 ppb, which is consistent with the typical ethane levels found in healthy controls (See section 6.4). Patient b, with an average breath ethane level of 11.54 ppb, was the only smoker, whose last cigarette had been only 30 min before the beginning of treatment. This explains the higher observed concentration. In addition to the low average breath ethane levels, the standard deviation across each patient's breath measurements was also low, and was typical of breath to breath fluctuations observed even in a healthy control (See figure 6.2, section 6.4). Breath ethane was therefore not seen to fluctuate significantly throughout the treatment.

8.4 Discussion

Although breath ethane has been previously analysed in patients who received ionising radiation [152], this was the first study in which breath ethane was monitored *during* the administration of radiation. Significant breath ethane elevation was not detected in any of the patients who participated in the trial. It is possible that breath ethane fluctuations may have been detected in a larger scale study, particularly if extremely sensitive patients had participated.

A number of difficulties were encountered in this trial. Firstly, the sampling equipment was designed on the basis of a treatment time of approximately 12 min, following discussions with clinical staff. Typically, the treatment involves the administration of radiation from 4 directions, separated by approximately 3 min. However, in practice the timing of the administration of the radiation varied significantly between patients. Patients were only situated on the treatment bed and wearing the mask for the required treatment time, which varied from 3 min (for patient 3 receiving 2-directional treatment) to between 5 min and 10 min 30 s for all other patients who received 4 directional treatment. The scale of this variation had not been anticipated when the system was designed. Although the calibration dial could be adjusted on the sampling rig to vary the time interval between collection and the flowrate of the pump was increased, the approximate treatment timing had to be first estimated for each patient. The clinical staff helped to anticipate treatment timings for each patient. However, in practice this was entirely dependent on the speed and ease with which the staff accurately repositioned each individual patient between changes in treatment direction. Therefore the timing of the collection of breath samples for each patient was not optimised.

Secondly, the use of a mask assembly was necessary to enable collection of breath samples without any additional movement from the patient. It was thought that potential breath ethane effects were likely to be more prominent in the first patient treatment fraction. However, asking patients to participate in the study on the first day of their treatment would be unfair given the apprehension they would already be experiencing. A compromise was reached by asking patients to participate on the day of their 3rd treatment fraction. However, many patients were still extremely anxious and uncomfortable with the idea of

wearing a mask. In addition, of those patients who did view the mask and decide to participate, a few patients did not comfortably tolerate the slight increase in breathing resistance. Therefore, while the sampling equipment was demonstrated to be successful in the first automated collection of breath ethane during radiotherapy treatment, it is clear that the technique is not feasible for use with all patients. Patients appear far more comfortable with single breath exhalations into a collection bag, the technique used in the dialysis study (see section 7.2.3), which was not possible for this study. This study has emphasised that issues encountered in breath analysis lie not only in the technical challenges in the ultra-sensitive gas detection and the interpretation of the results, but also in the practicality and feasibility of introducing breath monitoring in a variety of clinical areas.

Chapter 9

Intensive care study

This study provided pilot breath ethane data from ventilated patients to investigate the possible clinical potential and feasibility of breath ethane monitoring in intensive care. For the first time measurements were made *on-site* using the portable instrument.

9.1 Background

There are several populations of intensive care patients whose clinical management may benefit from early indicators of oxidative stress (OS). Sepsis, for example, is a major cause of mortality in intensive care units and is associated with increased OS [108, 153]. Therefore the detection of changes in OS may be useful in clinical detection and/or subsequent treatment of sepsis. Another potential group is patients who have suffered an acute central nervous system injury: After brain injury by ischemic or hemorrhagic stroke or trauma, the production of reactive oxygen species (ROS) may increase and could lead to tissue damage [154]. It is also possible that measures of OS may be useful for the clinical process of weaning patients off mechanical ventilation, as increased oxidative stress has been associated with diaphragm fatigue [155].

The overall usefulness of breath ethane monitoring, for the assessment of OS, in intensive care patients is unclear. Although breath ethane has been investigated in a range of clinical conditions and procedures it has not been studied extensively in intensive care patients. The aim of our study was to use the portable instrument on-site in a hospital to collect pilot data from ventilated patients receiving intensive care. This was to broadly investigate the possible clinical potential and feasibility of breath ethane monitoring in an intensive care unit (ICU).

9.2 Study design

The study took place in the neurosurgical Intensive Therapy Unit (ITU) at the Southern General hospital, Glasgow. The study was approved by the Multi Centre Research Ethics Committee for Scotland. Patients were selected for participation in the trial if they fell into one of the following four categories: Patients with possible/potential sepsis, patients with sub-arachnoid haemorrhage, patients who had suffered a traumatic brain injury (TBI) or patients who were being weaned off ventilation. Patients meeting this selection criteria had written consent obtained from a relative. The patients had their inspired and expired ventilatory gases sampled non-invasively and the ethane concentrations were immediately determined on-site using the portable ethane spectroscopy system. Initially the instrument was conveniently located in a room beside the ITU ward and the gas samples were measured manually. Later in the trial the instrument was located in the ITU ward and samples were measured using an automated system. The study was observational and non-invasive, involving no additional intervention beyond the routine procedures and therapies conventionally used in the ITU as part of their standard intensive care management. For each patient, the measured breath ethane levels were compared with the corresponding physiological data in order to investigate possible correlation.

9.2.1 Physiological data collection

Patients admitted to the ITU have clinical parameters such as heart rate, respiratory rate and arterial blood pressure (ABP) monitored and displayed on a screen above their bed. In addition, the DocVu system, currently being piloted in the ITU by the Brain-IT group [156], was used to record a range of other physiological data and it allows clinical staff to indicate the occurrence and time-stamp of specific medical procedures or clinical events. This system collects minute-by-minute data from the bedside monitor, along with additional comments entered into the system by clinical staff, and archives it automatically to an in-house server. Patient information such as name, date of birth and unit ID number, are also stored. However, for the purposes of this study, each patient was also allocated an anonymous Patient ID number, which was used for all further referrals to their clinical and breath ethane data.

9.2.2 Breath sample collection

The patient breath samples were obtained using a peristaltic pump (WM313, Watson-Marlow) which was connected to the ventilator using narrow bore (1.2 mm) side-stream sampling tubing (2734, Intersurgical). The pump, shown in figure 9.1, was used to continually draw gas from both the inspiratory and expiratory lines of the ventilator at a rate of 300 ml per minute (per line) and slowly fill two 5 l gas sample collection bags (Tedlar SKC). One sample bag was used for inspired gas and the other for expired gas. For safety, the pumping mechanism was disabled in the reverse flow direction ensuring that the flow of gases was solely from the ventilator and that no gas could accidentally be forced back into the ventilator lines.

A filter (Clear-Guard Bacterial & Viral 1644, Intersurgical) on each line of the ventilator tubing was used to protect the collection apparatus from contamination. The pump and sample bags were situated on top of the ventilator, as shown in figure 9.1b. The gas samples were immediately measured using the portable instrument, either manually or using the automated system. For each pair of gas sample bags, the measured inspired ethane concentration was subtracted from the measured expired ethane concentration.

The resulting subtracted ethane values were used to indicate the ethane contribution from the patient.

Manual ethane measurement

Initially the gas sample collection bags were manually replaced at intervals of approximately 10 min. All bags were labelled with the anonymous patient ID code and a bag sample code. Upon removal the samples were immediately measured using the portable instrument, conveniently located on-site in a medical physics room nearby the ITU ward. On-site measurement was extremely efficient and results were therefore made available immediately. On occasion, on-site measurement was not possible due to practical difficulties and in such cases the samples were stored and later measured in the lab.

A control experiment was run to check that no ethane was produced by the ventilator, pump or tubing. This experiment involved an identical set-up and analysis to that used with a patient, except an artificial lung was used in place of the patient.

Automated ethane measurement

After three patient datasets and a control dataset were obtained it was demonstrated that the gas collection process was running smoothly, although the manual sample measurement system was labour intensive. This manual system was then replaced by an automatic measurement system. This was made possible by bringing the portable ethane spectroscopy system into the ITU ward directly to the patient bedside. The instrument was placed out of the way of clinical staff, behind the patient's bed, ventilator and other clinical equipment as shown in figure 9.1 c.

After discussions with the medical physics team at the Southern General hospital it was decided that the portable instrument should not be used to draw gas samples directly from the ventilator. There are a number of reasons for this: Firstly, the portable instrument gas sampling rate is not easily reduced to the maximum gas removal rate from the ventilator

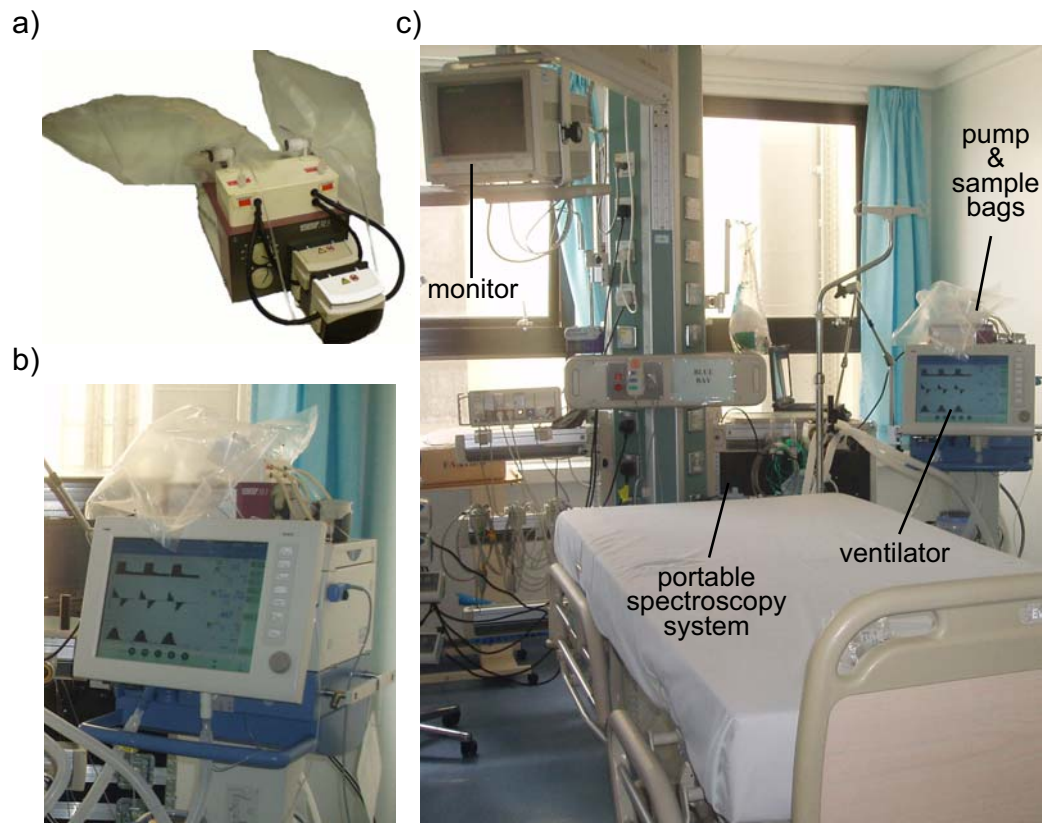


Figure 9.1: (a) The pump and sample bags used for breath gas collection. (b) The pump was situated on top of the ventilator. Inspired and expired breath gases were drawn from the ventilator and pumped into the sample bags. (c) The ITU ward in the Southern General Hospital. The portable instrument was conveniently situated behind the vacant bed, where disruption to clinical staff was minimal.

lines. Secondly, with the gas removal alternating between inspired and expired lines, the gas removal is much harder to compensate for via adjustment of the ventilator settings. Thirdly, it was desirable to automate the system quickly as the pilot study was well underway. The main priority of course was patient safety.

With the above points in mind it was decided the easiest approach would be to make use of the existing collection apparatus. The pump was connected as before to the ventilatory tubing and used to continually draw gas from both the inspiratory and expiratory lines of the ventilator. The gas was directed as previously, into two 5 l gas sample collection bags, one for inspired and the other for expired gas. At intervals of approximately 4 min, 1 l of gas was sequentially removed from the two sample bags and automatically analysed using the portable instrument. The sample bags essentially acted as buffer bags to enable a constant removal of gas from each line of the ventilator (300 ml min^{-1}) and allow subsequent removal by the instrument at regular intervals with a much higher flow rate ($\sim 2 \text{ l min}^{-1}$).

The average measured inspired and expired ethane concentrations were automatically calculated using the LabVIEW software. For each pair of sample bag measurements, the inspired levels were subtracted from the expired levels. These indicate the ethane contribution from the patient and results were updated immediately after measurement of each sample pair. The second-by-second ethane data was also recorded for each patient. Figure 9.1 shows the use of the portable instrument, ventilator and sample collection device with buffer bags (on top of the ventilator) during a trial run in the ward. This set-up was then used for the collection of patient data.

9.2.3 System modifications

In order to enable automatic collection, the portable instrument required a number of modifications: Firstly, normal operation of the instrument uses a 3-way valve to select between the sample measurement line and the zero-referencing (nitrogen) line and draw the selected gas into the Herriott cell. Following discussions with medical physics, it was decided it would not be practical to use a cylinder of nitrogen gas in the ITU for the instrument zero-referencing. The use of a large sample bag as a supply of nitrogen would prevent

longer-term automatic use. Instead, measurements of ethane in the inspired and expired gases were measured relative to the ambient ethane. While measured values of inspired and expired would no longer be absolute, the relative difference between them would remain mainly unaffected. This process required an additional 3-way valve for the selection of either inspired, expired or room air. The additional valve was added and the instrument LabVIEW software was modified to enable automatic selection between inspired, expired and ambient air. The software was also modified to automatically average the ethane concentration over the measurement intervals, subtract the inspired concentration from the expired concentration and plot the resultant subtracted ethane concentration against time. The filling and removal interval times, averaging times and response times could be adjusted via user controls on the front panel of the software.

Secondly, even with the reduced gas flow rate of 1.5 l min^{-1} into the instrument, this gas removal rate from the ventilator was thought to be possibly greater than the safe maximum. Therefore, after a period of gas removal from the sample bags the newly-added valve on the instrument was switched to draw room air into the instrument. This was for a sufficient time to allow the peristaltic pump to completely replenish the sample bags. The total time period used for measurement and replenishing of each pair of sample bags was 3 min 20 s. Continual filling of each bags at a rate of 300 ml per min resulted in a total fill volume of 1 l for each bag in each time interval. For measurement, gas was removed by the instrument for 25 s from each sample bag. This occurred at a flow rate of 1.5 l per min, corresponding to a removed volume from each bag of 625 ml. Therefore, the overall ‘filling rate’ was set to be higher than the overall ‘removal rate’ (averaged over the entire interval time) so that there was no risk of the gas volume in the bags being significantly reduced over time. In order to prevent the bags from bursting due to the excess gas, a small piercing was made on the inlet of each bag.

Thirdly, the gases were drawn into the instrument from the sample bags through narrow bore tubing lines. This tubing was used as the connectors were compatible with the ventilator connections and it could be easily obtained from the ITU for single use with each patient. The usual instrument flow rate of $\sim 3\text{ l min}^{-1}$ is set by an air filter and regulator valve on the inlet to the Herriott cell, with which a pressure of 40 mB is maintained and using wider bore tubing. However, the narrow tubing diameter of 1.2 mm reduced the gas flow rate to 1.5 l min^{-1} and reduced the pressure in the Herriott cell to 12 mbar. Figure 9.2

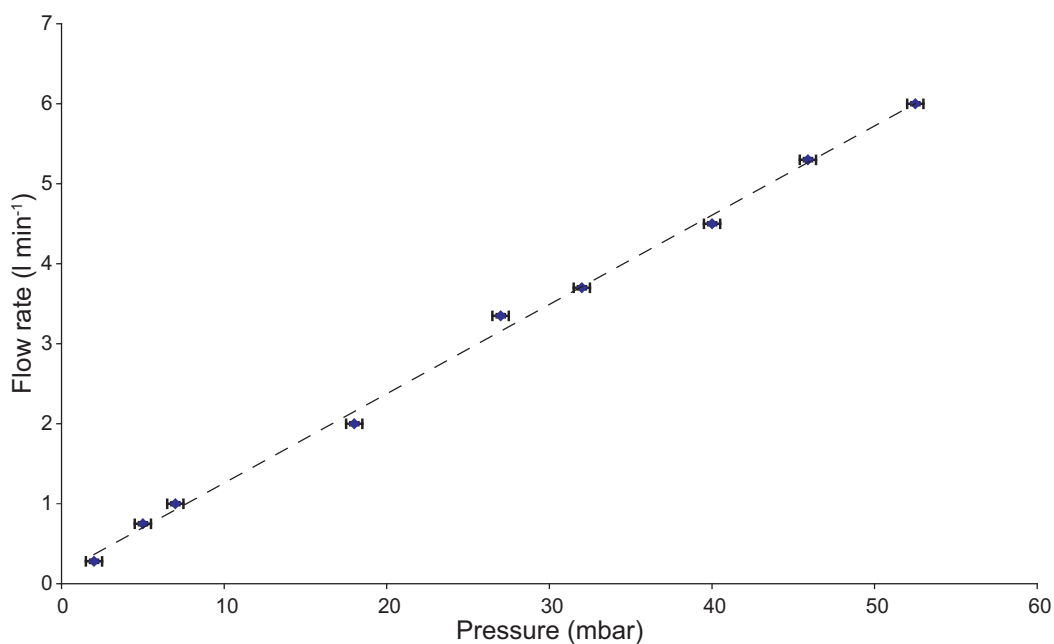


Figure 9.2: The gas flow rate of the instrument depends linearly on the Herriott cell pressure, which is adjusted using the regulator valve on the inlet to the cell.

shows that the flow rate depends linearly on the Herriott cell pressure. However a flow rate sensor was used for these measurements, instead of the usual bag filling technique, along with a change of tubing which altered the impedance of the system. This may account for the observed differences in the flowrate/pressure dependence compared with previously. During automated measurement the instrument was therefore operated at a lower pressure than normal. This, combined with other factors, resulted in the reduced instrument sensitivity of ~ 0.5 ppb. As mentioned in section 4.5.3, differences in ethane transition pressure broadening between the reference and sample cell (due to different background gases) may also be a source of error.

9.2.4 Ventilator modes

Initial tests were performed at the Southern General hospital with the medical physics department to ensure that the gas removal from the ventilators was completely safe for the

patient. The ventilators are operated in a number of different modes, depending on each patient's condition and their stage in the weaning process. A 'leak compensation' setting on the ventilators automatically increases the delivered volume of gas to compensate for any detected gas loss. It was necessary to determine the effect of gas removal during operation of a number of these different ventilator modes with the leak compensation setting switched on. The flow rate of the peristaltic pump used for sample collection was determined to be 300 ml min^{-1} from each line (inspiratory and expiratory). An experiment was performed using an artificial lung to determine the effect of gas removal at this rate on the ventilator readings in the following ventilator modes:

IPPV

Typically, patients entering the ITU are immediately put on an Intermittent Positive Pressure Ventilation (IPPV) mode. In this type of mode the ventilator delivers a preset number of breaths and tidal volume, but no allowance is made for any effort by the patient.

SIMV

In the Synchronized Intermittent Mandatory Ventilation (SIMV) mode the ventilator delivers preset breaths of a certain tidal volume. However, within the breath cycle time the ventilator also allows the patient to trigger a preset breath. If the patient does not trigger a breath in the cycle time, the ventilator again delivers a breath.

ASB

Assisted Spontaneous Breathing (ASB) modes are used to wean patients off the ventilator. Here the ventilator is triggered to deliver a preset breath only when the patient initiates a breath. However, auto-cycling is a problem that can occur if the ventilator interprets fluctuations in the circuit as a patient's attempt to initiate a breath.

9.2.5 Medical gases

The oxygen concentration in the inspired gas is set, monitored and adjusted via the ventilator settings. Ventilated patients are normally receiving inspired gas with oxygen levels between 30 % and 100 %. The required concentration is achieved using a mixture of medical air (containing 20 % oxygen) and medical oxygen (at 100 %). By varying the oxygen level in the inspired gas and measuring the resulting ethane concentration the approximate ethane concentrations in medical air and medical oxygen were determined.

9.3 Results

9.3.1 Ethane in medical gases

Figure 9.3 shows the measured ethane concentrations in inspiratory gas for a number of different oxygen concentration settings. Measurements of the inspired gas show significantly higher levels of ethane (10's of ppb) than typical room ethane levels (ppb).

Since the minimum inspired oxygen level of 20 % is achieved using 100 % medical air, the concentration of ethane in medical air was found to be 2.7 ppb (from extrapolation to the y-axis in figure 9.3). Similarly, 100 % inspired oxygen levels are achieved using 100 % medical oxygen, determined to be 40.82 ppb. Ideally, the inspired ethane concentration would be lower to make small fluctuations in the expired ethane concentration more distinguishable. However, this situation was unavoidable and therefore the inspired was carefully monitored and the measured levels were subtracted from the expired as described above.

Unfortunately the oxygen concentration could not be automatically recorded during this trial for potential correlation with measured changes in inspired ethane.

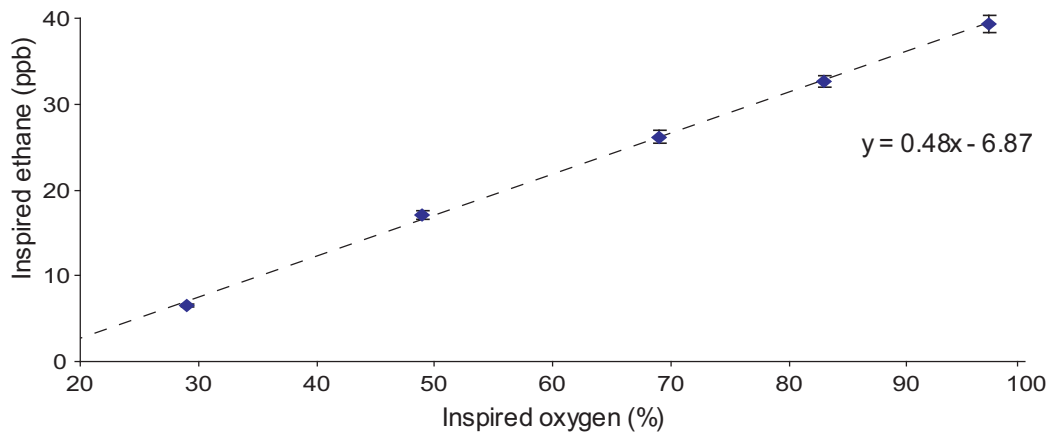


Figure 9.3: Measured ethane concentrations in inspiratory gas for a number of different oxygen concentration settings. The inspiratory gas is a mixture of medical air (20 % oxygen) and medical oxygen (at 100 %), with ethane concentrations for these gases determined to be 2.7 ppb and 39.3 ppb respectively.

9.3.2 Ventilator mode safety tests

The following safety test results for a number of ventilator modes were obtained for a gas removal rate of 300 ml min^{-1} from each line:

When operating in both the IPPV mode and the SIMV mode no disruption was caused to the simulated ventilator process. The delivered tidal volume was reduced by $\sim 100 \text{ ml}$ and this was easily compensated for manually in the input ventilator settings.

For the ASB mode, when the trigger level was set to a level of 2 (arbitrary units on ventilator display) the ventilator sometimes continually triggered the delivery of preset breaths. The trigger level could be increased and this auto-cycling stopped, but this would require greater patient effort to initiate a breath and could make the weaning process more difficult. It was decided by the medical physics department that the trigger level could be safely raised to a level of 5 on the ventilator to ensure no auto-cycling without compromising patient care.

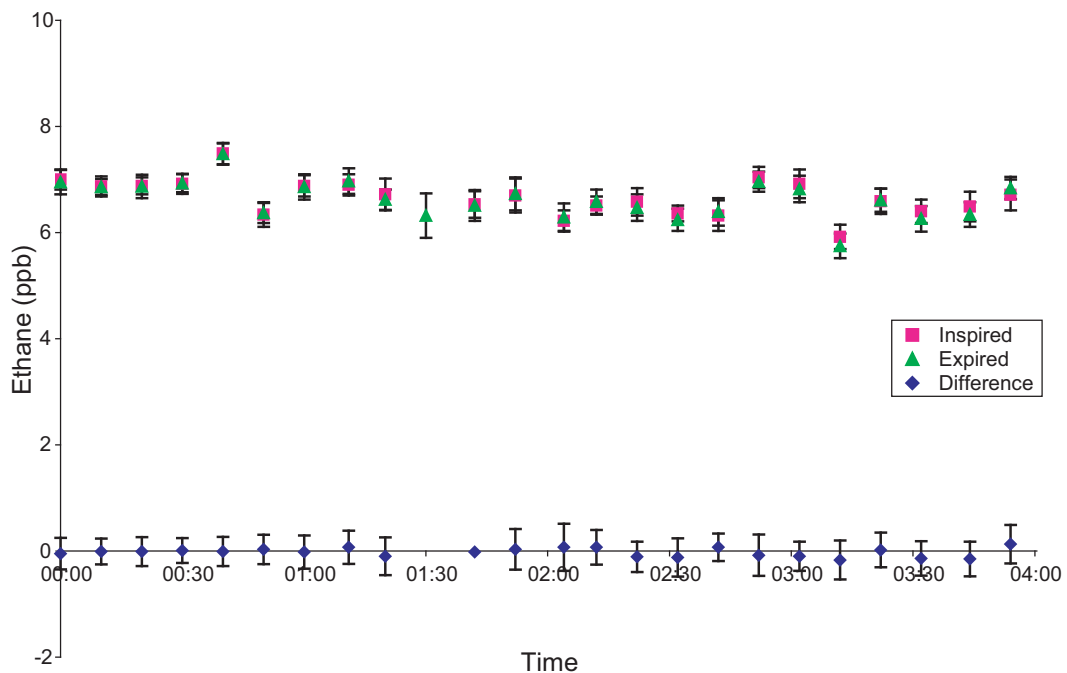


Figure 9.4: Control data obtained using an identical set-up as with a patient, except an artificial lung was used in place of a patient. Inspired, expired and subtracted ethane levels are shown. The mean subtracted ethane concentration was -0.03 ppb with a standard deviation of 0.08 ppb. These results confirm that there is no net ethane concentration difference between the inspired and expired air.

9.3.3 Control experiment

Gas samples were collected during a control experiment using an artificial lung for a total of four hours, with each pair of sample bags immediately analysed manually using the portable instrument. The plotted inspired, expired and subtracted ethane concentrations are shown in figure 9.4. The average value of the subtracted ethane values was -0.03 ppb with a standard deviation of 0.08 ppb. This suggests that no additional ethane is produced in the expiratory line and the subtracted ethane values obtained with a patient are attributable to the contribution from that patient's breath.

It can be seen that even for a constant oxygen concentration of 30% (determined by ventila-

tor settings) the inspired ethane levels were seen to fluctuate, with an average concentration of 6.66 ppb and standard deviation of 0.34 ppb. Instrument error in the measurement will have contributed to these fluctuations, and possibly also a changing ethane concentration in the room air which was used as a zero-reference. However it is also possible that the fluctuations were due to genuine changes in ethane concentration. One explanation is that the oxygen concentration was fluctuating. However, a real change of 1 ppb in ethane, for example from 7 ppb to 6 ppb would correspond to a change in oxygen from 29 % to 27 %. The ventilator is specified to monitor oxygen levels to an accuracy better than 1 % so it is unlikely that the oxygen concentration changed as much. A second explanation is that the concentration of ethane in the medical gases varies with time. The medical gases are supplied centrally and the mixing ratio is determined by the ventilator settings. However, we were assured by the medical physicists at the Southern General that the mixing process is extremely accurate and therefore it is unlikely that this is the cause. A further test was used to check that the instrument error does not fully account for these fluctuations in inspired ethane: The inspired and expired samples collected from one patient over several hours were measured in a random order after all the samples had been collected. The measured expired ethane concentrations still increased and decreased with the reported inspired ethane levels, demonstrating that instrument error is not the only cause and that the fluctuations are real.

A second control experiment¹ was performed to investigate the possible effect of changes in inspired oxygen (and therefore inspired ethane) and minute volume on the resultant net ethane. As can be seen from figure 9.5, inspired and expired ethane concentration appear to approximately follow the changes in oxygen concentration, which was varied between 50 % and 100 %. While the higher oxygen concentration led to an increase in the standard deviation of these ethane measurements there did not seem to be a significant effect on the net ethane concentration. As might be expected, a step increase in minute volume (e.g. from 11.7 l to 18.2 l at 16.20) did not appear to significantly affect the net ethane concentration.

¹These results were recorded in April 2008 as part of the ongoing clinical study. The gas samples were collected by a medical student at the Southern General hospital and were analysed by members of the project team in the Glasgow Optics group.

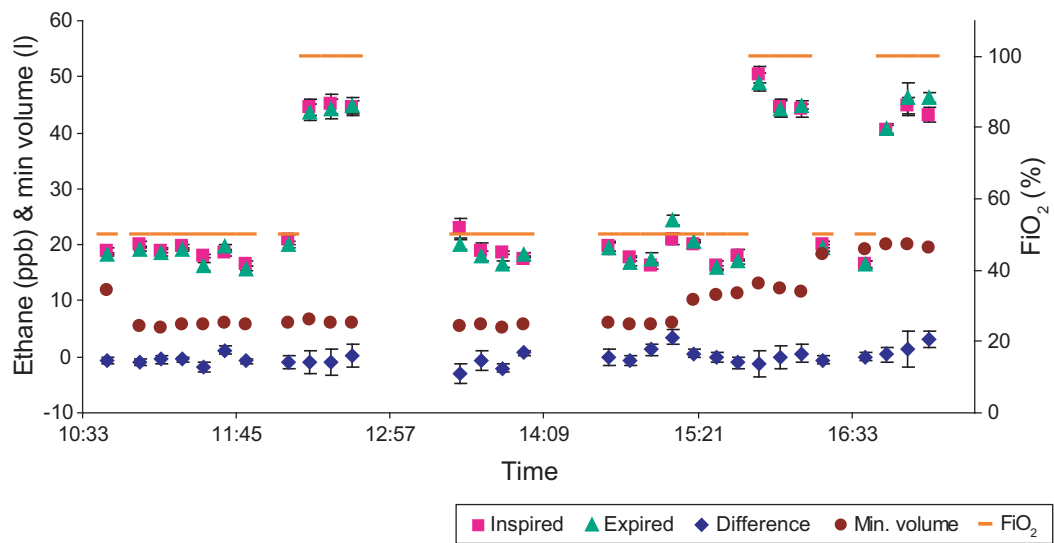


Figure 9.5: Second set of ITU control data obtained using an artificial lung in place of a patient. Inspired oxygen levels (FiO_2) and inspired volume per minute (min. volume) were changed and the inspired, expired and subtracted ethane concentrations were measured and recorded. Although increasing FiO_2 leads to larger errors it does not appear to have a significant effect on the net ethane concentration.

9.3.4 Manual measurement of breath ethane

For each patient the measured inspired and expired ethane concentrations were plotted against time. For each pair of sample bag measurements, the inspired levels were subtracted from the expired levels and the resulting subtracted ethane values were also plotted. For ease of presentation of the results each patient number simply refers to the order in which the patients participated in the trial.

Patient 1

Patient 1 was admitted to the ITU with a traumatic brain injury. Breath ethane was collected and measured manually as described above for seven hours. The inspired, expired and subtracted breath ethane values are plotted in figure 9.6. Physiological data was collected using the DocVu system as described above. A plot of several of these clinical parameters is given in appendix D.2. Over the sampling period the patient was clinically stable and the subtracted ethane levels were observed to be flat, with a mean ethane concentration of 0.26 ppb and standard deviation of 0.08 ppb. The reduction in inspired ethane concentration towards the end of the sampling period was due to a reduction in the patient's oxygen concentration.

Patient 2

Patient 2 was admitted to the ITU with a traumatic brain injury. Breath ethane was collected and measured manually for four and a half hours. Unfortunately the DocVu physiological data could not be recovered after sampling due to a technical problem. However the patient had been clinically stable over the sampling period. Subtracted ethane levels, shown in figure 9.7 were also relatively flat, with a mean ethane concentration of 0.16 ppb and standard deviation of 0.12 ppb.

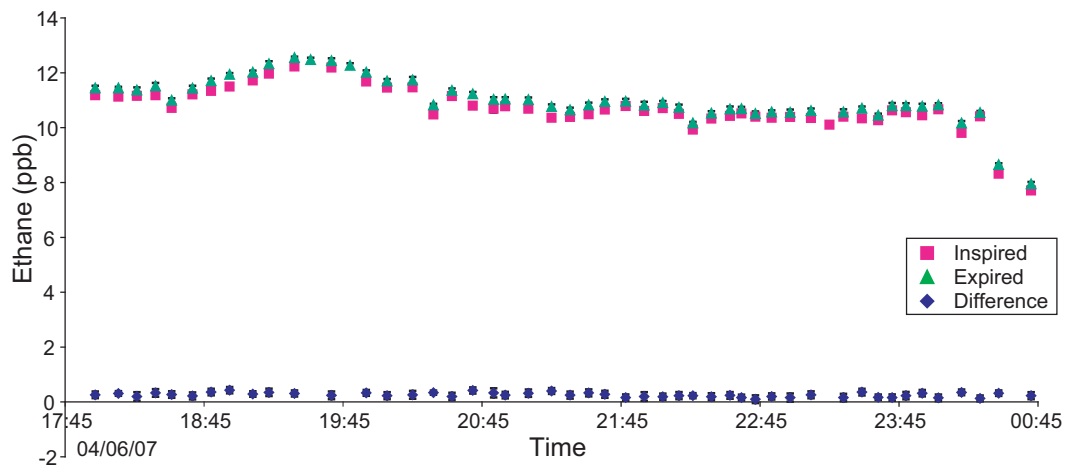


Figure 9.6: Inspired, expired and subtracted breath ethane levels for ITU patient 1. The subtracted ethane levels were observed to be flat with a mean concentration of 0.26 ppb and standard deviation of 0.08 ppb.

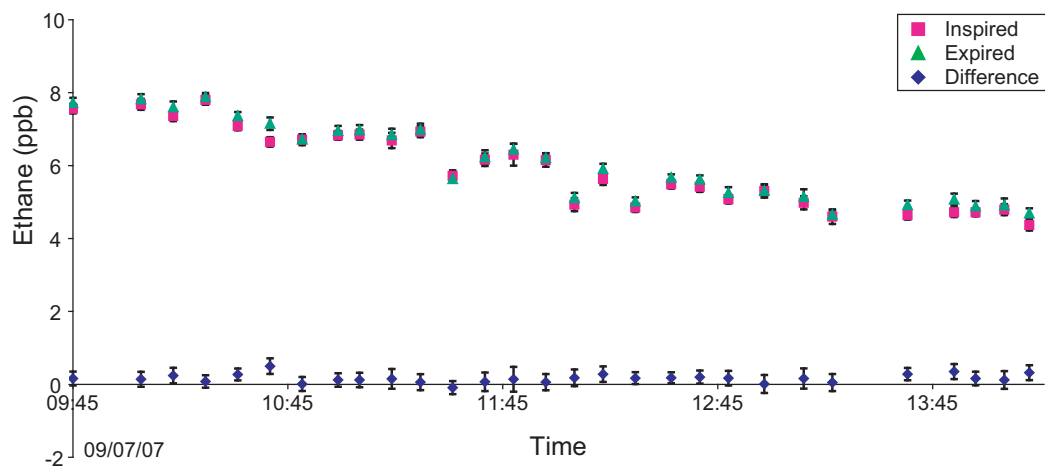


Figure 9.7: Inspired, expired and subtracted breath ethane levels for ITU patient 2. The subtracted breath ethane levels were observed to be fairly flat, with a mean concentration of 0.16 ppb and standard deviation of 0.12 ppb.

Patient 3

Patient 3 was also admitted to the ITU with a traumatic brain injury. Breath samples were collected and measured manually over four consecutive days. The inspired, expired

and subtracted breath ethane data collected over the four days is shown in figure 9.8. The observed subtracted ethane levels for the first three days were also relatively flat, with average baseline levels shown in table 9.1.

Day	Mean ethane concentration (ppb)	Standard deviation
1	0.80	0.29
2	1.57	0.47
3	0.31	0.26
4 (excl. peaks)	0.12	0.2

Table 9.1: Mean subtracted ethane concentration and standard deviation for each day of breath gas collection for ITU patient 3.

On the fourth day two peaks in breath ethane were observed. The first, observed at 11:46, was an increase of 1.82 ppb above the inspired ethane concentration. The second, observed at 15:12, was an increase of 5.23 ppb above the inspired concentration. Each peak was a measurement of a single sample bag, with the subsequent sample (10 min later) measuring baseline level again, as shown in table 9.1. It is possible, although extremely unlikely that the observed peaks could be caused by contamination of the sample bags used for the breath gas collection.

The DocVu clinical data for the four days is shown in appendix D.3. Interestingly, the patient had been heavily sedated on the first three days and on the fourth day, when ethane peaks were observed, had shown variation in their level of consciousness and greater fluctuations in their monitored physiology. There also appeared to be some trend downwards in blood pressure. No significant clinical events were recorded over the four days for which breath samples were collected. However on the fourth day at 15:10, just two minutes before the second peak was observed, a physical examination of the patient had begun.

9.3.5 Automated measurement of breath ethane

Patient 4

Patient 4 had suffered a subarachnoid haemorrhage (SAH). Breath samples were collected and measured on three consecutive days using the automated sampling system. On the second day, the instrument was thermally-cycled (as described in section 3.2) following poor performance that morning. Therefore sampling was resumed in the evening. The inspired, expired and subtracted breath ethane data collected over the three days is shown in figure 9.9. It is likely that the increased variation in the measured values of inspired and expired air reflect the fact that the instrument was zero-referencing using room air rather than nitrogen gas. Larger deviations are also seen in these measurements, which were obtained towards the end of the trial, due to a general slow deterioration of instrument performance over several months.

No significant peaks were observed in the subtracted breath ethane levels for the first two days. On the third day two peaks were observed. The first increase in breath ethane began at 13:10 and peaked at 13:42 with a value of 4.24 ppb with a standard deviation of 1.23 ppb. This coincided with the sedated patients family visiting. The second increase began at 18:47 and peaked at 19:06 with a value of 5.51 ppb and a standard deviation of 1.52 ppb. This coincided with the patient becoming agitated and requiring further sedation. The recorded physiological data is shown in appendix D.4. The ‘decay’ of the peaks in breath ethane using the automated system will have been affected by the filtering effect of the buffer bags. However the slow increases in ethane, this time measured over several sample bags, suggest that the increased rate of ethane production by the patient does extend over a period of ~ 30 min.

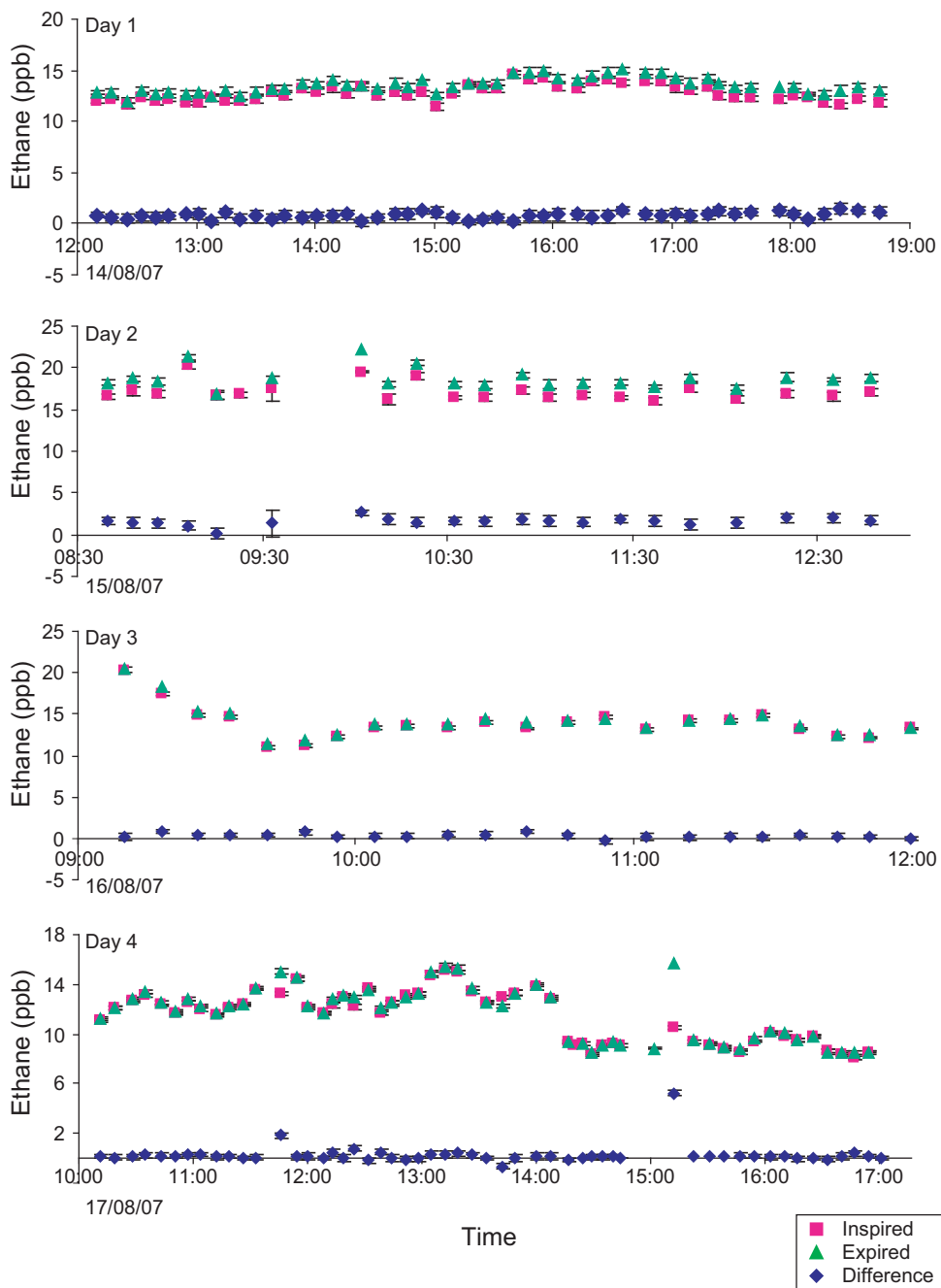


Figure 9.8: Inspired, expired and subtracted breath ethane levels for ITU patient 3 measured over four consecutive days.

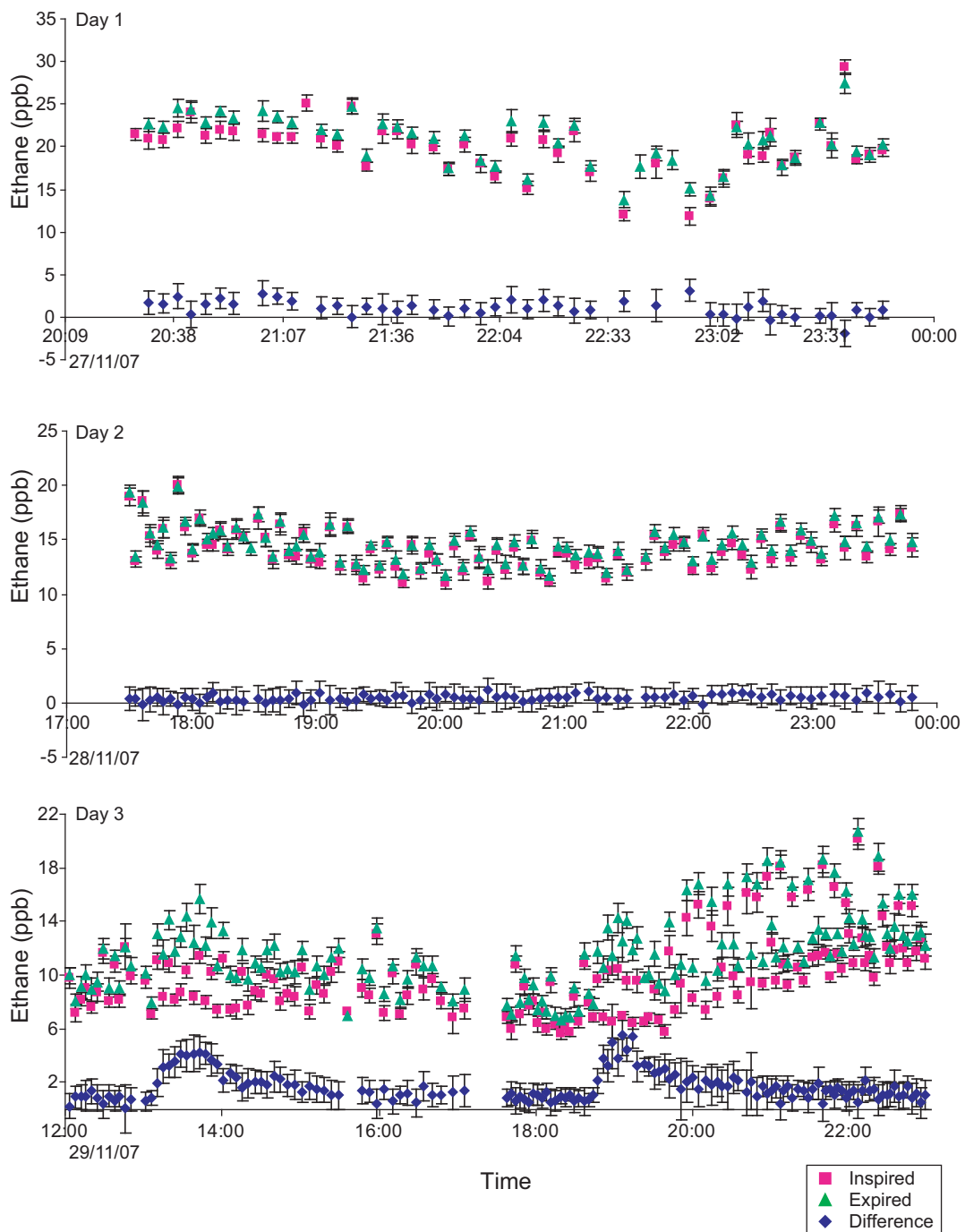


Figure 9.9: Inspired, expired and subtracted breath ethane levels for ITU patient 4 measured on three consecutive days.

9.4 Discussion

Breath ethane was non-invasively monitored in a number of ventilated patients in the ITU. Subtracted ethane concentrations were calculated from measurements of ethane of inspired and expired air. The subtraction technique appeared to give a good indication of the ethane contribution from the patient, even when the inspired ethane concentrations were much higher than this contribution. It is also interesting to note that these subtracted values also remained consistent when the inspired ethane concentration was adjusted, by an increase or reduction in oxygen. This is in contrast to the findings by Schubert et al that inspired substance concentrations can seriously affect the accuracy and reliability of breath analysis in mechanically ventilated patients and that a simple correction for inspired substance concentrations is not possible [157].

Very recently (July 2008) a letter was published reporting that peaks of ethane of short duration occur in breath of intensive care patients [158]. For the sample group of six patients, fewer breath ethane surges were observed for the three patients that had less serious conditions than the others. Peaks were observed more frequently in the three patients, and some were reported to occur along with recorded clinical events such as administration of drugs, pulmonary toilette and arrhythmias. The high frequency of sampling enabled short lived changes to be observed, although the sample measurement technique of gas chromatography required laboratory analysis [93].

In our pilot study, breath ethane peaks in the subtracted values of >1.5 ppb were observed in two out of the four patients for which breath gas was monitored before the end of November 2007. Since then, the portable instrument remained on-site in the Southern General (SG) hospital and the ITU trial was continued by other members of the team and their clinical collaborators. Further breath ethane peaks have since been observed in a patient with sepsis/spinal injury. In a study running in parallel with this one over the last year, breath samples were collected from a number of sepsis patients in the Intensive Care unit at Ninewells hospital, Dundee. These samples were also mainly measured using the portable instrument and several breath ethane peaks were observed.

The underlying cause of the ethane peaks is unclear as there appeared to be no significant

correlations between breath ethane and other recorded clinical data. However, during the ITU trial the breath ethane was seen to peak at times that correspond with an apparent increased patient awareness. Similar increases were observed in the ICU Ninewells study in a patient with spinal injury while being washed by the nursing staff and also while a patient was being prepared for a CT Scan. These observations suggest that anxiety or stress induces metabolic changes that generate ethane. The origin of the ethane is uncertain but it is possible that the central nervous system may be a major contributing tissue.

The limited number of patients currently monitored means it is difficult to correlate the measured ethane with physiological events. It may even be that the clinical markers currently monitored in the ITU are not appropriate for direct comparison with breath ethane, or that the changes in such markers may be subject to a significant delay. Future work would require much larger scale studies, allowing in depth statistical analysis to be performed. A larger scale follow-up study could be used to investigate if observed breath ethane increases are linked at all to patient outcomes. A similar type of study is currently being performed by the clinical physics department at the Southern General hospital where the DocVu real-time physiological data recording system is being tested. The clinical data that is currently recorded and displayed on the bedside monitor each second is being analysed and correlated with patient outcomes. The aim is for the potential optimisation of patient care in the ITU.

Chapter 10

Summary and conclusions

10.1 Summary

In this thesis the development of a portable spectroscopy system for the real-time detection of breath ethane has been described. The instrument has dimensions 1 m x 0.5 m x 1 m and incorporates a closed-loop cooling system, enabling a factor of 3 volume reduction compared with the lab-based system. In addition to a significant size reduction the previously achieved high performance has been not only been sustained but improved upon. A sensitivity of 70 ppt has been achieved based on a 1 Hz sampling rate. This corresponds to the detection of a minimum absorbance of 11 cm^{-1} . The performance of the instrument has been characterized and the factors affecting this performance have been explored. An accuracy of $> 78\%$ has been demonstrated when measured ethane concentrations were compared with empirical concentration, shown to be reproducible provided zero-referencing occurs at regular intervals. The instrument has been shown to have a linear response and is relatively insensitive to common contaminating species. Pressure and temperature fluctuations have been shown to have little effect, while shifting optical fringes and changing modal properties of the laser do contribute significantly to the working sensitivity.

An outdoor field trial was conducted in which ethane concentration data was gathered for the future development of gas dispersion and inverse models. Sub-ppb performance of the instrument was observed even when driving over relatively rough terrain increasing confidence in the robustness of the system.

The instrument was used in a number of pilot clinical studies, both as an off-line and an on-line analyser. In the dialysis study the real-time nature of the instrument was exploited to enable the rapid turnaround of large numbers of discrete breath samples. Breath ethane was monitored in patients as they received dialysis treatment and short term increases in breath ethane were detected in 14 out of the 24 patients at the onset of the treatment session. The observations are consistent with findings reported in the literature using other OS markers. Breath ethane was collected for the first time during radiotherapy treatment using a custom-designed automated sampling rig although no significant breath ethane increases were observed in the 6 patients.

The instrument was then located on-site at the Southern General hospital, Glasgow where inspired and expired breath samples were collected from ventilated patients in the Intensive Therapy Unit. Initially, the breath samples were collected and measured manually, with the convenient location of the instrument facilitating a rapid turnaround of sample analysis. Later in the trial the instrument was modified to enable automated collection and measurement of inspired and expired breath from ventilated patients. Significant increases in breath ethane were observed in two out of the four patients monitored in the ITU. This trial continued and the portable instrument is still in regular use, having replaced the previous lab-based system as the most sensitive, reliable breath ethane sensor.

10.2 Conclusions

On commencement of this project lead-salt lasers were the most practical choice of laser source for the portable instrument: They were commercially available, essentially 'plug and play' in our systems, and they had previously been used to achieve high performance in the lab-based systems. Therefore the portable instrument was based on these previous systems and its development benefited from the Glasgow Optics group's previous experience. The

key change in the way in which the laser is cooled has offered several advantages: The closed loop cooling cycle offers higher temperature stability and enables longer-term on-site use in a clinical setting. The induced vibrational noise from the cooling system does not have a significant effect on the sensitivity, due to the nature of the wavelength modulation technique. While the cooling system has enabled a reduction in size of the dewar and dispensed with the need for a liquid nitrogen dewar, the instrument is still a significant size at 1 m x 0.5 m x 1 m. The base, which encloses the compressor and scroll pump, accounts for approximately half the height of the instrument. If the laser did not require cryogenic cooling the base section would be unnecessary and the size would be reduced by a factor of two.

Alternative mid-IR sources offering room temperature operation could enable this. Additionally, a higher power source could achieve a high signal to noise ratio over a shorter pathlength. Despite a reduction in length as compared with lab-based systems, the multi-pass Herriott cell in the portable instrument still contributes significantly to the size of the instrument. Reducing the length of the Herriott cell requires the number of passes to be increased to sustain the pathlength, and therefore, sensitivity. As was shown, this is offset by mirror transmission losses and therefore there is a fundamental limit on the length reduction for a given laser power. At high powers, a lower number of passes will permit smaller cells to be used. The reduction in cell volume has the added advantage of increasing the gas response time. The portable instrument response time of ~ 2 s is currently limited by the cell volume of 3.2 l. For future breath analysis studies, especially by ‘side-stream’ sampling from a ventilator for example, a lower volume of gas required for analysis should be required.

Breath monitoring

In our breath analysis studies the portable ethane spectroscopy system enabled a large turnaround of breath samples at high sensitivity and selectivity. The dynamic breath ethane patterns observed in patients during dialysis treatment indicated increased oxidative stress at the onset of dialysis treatment. Further larger scale studies will be required to offer greater insight into the ethane elevation effect and potential clinical benefit of breath

ethane monitoring and the possibility of intervention. The key observation is the speed of the response, and following this trial our approach to breath sampling was modified to take this into account.

The portable instrument and corresponding gas sampling system enabled the first automated analysis of breath ethane in ventilated patients in an intensive therapy unit. Although samples were ‘averaged’ over periods of minutes, the automated technique allowed unsupervised use over periods of hours, and minimum disruption to clinical staff and visiting friends or family compared with the manual system. The control experiments demonstrated that the measured net ethane concentration between expired and inspired air was attributable to the patients.

These increases in the net exhaled ethane during visits by family and interventions by nursing staff suggest that stress or anxiety can trigger the production of ethane even in situations where other clinical parameters are not significantly altered. Results obtained across various studies were discussed with the clinical biochemist collaborating with our team. It was suggested the breath ethane data collected to date point to alterations in cerebral activity as the causative factor in elevated ethane. This could have important implications for further breath ethane studies, and applications of the technology.

10.3 Future work

Further advances in both laser technology and spectroscopic techniques will enable future development of compact, robust gas sensors with high sensitivity and selectivity. There have been a number of advances in compact laser technologies for the generation of widely tunable mid-IR radiation around 3 μm . Recently, a limited number of alternative sources have become commercially available. For example, M Squared Lasers Ltd (Glasgow, UK) produce a widely tunable, pulsed OPO (Firefly-IR) with an ‘idler’ wavelength range of ~ 2.4 to 4.7 μm . Despite the high average power (> 100 mW at 350 kHz) the linewidth of several GHz is a limiting factor. Aculight (Bothell, WA, USA) also produce a tunable, single frequency OPO (Argos Model 2400) with idler wavelength range of 3.2–3.9 μm with a linewidth < 1 MHz and power > 1 W. Multimode interband cascade lasers designed for

operation between 3 and 4 μm are available from Maxion technologies, Inc (College Park, MD, USA) [159].

QC lasers are potential alternatives that may offer room temperature and high power around 3 μm in the near future for spectroscopic gas sensing. Researchers and collaborators at the Jet Propulsion Lab (JPL) are developing a new generation of miniature, room-temperature mid-IR QCL spectrometers for measurement of atmospheric and planetary gases, including ethane. Currently, the Glasgow Optics group are working on a UK collaborative interdisciplinary project to develop a trace gas sensor based on quantum cascade lasers for oil and gas prospecting. The collaboration comprises the Compound Semiconductor Technologies (CST), the Universities of Sheffield and Glasgow, Shell Global Solutions and laser system specialist Cascade Technologies and is funded by the UK government's previous Department of Trade and Industry (DTI) [160]. The QCL structures are being developed at the University of Sheffield, using novel antimonide-based epitaxy, which will be used to target the absorption band of ethane at 3.34 μm . Working with the electronics and electrical engineering department at Glasgow, CST will fabricate laser devices from the material produced at Sheffield. Cascade will provide module-level packaging and control electronics. The Glasgow Optics group will then develop the photoacoustic instrument, in conjunction with Shell, and it will be then be tested in a number of field trials.

In healthcare, ethane is of considerable interest as a marker of OS. A number of researchers and collaborators are keen to build on the previous work in ethane breath analysis using new online analysers. Preliminary studies such as those described in this thesis, point to the need for frequent sample collection to observe short-lived changes in breath ethane. In contrast to studies which suggest that ethane may have diagnostic potential [75], our results suggest ethane has more potential for clinical monitoring. More research is needed to truly determine if breath monitoring of ethane will be feasible in the future, and more importantly, if it will be clinically useful. It is only with more extensive research, and larger scale studies that this will become clear. As has been shown with the case of NO, the measurement of certain gases is actually being incorporated into clinical practice. This has been made possible by the development of low cost, 'turn-key', portable breath gas analysers. For other breath gases, such as ethane, the measurement technologies require further development. Breath analysis is a growing field with exciting prospects, despite a number of challenges to be overcome. As the field of breath analysis expands and breath

gas detection methods improve there is a growing need for standardization of breath sampling techniques [90, 161]. While technological development, particularly of laser-based gas sensors, will overcome a number of obstacles, a great deal of progress has been, and will continue to be made, through a collaborative and interdisciplinary approach.

Appendix A

Circuit diagrams

APPENDIX A. CIRCUIT DIAGRAMS

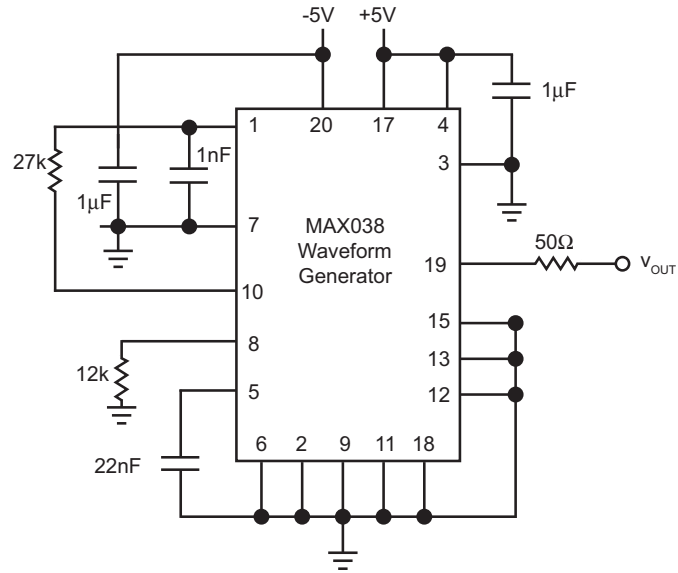


Figure A.1: A sinusoidal waveform used to modulate the laser wavelength modulation is generated using a waveform generator (MAX038CPP, Maxim).

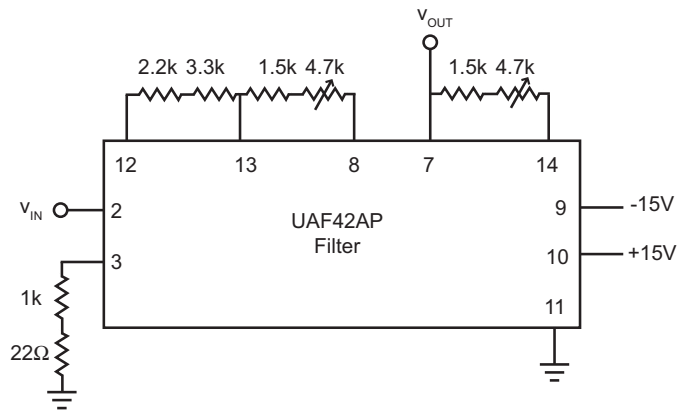


Figure A.2: A bandpass filter (UAF42AP Burr-Brown series, Texas Instruments) is used to filter the generated sinusoidal waveform and also the detected AC signals from the photodetector modules.

APPENDIX A. CIRCUIT DIAGRAMS

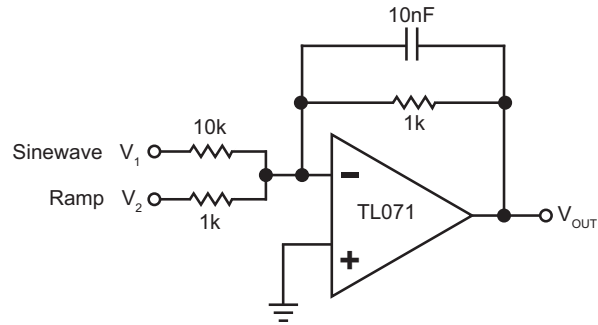


Figure A.3: A summing op-amp (TL071, Texas Instruments) was used to add the sinusoidal waveform to the ramp signal.

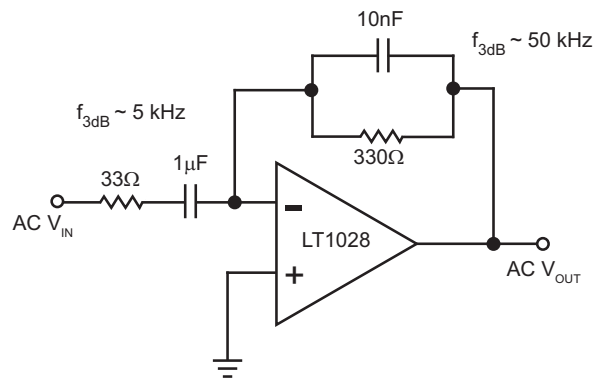


Figure A.4: Before being filtered the detected AC signals at 16 kHz from the photodetector modules were amplified using a low noise op-amp (LT1028) with an AC gain of ~ 10 .

Appendix B

Rayleigh range approximation

Two key parameters of a Gaussian beam are beam size, ω , and wavefront curvature, R_W , as a function of distance, z . The position $z = 0$, where $\omega = \omega_{min} = \omega_0$, is called the beam waist. The wavefront curvature is a minimum at the Rayleigh range z_R .

We have¹

$$\omega(z) = \omega_0 \sqrt{1 + \left(\frac{z}{z_R}\right)^2} \quad (\text{B.1})$$

$$R_W(z) = \frac{1}{z}(z^2 + z_R^2) \quad (\text{B.2})$$

For a confocal cavity the two mirrors, each of radius of curvature, R , are placed at the Rayleigh range, z_R , and we have

$$2z_R = d = R = R_W(z = z_R) \quad (\text{B.3})$$

Rewriting equation B.2 for z gives

$$z = \frac{R}{2} \pm \sqrt{\frac{R^2 - 4z_R^2}{4}} \quad (\text{B.4})$$

¹The following working was modified from notes taken during the Modern and Nonlinear Optics undergraduate lectures delivered by Prof Miles Padgett at the University of Glasgow

APPENDIX B. RAYLEIGH RANGE APPROXIMATION

Using $d = 2z$ and B.4 we obtain the following expression for z_{r}

$$z_{\text{r}} \simeq \sqrt{\frac{d(2R - d)}{4}} \quad (\text{B.5})$$

Appendix C

Radiotherapy sampling equipment staff instructions

APPENDIX C. RADIOTHERAPY SAMPLING EQUIPMENT STAFF INSTRUCTIONS

Breath Ethane Radiotherapy Trial - Instructions for staff

INITIAL SET-UP

(Could be done by staff while previous patient is still in treatment room)



1. Flick switch on black sampling rig to 'RESET'

2. Plug in extension reel at wall and turn power ON. [The 2 rows of green lights show that the connections

between rig and sample bags are now closed]

3. Press Power switch 'ON' at back of pump

4. Press green 'START' button on pump (Speed: 400 rpm)



5. Holding the tap nozzle as shown, open all 12 bags by turning taps anti-clockwise (2 turns)

IMMEDIATELY BEFORE TREATMENT

6. Fit patient with mask and secure with mask strap



7. Immediately after mask is secured, flick switch on black sampling rig to START

IMMEDIATELY AFTER TREATMENT



8. Immediately before patient mask is removed, flick switch on black sampling rig to RESET

9. Finally close all 12 bags by turning taps clockwise until they are tightly sealed



Figure C.1: The instruction sheet for operation of the sampling equipment developed to collect breath samples from patients receiving radiotherapy treatment. The sheet was distributed to clinical staff in the Radiotherapy unit, Ninewells hospital, Dundee.

Appendix D

ITU patient physiological data

The DocVu system currently being piloted in the ITU by the Brain-IT group [156] was used during the breath ethane study to record a range of physiological data.

The recorded patient physiological data corresponding to the dates and times of breath ethane sampling are shown in figures D.2–D.4. For a key to the parameters shown in all three figures, please refer to figure D.1. A point to note is that the unfeasible dramatic increases in certain physiological parameters was often as a result of an interruption to the sensor due to a clinical assessment or treatment procedure. For example, the apparent increases in central venous pressure from ~ 20 to ≥ 100 are artefacts.

APPENDIX D. ITU PATIENT PHYSIOLOGICAL DATA

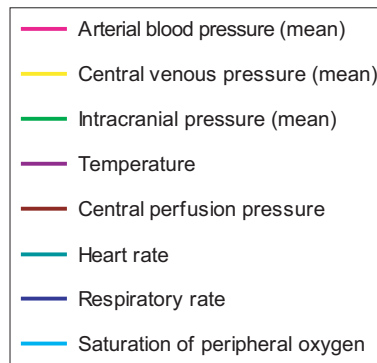


Figure D.1: Key to displayed physiological data collected from ventilated ITU patients using the DocVu system.

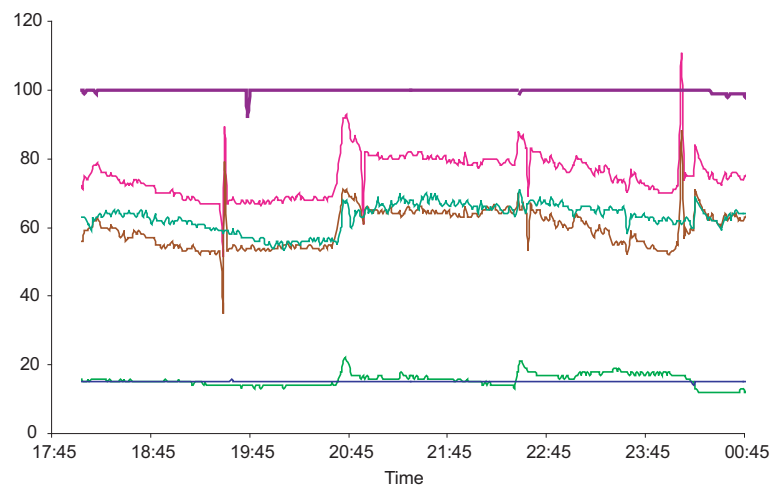


Figure D.2: DocVu data for patient 1 recorded on 4/06/07. Refer to figure D.1 for key.

APPENDIX D. ITU PATIENT PHYSIOLOGICAL DATA

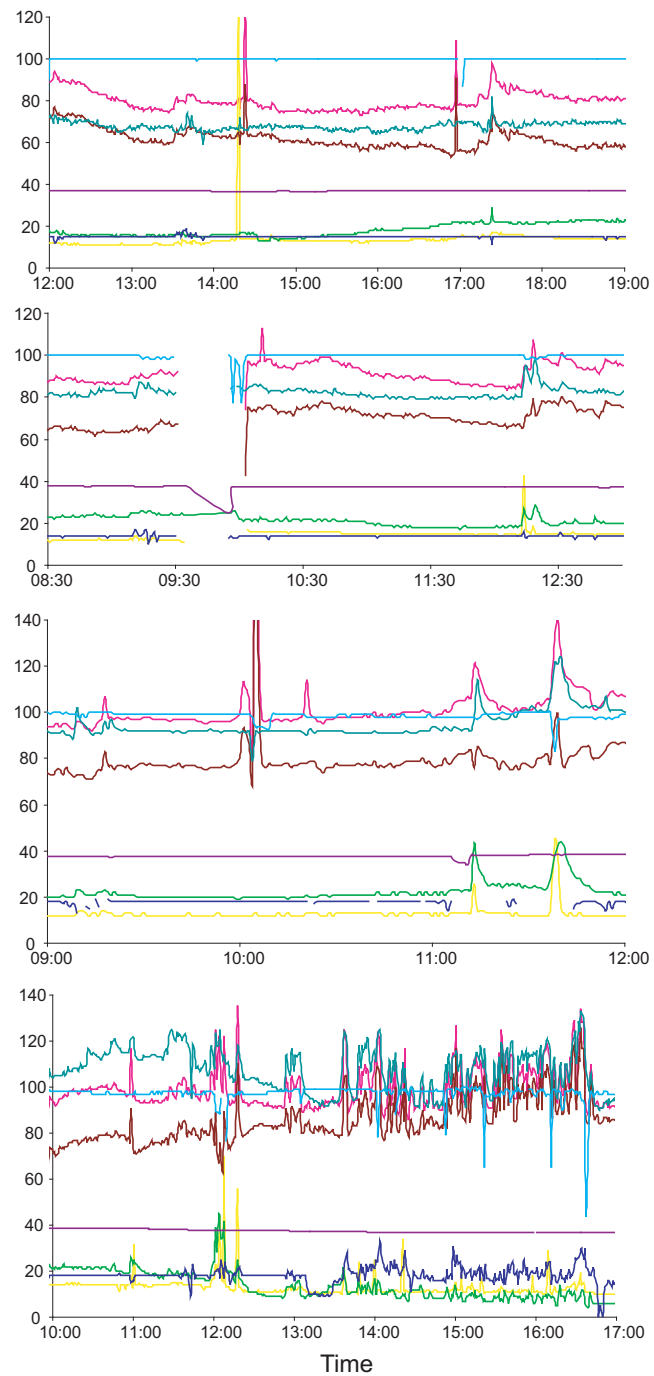


Figure D.3: DocVu data for patient 3 recorded on four consecutive days 14/08/07–17/08/07. Refer to figure D.1 for key.

APPENDIX D. ITU PATIENT PHYSIOLOGICAL DATA

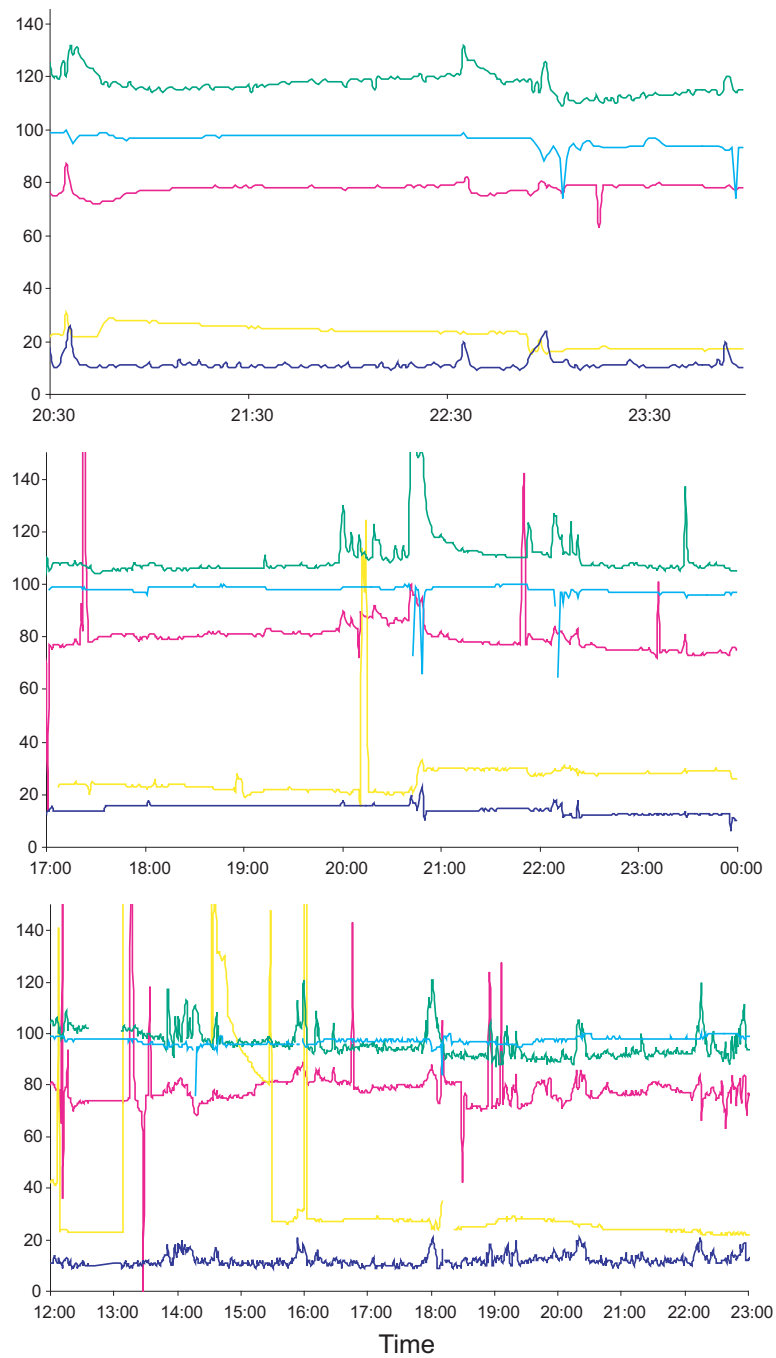


Figure D.4: DocVu data for patient 4 recorded on three consecutive days 27/11/07–29/11/07. Refer to figure D.1 for key.

Bibliography

- [1] G. M. Barrow. *Physical Chemistry*. McGraw-Hill International Editions, 1988.
- [2] J. R. Mourant, R. R. Gibson, T. M. Johnson, S. Carpenter, K. W. Short, Y. R. Yamada, and J. P. Freyer. Methods for measuring the infrared spectra of biological cells. *Physics in Medicine and Biology*, 48(2):243–257, 2003.
- [3] A spectrum of an extrasolar planet. L. J. Richardson, D. Deming, K. Horning, S. Seager and J. Harrington. *Nature*, 445:892–895, 2007.
- [4] W. Demtröder and M. Inguscio, editors. *Applied laser spectroscopy*. Plenum publishing corporation, 1990.
- [5] A. W. Mantz. A review of the applications of tunable diode laser spectroscopy at high sensitivity. *Microchem. J.*, 50(3):351–364, 1994.
- [6] W. Demtröder. *Laser spectroscopy: Basic concepts and instrumentation*, chapter Laser Raman Spectroscopy. Springer, 2002.
- [7] W. Koechner and M. Bass. *Solid-State Lasers*, chapter Nonlinear Devices, pages 339–386. Springer, 2003.
- [8] P. Werle. A review of recent advances in semiconductor laser based gas monitors. *Spectrochim. Acta, Part A*, 54(2):197–236, 1998.
- [9] W. Lindinger, A. Hansel, and A. Jordan. On-line monitoring of volatile organic compounds at pptv levels by means of proton-transfer-reaction mass spectrometry

BIBLIOGRAPHY

- (PTR-MS) medical applications, food control and environmental research. *Int. J. Mass Spectrom. Ion Processes*, 173(3):191–241, 1998.
- [10] M. R. McCurdy, Y. Bakhirkin, G. Wysocki, R. Lewicki, and F. K. Tittel. Recent advances of laser-spectroscopy-based techniques for applications in breath analysis. *J. Breath Res.*, 1(1):014001 (12pp), 2007.
- [11] M. J. Thorpe, D. Balslev-Clausen, M. S. Kirchner, and J. Ye. Cavity-enhanced optical frequency comb spectroscopy: Application to human breath analysis. *Opt. Express*, 16(4):2387–2397, 2008.
- [12] P. Spanel and S. D. Smith. Selected ion flow tube: A technique for quantitative trace gas analysis of air and breath. *Med. Biol. Eng. Comput.*, 34(6):409–419, 1996.
- [13] P. Mürtz, L. Menzel, W. Bloch, A. Hess, O. Michel, and W. Urban. LMR spectroscopy: A new sensitive method for on-line recording of nitric oxide in breath. *J. Appl. Physiol.*, 86(3):1075–1080, 1999.
- [14] M. W. Sigrist, R. Bartlome, D. Marinov, J. M. Rey, D. E. Vogler, and H. Wächter. Trace gas monitoring with infrared laser-based detection schemes. *Appl. Phys. B*, 90:289–300, 2008.
- [15] S. Schilt, L. Thvenaz, M. Nikès, L. Emmenegger, and C. Hügli. Ammonia monitoring at trace level using photoacoustic spectroscopy in industrial and environmental applications. *Spectrochim. Acta, Part A*, 60(14):3259–3268, 2004.
- [16] R. F. Curl and F. K. Tittel. Tunable infrared laser spectroscopy. *Annu. Rep. Prog. Chem. Sect. C*, 98:217–270, 2002.
- [17] F. K. Tittel, D. Richter, and A. Fried. *Solid-state Mid-Infrared Laser Sources*, chapter Mid-Infrared Laser Applications in Spectroscopy, pages 445–510. Springer, 2003.
- [18] B. Di Bartolo and O. Forte. *Advances in spectroscopy for lasers and sensing*. Springer, 2006.
- [19] F. K. Tittel, G. Wysocki, A. Kosterev, and Y. Bakhirkin. *Mid-Infrared Coherent Sources and Applications*, chapter Semiconductor laser based trace gas sensor technology: Recent advances and applications, pages 467–493. Springer, 2007.

BIBLIOGRAPHY

- [20] C. Fischer and M. W. Sigrist. *Solid-state Mid-Infrared Laser Sources*, chapter Mid-IR Difference Frequency Generation, pages 131–136. Springer, 2003.
- [21] S. Schilt, A. Vicet, R. Werner, M. Mattiello, L. Thévenaz, A. Salhi, Y. Rouillard, and J. Koeth. Application of antimonide diode lasers in photoacoustic spectroscopy. *Spectrochim. Acta, Part A*, 60(14):3431–3436, 2004.
- [22] M. Tacke. Lead-salt lasers. *Phil. Trans. R. Soc. Lond. A*, 359(1780):547–566, 2001.
- [23] F. G. Smith and T. A. King. *Optics and Photonics - An Introduction*. Wiley, 2000.
- [24] S.M.Sze. *Semiconductor Devices: Physics and Technology*. Wiley, 2001.
- [25] G. Duxbury, N. Langford, M. T. McCulloch, and S. Wright. Quantum cascade semiconductor infrared and far-infrared lasers: From trace gas sensing to non-linear optics. *Chem. Soc. Rev.*, 34:921–934, 2005.
- [26] F. K. Tittel, Y. Bakhirkin, A. Kosterev, and G. Wysocki. Recent advances in trace gas detection using quantum and interband cascade lasers. *Rev. Laser Eng.*, 34:275–282, 2006.
- [27] C. Gmachl, F. Capasso, D. L. Sivco, and A. Y. Cho. Recent progress in quantum cascade lasers and applications. *Rep. Prog. Phys.*, 64:1533–1601, 2001.
- [28] D. Hofstter and J. Faist. *Solid-state Mid-Infrared Laser Sources*, chapter High performance quantum cascade lasers and their applications, pages 61–96. Springer, 2003.
- [29] J. Faist, F. Capasso, D. L. Sivco, C. Sirtori, A. L. Hutchinson, and A. Y. Cho. Quantum Cascade Laser. *Science*, 264(5158):553–556, 1994.
- [30] A. Kosterev, G. Wysocki, Y. Bakhirkin, S. So, R. Lewicki, M. Fraser, F. Tittel, and R. F. Curl. Application of quantum cascade lasers to trace gas analysis. *Appl. Phys. B*, 90(2):165–176, 2008.
- [31] D. G. Revin, J. W. Cockburn, M. J. Steer, R. J. Airey, M. Hopkinson, A. B. Krysa, L. R. Wilson, and S. Menzel. InGaAs/AlAsSb/InP quantum cascade lasers operating at wavelengths close to 3 μm . *Appl. Phys. Lett.*, 90(2):021108, 2007.
- [32] R. Q. Yang, C. J. Hill, and Y. Qiu. Mid-IR interband cascade lasers. *MRS Fall Meeting*, 2005.

BIBLIOGRAPHY

- [33] K. Vodopyanov. *Solid-state Mid-Infrared Laser Sources*, chapter Pulsed Mid-IR Optical Parametric Oscillators, pages 141–172. Springer, 2003.
- [34] S. Stry, P. Hering, and M. Mürtz. Portable difference-frequency laser-based cavity leak-out spectrometer for trace-gas analysis. *Appl. Phys. B*, 75(2-3):297–303, 2002.
- [35] F. Müller, A. Popp, F. Kühnemann, and S. Schiller. Transportable, highly sensitive photoacoustic spectrometer based on a continuous-wave dual-cavity optical parametric oscillator. *Opt. Express*, 11(22):2820–2825, 2003.
- [36] S. Schilt, L. Thévenaz, and P. Robert. Wavelength modulation spectroscopy: combined frequency and intensity laser modulation. *Appl. Opt.*, 42(33):6728–6738, 2003.
- [37] D. S. Bomse, A. C. Stanton, and J. A. Silver. Frequency modulation and wavelength modulation spectroscopies: Comparison experimental methods using a lead-salt diode laser. *Appl. Opt.*, 31(6):718–731, 1992.
- [38] M. Gehrtz, G. C. Bjorklund, and E. A. Whittaker. Quantum-limited laser frequency-modulation spectroscopy. *J. Opt. Soc. Am. B*, 2(9):1510–1526, 1985.
- [39] G. Berden, R. Peeters, and G. Meijer. Cavity ring-down spectroscopy: Experimental schemes and applications. *Int. Rev. Phys. Chem.*, 19(4):565–607, 2000.
- [40] M. W. Sigrist. Trace gas monitoring by laser photoacoustic spectroscopy and related techniques (plenary). *Rev. Sci. Instrum.*, 74(1):486–490, 2003.
- [41] A. Miklós, P. Hess, and Z. Bozóki. Application of acoustic resonators in photoacoustic trace gas analysis and metrology. *Rev. Sci. Instrum.*, 72(4):1937–1955, 2001.
- [42] G. Gibson, S. D. Monk, and M. Padgett. A field-portable, laser-diode spectrometer for the ultra-sensitive detection of hydrocarbon gases. *J. Mod. Opt.*, 49(5):769–76, 2002.
- [43] B. Hirst, G. Gibson, S. Gillespie, I. Archibald, O. Podlaha, K. D. Skeldon, J. Courtial, S. Monk, and M. Padgett. Oil and gas prospecting by ultra-sensitive optical gas detection with inverse gas dispersion modelling. *Geophys. Res. Lett.*, 31, 2004.
- [44] K. D. Skeldon, G. M. Gibson, C. A. Wyse, L. C. McMillan, S. D. Monk, C. Longbottom, and M. J. Padgett. Development of high resolution real-time sub-ppb ethane

BIBLIOGRAPHY

- spectroscopy and some pilot studies in life science. *Appl. Opt.*, 44(22):4712–4721, 2005.
- [45] K. D. Skeldon, C. S. Patterson, C. A. Wyse, G. M. Gibson, M. J. Padgett, C. Longbottom, and L. C. McMillan. The potential offered by real-time, high-sensitivity monitoring of ethane in breath and some pilot studies using optical spectroscopy. *J. Opt. A: Pure Appl. Opt.*, 7:376–384, 2005.
- [46] K. D. Skeldon, L. C. McMillan, C. A. Wyse, S. D. Monk, G. Gibson, C. Patterson, T. France, C. Longbottom, and M. J. Padgett. Application of laser spectroscopy for measurement of exhaled ethane in patients with lung cancer. *Resp. Med.*, 100(2):300–306, 2006.
- [47] H. Dahnke, D. Kleine, P. Hering, and M. Murtz. Real-time monitoring of ethane in human breath using mid-infrared cavity leak out spectroscopy. *Appl. Phys. B*, 72(8):971–975, 2001.
- [48] G. von Basum, H. Dahnke, D. Halmer, P. Hering, and M. Mürtz. Online recording of ethane traces in human breath via infrared laser spectroscopy. *J. Appl. Physiol.*, 95(6):2583–2590, 2003.
- [49] A. Popp, F. Müller, F. Kühnemann, S. Schiller, G. von Basum, H. Dahnke, P. Hering, and M. Murtz. Ultra-sensitive mid-infrared cavity leak-out spectroscopy using a cw optical parametric oscillator. *Appl. Phys. B*, 75(6-7):751–754, 2002.
- [50] G. von Basum, D. Halmer, P. Hering, M. Mürtz, S. Schiller, F. Müller, A. Popp, and F. Kühnemann. Parts per trillion sensitivity for ethane in air with an optical parametric oscillator cavity leak-out spectrometer. *Opt. Lett.*, 29(8):797–799, 2004.
- [51] D. Halmer, S. Thelen, P. Hering, and M. Mürtz. Online monitoring of ethane traces in exhaled breath with a difference frequency generation spectrometer. *Appl. Phys. B*, 85(2-3):437–443, 2006.
- [52] F. Müller, A. Popp, S. Schiller, and F. Kühnemann. Cw-OPO-based photoacoustic spectrometer for highly sensitive detection of ethane and other volatile organic compounds. In A. A. Oraevsky and L. V. Wang, editors, *Photons Plus Ultrasound: Imaging and Sensing.*, volume 5320, pages 138–144. SPIE, 2004.

BIBLIOGRAPHY

- [53] M. M. J. W. van Herpen, S. Li, S. E. Bisson, and F. J. M. Harren. Photoacoustic trace gas detection of ethane using a continuously tunable, continuous-wave optical parametric oscillator based on periodically poled lithium niobate. *Appl. Phys. Lett.*, 81(7):1157–1159, 2002.
- [54] M. M. J. W. van Herpen, S. E. Bisson, A. K. Y. Ngai, and F. J. M. Harren. Combined wide pump tuning and high power of a continuous-wave, singly resonant optical parametric oscillator. *Appl. Phys. B*, 78(3-4):281–286, 2004.
- [55] Y. A. Bakhirkin, G. Wysocki, M. P. Fraser, R. Q. Yang, and F. K. Tittel. Sensitive, real-time interband cascade laser based sensor for ethane monitoring. In *Optical Society of America - CLEO/QELS Conference*, pages 1–2, May 2007.
- [56] G. Wysocki, Y. Bakhirkin, S. So, F. Tittel, C. Hill, R. Yang, and M. Fraser. Dual interband cascade laser based trace gas sensor for environmental monitoring. *Appl. Opt.*, 46(33):8202–8210, 2007.
- [57] K. R. Parameswaran, R. T. Wainner, D. I. Rosen, D. M. Sonnenfroh, and M. G. Allen. Ethane spectroscopy for breath analysis using a mid-infrared interband cascade laser. In *Laser Applications to Chemical, Security and Environmental Analysis*, pages 1–2, May 2008.
- [58] Barbara H. Stuart. *Infrared spectroscopy: Fundamentals and applications*, chapter Organic molecules. Wiley, 2004.
- [59] <http://www.hitran.com>.
- [60] D. R. Herriott and H. J. Schulte. Folded optical delay lines. *Appl. Opt.*, 4(8):883–889, 1965.
- [61] A. M. Russell and D. A. Torchia. Harmonic analysis in systems using phase-sensitive detectors. *Rev. Sci. Instrum.*, 33:1475, 1962.
- [62] K. Duffin, A. J. McGettrick, W. Johnstone, G. Stewart, and D. G. Moodie. Tunable diode-laser spectroscopy with wavelength modulation: A calibration-free approach to the recovery of absolute gas absorption line shapes. *J. Lightwave Technol.*, 25:3114 – 3125, 2007.

BIBLIOGRAPHY

- [63] J. B. McManus, P. L. Kebabian, and M. S. Zahniser. Astigmatic mirror multipass absorption cells for long-path-length spectroscopy. *Appl. Opt.*, 34(18):3336–3348, 1995.
- [64] C. S. Patterson, L. C. McMillan, C. Longbottom, G. M. Gibson, M. J. Padgett, and K. D. Skeldon. Portable optical spectroscopy for accurate analysis of ethane in exhaled breath. *Meas. Sci. Technol.*, 18:1459–1464, 2007.
- [65] J.-M. Liu. *Photonic Devices*. Cambridge University Press, 2005.
- [66] S. D. Monk. *Ultra sensitive detection of hydrocarbons using wavelength modulation spectroscopy*. PhD thesis, University of Glasgow, Department of Physics and Astronomy, 2003.
- [67] A. S. Pine and S. C. Stone. Torsional tunneling and A1-A2 splittings and air broadening of the RQ^0 and RQ^3 subbranches of the ν_7 band of ethane. *Journal of Molecular Spectroscopy*, 175(1):21–30, 1996.
- [68] B. van Well, S. Murray, J. Hodgkinson, R. Pride, R. Strzoda, G. Gibson, and M. Padgett. An open-path, hand-held laser system for the detection of methane gas. *J. Opt. A: Pure Appl. Opt.*, 7(6):S420–S424, 2005.
- [69] L. C. Thomson, B. Hirst, G. Gibson, S. Gillespie, P. Johathan, K. D. Skeldon, and M. J. Padgett. An improved algorithm for locating a gas source using inverse methods. *Atmos. Environ.*, 41(6):1128–1134, 2007.
- [70] Y. Ma, Z. Boybeyi, S. Hanna, and K. Chayantrakom. Plume dispersion from the mvp field experiment. analysis of surface concentration and its fluctuations. *Atmos. Environ.*, 39(17):3039–3054, 2005.
- [71] R. R. Draxler. Determination of atmospheric diffusion parameters. *Atmos. Environ.*, 10(2):99–105, 1976.
- [72] R. H. Brown and T. H. Risby. *Disease markers in exhaled breath*, chapter 13. New York: Dekker, 2003.
- [73] L. Pauling, A. B. Robinson, R. Teranishi, and P. Cary. Quantitative analysis of urine vapor and breath by gas-liquid partition chromatography. *Proc. Nat. Acad. Sci. U.S.A.*, 68(10):2374–2376, 1971.

BIBLIOGRAPHY

- [74] M. Phillips, J. Herrera, S. Krishnan, M. Zain, J. Greenberg, and R. N. Cataneo. Variation in volatile organic compounds in the breath of normal humans. *J. Chromatogr. B*, 729(1-2):75–88, 1999.
- [75] W. Miekisch, J. K. Schubert, and G.F.E. Noeldge-Schomburg. Diagnostic potential of breath analysis - focus on volatile organic compounds. *Clin. Chim. Acta*, 347(1-2):25–39, 2004.
- [76] M. Phillips. Method for the collection and assay of volatile organic compounds in breath. *Anal. Biochem.*, 247(2):272–278, 1997.
- [77] <http://www.nhs.uk/conditions/blood-tests>.
- [78] A. D. Smith, J. O. Cowan, K. P. Brassett, G. P. Herbison, and D. R. Taylor. Use of exhaled nitric oxide measurements to guide treatment in chronic asthma. *N. Engl. J. Med.*, 352(21):2163–2173, 2005.
- [79] M. Yamaya, M. Hosoda, S. Ishizuka, M. Monma, T. Matsui, T. Suzuki, K. Sekizawa, and H. Sasaki. Relation between exhaled carbon monoxide levels and clinical severity of asthma. *Clin. Exp. Allergy*, 31(3):417–422, 2001.
- [80] C. Brindicci, K. Ito, O. Resta, N. B. Pride, P. J. Barnes, and S. A. Kharitonov. Exhaled nitric oxide from lung periphery is increased in COPD. *Eur. Respir. J.*, 26(1):52–59, 2005.
- [81] P. Montuschi, S. A. Kharitonov, and P. J. Barnes. Exhaled carbon monoxide and nitric oxide in copd. *Chest*, 120(2):496–501, 2001.
- [82] H. E. Elphick, E. A. Demoncheaux, S. Ritson, T. W. Higenbottam, and M. L. Everard. Exhaled nitric oxide is reduced in infants with cystic fibrosis. *Thorax*, 56(2):151–152, 2001.
- [83] P. Paredi, P. L. Shah, P. Montuschi, P. Sullivan, M. E. Hodson, S. A. Kharitonov, and P. J. Barnes. Increased carbon monoxide in exhaled air of patients with cystic fibrosis. *Thorax*, 54(10):917–920, 1999.
- [84] P.E Silkoff, M. Carlson, T. Bourke, R. Katial, E. Ogren, and S. J. Szefer. The aerocrine exhaled nitric oxide monitoring system NIOX is cleared by the us food and

BIBLIOGRAPHY

- drug administration for monitoring therapy in asthma. *J. Allergy Clin. Immunol.*, 114(5):1241–1256, 2004.
- [85] D. R. Taylor, M. W. Pijnenburg, A. D. Smith, and J. C. De Jongste. Exhaled nitric oxide measurements: Clinical application and interpretation. *Thorax*, 61(9):817–827, 2006.
- [86] B. Khalili, P. B. Boggs, and S. L. Bahna. Reliability of a new hand-held device for the measurement of exhaled nitric oxide. *Allergy*, 62(10):1171–1174, 2007.
- [87] K. Alving, C. Janson, and L. Nordvall. Performance of a new hand-held device for exhaled nitric oxide measurement in adults and children. *Respir. Res.*, 7:67, 2006.
- [88] W. Miekisch, J. K. Schubert, D. A. Vagts, and K. Geiger. Analysis of Volatile Disease Markers in Blood. *Clin. Chem.*, 47(6):1053–1060, 2001.
- [89] W. Cao and Y. Duan. Breath analysis: Potential for clinical diagnosis and exposure assessment. *Clin. Chem.*, 52(5):800–811, 2006.
- [90] T. H. Risby and S. S. Sehnert. Clinical application of breath biomarkers of oxidative stress status. *Free Radic. Biol. Med.*, 27(11/12):1182–1192, 1999.
- [91] M. Phillips, K. Gleeson, J. M. B. Hughes, J. Greenberg, R. N. Cataneo, L. Baker, and W. P. McVay. Volatile organic compounds in breath as markers of lung cancer: A cross-sectional study. *Lancet*, 353(9168):1930–1933, 1999.
- [92] S. Thelen, W. Miekisch, D. Halmer, J. Schubert, P. Hering, and M. Mürtz. Inter-comparison of infrared cavity leak-out spectroscopy and gas chromatography-flame ionization for trace analysis of ethane. *Anal. Chem.*, 80(8):2768–2773, 2008.
- [93] O. Dale, H. Bergum, T. Lund, T. Nilsen, P. Aadahl, and R. Stenseth. A validated method for rapid analysis of ethane in breath and its application in kinetic studies in human volunteers. *Free Radical Res.*, 37(8):815–21, 2003.
- [94] Z. Cao, W. J. Buttner, and J. R. Stetter. The properties and applications of amperometric gas sensors. *Electroanalysis*, 4(3):253–266, 1992.
- [95] C. Roller, K. Namjou, J. D. Jeffers, M. Camp, A. Mock, P. J. McCann, and J. Grego. Nitric oxide breath testing by tunable-diode laser absorption spectroscopy: Application in monitoring respiratory inflammation. *Appl. Opt.*, 41(28):6018–6029, 2002.

BIBLIOGRAPHY

- [96] E. V. Stepanov, P. V. Zyrianov, and V. A. Miliaev. Single-breath NO detection with tunable diode lasers for pulmonary disease diagnosis. *ALT'98 Selected Papers on Novel Laser Methods in Medicine and Biology*, 3829(1):103–109, 1999.
- [97] E. V. Stepanov, M. V. Daraselia, P. V. Zyrianov, Y. A. Shulagin, and V. A. Skrupskii. Monitoring of endogenous carbon monoxide dynamics in human breath by tunable diode laser. In *Biomedical Optoelectronics in Clinical Chemistry and Biotechnology*, volume 2629, pages 24–34. SPIE, 1996.
- [98] B. W. M. Moeskops, H. Naus, S. M. Cristescu, and F. J. M. Harren. Quantum cascade laser-based carbon monoxide detection on a second time scale from human breath. *Appl. Phys. B*, 82(4):649–654, 2006.
- [99] T. Fritsch, P. Hering, and M. Mürtz. Infrared laser spectroscopy for online recording of exhaled carbon monoxide; A progress report. *J. Breath Res.*, 1(1):014002 (8pp), 2007.
- [100] L. R. Narasimhan, W. Goodman, and C. K. Patel. Correlation of breath ammonia with blood urea nitrogen and creatinine during hemodialysis. *Proc. Nat. Acad. Sci. U.S.A.*, 98(8):4617–4621, 2001.
- [101] J. Manne, O. Sukhorukov, W. Jager, and J. Tulip. Pulsed quantum cascade laser-based cavity ring-down spectroscopy for ammonia detection in breath. *Appl. Opt.*, 45(36):9230–9237, 2006.
- [102] P. A. Riley. Free radicals in biology: Oxidative stress and the effects of ionizing radiation. *Int. J. Radiat. Biol.*, 65(1):27–33, 1994.
- [103] P. M. Abuja and R. Albertini. Methods for monitoring oxidative stress, lipid peroxidation and oxidation resistance of lipoproteins. *Clin. Chim. Acta*, 306(1-2):1–17, Apr 2001.
- [104] H. Sies. Oxidative stress: Oxidants and antioxidants. *Exp. Physiol.*, 82(2):291–295, 1997.
- [105] S. M. Gordon, J. P. Szidon, B. K. Krotoszynski, R. D. Gibbons, and H. J. O'Neill. Volatile organic compounds in exhaled air from patients with lung cancer. *Clin. Chem.*, 31(8):1278–1282, 1985.

BIBLIOGRAPHY

- [106] R. K. Brown and F. J. Kelly. Role of free radicals in the pathogenesis of cystic fibrosis. *Thorax*, 49(8):738–742, 1994.
- [107] P. Paredi, S. A. Kharitonov, D. Leak, S. Ward, D. Cramer, and P. J. Barnes. Exhaled ethane, a marker of lipid peroxidation, is elevated in chronic obstructive pulmonary disease. *Am. J. Respir. Crit. Care Med.*, 162(2):369–373, 2000.
- [108] J. M. Gutteridge and J. Mitchell. Redox imbalance in the critically ill. *Br. Med. Bull.*, 55(1):49–75, 1999.
- [109] P. J. Barnes. Reactive oxygen species and airway inflammation. *Free Radic. Biol. Med.*, 9(3):235–43, 1990.
- [110] M. P. Habib, N. C. Clements, and H. S. Garewal. Cigarette smoking and ethane exhalation in humans. *Am. J. Respir. Crit. Care Med.*, 151(5):1368–1372, 1995.
- [111] F. J. Kelly. Oxidative stress: Its role in air pollution and adverse health effects. *Occup. Environ. Med.*, 60(8):612–616, 2003.
- [112] B. Descamps-Latscha, T. Drüeke, and V. Witko-Sarsat. Dialysis-induced oxidative stress: Biological aspects, clinical consequences, and therapy. *Semin. Dial.*, 14(3):193–199., 2001.
- [113] W. A. Pryor. Measurement of oxidative stress status in humans. *Cancer Epidemiol. Biomarkers Prev.*, 2(3):289–292, 1993.
- [114] L. J. Roberts and J.D. Morrow. Measurement of F2-isoprostanes as an index of oxidative stress in vivo. *Free Radic. Biol. Med.*, 28(4):505–513, 2000.
- [115] S. T. Mayne. Antioxidant Nutrients and Chronic Disease: Use of Biomarkers of Exposure and Oxidative Stress Status in Epidemiologic Research. *J. Nutr.*, 133(3):933S–940S, 2003.
- [116] C. A. Riely, G. Cohen, and M. Lieberman. Ethane evolution: A new index of lipid peroxidation. *Science*, 183(121):208–210, 1974.
- [117] E. Aghdassia and J. P. Allard. Breath alkanes as a marker of oxidative stress in different clinical conditions. *Free Radic. Biol. Med.*, 28(6):880–886, 2000.

BIBLIOGRAPHY

- [118] J. R. Springfield and M. D. Levitt. Pitfalls in the use breath pentane measurements to assess lipid peroxidation. *J. Lipid Res.*, 35:1497–1504, 1994.
- [119] B. Halliwell and J. M. C. Gutteridge. *Free radicals in biology and medicine*. Oxford Science Publications, third edition edition, 1999.
- [120] C. M. Kneepkens, G. Lepage, and C. C. Roy. The potential of the hydrocarbon breath test as a measure of lipid peroxidation. *Free Radic. Biol. Med.*, 17(2):127–160, 1994.
- [121] K. A. Andreoni, M. Kazui, D. E. Cameron, D. Nyhan, S. S. Sehnert, C. A. Rohde, G. B. Bulkley, and T. H. Risby. Ethane: A marker of lipid peroxidation during cardiopulmonary bypass in humans. *Free Radic. Biol. Med.*, 26(3-4):439–445, 1999.
- [122] R. Stenseth, T. Nilsen, R. Haaverstad, N. Vitale, and O. Dale. Frequent sampling allows detection of short and rapid surges of exhaled ethane during cardiac surgery. *Perfusion*, 22(6):391–396, 2007.
- [123] I. S. Young and J. McEneny. Lipoprotein oxidation and atherosclerosis. *Biochem. Soc. Trans.*, 29:358–362, 2001.
- [124] S. Solberg, C. Dye, N. Schmidbauer, A. Herzog, and R. Gehrig. Carbonyls and nonmethane hydrocarbons at rural european sites from the mediterranean to the arctic. *J. Atmos. Chem.*, 25(1):33–66, 1996.
- [125] B. K. Do, H. S. Garewal, N. C. Clements, Y. M. Peng, and M. P. Habib. Exhaled ethane and antioxidant vitamin supplements in active smokers. *Chest*, 110(1):159–164, 1996.
- [126] T. Nguyen-Khoa, Z. A. Massy, J. P. De Bandt, M. Kebede, L. Salama, G. Lambrey, V. Witko-Sarsat, T. B. Dreke, B. Lacour, and M. Thvenin. Oxidative stress and haemodialysis: Role of inflammation and duration of dialysis treatment. *Nephrol. Dial. Transplant.*, 16(2):335–340, 2001.
- [127] E. Dursun, T. Ozben, G. Süleymanlar, B. Dursun, and G. Yakupoglu. Effect of hemodialysis on the oxidative stress and antioxidants. *Clin. Chem. Lab. Med.*, 40(10):1009–1013, 2002.

BIBLIOGRAPHY

- [128] E. Dursun, B. Dursun, G. Suleymanlar, and T. Ozben. Effect of haemodialysis on the oxidative stress and antioxidants in diabetes mellitus. *Acta Diabetol.*, 42(3):123–128, 2005.
- [129] G. J. Handelman, L. M. Rosales, D. Barbato, J. Luscher, R. Adhikarla, R. J. Nicolosi, F. O. Finkelstein, C. Ronco, G. A. Kaysen, N. A. Hoenich, and N. W. Levin. Breath ethane in dialysis patients and control subjects. *Free Radic. Biol. Med.*, 35(1):17–23, 2003.
- [130] R.A. Ward and K. R. McLeish. Oxidant stress in hemodialysis patients: what are the determining factors? *Artif. Organs*, 27(3):230–236, 2003.
- [131] G. J. Handelman. Efforts to determine the role of oxidant stress in dialysis outcomes. *Semin. Dial.*, 16(6):488–491, 2003.
- [132] G. J. Handelman. Current studies on oxidant stress in dialysis. *Blood Purif.*, 21(1):46–50, 2003.
- [133] R. A. Ward and K. R. McLeish. Hemodialysis with cellulose membranes primes the neutrophil oxidative burst. *Artif. Organs*, 19(8):801–807, 1995.
- [134] J. P. Cristol, J. Y. Bosc, S. Badiou, M. Leblanc, R. Lorrho, B. Descomps, and B. Canaud. Erythropoietin and oxidative stress in haemodialysis: Beneficial effects of vitamin e supplementation. *Nephrol. Dial. Transplant.*, 12(11):2312–2317, 1997.
- [135] O. Ziouzenkova, L. Asatryan, C. Tetta, M. L. Wratten, J. Hwang, and A. Sevastian. Oxidative stress during ex vivo hemodialysis of blood is decreased by a novel hemolipodialysis procedure utilizing antioxidants. *Free Radic. Biol. Med.*, 33(2):248–258, 2002.
- [136] H. Miyazaki, H. Matsuoka, H. Itabe, M. Usui, S. Ueda, S. Okuda, and T. Imaizumi. Hemodialysis impairs endothelial function via oxidative stress: Effects of vitamin E-coated dialyzer. *Circulation*, 101(9):1002–1006, 2000.
- [137] S. Banni, L. Lucchi, A. Baraldi, B. Botti, G. Cappelli, F. Corongiu, M. A. Dessi, A. Tomasi, and E. Lusvarghi. No direct evidence of increased lipid peroxidation in hemodialysis patients. *Nephron*, 72(2):177–183., 1996.

BIBLIOGRAPHY

- [138] M. A. Spittle, N. A. Hoenich, G. J. Handelman, R. Adhikarla, P. Homel, and N. W. Levin. Oxidative stress and inflammation in hemodialysis patients. *Am J Kidney Dis*, 38(6):1408–1413, Dec 2001.
- [139] K. Stevenson, K. Radhakrishnan, C. S. Patterson, L. C. McMillan, K. D. Skeldon, L. Buist, M. Padgett, and P. G. Shiels. Breath ethane peaks during a single haemodialysis session and is associated with time on dialysis. *J. Breath Res.*, 2(2):026004 (8pp), 2008.
- [140] R. A. Ward, R. Ouseph, and K. R. McLeish. Effects of high-flux hemodialysis on oxidant stress. *Kidney Int.*, 63(1):353–359, 2003.
- [141] T. Kuwahara, M. Markert, and J. P. Wauters. Neutrophil oxygen radical production by dialysis membranes. *Nephrol. Dial. Transplant.*, 3(5):661–665, 1988.
- [142] S. Sezer, E. Tural, A. Bilgic, D. Aldemir, S. Turkoglu, Z. Arat, F. N. Ozdemir, and M. Haberal. Impact of nutritional status on oxidative stress in hemodialysis patients with/without inflammatory state. *Nephrol. Dial. Transplant.*, 20(Suppl. 5):v131, 2005.
- [143] F. Galli and C. Ronco. Oxidant stress in hemodialysis. *Nephron*, 84(1):1–5, 2000.
- [144] C. S. Patterson, L. C. McMillan, K. Stevenson, K. Radhakrishnan, P. G. Shiels, M. J. Padgett, and K. D. Skeldon. Dynamic study of oxidative stress in renal dialysis patients based on breath ethane measured by optical spectroscopy. *J. Breath Res.*, 1(2):026005, 2007.
- [145] Radiotherapy: Developing a world class service for england. Technical report, Department of Health, 2007.
- [146] <http://www.goingfora.com>.
- [147] N. G. Burnet, J. Johansen, I. Turesson, J. Nyman, and J. H. Peacock. Describing patients normal tissue reactions: Concerning the possibility of individualising radiotherapy dose prescriptions based on potential predictive assays of normal tissue radiosensitivity. *Int. J. Cancer (Pred. Oncol.)*, 79(6):606–613, 1998.

BIBLIOGRAPHY

- [148] S. Tucker, F. Geara, L. Peters, and W. Brock. How much could the radiotherapy dose be altered for individual patients based on a predictive assay of normal-tissue radiosensitivity? *Radiother. Oncol.*, 38(2):103–113, 1996.
- [149] M. Baumann and T. Holscher. Towards genetic prediction of radiation responses: Estro’s genepi project. *Radiother. Oncol.*, 69(2):121–125, 2003.
- [150] Communication with Professor Alistair Munro, Surgery and Molecular Oncology, Ninewells hospital.
- [151] G. M. Ross. Induction of cell death by radiotherapy. *Endocr. Relat. Cancer*, 6(1):41–44, 1999.
- [152] V.E. Arterbery, W. A. Pryor, L. Jiang, S. S. Sehnert, W. M. Foster, and T. Risby. Breath ethane generation during clinical total body irradiation as a marker of oxygen-free-radical mediated lipid peroxidation: A case study. *Free Radic. Biol. Med.*, 17(6):569–576, 1994.
- [153] J. Macdonald, H. F. Galley, and N. R. Webster. Oxidative stress and gene expression in sepsis. *Br. J. Anaesth.*, 90(2):221–232, 2003.
- [154] Y. Gilgun-Sherki, Z. Rosenbaum, B. Melamed, and D. Offen. Antioxidant Therapy in Acute Central Nervous System Injury: Current State. *Pharmacol. Rev.*, 54(2):271–284, 2002.
- [155] C. Goodyear-Bruch and J. D. Pierce. Oxidative stress in critically ill patients. *Am. J. Crit. Care*, 11(6):543–51, 2002.
- [156] <http://www.brainit.org>.
- [157] J. K. Schubert, K. Geiger W. Miekisch, T. Birken, and G. F. E. Nldge-Schomburg. Impact of inspired substance concentrations on the results of breath analysis in mechanically ventilated patients. *Biomarkers*, 10(2-3):138–152, 2005.
- [158] O. Dale, T. Nilsen, T. Bjrgaas, A. Borkamo, and P. Aadahl. The time course of exhaled ethane in six intensive care cases. *Acta Anaesthesiol. Scand.*, 52(6):869–871, 2008.
- [159] <http://www.maxion.com>.

BIBLIOGRAPHY

- [160] G. Purvis. MWIR centre field in R& D. *III-Vs Review*, 19(8):20–25, 2006.
- [161] Wolfram Mickisch, Sabine Kischkel, Annika Sawacki, Tina Liebau, Maren Mieth, and Jochen K Schubert. Impact of sampling procedures on the results of breath analysis. *J. Breath Res.*, 2(2):026007 (7pp), 2008.

Portable optical spectroscopy for accurate analysis of ethane in exhaled breath

Claire S Patterson¹, Lesley C McMillan²,
Christopher Longbottom², Graham M Gibson¹,
Miles J Padgett¹ and Kenneth D Skeldon¹

¹ Department of Physics and Astronomy, University of Glasgow, Glasgow, UK

² Centre for Clinical Innovation, Division of Community Health Sciences,
University of Dundee, Dundee, UK

E-mail: c.patterson@physics.gla.ac.uk and k.skeldon@physics.gla.ac.uk

Received 11 January 2007, in final form 12 February 2007

Published 20 March 2007

Online at stacks.iop.org/MST/18/1459

Abstract

We report on a maintenance-free, ward-portable, tunable diode laser spectroscopy system for the ultra-sensitive detection of ethane gas. Ethane is produced when cellular lipids are oxidized by free radicals. As a breath biomarker, ethane offers a unique measure of such oxidative stress. The ability to measure real-time breath ethane fluctuations will open up new areas in non-invasive healthcare. Instrumentation for such a purpose must be highly sensitive and specific to the target gas. Our technology has a sensitivity of 70 parts per trillion and a 1 s sampling rate. Based on a cryogenically cooled lead-salt laser, the instrument has a thermally managed closed-loop refrigeration system, eliminating the need for liquid coolants. Custom LabVIEW software allows automatic control by a laptop PC. We have field tested the instrument to ensure that target performance is sustained in a range of environments. We outline the novel applications underway with the instrument based on an *in vivo* clinical assessment of oxidative stress.

Keywords: ethane, breath, oxidative stress, infrared

(Some figures in this article are in colour only in the electronic version)

1. Introduction

There is increasing interest among clinicians in the field of breath analysis. This is due in part to the relatively recent advent of accurate real-time measurement technologies. While the field of optical sensors in medicine has progressed in areas such as imaging technology [1] and adoption of new laser treatments [2], there is also a significantly important movement towards breath measurement technologies. Of interest to clinicians are techniques that target gases with known biochemical pathways [3–5]. Due to its proven role as a biomarker for free-radical-induced cell attack, ethane is of particular interest [6]. Oxidative attack on cell membrane lipids (lipid peroxidation) is regulated by the balance between free-radical production and scavenging within the body [7].

The resulting equilibrium is referred to as the level of oxidative stress (OS) [8]. Ethane is thus an excellent indicator of OS and its presence in breath could offer non-invasive, dynamic assessment of ongoing cell damage. Almost all clinical studies involving ethane have been conducted using non-real-time techniques such as gas chromatography (GC) coupled with mass spectroscopy and other variants. Such work has been pivotal in stimulating interest in ethane and while improved GC improved methods have been developed [9], the real potential of ethane as an adoptable measure of dynamic OS has been hampered by the absence of real-time technology of sufficient sensitivity. Here we describe a compact, sub-part-per-billion, maintenance-free ethane spectroscopy system. This enables continuous non-invasive *in vivo* assessment of oxidative stress in a hospital setting.

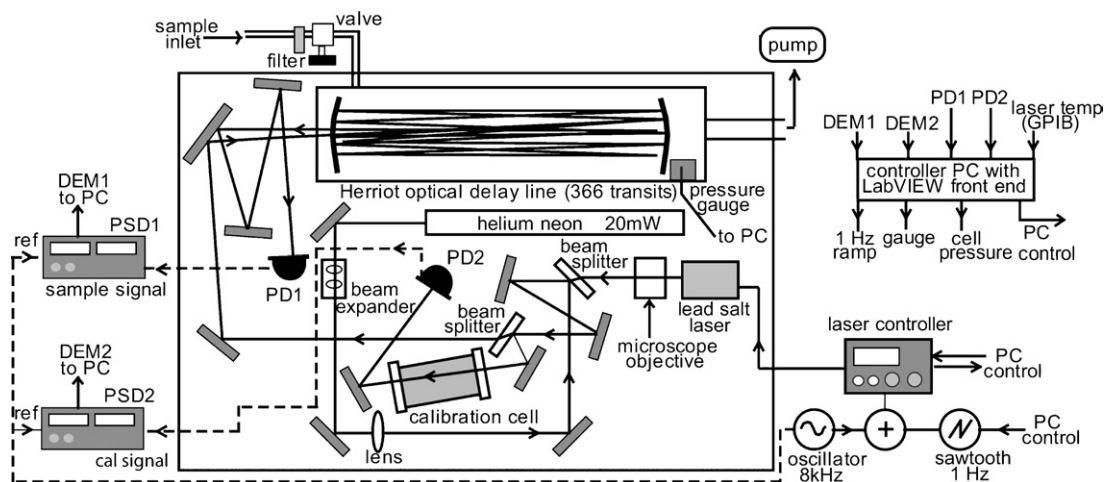


Figure 1. Schematic of the optical configuration. All optics are mounted on a 90 cm by 45 cm lightweight optical table.

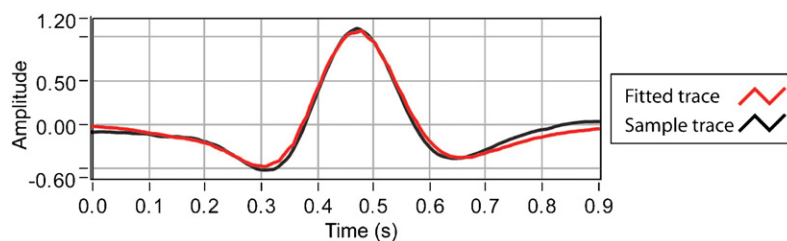


Figure 2. 2f sample lineshape and fitted lineshape as the laser wavelength is scanned over the ethane transition. A LabVIEW least squares fitting algorithm is used to calculate the ethane concentration.

2. Description of the spectroscopy system

Our instrument is based on highly resolved absorption spectroscopy across a transition for ethane gas at 2990.09 cm^{-1} . A schematic of the optical configuration is shown in figure 1. A cryogenically cooled lead-salt laser diode (IR-2990-GMP-WM, Laser Components) emits $\sim 0.2\text{ mW}$ of light which passes through a Herriott optical sample cell, 0.55 m in length. The light undergoes 366 passes and exits onto a low noise thermo-electrically cooled HgZnCdTe photodetector PD1 (VIGO PVI-2TE). Sample gas is drawn through a sample inlet pipe to the Herriott cell by a 240 l min^{-1} pump (Varian, Inc.). An air filter and regulator valve on the inlet to the cell maintains a pressure of $40\text{ mbar} \pm 2\%$ corresponding to a sample inlet flow rate of 3 l min^{-1} . Around 5% of the light is split off before the Herriott cell and directed through a 10 cm reference cell containing a known concentration of ethane also at 40 mbar and onto a second photodetector PD2. This allows for continual calibration and wavelength stability checks. A second harmonic wavelength modulation scheme is used, whereby the laser light is sine-wave modulated at 8 kHz and continually ramped through the ethane transition at 1 Hz. The reported sample cell concentration is based on curve fitting between the demodulated signals from PD1 and PD2. See figure 2. This is achieved using a least squares fitting algorithm in the LabVIEW software, which compares the 2f lineshape from the sample channel to that of the reference channel and reports coefficients for the scaling factor and offset. The

former of these coefficients is used to calculate the ethane concentration.

As the height of the ethane transition in the sample and reference channels is linearly proportional to the dc light levels at PD1 and PD2 respectively, the calculated concentration is also multiplied by the ratio of the light levels at PD1 and PD2. This normalizes for changes in the overall light level and also for relative changes in the dc levels between the photodetectors. The entire modulation scheme and data analysis process is controlled by custom-written LabVIEW software controlling a commercial laser controller (Profile PRO8000).

All electronics for modulation and signal processing is designed in house with the exception of two PSDs (Femto LIA-MV-200-H). The laser cooling is achieved by a closed-loop compressor and throttle. The instrument is thus completely self-contained, and the only additional requirement is hydrocarbon-free nitrogen gas for zero referencing. With the above configuration, we have achieved a working sensitivity of 70 parts per trillion (ppt) with a 1 Hz sample rate. This equates to a minimum detectable absorption coefficient for ethane of $1.05 \times 10^{-9}\text{ cm}^{-1}\text{ Hz}^{-\frac{1}{2}}$. Further details about the second derivative modulation spectroscopy technique can be found in [10, 11].

3. Design aspects essential for clinical use

Our instrument offers essential enhancements over previous technologies. Firstly, the physical dimensions of the system

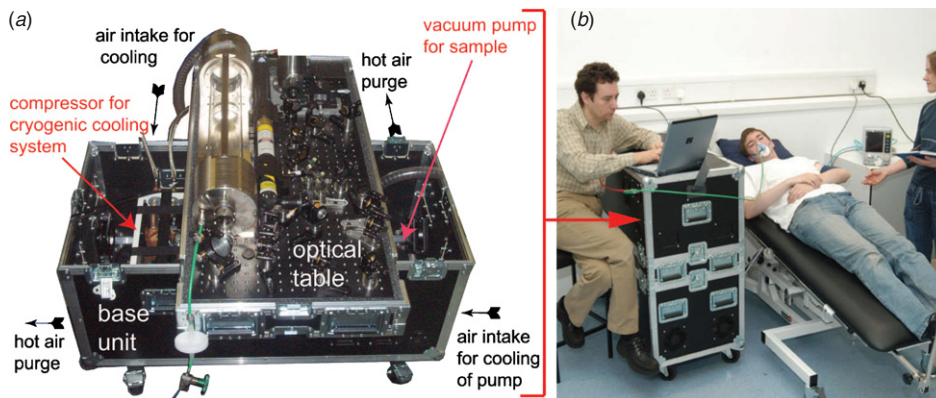


Figure 3. (a) The optical table section has been rotated to show the compressor and vacuum pump positions in the base. Thermal management is achieved via cooling fans with air flow controlled by foam partitioning. (b) The packaged instrument measures $1 \text{ m} \times 0.5 \text{ m} \times 1 \text{ m}$ (L \times W \times H), allowing ease of transportation to the bedside.

are $1 \text{ m} \times 0.5 \text{ m} \times 1 \text{ m}$ (length \times width \times height), occupying three times less volume and footprint compared with our own previously published best performance [10].

Furthermore, the self-contained cooling system dispenses with the need for liquid nitrogen, enabling use in a clinical environment. Issues such as intermittent filling with liquid nitrogen, requiring temperature re-equilibration, have been eliminated. We observe continuous operation over several days with steady operating parameters and consistent sensitivity. The closed-loop cooling system has enabled a more compact laser cold finger to be incorporated, and thus the entire laser dewar has been downsized by around a factor of 2 in volume from our lab-based system. To accommodate these design aspects, the instrument has been arranged in three sections as shown in figure 3(a). The base houses two sections containing compressor and vacuum pump, each with separate thermal management. The third (upper) section consists of the optical table on which the laser and optics are mounted. The complete instrument, being used in a physiology study, is shown in figure 3(b).

4. Performance of the spectroscopy system

The working sensitivity (70 ppt) is determined by the standard deviation measured over 1 min as hydrocarbon-free nitrogen gas is drawn through the sample cell. Example breath ethane measurements for both online and offline samples are shown in figures 4(a)–(d). In particular, online sampling allows the increase in ethane associated with the gas exchange regions within the lung to be observed over the course of a single exhalation (the so-called alveolar gradient). This level of resolution may provide additional clinical information over and above time-averaged ethane elevations.

We consider the accuracy of our instrument in terms of its absolute calibration and reproducibility. To address these issues we have performed various measurements, examples of which are shown in figure 5. In figure 5(a), a typical graph of measured concentration versus empirically calculated concentration is shown. Figure 5(b) shows the basic concentration reproducibility associated with measuring a constant ethane sample over a period of hours. Further details of the accuracy associated with our spectroscopic approach can be found in [10].

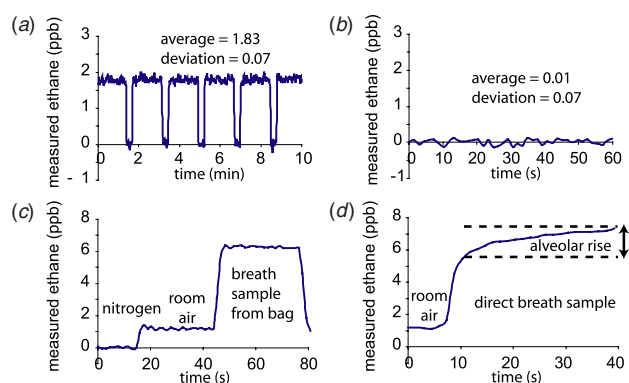


Figure 4. The performance of the ethane sensor. (a) Room air measured over 10 min, with regular nitrogen zero referencing. (b) Nitrogen gas measured over 60 s. (c) Room air followed by a breath sample contained in a Tedlar sample bag. (d) Room air followed by a breath sample exhaled directly into the instrument, whereupon the rise in ethane can be detected over a single breath

4.1. Zero referencing and absolute calibration

To provide a zero reference for the ethane figure, hydrocarbon-free nitrogen gas is measured for 12 s in every minute. This technique primarily eliminates optical fringing in the Herriott cell, which can affect the sample 2f lineshape. Optical fringing does not significantly affect the reference 2f lineshape since the reference cell contains a high concentration of ethane (500 ppm), and therefore the transition height is considerably larger than that of the fringes. As an additional measure to suppress optical fringing, the reference cell is placed in the beam path at an angle. In situations where the difference in ethane between two sources is to be examined, the zero reference can be taken as one of these sources, eliminating the need for an external reference such as nitrogen. Thus, in one of our most interesting clinical applications, namely the monitoring of intubated patients in intensive care wards, we can use the inspired and expired ports of the breathing ventilator and measure only the excess ethane contributed by the patient.

In addition, calibration is independently confirmed using a hydrocarbon reference standard certified in accordance with ISO9001 (National Physical Laboratory). This contains ethane

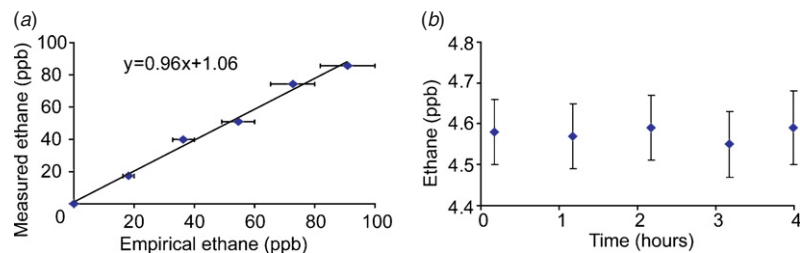


Figure 5. (a) A sequence of measured ethane concentrations showing the level of agreement with empirically calculated ethane concentrations. (b) Reproducibility of measurements of a constant ethane sample over a period of hours. The readings agree to within 0.07 parts per billion.

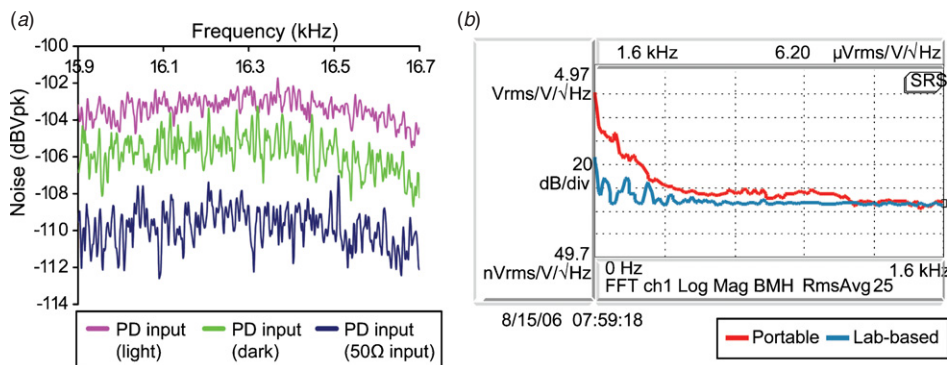


Figure 6. (a) Noise spectra measured post-photodetector electronics but pre-PSDs. The contributions due to shot noise, photodetector dark noise and electronic circuit noise (circuit grounded at photodetector input with a 50 Ω terminator) are shown. (b) Comparison of dc-coupled intensity noise measured at the sample cell photodetectors in our new instrument and existing lab-based system. Despite clear coupling of vibration from the compressor and pump housed within the new unit, potential up-conversion of this noise has no noticeable effect on measured sensitivity.

at 4.01 parts per billion (ppb) with a certification accuracy of 2%.

4.2. Factors affecting performance

Noise contributions from the detectors and electronics were measured using a Stanford Research Systems SR780 analyser. The sensitivity of the instrument is limited by a combination of photon shot noise, electronic noise and optical fringing. The basic electronic and photon shot noise is shown in figure 6(a). The photon shot noise at the sample detector equates to a fundamental sensitivity of around 20 ppt. As can be seen from figure 6(a), the carefully designed electronics do not compromise the shot noise figure. However, in practice, the sensitivity is limited by more subtle effects that are difficult to quantify, such as shifting interference patterns due to optical fringing and variation in mode purity. We have considerable experience with lead-salt laser spectroscopy systems and have noted that over a number of years the modal properties can decline.

Vibrational noise is introduced from the compressor and vacuum pump within the base compartment of the instrument. However, the overall sensitivity is not compromised as compared to our lab-based system in which the pump is isolated and liquid nitrogen is used. A comparison of the dc-coupled light level from the sample cell photodetector in our lab-based system and the portable instrument is shown in figure 6(b). Despite the considerable increase in vibration-induced light noise at the photodetectors, there is no up-

conversion of this noise compromising the signal at the detected frequency. It is reassuring that the coupling of such noise is so small since it would otherwise be difficult to suppress given the need for a compact design.

We should point out that we do not actively control the pressure or temperature of either the reference or sample cells in our configuration. While fluctuations here will have a small impact on accuracy via relative variations in the 2f lineshape, we find that optical issues mentioned above impact on sensitivity and accuracy to a much greater extent. Having said this, we do monitor sample cell pressure carefully and strive to keep the operating pressure to within 2% of 40 mbar. The reference cell pressure can be monitored via the width of the 2f lineshape displayed in the reference channel of the instrument. Additionally, the reference cell pressure is manually checked every few months and refilled if necessary. Finally, although the temperatures of the cells are not actively controlled, we find that the operating performance of the enclosed system does not depend on ambient temperature and we have seen good performance across a range of temperatures both indoor and outdoor.

4.3. The choice of laser

The modal properties of the laser are crucial in occupying a contaminant-free part of the infrared (IR) spectrum. We have found that a single mode operation at one of two transitions, 2986.73 cm^{-1} and 2990.09 cm^{-1} , is essential for our reported ethane sensitivity. While not an easily quantifiable source

of noise in terms of sensitivity reporting, we consider it a significant contributor to practical sensitivity. However, despite the perceived disadvantages of lead-salt lasers relating to reliability and longevity, we find that their use in our application offers many advantages. As indicated above, despite long-term modal changes in their output, we have shown them to be compatible with the requirements of a maintenance-free instrument. Given the need for cryogenic cooling, they are nevertheless compact and offer the necessary tuning for spectroscopic applications.

Until the commercial availability of mid-IR laser sources improves, probably by the development of mid-IR quantum cascade lasers (QCLs), lead-salt systems are likely to provide the most robust use in a compact design. Of course, we look to the future potential offered by higher power QCLs. If the need for cryogenic cooling can be relaxed, then a further generation of our technology would be made possible in terms of size, weight and perhaps, above all, cost. Alternative mid-IR laser sources include optic parametric oscillators [12] and difference frequency generators [13]. Several groups have reported sensitive ethane detection combining such sources with photoacoustic [14] or cavity leak-out [15, 16] spectroscopy. However as far as we are aware, no competing technique offers our combination of field-tested ultra-sensitivity (70 ppt), automatic operation, portability and real-time analysis.

Finally, we should point out that in addition to running the instrument indoors we have tested its robustness in a more hostile outdoor environment. By using a 4 kW portable generator, we have measured ambient ethane levels from within a moving vehicle. We achieved sub-ppb sensitivity while moving at speeds of up to 3 m s^{-1} over relatively rough terrain, as the system is highly robust to vibration and is liquid nitrogen free. This demonstrates its suitability to environmental or industrial monitoring, an area on which much of our earlier work was focused [17, 18].

5. Conclusion

We have demonstrated a novel, maintenance-free, lead-salt optical spectroscopy system for trace ethane detection. The ruggedized, portable design offers ease of use in a hospital environment. A closed-loop cooling system within a custom-built casing with careful thermal management has removed the need for liquid nitrogen cooling of the laser diode. All aspects of the wavelength modulation scheme, signal analysis and data processing are controlled by custom-written software requiring little or no operator intervention.

An analysis of the noise sources that limit our performance suggests that we are operating within 10 dB of the photon shot noise limit. Vibration induced by the compressor and vacuum pump introduces considerable intensity noise in the detected light signals at the photodetectors, but does not couple into the demodulated signals. Our achieved sensitivity of 70 ppt for a 1 s sampling rate offers an unparalleled performance for breath ethane measurement where typical concentrations are of order 1 ppb. The fast sampling allows analysis of the varying ethane concentration over the course of one breath, paving the way for on-site measurement of alveolar gradients.

We believe our work is particularly timely, given the current clinical interest in oxidative stress and the need for non-invasive assessment techniques. Many clinicians are familiar only with non-real-time processes for breath gas measurement, highlighting the need to raise awareness and discussion within the medical community of the opportunities created by optical spectroscopy. Currently, we are collaborating with various medical consultants and have in place a selection of ethics applications, some of which are now granted, for forthcoming trials. For example, we have approval for a study investigating oxidative stress in sepsis patients within intensive care wards. We are also exploring the potential of an ethane breath test as a dose mediator in radiotherapy treatment.

Acknowledgments

The work was funded primarily by a Scottish Enterprise Proof of Concept Award. L C McMillan along with our ongoing clinical evaluations are funded by an award from the Department of Health under the NEAT scheme. K D Skeldon would also like to acknowledge financial support from the NESTA, BBSRC and DTI. C S Patterson and G M Gibson acknowledge financial support from Unilever and the EPSRC respectively.

References

- [1] Hoheisel M 2006 Review of medical imaging with emphasis on X-ray detectors *Nucl. Instrum. Methods A* **563** 215–24
- [2] Huttmann G, Yao C and Endl E 2005 New concepts in laser medicine: towards a laser surgery with cellular precision *Med. Laser Appl.* **20** 135–9
- [3] Miekisch W, Vagts D A, Schubert J K and Geiger K 2001 Analysis of volatile disease markers in blood *Clin. Chem.* **47** 1053–60
- [4] Risby T H and Sehnert S S 1999 Clinical application of breath biomarkers of oxidative stress status *Free Rad. Biol. Med.* **27** 1182–92
- [5] Miekisch W, Noeldge-Schomburg G F E and Schubert J K 2004 Diagnostic potential of breath analysis—focus on volatile organic compounds *Clin. Chim. Acta.* **347** 25–39
- [6] Aghdassia E and Allard J P 2000 Breath alkanes as a marker of oxidative stress in different clinical conditions *Free Rad. Biol. Med.* **28** 880–6
- [7] Brown R H and Risby T H 2003 *Disease Markers in Exhaled Breath* (New York: Dekker) chapter 13
- [8] Halliwell B and Gutteridge J M C 1999 *Free Radicals in Biology and Medicine* (Oxford: Oxford Science Publications)
- [9] Dale O, Bergum H, Lund T, Nilsen T, Aadahl P and Stenseth R 2003 A validated method for rapid analysis of ethane in breath and its application in kinetic studies in human volunteers *Free Rad. Res.* **37** 815–21
- [10] Skeldon K D, Gibson G M, Wyse C A, McMillan L C, Monk S D, Longbottom C and Padgett M J 2005 Development of high resolution real-time sub-ppb ethane spectroscopy and some pilot studies in life science *Appl. Opt.* **44** 4712–21
- [11] Skeldon K D, Patterson C, Wyse C A, Gibson G M, Padgett M J, Longbottom C and McMillan L C 2005 The potential offered by real-time, high-sensitivity monitoring of ethane in breath and some pilot studies using optical spectroscopy *J. Opt. A: Pure Appl. Opt.* **7** 376–84
- [12] Stothard D J M, Lindsay I D and Dunn M H 2004 Continuous-wave pump-enhanced optical parametric

- oscillator with ring resonator for wide and continuous tuning of single-frequency radiation *Opt. Exp.* **12** 502–11
- [13] Richter D, Fried A, Wert B P, Walega J G and Tittel F K 2002 Development of a tunable mid-IR difference frequency laser source for highly sensitive airborne trace gas detection *Appl. Phys. B* **75** 281–8
- [14] Mueller F, Popp A, Schiller S and Kuehnemann F 2004 Cw-OPO-based photoacoustic spectrometer for highly sensitive detection of ethane and other volatile organic compounds *Photons Plus Ultrasound: Imaging and Sensing* ed A A Oraevsky and L V Wang (*Proc. SPIE* vol 5320) pp 138–44
- [15] von Basum G, Halmer D, Hering P, Mürtz M, Schiller S, Müller, Popp F A and Kühnemann F 2004 Parts per trillion sensitivity for ethane in air with an optical parametric oscillator cavity leak-out spectrometer *Opt. Lett.* **29** 797–9
- [16] Halmer D, Thelen S, Hering P and Mürtz M 2006 Online monitoring of ethane traces in exhaled breath with a difference frequency generation spectrometer *Appl. Phys. B* **85** 437–43
- [17] Gibson G, Monk S D and Padgett M 2002 A field-portable, laser-diode spectrometer for the ultra-sensitive detection of hydrocarbon gases *J. Mod. Opt.* **49** 769–76
- [18] Hirst B, Gibson G, Gillespie S, Archibald I, Podlaha O, Skeldon K D, Courtial J, Monk S and Padgett M 2004 Oil and gas prospecting by ultra-sensitive optical gas detection with inverse gas dispersion modelling *Geophys. Res. Lett.* **31** L12115

Dynamic study of oxidative stress in renal dialysis patients based on breath ethane measured by optical spectroscopy

Claire S Patterson¹, Lesley C McMillan², Karen Stevenson³,
Kamaraj Radhakrishnan³, Paul G Shiels³, Miles J Padgett¹
and Kenneth D Skeldon¹

¹ Department of Physics and Astronomy, University of Glasgow, Glasgow G12 8QQ, UK

² Centre for Clinical Innovation, Division of Community Health Sciences, University of Dundee, Dundee, UK

³ University Department of Surgery, Glasgow Royal Infirmary, Glasgow, UK

E-mail: c.patterson@physics.gla.ac.uk

Received 11 July 2007

Accepted for publication 30 October 2007

Published 6 December 2007

Online at stacks.iop.org/JBR/1/026005

Abstract

The application of optical spectroscopy for rapid accurate measurement of breath biomarkers has opened up new possibilities for monitoring and diagnostics in recent years. Here, we report on how our recent advances in optical detection of ethane have enabled us to record dynamic breath ethane patterns for patients undergoing kidney dialysis. Ethane is well established as a breath biomarker for free radical induced cell degradation. Moreover, renal dialysis is known to induce such oxidative attack, and our measurements may offer insight into the nature of this assault. Specifically, we have discovered that patients undergo significant breath ethane elevation at the beginning of each dialysis session. We have found an inverse relationship between the magnitude of this effect and number of months patients have been receiving treatment. We comment on how further refinements of our technology will allow a more detailed evaluation of the ethane elevation effect and ultimately lead to the assessment of potential interventions.

(Some figures in this article are in colour only in the electronic version)

1. Introduction

Over the last two decades, evidence linking oxidative stress and dialysis has grown. A number of groups have reported elevation in markers of oxidative stress in haemodialysis patients compared with healthy control groups [1–4]. While increased oxidative stress is considered to be a major factor in morbidity and mortality in dialysis patients [5], the factors contributing to this increase are not clear [6, 7]. Suggested causes include the uremic state [6], vitamin C deficiency [8], inflammatory status and duration of treatment [1]. In particular, it has been reported that the dialysis treatment *per se* may cause oxidative damage due to dialysate quality or dialyzing membranes, possibly by the stimulation of primed neutrophils [6, 9]. Techniques directed towards preventing

the damage from oxidative stress are under investigation, such as the effect of antioxidants [10, 11] and bio-compatible or vitamin E-coated membranes [12].

A number of biomarkers can be used for the measurement of oxidative stress. Blood markers include malondialdehyde (MDA), thiobarbituric acid reactive substances (TBARS), F₂-isoprostanes, glutathione (GSH) and oxidized low density lipoproteins (LDL) [5, 13–15]. Breath markers of oxidative stress such as exhaled hydrocarbons offer the advantage of non-invasive monitoring [16]. Here, we have focused on ethane as a well-established marker of oxidative stress [17–19]. Ethane is a product of free-radical-induced lipid peroxidation of omega-3 fatty acids in the cell membrane [20]. It is a particularly good marker of oxidative stress for several reasons. Its means of generation is well understood [16] and

other potential sources (for example, from the metabolism of bacteria in the colon) are not considered to contribute significantly [21]. Most importantly, however, ethane appears in the breath within seconds of the release of free radicals in the tissue [22]. Being both poorly metabolized and poorly soluble in the body, volatile ethane diffuses rapidly into the bloodstream and is transported to the lungs where it is exhaled [21]. This speed facilitates non-invasive patient monitoring applications when an appropriately periodic and rigorous sampling regime is used. Such monitoring has been recognized as important for gaining insight into oxidative damage in various clinical conditions [16, 23].

Past studies of oxidative stress using breath ethane have often involved only a small number of 'one-off' measurements, for example, before and after a treatment session. However, this approach lacks the resolution to track rapid or short-lived effects and this may have contributed to inconsistent results seen in the literature [4, 24].

Methods based on gas chromatography are generally time consuming for large numbers of samples, although improved methods have been developed for sequential breath sampling [25]. Optical techniques are inherently better suited to breath monitoring applications due to the combination of sensitivity and speed. For example, Narasimhan *et al* used photoacoustic spectroscopy to measure breath ammonia in patients undergoing haemodialysis treatment [26]. Cavity-ring down spectroscopy also enables rapid breath ammonia detection [27]. Such techniques are of interest for possible monitoring of kidney function and efficacy of dialysis.

Similarly, real-time techniques for the measurement of ethane could open up a new window on the monitoring of oxidative stress. Real-time ethane detection is currently only possible using optical techniques, such as cavity leak-out spectroscopy [28, 29] and our adopted technique of wavelength modulation absorption spectroscopy. Another sensitive technique is photoacoustic spectroscopy [30], although measurement integration times are typically longer than 1s.

The aim of this study was to monitor dialysis patients' changing ethane levels at regular intervals during single dialysis sessions. We achieved this using an ultra-sensitive laser absorption spectroscopy system developed within our team [31, 32] and located a short distance from the dialysis clinics used in the study. The system offers real-time measurement of ethane at the trace levels present in exhaled breath. Due to practical constraints, this pilot study involved breath collection using sample bags which were subsequently measured in the laboratory. While the real-time nature of our technique was therefore not fully exploited, it did facilitate the rapid turnaround of a large number of samples. We plan to employ our technology directly in the ward in future studies.

2. Materials and methods

2.1. Participants

Thirty subjects were recruited from patients presenting at the renal dialysis clinics at Glasgow Western Infirmary and

Glasgow Gartnavel General Hospital. Patients were recruited subject to the requirement that they were non-smokers and had not consumed alcohol for at least 12 h prior to their arrival at the clinic. This was to minimize the risk of known contamination issues. Six sets of patient samples were later excluded: four due to anaesthetic contamination, one due to unexplained excessive background fluctuation that swamped the breath samples and the other due to an inconsistent patient breathing technique.

The remaining 24 patients (age 65 ± 16 yr, mean \pm SD, range 39–85 yr) comprised 19 males and 5 females. Patients had been on dialysis for periods ranging from 4 days to 12 years and received three four-hourly sessions (typically) per week using Polyflux[®] dialysis membranes. The distribution in this period was highly positively skewed (median 10 months, range 0.1–141 months).

Patients receiving dialysis treatment had a wide variety of underlying conditions including renovascular disease, polycystic kidney disease, glomerulonephritis, obstructive uropathy, IgA nephropathy, membranous nephropathy and diabetic nephropathy. Five out of the twenty four patients were diabetic.

Informed consent was obtained from all participants and the study was approved by the Ethics committee of Universities West of Scotland NHS Trust.

2.2. Measurement of breath ethane using laser spectroscopy

Ethane concentrations were analysed using a laser spectroscopy system developed at Glasgow University. This technology is recognized as state-of-the-art in the field of trace gas detection.

The technology, photographed in figure 1 and schematically illustrated in figure 2, is summarized below. We perform high resolution absorption spectroscopy targeted at $\sim 3.4 \mu\text{m}$ (2990.09 cm^{-1}) using a cryogenically-cooled, tunable, lead-salt diode laser (IR-2990-GMP-WM, Laser Components). This absorption line is well separated from common contaminating species in the mid-IR window such as water and methane. The laser light is directed along two main optical paths: the principal path contains a Herriott optical delay line (AMAC-100, Aerodyne) with an optical path of >150 m, through which the target gas sample is drawn by a $240 \text{ litre min}^{-1}$ rotary pump (Varian, Inc.). The other path contains a short reference cell filled with a known ethane concentration. The laser light from each path is detected using two thermo-electrically cooled HgZnCdTe photodetectors, PD1 and PD2 (PVI-2TE Vigo). A helium–neon laser is used for alignment. A second derivative modulation scheme is used where the laser wavelength is modulated at 8 kHz and ramped through the ethane transition at 1 Hz. The signals are demodulated using two phase sensitive detectors, PSD1 and PSD2 (LIA-MV-200-H, Femto). The reported sample cell concentration is based on least-squares fitting between the demodulated signals, DEM1 and DEM2, from photodetectors PD1 and PD2 (see figure 2). A thermally-managed closed-loop cooling system (CryoTiger) eliminates the need for liquid coolants, enabling long term, uninterrupted use. The system



Figure 1. The ultra-sensitive, real-time ethane spectroscopy system developed at the University of Glasgow. The instrument with dimensions 1 m × 0.5 m × 1 m ($L \times W \times H$) is completely self-contained.

has a sensitivity of 70 parts per trillion, and data are returned at the rate of one value every second: essentially real-time data. All aspects of instrument control are automated by custom-written LabVIEW software, which controls a commercial laser controller (Profile PRO8000).

The instrument is arranged in three sections: the base houses the compressor, used to cool the laser, and vacuum pump, used to draw the gas into the sample cell, each with separate thermal management. The upper section, which can be completely separated from the base, supports the optical table on which the laser and optics are mounted, the laser controller and the detection electronics. Finally, there is a lid, which can also be removed. The instrument, with dimensions 1 m × 0.5 m × 1 m ($L \times W \times H$) is thus completely self-contained as shown in figure 1.

Our confidence in our reported data stems from a reliable and reproducible instrument performance as previously reported in [31]. The instrument self-calibrates every second using the in-built ethane reference cell. In addition, hydrocarbon-free nitrogen gas (BOC Ltd) is measured for 12 s in every minute as a zero reference. The absolute accuracy is also regularly checked using a hydrocarbon reference standard supplied by the National Physical Laboratory. This standard contains ethane at 4 ppb with a tolerance of 2% certified in accordance with a ISO9001 specification technique, and allows independent confirmation of the ethane measurement at the typical levels measured in the study.

A key advantage of this technology is that the direct analysis of gas samples requires no cooling or pre-concentration. Therefore each breath sample was analysed

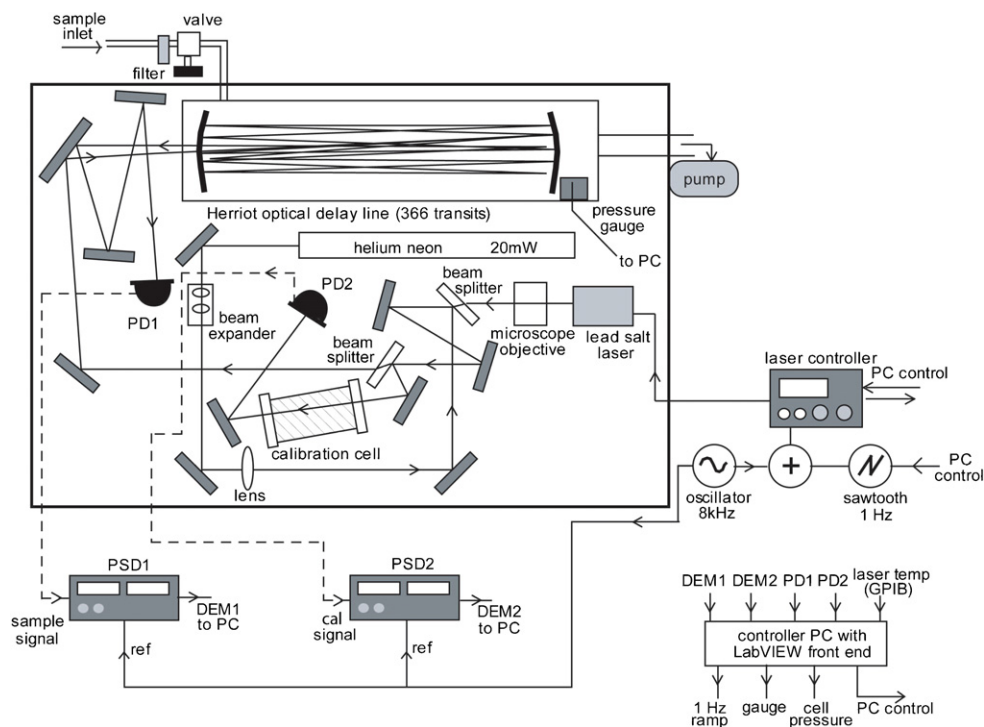


Figure 2. A schematic of the optical configuration. Patterson *et al* [31] provides the necessary information to reproduce the technology described in this report.

in less than 1 min. For example, the 38 samples collected for each patient (as described below) required a total measurement time of less than 40 min. Typically, we collected and analysed the breath ethane of four patients in a day. The total number of samples analysed in the study was >1000. This technique represents a considerable improvement in measurement efficiency and sample turnaround compared to other methods of sub-ambient ethane detection.

Further details of the system and its performance have been reported previously [31, 32] and further details can be obtained from the authors. The current system incorporates a laser with a tuning range that has enabled methane detection and could enable ethylene detection. The technology could be easily adapted to monitor other hydrocarbons such as propane, butane or pentane by use of a laser with the appropriate wavelength tuning range. Given the crucial role the laser plays in our system, the future progress and general cost-effectiveness of such instrumentation is strongly coupled to new developments in quantum cascade laser and optical parametric oscillator technology in the mid-IR range [33].

2.3. Study design

As previously outlined, the aim of the study was to monitor the oxidative stress level of patients during a single visit to the dialysis clinic by way of regular measurement of breath ethane. Each patient acted as their own control. Baseline breath ethane levels vary between individuals and therefore, in order to validate the comparison of patient data, we measured the extent of the change in each patient's breath ethane level from their respective baseline level. In other words, a common datum was defined with respect to patient baseline breath ethane levels by setting these to zero.

Healthy volunteers in close proximity to the patients also provided a concurrent series of breath samples using the same exhalation technique. This secondary control set was in order to verify that the observed effect was solely attributable to patient response and independent of environmental factors.

Frequent sampling throughout the whole of the treatment session was incompatible with the overriding requirement for good patient care. Fortunately, our early work had indicated raised exhaled ethane levels at the beginning of the treatment session and so the most rapid sampling was confined to this period.

The collection protocol was set at one sample every 2 min during an 8 min period prior to dialysis, then every 2 min for the first 10 min of dialysis followed by every 5 min during the next 20 min. Three samples were then collected at 10 min intervals and subsequent samples were collected at hourly intervals with a final sample being collected at the end of the dialysis session. The definition of the start of dialysis here is the point at which the dialysis machine commenced the blood flow returning to the patient, typically a few minutes after the initial attachment and flushing of the lines with saline. Precise times of breath collection were subject to small variations (typically ± 10 s) to avoid interference with clinical procedures or interventions. Patient care was considered paramount throughout.

Samples were collected in 5 litre ethane-impermeable bags (Tedlar, SKC Ltd). Patients exhaled through a disposable

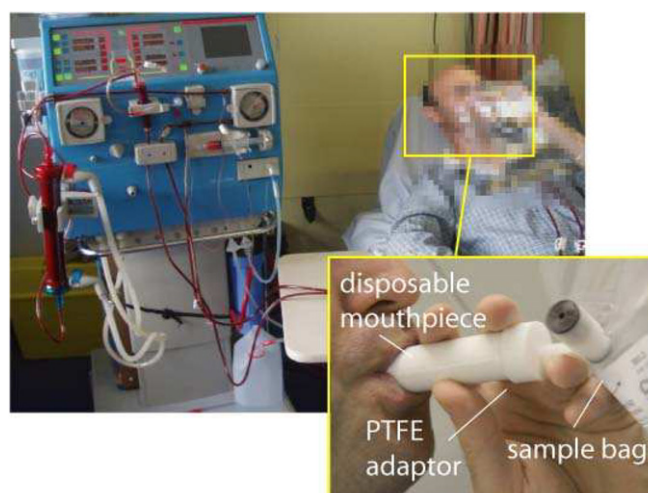


Figure 3. Breath samples were collected using a simple single breath filling technique into SKC Tedlar sample bags.

cardboard mouthpiece (Bedfont Scientific Ltd), connected to the sample bags by a Teflon mouthpiece adaptor. The setup is shown in figure 3.

2.3.1. Breath sampling. To standardize the protocol, a consistent breath sampling technique was adopted. Each breath sample was a single expiration of vital capacity. Patients found this approach easy to reproduce as is evident from the consistent longitudinal baseline measurements. The initial deep inhalation ensured each exhalation was more than minimum volume (1 litre) required for ultra-precise ethane measurement. For each breath sample collected, a corresponding room air sample was obtained using an oil-free hand pump and corrected breath ethane measurements were obtained by subtraction of these ambient ethane levels.

2.3.2. Contamination issues. Our spectroscopic window is extremely small, covering the width of our target ethane transition and no more. Consequently, we find contamination issues from other commonly present gases to be effectively eliminated. These include other VOCs and other compounds. The use of a second derivative detection scheme reduces the effects of a broadband absorption (e.g. water or isoprene) in the vicinity of the ethane transition. Methane and ethylene do have sharp absorption features neighbouring the ethane transition; however, contamination only occurs at concentrations of these gases much higher than levels found in ambient air and breath.

Importantly, the presence of contaminants is easily established using our detection technique. Any contamination causes distortion of the displayed ethane transition shape and constant monitoring of this via a curve-fitting algorithm provides a continuous check against such contamination.

All sampling equipment used was checked for the production of ethane and/or contaminants and no source of either was found. Commonly used hospital cleaning solutions were investigated as sources of contamination. Chlorohexadine gluconoate solution is typically used for patients for whom access is by way of a central line. In

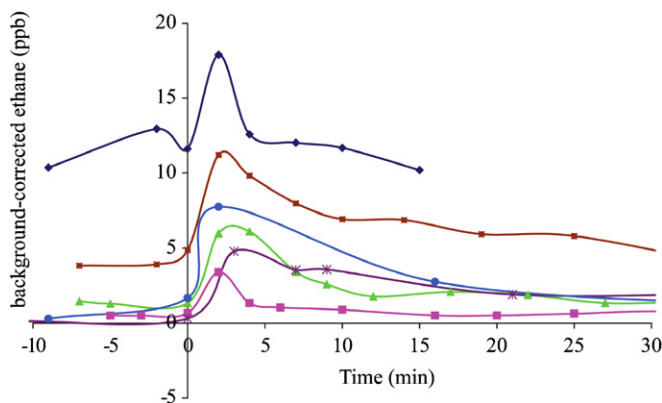


Figure 4. Elevation of ethane in first 30 min of dialysis, plotted for six patients. These values have been corrected for ambient ethane levels.

the case of fistula access, chlorohexadine gluconoate solution containing ethanol is used. The detection technique is insensitive to both of these compounds. However, ethyl chloride, often used as a local anaesthetic, was found to be a contaminant and was therefore avoided.

In this study, samples from four patients were affected by contamination due to ethyl chloride and were discarded. We can verify that the observed increases in breath ethane reported here were not due to contamination.

2.4. Data analysis

Data are presented as mean \pm standard deviation or median and range. The data were plotted to show the relationships between the magnitude of the ethane peak and other clinical scores, including period on dialysis, age, gender and comorbidity factors. The Student t-test was used and where data were found not to conform to the parameters of a normal distribution, significance testing was performed using a Mann–Whitney test for non-parametric data. Statistical significance was accepted at $P < 0.05$.

3. Results

Patient breath ethane measurements were corrected for the ambient air ethane by subtracting corresponding values and plotted against time. This standard technique [16, 34] takes account of modest variations in ambient ethane levels. A key advantage of our technology is that it enables the resolution of even relatively small changes in breath ethane above higher ambient levels. Other techniques include the breathing of purified air [18], a technique we considered unsuitable for this trial due to practical constraints. Significant short-lived increases in breath ethane were observed in 14 out of 24 patients within the first few minutes of the dialysis session. For clarity, since these peaks are largely coincident, a subset of six representative examples of the 24 are illustrated in figure 4. The effect was not observed in the healthy volunteers who acted as the secondary control group (see figure 5) and no further elevated breath ethane levels were observed at any time after the initial 30 min of the treatment session.

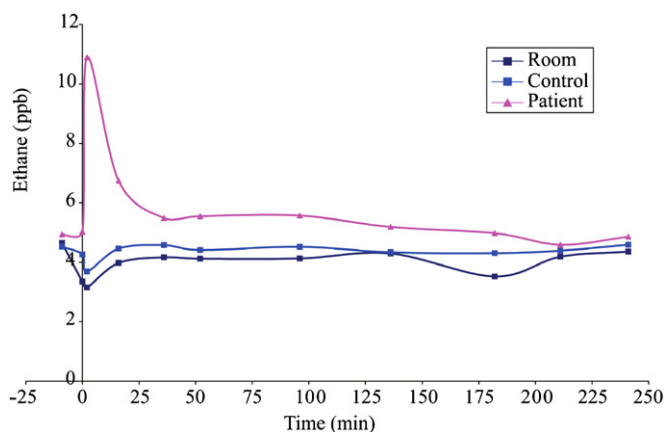


Figure 5. Comparison of room ethane, breath samples taken from a control subject and breath samples taken from a dialysis patient. This robustly demonstrates that the ethane elevation effect is confined to the patient.

Breath ethane levels prior to dialysis treatment (patient baseline levels) are seen to vary between individuals (median 0.6 ppb, range 0–12 ppb). This is seen in the positioning of the (background-corrected) traces along the y-axis in figure 4.

Ethane is a ubiquitous marker of oxidative stress and therefore a large number of factors will contribute to baseline ethane levels. In order to assess the contribution from the dialysis treatment *per se* the datasets were normalized by setting a common zero baseline ethane level. The peak level of ethane (PE) was defined as follows:

$$PE = E_{\max} - E_0, \quad (1)$$

where E_{\max} is the maximum background-corrected breath ethane concentration measured within approximately 5 min of start of dialysis and E_0 is the mean background-corrected breath ethane concentration measured prior to the start of dialysis.

The peak ethane measurements presented therefore correspond to the net change in breath ethane concentration. Peak ethane values for each of the 24 patients along with corresponding patient clinical data is shown in figure 6.

The distribution in peak levels of ethane generated by equation (1) was also highly positively skewed; median = 0.7 ppb, and range 0.1–14.9 ppb. The distribution in the Peak levels was not found to correlate with age. However, the distribution was found to be significantly different in the two patient groups that used either a fistula or a central line for access. (Mann–Whitney test significant at 0.0069). For patients with a fistula access ($n = 19$) the median Peak level of ethane = 0.5 ppb, range 0.1–14.9 ppb. For patients with a central line ($n = 5$) the median peak level of ethane = 6.3 ppb; range 2.9–7.5 ppb. However, this is likely to be misleading since patients new to dialysis treatment tend not to have had a fistula provided yet. Period on dialysis and fistula use are therefore not independent and the ethane peak levels were found to be strongly dependent on the former.

A significant correlation was found between peak level of ethane and period on dialysis (PoD) (see figure 7(a)).

Patient	Underlying condition	Diabetes present (1=yes)	Period on dialysis (months)	Age (yrs)	Type of access (1=fistula)	Peak level of ethane (ppb)
1	Diabetic Nephropathy	1	4	43	0	4.77
2		1	4	74	1	7.45
3		1	15	48	0	3.02
4		1	1	82	1	4.66
5	Drug Induced-Lithium	0	11	80	1	0.85
6	Glomerulonephritis	0	60	57	1	0.34
7		0	141	39	1	0.15
8		0	4	39	1	0.31
9	IgA nephropathy	0	20	72	1	0.28
10		0	120	72	1	0.47
11		0	0.1	47	0	6.28
12	Membranous Nephropathy	0	6	85	0	7.28
13	Obstructive Uropathy	0	15	66	1	0.52
14		0	0.3	44	1	14.93
15	Polycystic kidney disease	0	60	50	1	0.62
16		0	115	77	1	0.13
17	Renovascular disease	0	6	67	1	0.15
18		0	6	79	1	0.4
19		0	28	81	1	1.88
20		1	4.5	75	0	2.9
21		0	5	78	1	0.22
22	Unknown	0	10	76	1	1.68
23		0	10	83	1	1.35
24		0	17	49	1	0.2

Figure 6. Clinical data and corresponding measured peak ethane values for the 24 recruited patients in the study.

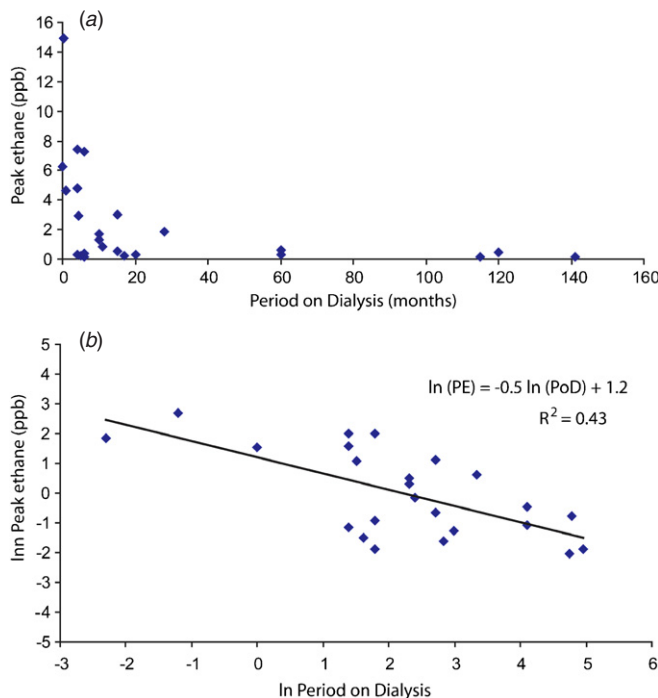


Figure 7. (a) Peak ethane dependence on period on dialysis. (b) The same data transformed to a natural log–log scatterplot.

Both variables demonstrated lognormal distributions and a natural log–log plot (figure 7(b)) yielded a linear relationship ($R^2 = 0.43$). The equation of the fitted line is

$$\ln(\text{PE})_{\text{all data}} = -0.5(\ln \text{PoD}) + 1.2. \quad (2)$$

Modified Charlson co-morbidity scores (CCS) were calculated for all patients (median 5, range 2–11). No significant correlation was found between peak level of ethane and age, gender or co-morbidity. Although peak ethane appeared to be higher in diabetic patients (median 4.7 ppb, range 2.9–7.5 ppb) than non-diabetic patients (median 0.5 ppb,

range 0.1–14.9 ppb), it was shown that diabetic status was not independent of fistula use and period on dialysis. This is discussed further in [36].

4. Discussion

We have monitored changes in oxidative stress during dialysis treatment using exhaled ethane as a biomarker. As shown in figures 4 and 5 we observed a single, short-lived ethane peak on commencement of dialysis, suggesting that there is a significant increase in oxidative stress at this time.

The absence of this effect in both of the concurrent sample sets of ambient air and exhaled breath from the healthy volunteers (see figure 5) confirms that the effect is solely attributable to patient response. The control trace essentially mirrors the relatively flat background air trace. It should be pointed out of course that the healthy volunteers did not receive dialysis treatment. This set of controls should not be confused with the primary control group. In this longitudinal study, the patients acted as their own control in the strictest sense. Each patient provided a series of samples that were referenced to the their own baseline breath ethane level, that is, the level measured immediately before the start of their treatment session.

The peaks in breath ethane are unlikely to be due to a reservoir of ethane stored in tissue since ethane is highly volatile and poorly metabolized, rapidly diffusing into the blood stream upon production [22]. Possible errors due to inconsistent breath sampling were reduced using the breath sampling protocol described in section 2.3.1. The consistency of the observed ethane elevation effect (observed in 14 out of the 24 patients) with ethane concentrations significantly higher than the breath to breath fluctuations found even in healthy controls suggests that the effect could not be solely attributable to patient breathing dynamics.

It is recognized that a large number of factors affect the overall oxidative stress status of dialysis patients, such as age, lifestyle and underlying condition. For example, a higher level of oxidative stress has been reported in diabetic haemodialysis patients [3]. While we recognize these factors, this pilot study focused specifically on the detection of rapid changes in oxidative stress associated with the dialysis treatment *per se*. Normalizing peak ethane levels to the patients' baseline ethane levels enabled us to look at this short-term effect across a limited number of patients with a broad range of underlying conditions. Ethane is a ubiquitous marker of oxidative stress and baseline ethane levels are known to vary considerably even between healthy control patients [35] and can even vary significantly in a healthy individual from day to day. For this reason it is difficult to extract relevant information from a single measurement of baseline ethane from individual patients in a study with small patient numbers. No significant relationship was found between baseline ethane level and pathology in this pilot study. However, trends may become apparent in a larger scale study (see below). A paper is in preparation by our clinical collaborators in which the potential biological and clinically relevant factors affecting breath ethane production are further explored [36].

The relatively low level of noise in the expired ethane traces indicate that the consistent breath sampling protocol worked well and that possible variation in patient respiratory rate, expired volume and background ethane had a minimal effect.

It is important to note that the peak ethane measured for each patient is a conservative estimate of the true maximum. This is due to the finite sampling intervals and the consequential limited resolution with respect to the changing breath ethane concentration. This may explain the spread in the data shown in figure 7 and the relatively low value of R^2 in figure 7(b). More frequent sampling could help reduce this spread. However, in practice, acquiring breath samples from a patient more regularly than at 2 min intervals is difficult without disrupting clinical care.

Clearly the speed of the ethane response highlights the need for regular, continual sampling for the detection of such transient events. For example, had patient breath sampling been limited to pre- and post-dialysis, the effect would have been missed completely and the false conclusion drawn that ethane levels (and oxidative stress) are unchanged during dialysis treatment. This could explain the conflicting results from a number of previous studies of lipid peroxidation in dialysis patients [4, 24]. Our results are consistent with the findings of Ward *et al* [9, 37] that neutrophil priming, as a consequence of interaction with dialysis membranes, results in a respiratory burst that can lead to lipid peroxidation. Kuwahara *et al* also noted this neutrophil activation [38].

Figure 7(a) suggests that haemodialysis patients do become conditioned to their treatment regime relatively quickly, since peak ethane levels decrease exponentially with period on dialysis. This is in keeping with findings of Sezer *et al* that oxidative stress was negatively correlated with dialysis duration [39].

Since the observed ethane fluctuations are transient, suggesting only short-term periods of oxidative stress, it is unknown if there are any significant long-term consequences of this oxidative damage. It will be important to establish if the repetition of such events have an effect on morbidity or mortality outcomes. If so, it may be that the use of an appropriate intervention could reduce the oxidative stress response in patients new to dialysis treatment. Recent approaches include haemolipodialysis, infusion of antioxidants by dialysate and the use of vitamin E bonded membranes [7, 12, 40]. Breath ethane is a specific marker of lipid peroxidation, which antioxidants such as vitamin E can reduce. Therefore, breath ethane monitoring could offer useful assessment of oxidative stress during haemodialysis and the effect of vitamin E-bonded membranes. For example, previous studies in other areas have shown that the production of breath ethane arising from reperfusion injury during organ transplantation [18] or during cardio pulmonary bypass [41] could be reduced using radical scavenging species. A review by Abuja and Albertini [23] suggests that the increasing use of antioxidants in medicine will lead to the requirement for monitoring of oxidative stress in a laboratory or hospital in the future.

Future studies with a much greater patient number and a more uniform sample will be necessary in order to determine

the potential clinical benefit of such monitoring during dialysis. In this pilot study, practical constraints prevented the recruitment of the ideal patient group, resulting in highly skewed patient statistics (see section 2.1), which may have contributed to the R^2 value in figure 7. Increased patient numbers will also enable better understanding of the variability in baseline levels of ethane among the patients and the possible relationship with pathology and other factors.

In this study, we have exploited the real-time nature of our technology to enable the rapid turnaround of large numbers of discrete breath samples. However, our real-time technology has recently been developed into a ward-portable form for on-site use [31]. This will allow us to further resolve changes in breath ethane. We now have the ability to embark on future studies where continuous ethane monitoring can be supported. This is likely to offer greater insight into the ethane elevation effect and the factors contributing to oxidative stress during dialysis.

Acknowledgments

We are indebted to the staff and patients of the dialysis clinics of Gartnavel General Hospital and the Western Infirmary, both in Glasgow. Their cheerful assistance was much appreciated. The advice and help of Ms Laura Buist and Dr Colin Geddes were also gratefully received. CP would like to acknowledge the financial support of Unilever and EPSRC. Similarly, LM is grateful to NEAT and KS would like to thank DTI, NESTA and HRH. KR and PS would like to acknowledge their funding by Novartis and Darlinda's Charitable Trust, respectively. Finally, we would like to acknowledge the supplementary financial and general infrastructure support provided by The University of Glasgow.

References

- [1] Nguyen-Khoa T, Massy Z A, De Bandt J P, Kebed M, Salama L, Lambrey G, Witko-Sarsat V, Drüeke T B, Lacour and Thévenin M 2001 Oxidative stress and haemodialysis: role of inflammation and duration of dialysis treatment *Nephrol. Dial. Transplant.* **16** 335–40
- [2] Dursun E, Ozben T, Süleymanlar S, Dursun B and Yakupoglu G 2002 Effect of hemodialysis on the oxidative stress and antioxidants *Clin. Chem. Lab. Med.* **40** 1009–13 (DOI:10.1515/CCLM.2002.175)
- [3] Dursun E, Dursun B, Suleymanlar G and Ozben T 2005 Effect of haemodialysis on the oxidative stress and antioxidants in diabetes mellitus *Acta. Diabetol.* **42** 123–8 (DOI:10.1007/s00592-005-0191-1)
- [4] Handelman G J *et al* 2003 Breath ethane in dialysis patients and control subjects *Free Radic. Biol. Med.* **35** 17–23 (DOI:10.1016/S0891-5849(03)00183-7)
- [5] Descamps-Latscha B, Drüeke T and Witko-Sarsat V 2001 Dialysis-induced oxidative stress: biological aspects, clinical consequences, and therapy *Semin. Dial.* **14** 193–9 (DOI:10.1046/j.1525-139X.2001.00052)
- [6] Ward R A and McLeish K R 2003 Oxidant stress in hemodialysis patients: what are the determining factors? *Artif. Organs* **27** 230–6 (DOI:10.1046/j.1525-1594.2003.07170.x)
- [7] Handelman G J 2003 Efforts to determine the role of oxidant stress in dialysis outcomes *Semin. Dial.* **16** 488–91 (DOI:10.1046/j.1525-139X.2003.16105.x)

- [8] Handelman G J 2003 Current studies on oxidant stress in dialysis *Blood Purif.* **21** 46–50 (DOI:10.1159/000067868)
- [9] Ward R A and McLeish K R 1995 Hemodialysis with cellulose membranes primes the neutrophil oxidative burst *Artif. Organs* **19** 801–7
- [10] Cristol J P, Bosc J Y, Badiou S, Leblanc M, Lorrho R, Descomps B and Canaud B 1997 Erythropoietin and oxidative stress in haemodialysis: beneficial effects of vitamin E supplementation *Nephrol. Dial. Transplant.* **12** 2312–7
- [11] Ziouzenkova O, Asatryan L, Tetta C, Wratten M L, Hwang J and Sevanian A 2002 Oxidative stress during ex vivo hemodialysis of blood is decreased by a novel hemodialysis procedure utilizing antioxidants *Free Radic. Biol. Med.* **33** 248–58 (DOI:10.1016/S0891-5849(02)00875-4)
- [12] Miyazaki H, Matsuoka H, Itabe H, Usui M, Ueda S, Okuda S and Imaizumi T 2000 Hemodialysis impairs endothelial function via oxidative stress: effects of vitamin E-coated dialyzer *Circulation* **101** 1002–6
- [13] Pryor W A 1993 Measurement of oxidative stress status in humans *Cancer Epidemiol. Biomarkers Prev.* **2** 289–92
- [14] Roberts L J and Morrow J D 2000 Measurement of F₂-isoprostanes as an index of oxidative stress in vivo *Free Radic. Biol. Med.* **28** 505–13 (DOI:10.1016/S0891-5849(99)00264-6)
- [15] Mayne S T 2003 Antioxidant nutrients and chronic disease: use of biomarkers of exposure and oxidative stress status in epidemiologic research *J. Nutr.* **133** 933S–40S
- [16] Miekisch W, Noeldge-Schomburg G F E and Schubert J K 2004 Diagnostic potential of breath analysis—focus on volatile organic compounds *Clin. Chim. Acta* **347** 25–39 (DOI:10.1016/j.cccn.2004.04.023)
- [17] Riely C A, Cohen G and Lieberman M 1974 Ethane evolution: new index of lipid peroxidation *Science* **183** 208–10 (DOI:10.1126/science.183.4121.208)
- [18] Risby T H and Sehnert S S 1999 Clinical application of breath biomarkers of oxidative stress status *Free Rad. Biol. Med.* **27** 1182–92 (DOI:10.1016/S0891-5849(99)00212-9)
- [19] Aghdassi E and Allard J P 2000 Breath alkanes as a marker of oxidative stress in different clinical conditions *Free Rad. Biol. Med.* **28** 880–6 (DOI:10.1016/S0891-5849(00)00189-1)
- [20] Halliwell B and Gutteridge J M C 1999 *Free Radicals in Biology and Medicine* 3rd edn (Oxford: Oxford Science Publications) (DOI:10.1016/S1357-2725(99)00059-X)
- [21] Kneepkens C M, Lepage G and Roy C C 1994 The potential of the hydrocarbon breath test as a measure of lipid peroxidation *Free Rad. Biol. Med.* **17** 127–60 (DOI:10.1016/0891-5849(94)90110-4)
- [22] Brown R H and Risby T H 2003 *Disease Markers in Exhaled Breath* (New York: Dekker) chapter 13
- [23] Abuja P M and Albertini R 2001 Methods for monitoring oxidative stress, lipid peroxidation and oxidation resistance of lipoproteins *Clin. Chim. Acta* **306** 1–17
- [24] Banni S, Lucchi L, Baraldi A, Botti B, Cappelli G, Corongiu F, Dessi M A, Tomasi A and Lusvardi E 1996 No direct evidence of increased lipid peroxidation in hemodialysis patients *Nephron* **72** 177–83 (DOI:10.1046/j.1525-1594.2000.06626.x)
- [25] Dale O, Bergum H, Lund T, Nilsen T, Aadahl P and Stenseth R 2003 A validated method for rapid analysis of ethane in breath and its application in kinetic studies in human volunteers *Free Rad. Res.* **37** 815–21 (DOI:10.1080/1071576031000107353)
- [26] Narasimhan L R, Goodman W and Patel C K 2001 Correlation of breath ammonia with blood urea nitrogen and creatinine during hemodialysis *Proc. Natl. Acad. Sci. USA* **98** 4617–21 (DOI:10.1073/pnas.071057598)
- [27] Manne J, Sukhorukov O, Jäger W and Tulip J 2006 Pulsed quantum cascade laser-based cavity ring-down spectroscopy for ammonia detection in breath *Appl. Opt.* **45** 9230–7
- [28] Halmer D, Thelen S, Hering P and Mürtz M 2006 Online monitoring of ethane traces in exhaled breath with a difference frequency generation spectrometer *Appl. Phys. B* **85** 437–43 (DOI:10.1007/s00340-006-2288-9)
- [29] Dahnke H, Kleine D, Hering P and Mürtz M 2001 Real-time monitoring of ethane in human breath using mid-infrared cavity leak out spectroscopy *Appl. Phys. B* **72** 971–5 (DOI:10.1007/s003400100609)
- [30] van Herpen M M J W, Li S, Bisson S E and Harren F J M 2002 Photoacoustic trace gas detection of ethane using a continuously tunable, continuous-wave optical parametric oscillator based on periodically poled lithium niobate *Appl. Phys. Lett.* **81** 1157–9 (DOI:10.1063/1.1500410)
- [31] Patterson C S, McMillan L C, Longbottom C, Gibson G M, Padgett M J and Skeldon K D 2007 Portable optical spectroscopy for accurate analysis of ethane in exhaled breath *Meas. Sci. Technol.* **18** 1459–64 (DOI:10.1088/0957-0233/18/5/035)
- [32] Skeldon K D, Patterson C, Wyse C A, Gibson G M, Padgett M J, Longbottom C and McMillan L C 2005 The potential offered by real-time, high-sensitivity monitoring of ethane in breath and some pilot studies using optical spectroscopy *J. Opt. A: Pure Appl. Opt.* **7** 376–84 (DOI:10.1088/1464-4258/7/6/019)
- [33] Revin D G, Cockburn J W, Steer M J, Airey R J, Hopkinson M, Krysa A B, Wilson L R and Menzel S 2007 InGaAs/AlAsSb/InP quantum cascade lasers operating at wavelengths close to 3 μm *Appl. Phys. Lett.* **90** 1108–10 (DOI:10.1063/1.2431035)
- [34] Phillips M, Gleeson K, Hughes J M B, Greenberg J, Cataneo R N, Baker L and McVay W P 1999 Volatile organic compounds in breath as markers of lung cancer: a cross-sectional study *Lancet* **353** 1930–3 (DOI:10.1016/S0140-6736(98)07552-7)
- [35] Skeldon K D, McMillan L C, Wyse C A, Monk S D, Gibson G, Patterson C, France T, Longbottom C and Padgett M J 2006 Application of laser spectroscopy for measurement of exhaled ethane in patients with lung cancer *Resp. Med.* **100** 300–6 (DOI:10.1016/j.rmed.2005.05.006)
- [36] Stevenson K, Radhakrishnan K, Patterson C S, McMillan L C, Skeldon K D, Buist L, Padgett M and Shiels P G 2007 Breath ethane peaks during a single haemodialysis session and is associated with time on dialysis (in preparation)
- [37] Ward R A, Ouseph R and McLeish K R 2003 Effects of high-flux hemodialysis on oxidant stress *Kidney Int.* **63** 353–9 (DOI:10.1046/j.1523-1755.2003.00741.x)
- [38] Kuwahara T, Markert M and Wauters J P 1988 Neutrophil oxygen radical production by dialysis membranes *Nephrol. Dial. Transplant.* **3** 661–5
- [39] Sezer S, Tutal E, Bilgic A, Aldemir D, Turkoglu S, Arat Z, Ozdemir F N and Haberal M 2005 Impact of nutritional status on oxidative stress in hemodialysis patients with/without inflammatory state *Nephrol. Dial. Transplant.* **20** v131
- [40] Galli F and Ronco C 2000 Oxidant stress in hemodialysis *Nephron* **84** 1–5 (DOI:10.1159/000045531)
- [41] Andreoni K A, Kazui M, Cameron D E, Nyhan D, Sehnert S S, Rohde C A, Bulkley G B and Risby T H 1999 Ethane: a marker of lipid peroxidation during cardiopulmonary bypass in humans *Free Radic. Biol. Med.* **26** 439–45 (DOI:10.1016/S0891-5849(98)00220-2)